

University of Southampton Research Repository ePrints Soton

Copyright © and Moral Rights for this thesis are retained by the author and/or other copyright owners. A copy can be downloaded for personal non-commercial research or study, without prior permission or charge. This thesis cannot be reproduced or quoted extensively from without first obtaining permission in writing from the copyright holder/s. The content must not be changed in any way or sold commercially in any format or medium without the formal permission of the copyright holders.

When referring to this work, full bibliographic details including the author, title, awarding institution and date of the thesis must be given e.g.

AUTHOR (year of submission) "Full thesis title", University of Southampton, name of the University School or Department, PhD Thesis, pagination

UNIVERSITY OF SOUTHAMPTON
FACULTY OF PHYSICAL SCIENCES AND ENGINEERING
SCHOOL OF ELECTRONICS AND COMPUTER SCIENCE

Detection for
Multiple-Input Multiple-Output Systems:
Probabilistic Data Association and Semidefinite
Programming Relaxation

by

Shaoshi Yang

BEng, MEng

*A thesis for the degree of
Doctor of Philosophy
at the University of Southampton*

December 2013

Supervisor: *Professor Lajos Hanzo*

FREng, FIEEE, FIET, FEURASIP

Chair in Telecommunications

Communications, Signal Processing and Control Group

School of Electronics and Computer Science

University of Southampton

Southampton, SO17 1BJ

United Kingdom

Dedicated to my dearly beloved parents and wife.

UNIVERSITY OF SOUTHAMPTON

ABSTRACT

FACULTY OF PHYSICAL SCIENCES AND ENGINEERING

School of Electronics and Computer Science

Doctor of Philosophy

DETECTION FOR MULTIPLE-INPUT MULTIPLE-OUTPUT SYSTEMS:
PROBABILISTIC DATA ASSOCIATION AND SEMIDEFINITE PROGRAMMING
RELAXATION

by Shaoshi Yang

As a highly effective physical-layer interference management technique, the joint detection of a vector of non-orthogonal information-bearing symbols simultaneously transmitted over multiple-input multiple-output (MIMO) channels is of fundamental importance for high-throughput digital communications. This is because the generic mathematical model of MIMO detection underpins a wide range of relevant applications including (but not limited to) the equalization of dispersive band-limited channels imposing intersymbol interference (ISI), the multiuser detection (MUD) in code-division multiple-access (CDMA) systems and the multi-stream detection for multiple-antenna based spatial-division multiplexing (SDM) systems. With the evolution of wireless networks, the “virtual MIMO” concept was conceived, which is also described by the generic mathematical MIMO model. MIMO detection becomes even more important, because the achievable performance of spectrum-efficient wireless networks is typically interference-limited, rather than noise-limited.

In this thesis, a pair of detection methods that are well-suited for large-scale MIMO systems are investigated. The first one is the probabilistic data association (PDA) algorithm, which is essentially an interference-modelling approach based on iterative Gaussian approximation. The second one is the semidefinite programming (SDP) relaxation based approach, which approximates the optimal maximum likelihood (ML) detection problem to a convex optimization problem. The main advantage of both methods is that they impose a moderate computational complexity that increases as a polynomial function of the problem size, while providing competitive performance.

The contributions of this thesis can be broadly categorized into two groups. The first group is related to the design of virtually antipodal (VA) detection of rectangular M -ary quadrature amplitude modulation (M -QAM) symbols transmitted in SDM-MIMO systems. As a foundation, in the first parts of Chapter 2 and Chapter 3 the rigorous mathematical relationship between the vector space of transmitted bits and that of transmitted rectangular M -QAM

symbols is investigated. Both linear and nonlinear bit-to-symbol mappings are considered. It is revealed that the two vector spaces are linked by linear/quasi-linear transformations, which are explicitly characterized by certain transformation matrices. This formulation may potentially be applicable to many signal processing problems of wireless communications. For example, when used for detection of rectangular M -QAM symbol vector, it enables us to transform the conventional three-step “signal-to-symbol-to-bits” decision process to a direct “signal-to-bits” decision process. More specifically, based on the linear VA transformation, in Chapter 2 we propose a unified bit-based PDA (B-PDA) detection method for linear natural mapping aided rectangular M -QAM symbols transmitted in SDM-MIMO systems. We show that the proposed linear natural mapping based B-PDA approach attains an improved detection performance, despite dramatically reducing the computational complexity in contrast to the conventional symbol-based PDA detector. Furthermore, in Chapter 3 a quasi-linear VA transformation based generalized low-complexity semidefinite programming relaxation (SDPR) detection approach is proposed for Gray-coded rectangular M -QAM signalling over MIMO channels. Compared to the linear natural mapping based B-PDA of Chapter 2, the quasi-linear VA transformation based SDPR method is capable of directly deciding on the information bits of the ubiquitous Gray-mapping aided rectangular M -QAM by decoupling the M -QAM constellation into several 4-QAM constellations. Moreover, it may be readily combined with the low-complexity bit-flipping based “hill climbing” technique for exploiting the unequal error protection (UEP) property of rectangular M -QAM, and the resultant VA-SDPR detector achieves the best bit-error rate (BER) performance among the known SDPR-based MIMO detectors conceived for high-order QAM constellations, while still maintaining the same order of polynomial-time worst-case computational complexity. Additionally, we reveal that the linear natural mapping based VA detectors attain the same performance provided by the binary reflected Gray mapping based VA detectors, but the former are simpler for implementation. Therefore, only if there are other constraints requiring using the nonlinear Gray mapping, it is preferable to use the linear natural mapping rather than the Gray mapping, when the VA detectors are used in uncoded MIMO systems.

The second group explores the application of the PDA-aided detectors in some more sophisticated systems that are of great interest to the wireless research community. In particular, the design of iterative detection and decoding (IDD) schemes relying on the proposed low-complexity PDA methods is investigated for the turbo-coded MIMO systems in Chapter 4 and 5. It has conventionally been regarded that the existing PDA algorithms output the estimated symbol-wise *a posteriori* probabilities (APPs) as soft information. In Chapter 4 and 5, however, we demonstrate that these probabilities are not the true APPs in the rigorous mathematical sense, but a type of nominal APPs, which are unsuitable for the classic architecture of IDD receivers. Moreover, our study shows that the known methods of calculating the bit-wise extrinsic logarithmic likelihood ratios (LLRs) are no longer applicable to the

conventional PDA based methods when detecting M -ary modulation symbols. Additionally, the existing PDA based MIMO detectors typically operate purely in the probabilistic domain. Therefore, the existing PDA methods are not readily applicable to IDD receivers. To overcome this predicament, in Chapter 4 and Chapter 5 we propose the approximate Bayes' theorem based logarithmic domain PDA (AB-Log-PDA) and the exact Bayes' theorem based logarithmic domain PDA (EB-Log-PDA) detectors, respectively. We present the approaches of calculating the bit-wise extrinsic LLRs for both the AB-Log-PDA and the EB-Log-PDA, which makes them well-suited for IDD receivers. Furthermore, we demonstrate that invoking inner iterations within the PDA algorithms – which is common practice in PDA-aided uncoded MIMO systems – would actually degrade the IDD receiver's performance, despite significantly increasing its overall computational complexity. Additionally, we investigate the relationship between the extrinsic LLRs of the proposed EB-Log-PDA and of the AB-Log-PDA. It is also shown that both the proposed AB-Log-PDA- and the EB-Log-PDA-based IDD schemes dispensing with any inner PDA iterations are capable of achieving a performance comparable to that of the optimal maximum *a posteriori* (MAP) detector based IDD receiver in the scenarios considered, despite their significantly lower computational complexity. Finally, in Chapter 6, a base station (BS) cooperation aided distributed soft reception scheme using the symbol-based PDA algorithm and soft combining (SC) is proposed for the uplink of multiuser multicell MIMO systems. The realistic 19-cell hexagonal cellular model relying on radical unity frequency reuse (FR) is considered, and local cooperation based message passing is used instead of a global message passing chain for the sake of reducing the backhaul traffic. We show that despite its moderate complexity and backhaul traffic, the proposed distributed PDA (DPDA) aided SC (DPDA-SC) reception scheme significantly outperforms the conventional non-cooperative benchmarks. Furthermore, since only the index of the quantized converged soft information has to be exchanged between collaborative BSs for SC, the proposed DPDA-SC scheme is relatively robust to the quantization errors of the soft information exchanged. As an appealing benefit, the backhaul traffic is dramatically reduced at a negligible performance degradation.

Declaration of Authorship

I, **Shaoshi Yang**, declare that the thesis entitled

**Detection for Multiple-Input Multiple-Output Systems: Probabilistic Data
Association and Semidefinite Programming Relaxation**

and the work presented in it are my own and have been generated by me as the result of my own original research. I confirm that:

1. This work was done wholly or mainly while in candidature for a research degree at this University;
2. Where any part of this thesis has previously been submitted for a degree or any other qualification at this University or any other institution, this has been clearly stated;
3. Where I have consulted the published work of others, this is always clearly attributed;
4. Where I have quoted from the work of others, the source is always given. With the exception of such quotations, this thesis is entirely my own work;
5. I have acknowledged all main sources of help;
6. Where the thesis is based on work done by myself jointly with others, I have made clear exactly what was done by others and what I have contributed myself;
7. Parts of this work have been published, as seen in the list of publications.

Signed: Shaoshi Yang

Date: 3 December 2013

Acknowledgements

There are many people I would like to acknowledge for making my experience in the University of Southampton one of the most important and rewarding periods during my life.

I would like to express my heartfelt gratitude to Professor Lajos Hanzo for his outstanding supervision and continuous support throughout my research adventure. His insightful guidance and enthusiastic encouragement have greatly transformed my thoughts not only on research but also on life. He, as a role model with charming personality, granted much freedom to me for exploring the research problems of interest to me. Most importantly, I would like to appreciate him for his invaluable friendship.

Many thanks also to my colleagues and the staff of the research group, both past and present, for their generous help throughout my research. I would like to thank Prof. Lie-Liang Yang, Prof. Sheng Chen, Dr. Robert G. Maunder, Dr. Li Wang, Dr. Soon Xin Ng, Dr. Rong Zhang, Dr. Lingkun Kong, Dr. Wang Yao, Dr. Shinsuke Ibi, Dr. Shinya Sugiura, Dr. Yosef Akhtman, Dr. Jiayi Zhang, Chao Xu, Li Li, Dandan Liang *et al.*, too numerous to mention here explicitly.

I would also like to express my great appreciation to my parents and my siblings for their love and support. Thanks also due to Prof. Tiejun Lv and Prof. Daoben Li at BUPT, for cultivating in me the first piece of taste of research. Special thanks also to Dr. Ming Lei and Dr. Hongmei Sun, for their guidance and friendship during my internship in Intel Labs China. Finally, to my beloved wife, Junhua Zhou, for her deep love, persistent support and considerate care to me.

The financial support of the School of Electronics and Computer Science, University of Southampton, and of the China Scholarship Council (CSC) is also gratefully acknowledged.

List of Publications

Journal Papers:

1. **Shaoshi Yang**, Tiejun Lv, Robert G. Maunder and Lajos Hanzo, “From nominal to true *a posteriori* probabilities: an exact Bayesian theorem based probabilistic data association approach for iterative MIMO detection and decoding”, *IEEE Transactions on Communications*, vol. 61, no. 7, pp. 2782-2793, July 2013.
2. Kent Tsz Kan Cheung, **Shaoshi Yang** and Lajos Hanzo, “Achieving maximum energy-efficiency in multi-relay OFDMA cellular networks: a fractional programming approach”, *IEEE Transactions on Communications*, vol. 61, no. 7, pp. 2746-2757, July 2013.
3. **Shaoshi Yang**, Tiejun Lv and Lajos Hanzo, “Semidefinite programming relaxation based virtually antipodal detection for MIMO systems using Gray-coded high-order QAM”, *IEEE Transactions on Vehicular Technology*, vol. 62, no. 4, pp. 1667-1677, May 2013.
4. **Shaoshi Yang**, Li Wang, Tiejun Lv and Lajos Hanzo, “Approximate Bayesian probabilistic-data-association-aided iterative detection for MIMO systems using arbitrary M -ary modulation”, *IEEE Transactions on Vehicular Technology*, vol. 62, no. 3, pp. 1228-1240, March 2013.
5. **Shaoshi Yang**, Tiejun Lv, Robert G. Maunder and Lajos Hanzo, “Distributed probabilistic-data-association-based soft reception employing base station cooperation in MIMO-aided multiuser multicell systems”, *IEEE Transactions on Vehicular Technology*, vol. 60, no. 7, pp. 3532-3538, September 2011.
6. **Shaoshi Yang**, Tiejun Lv, Robert G. Maunder and Lajos Hanzo, “Unified bit-based probabilistic data association aided MIMO detection for high-order QAM constellations”, *IEEE Transactions on Vehicular Technology*, vol. 60, no. 3, pp. 981-991, March 2011.
7. Kent Tsz Kan Cheung, **Shaoshi Yang** and Lajos Hanzo, “Spectral and energy spectral efficiency optimization of joint transmit and receive beamforming based multi-relay MIMO-OFDMA cellular networks”, *submitted to IEEE Transactions on Wireless Communications*.
8. Xinyi Xu, **Shaoshi Yang**, Rong Zhang, Qiuping Zhu and Lajos Hanzo, “Pervasive distributed antennas and mobile relays for fractional frequency reuse based multicell multiuser networks”, *submitted to IEEE Transactions on Vehicular Technology*.

Conference Papers:

1. **Shaoshi Yang**, Lajos Hanzo, “Exact Bayes’ theorem based probabilistic data association for iterative MIMO detection and decoding”, in *Proc. IEEE 56th Global Communications Conference (GLOBECOM 2013)*, Atlanta, USA, December 2013.
2. Kent Tsz Kan Cheung, **Shaoshi Yang**, Lajos Hanzo, “Maximizing Energy-Efficiency in Multi-Relay OFDMA Cellular Networks”, in *Proc. IEEE 56th Global Communications Conference (GLOBECOM 2013)*, Atlanta, USA, December 2013.
3. **Shaoshi Yang**, Lajos Hanzo, “Iterative detection and decoding using approximate Bayesian theorem based PDA method over MIMO Nakagami- m fading channels”, in *Proc. IEEE 55th Global Communications Conference (GLOBECOM 2012)*, Anaheim, USA, December 2012, pp. 3588-3593.
4. **Shaoshi Yang**, Lajos Hanzo, “Semidefinite programming relaxation based virtually antipodal detection for Gray coded 16-QAM MIMO signalling”, in *Proc. IEEE 54th Global Communications Conference (GLOBECOM 2011)*, Houston, USA, December 2011, pp. 1-5.
5. **Shaoshi Yang**, Tiejun Lv and Lajos Hanzo, “Base station cooperation in MIMO-aided multi-user multi-cell systems employing distributed probabilistic data association based soft reception”, in *Proc. IEEE 46th International Conference on Communications (ICC 2011)*, Kyoto, Japan, June, 2011, pp. 1-5.
6. **Shaoshi Yang**, Tiejun Lv and Lajos Hanzo, “Unified bit-based probabilistic data association aided MIMO detection for high-order QAM”, in *Proc. IEEE 12th Wireless Communications and Networking Conference (WCNC 2011)*, Cancun, Mexico, March 2011, pp. 1629-1634.

List of Symbols

General notation

\mathbf{A}	boldface uppercase letters denote matrices.
a_{ij}	the element of the matrix \mathbf{A} at row i , column j .
\mathbf{x}	boldface lowercase letters denote column vectors.
x	standard lowercase letters denote scalars.
x_i	the i th element of the vector \mathbf{x} .
$\text{Diag}\{\mathbf{x}\}$	a diagonal matrix with \mathbf{x} being its diagonal elements.
$\text{diag}\{\mathbf{A}\}$	a vector comprised of the diagonal elements of the matrix \mathbf{A} .
$\text{Trace}(\mathbf{A})$	trace of matrix \mathbf{A} .
\mathbf{A}^*	elementwise complex conjugate of the matrix \mathbf{A} .
\mathbf{A}^T	transpose of the matrix \mathbf{A} .
\mathbf{A}^H	Hermitian transpose of the matrix \mathbf{A} .
\mathbf{A}^{-1}	inverse of the square matrix \mathbf{A} .
\mathbf{A}^\dagger	Moore-Penrose inverse (pseudoinverse) of the matrix \mathbf{A} .
$\hat{\mathbf{x}}$	estimate of the vector \mathbf{x} .
$\mathcal{E}(\cdot)$	Expectation operator.
$\mathcal{V}(x)$	Variance of random variable x .
$\mathcal{C}(\cdot)$	Covariance (matrix) operator.
$\mathcal{C}_p(\cdot)$	Pseudo-covariance (matrix) operator.
$\Re(\mathbf{A})$	elementwise real part of the matrix \mathbf{A} .
$\Im(\mathbf{A})$	elementwise imaginary part of the matrix \mathbf{A} .
\mathbf{I}_N	the $(N \times N)$ -element identity matrix.
$\mathbf{1}_N$	the dimension- N column vector of ones.
\mathbb{R}	the field of real numbers.
\mathbb{C}	the field of complex numbers
\mathbb{Z}	the set of all integers.
\mathbb{Z}^+	the set of all positive integers.
$\ \cdot\ _2$	the Euclidean norm of a vector.
$\ \cdot\ _F$	the Frobenius norm of a matrix.
$\min(\cdot)$	minimization operator
$\max(\cdot)$	maximization operator

Special symbols

\mathbf{b}	source bit vector.
\mathbf{c}	encoded bit vector.
\mathbf{s}	modulated symbol vector.
\mathbf{n}	additive white Gaussian noise (AWGN) vector.
\mathbf{y}	baseband received signal vector.
N_0	one-sided power spectrum density of AWGN.
σ^2	the power of AWGN per dimension.
N_t	the number of transmitting antennas.
N_r	the number of receiving antennas.
$N_t \times N_r$	an MIMO system with N_t transmitting and N_r receiving antennas.
E_b	energy per bit.
E_s	energy per symbol.
\mathbf{e}_i	a column vector whose i th element is equal to 1 and the other elements are equal to 0.
$F(\mathbf{x})$	the cumulative distribution function (CDF) of random variable \mathbf{x} .
$f(\mathbf{x})$	the probability density function (PDF) of random variable \mathbf{x} .
\mathbf{H}	MIMO channel matrix.
\mathbf{h}_i	the i th column vector of \mathbf{H} ; associated with the i th transmitting antenna.
h_{ji}	the channel fading coefficient between the i th transmitting antenna and the j th receiving antenna.
M_c	number of bits per constellation symbol.
M	size of the modulation constellation.
R	channel coding rate.
\oplus	addition operator in GF(2) (the XOR operator of two binary scalars).
\boxplus	elementwise XOR operator of two binary vectors/matrices.
\otimes	elementwise multiplication operator of two vectors/matrices.
$\mathbf{X} \succeq 0$	\mathbf{X} is a positive semidefinite (PSD) matrix.
$\mathbf{X} \succ 0$	\mathbf{X} is a positive definite (PD) matrix.
$\text{abs}(\cdot)$	elementwise absolute value function.
\mathbb{A}	constellation alphabet.
\propto	is proportional to.

Contents

Abstract	v
Declaration of Authorship	ix
Acknowledgements	xi
List of Publications	xiii
List of Symbols	xv
Contents	xvii
1 Introduction	1
1.1 The Nature of Co-Channel Interference	3
1.2 Concept and Generality of MIMO Detection	6
1.3 Formal Definition of the MIMO Detection Problem	8
1.4 MIMO System Model for Linear Memoryless Channels	10
1.5 MIMO System Model for Dispersive Channels Exhibiting Memory	11
1.6 Complex-Valued versus Real-Valued MIMO System Model	12
1.7 An Introductory Example of SDM-MIMO Systems	13
1.8 History and State-of-the-Art of MIMO detection	14
1.8.1 Optimum MIMO Detector	15
1.8.2 Linear MIMO Detectors	19
1.8.3 Interference Cancellation Aided MIMO Detectors	24
1.8.4 Tree-Search MIMO Detectors	26
1.8.5 Probabilistic Data Association Based Detector	31
1.8.6 Semidefinite Programming Relaxation Based Detector	33
1.9 Organization and Novel Contributions of the Thesis	34
1.9.1 Organization	34
1.9.2 Novel Contributions	37
2 Unified Bit-Based PDA Aided MIMO Detection for High-Order QAM Constellations	41
2.1 Introduction	41
2.2 Problem Statement	44
2.3 UMR of QAM: Linear Natural Bit-to-Symbol Mapping	45
2.3.1 Even-Throughput Rectangular QAM	46
2.3.1.1 4-QAM	46
2.3.1.2 16-QAM	47

2.3.1.3	64-QAM	47
2.3.2	Odd-Throughput Rectangular QAM	48
2.3.2.1	BPSK	48
2.3.2.2	8-QAM	49
2.3.2.3	32-QAM	49
2.3.3	General M -QAM	49
2.4	UMR of QAM: Nonlinear Gray Bit-to-Symbol Mapping	50
2.4.1	16-QAM	51
2.4.2	64-QAM	52
2.4.3	General M -QAM	54
2.5	B-PDA MIMO Detection based on UMR	56
2.5.1	Basic Detection Algorithm	56
2.5.2	Example of the B-PDA	58
2.5.3	Discussions	63
2.5.3.1	Positive versus Negative Impact of UMR	63
2.5.3.2	Impact of Constellation Labelling on BER/SER Performance	67
2.5.3.3	Practical Feasibility of UMR for Gray Mapping	67
2.5.4	Computational Complexity Analysis	67
2.6	Simulation Results	70
2.7	Chapter Summary and Conclusions	74
3	Semidefinite Programming Relaxation Based Virtually Antipodal MIMO Detection for Gray-Coded High-Order QAM	75
3.1	Introduction	75
3.2	Basics of Convex Optimization and Semidefinite Programming	78
3.2.1	Convex Optimization	78
3.2.2	Semidefinite Programming	83
3.2.2.1	Several Widely Used Forms of SDP	83
3.2.2.2	Example of SDP	85
3.3	System Model and Problem Statement	86
3.4	Revisiting Gray-Mapping Aided M -QAM	87
3.5	DVA-SDPR Detector	91
3.5.1	DVA-SDPR Formulation	91
3.5.2	DVA-SDPR Solving Method	93
3.5.3	Performance Refinement Using Bit-Flipping	95
3.5.4	Computational Complexity Analysis	95
3.6	Simulation Results and Discussions	96
3.6.1	Simulation Results	96
3.6.2	Discussions	100
3.7	Chapter Summary and Conclusions	102
4	Approximate Bayes' Theorem Based PDA for Iterative MIMO Detection and Channel Decoding	105
4.1	Introduction	105
4.2	System Model	109
4.3	Interference-Plus-Noise Distribution Analysis	111
4.4	AB-Log-PDA Relying on <i>A Priori</i> Soft Feedback From the FEC Decoder	114

4.5	Extrinsic LLR Calculation Using the Output of AB-Log-PDA	118
4.5.1	Challenges in Calculating Extrinsic LLRs for PDA Based Methods	119
4.5.2	Calculating Extrinsic LLRs for AB-Log-PDA	121
4.6	Simulation Results and Discussions	122
4.6.1	Performance of the AB-Log-PDA based IDD	123
4.6.2	Computational Complexity Analysis	131
4.7	Chapter Summary and Conclusions	134
5	Exact Bayes' Theorem Based PDA for Iterative MIMO Detection and Channel Decoding	135
5.1	Introduction	135
5.2	System Model	137
5.3	The EB-Log-PDA with A Priori Soft Feedback From The FEC decoder	138
5.4	Extrinsic LLR Calculation For EB-Log-PDA	142
5.4.1	Method of Calculating the Extrinsic LLRs for EB-Log-PDA	142
5.4.2	On the Relationship Between the Extrinsic LLRs of the EB-Log-PDA and AB-Log-PDA	145
5.5	Simulation Results and Discussions	148
5.5.1	Convergence and Performance of the EB-Log-PDA based IDD	148
5.5.2	Impact of Inner PDA Iterations on the EB-Log-PDA Based IDD	150
5.5.3	Relationship between Extrinsic LLRs of EB-Log-PDA and AB-Log-PDA	152
5.5.4	Computational Complexity Comparison	154
5.6	Chapter Summary and Conclusions	155
6	Distributed PDA Based Soft Reception for Base Station Cooperation in Multiuser Multicell MIMO Systems	157
6.1	Introduction	157
6.2	Hexagonal Cellular Network Model	160
6.3	Cooperative Distributed Soft Reception	163
6.3.1	Signal Model	163
6.3.2	Parallel Detection Using the PDA Algorithm	164
6.3.3	Parallel Message Exchange via Unified-Client-Server Mode	167
6.3.4	Soft Combining (SC) and Final Decision	167
6.3.5	Complexity Analysis	168
6.4	Simulation Results and Discussions	168
6.4.1	Perfect CSI	169
6.4.2	Imperfect CSI	171
6.4.3	Impact of Quantization on the Backhaul Traffic and Performance	172
6.4.4	Rank-Deficient Scenario	173
6.4.5	Convergence Property	173
6.4.6	Complexity Comparison	174
6.5	Chapter Summary and Conclusions	175
7	Conclusions and Future Research	177
7.1	Summary and Conclusions	178
7.2	Future Work	188

Glossary	i
List of Figures	vii
List of Tables	xi
Bibliography	xiii
Author Index	xliii

Introduction

THE multimedia data traffic conveyed by the global mobile networks has been soaring [1–5], and this trend is set to continue, as indicated by Cisco’s visual networking index (VNI) forecast [6, 7]. More specifically,¹ as predicted in Fig. 1.1, the global mobile data traffic will increase 13-fold between 2012 and 2017, which translates to a compound annual growth rate (CAGR) of 66% for the period spanning from 2012 to 2017, reaching 11.2 exabytes (EB), i.e. 10^{18} bytes per month by 2017 [6, 7]. As seen from Fig. 1.2, this explosive growth is mainly fuelled by the prevalence of smartphones and tablets, as well as by the emergence of machine-to-machine (M2M) communications [8–19]. As a consequence of the combined effect of this trend and the constraints imposed by the paucity of radio spectrum, as exemplified by the overcrowded frequency allocation chart of the United States [20], future communication systems have to resort to the employment of multiple-input multiple-output (MIMO) transmission techniques for achieving both high spectrum-efficiency [21–25] and high energy-efficiency [25, 26].

The joint detection of multiple symbols in MIMO systems is of central importance for the sake of realizing the substantial benefits of various MIMO techniques. This is because the co-channel interference (CCI) routinely encountered in MIMO-based communication systems constitutes a fundamental limiting characteristic [24, 27–36]. Unfortunately, the optimum MIMO detection problem was proven nondeterministic polynomial-time hard (NP-hard) [37–39], thus all known algorithms conceived for solving the problem optimally have a complexity exponentially increasing with the number of decision variables. As a result, the computational complexity of the optimum maximum-likelihood (ML) criterion or the maximum *a posteriori* (MAP) criterion based MIMO detection algorithms become excessive as the number of decision variables increases. Hence low-complexity, yet high-performance suboptimum MIMO detection algorithms are needed for practical MIMO applications.

¹Fig. 1.1 and Fig. 1.2 are reprinted from the Cisco VNI white paper [6], with permission of Cisco.

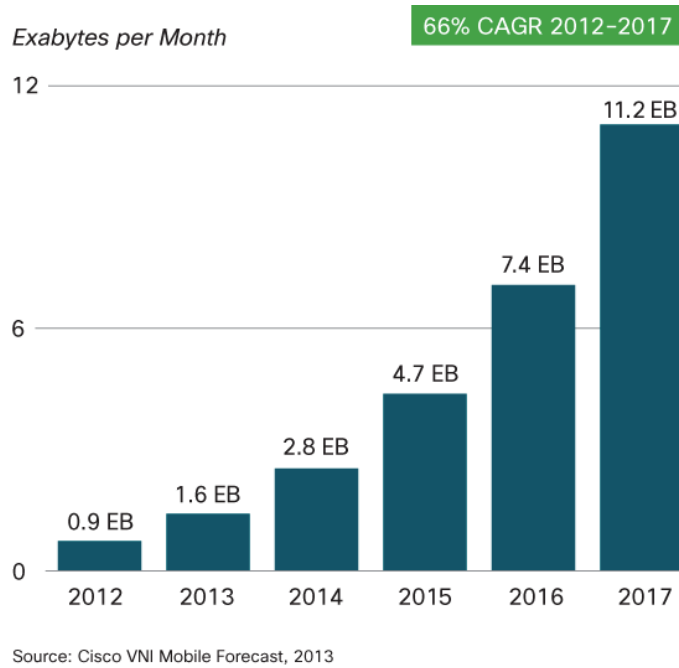
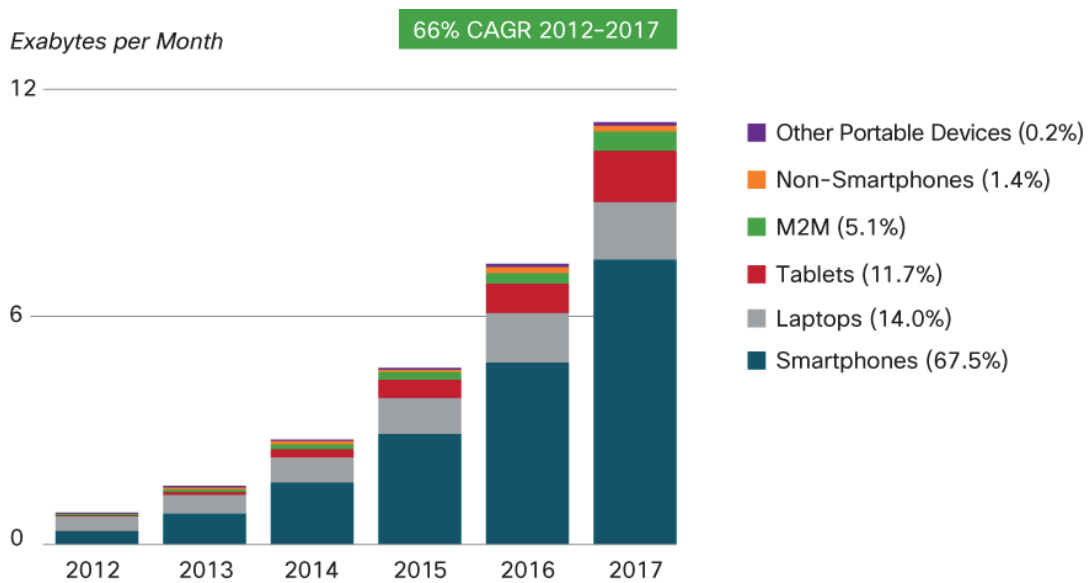


FIGURE 1.1: Cisco VNI: global mobile data traffic forecast, 2012-2017.



Figures in legend refer to traffic share in 2017.
Source: Cisco VNI Mobile Forecast, 2013

FIGURE 1.2: Cisco VNI: share of different devices in the global mobile traffic forecast, 2012-2017.

In this thesis, complexity-scalable MIMO detection methods are conceived for large-scale MIMO systems [25]. The first method considered is the probabilistic data association (PDA) algorithm [40–47], which is essentially an interference-modelling approach based on iterative Gaussian approximation. The second method considered is the semidefinite programming relaxation (SDPR) based approach [48, 49], which approximates the optimal ML detection problem by a readily-solvable convex optimization problem. The greatest advantage of both methods is that they impose a low computational complexity, which increases as a polynomial function of the number of decision variables, while providing a competitive performance. Compared to other mainstream suboptimum MIMO detection methods [50–53] such as the linear zero-forcing (ZF) detector, the linear minimum mean-square error (MMSE) detector, the successive interference cancellation (SIC) detector, and the sphere decoding (SD) detector [54–83], neither the PDA nor the SDPR method has been well investigated in sufficient depth, and hence there remains some significant open problems to be solved.

To gain profound insights into the intricacies of the MIMO detection problem, and in particular into the PDA and the SDPR based MIMO detectors, let us briefly reflect on the nature of the CCI in the following section.

1.1 The Nature of Co-Channel Interference

The nature of CCI depends on the specific context. In this thesis, it is defined in its most generic form as *the interfering signal imposed by multiple transmissions taking place on channels which are mutually correlated*. The channel-induced correlation may be observed in one or more domains of frequency, time and space, as shown in Fig. 1.3. To recover the desired signal at the receiver, the desired signal has to be distinguishable from the interference in *at least* one domain. In the extreme case, if the multiple transmissions are highly correlated in all domains, then it may become impossible to recover the desired signal by any means.

In essence, the CCI originates from signal-feature-overlapping of multiple transmissions. For example, in spectrum-efficient communication systems such as the code-division multiplexing /multiple-access (CDM/CDMA) systems [84–86] and the space-division multiplexing /multiple-access (SDM/SDMA) systems [21, 36, 87–93], multiple transmissions are often deliberately arranged to take place simultaneously over the same frequency band. These “frequency sharing” and “time sharing” strategies result in a “frequency-overlapping” and a “time-overlapping” phenomenon, respectively. It is worth pointing out that as far as radio waves are concerned, rigorously the CCI always tends to exist in the frequency, time and space domains. For example, when no deliberate frequency-overlapping is arranged, the “frequency-overlapping” is due to the underlying fact that *for all realizable, time-limited*

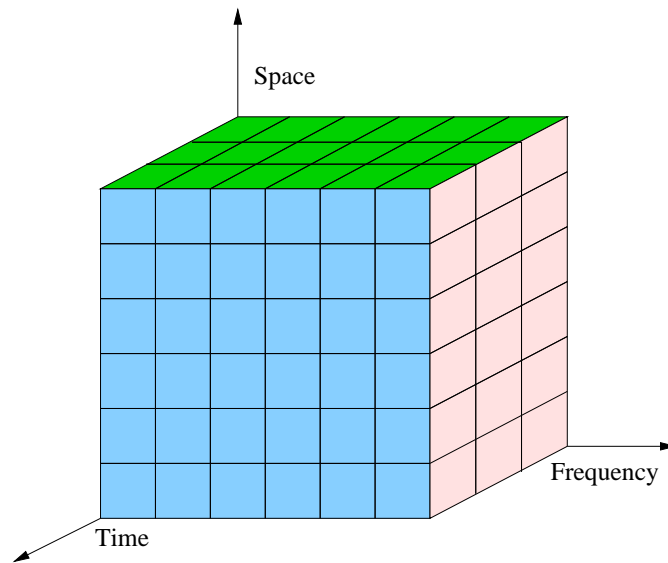


FIGURE 1.3: The multiple signals have to be distinguishable in at least one of the three fundamental domains of time, frequency and space.

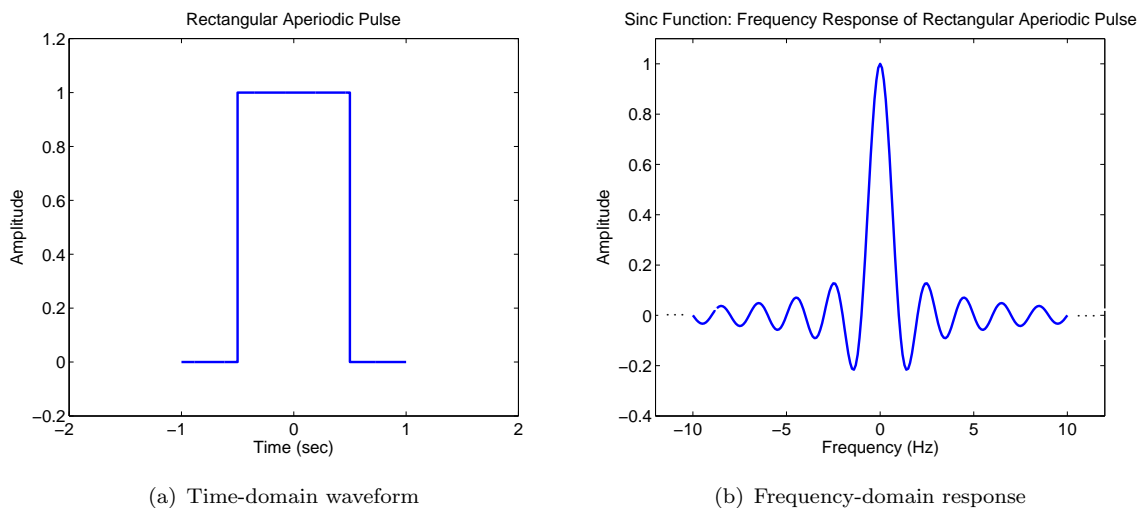


FIGURE 1.4: All realizable, duration-time limited waveforms has a infinite frequency band.

radio waveforms, their absolute bandwidth is infinite [94, 95], as shown in Fig. 1.4. In other words, *every active radio transmitter has an impact on every operating radio receiver*. Similarly, for a strictly bandwidth-limited signal, its time duration has to be infinite. With respect to the space domain, it is well known that the propagation of electromagnetic energy in free space is determined by the inverse square law [21, 93, 96], i.e. we have $S = P_t/4\pi d^2$, where S is the power per unit area or power spatial density (in Watts per metre-squared) at distance d , and P_t is the total power transmitted (in Watts). Hence, theoretically, the radio signals cannot be stopped, they are only attenuated in the frequency, time and space domains.

In engineering practice, fortunately, by using well-designed filters [97, 98], typically the wave-

form of the time-limited signal can be shaped so that most energy of the signal can be kept within a given limited frequency-band, and thus the signal energy leakage outside the target frequency-band can be reduced to a sufficiently low level. Similarly, in the space domain, two transmissions taking place at a sufficiently far distance can also be regarded as non-interfering with each other. Therefore, despite the fact that the signal-feature-overlapping in frequency, time and space domains is inevitable from the theoretic point of view, in practical spectrum-efficient systems we can typically assume that the signal-feature-overlapping in these three domains is a result of a deliberate design. In this context, *the signals are made as much distinguishable as possible in one domain, and as much overlapping as possible in the remaining domains*. Our task is to recover the desired signal based on this deliberate arrangement.

Since the frequency, time and space domains represent the fundamental physical features of signal transmission, each of them corresponds to a distinct multiplexing/multiple-access scheme [99], namely the frequency-division multiplexing/multiple-access (FDM/FDMA), time-division multiplexing/multiple-access (TDM/TDMA), and SDM/SDMA, respectively. It is worth noting that compared to these three fundamental domains, the spreading code sequences used in CDM/CDMA systems do *not* constitute an independent domain. This is because the orthogonality of the spreading code sequences is essentially *a special case of time-domain orthogonality*. In systems using spreading codes, in principle we pursue to transmit orthogonal code sequences to minimize the inter-code interference. Although it is mathematically possible to construct perfectly orthogonal code sequences, the orthogonality of these code sequences is typically degraded in practical transmissions [86]. Moreover, since the number of theoretically orthogonal code sequences is rather limited, often quasi-orthogonal code sequences are adopted in practice [86]. Therefore, typically substantial interference is imposed by the non-orthogonality of spreading code sequences in practical CDM/CDMA systems [100].

In analogy to CDM/CDMA, the conventional frequency division pattern, time division pattern and space division pattern can also be regarded as a special case of “spreading codes” in the frequency domain, time domain and space domain, respectively. Note, however, that there exist a certain degree of differences in terms of *their multiplexing/multiple-access resolution* in these three domains. More specifically, in practice, by using guard intervals in the corresponding domain, a good resolution of frequency division and time division may be readily maintained – in other words, the orthogonality of “spreading codes” in frequency- and time-division systems may be relatively easy to obtain [99]. By contrast, the resolution of space division tends to be undermined by the physical size of transmitters/receivers and by the random propagation channel, hence typically substantial interference is imposed by the non-orthogonality of “spreading codes” in practical space-division systems [21, 36, 87–93]. This is similar to the case in CDM/CDMA systems, and explains why MIMO detection typically represents a more significant problem in CDM/CDMA systems and in SDM/SDMA

systems than in FDM/FDMA and TDM/TDMA systems.

In this thesis, the CCI considered mainly refers to the interference in SDM/SDMA or CDMA/CDMA systems, where multiple transmissions often take place *simultaneously*, or *partially simultaneously* over the same frequency. Depending on specific applications, CCI is often alternatively termed as intersymbol interference (ISI), interchannel interference (ICI), interantenna interference (IAI), multiuser interference (MUI), multiple-access interference (MAI), and multiple-stream interference (MSI) etc.

1.2 Concept and Generality of MIMO Detection

As a family of physical-layer CCI management techniques, MIMO detection deals with the joint detection of several information-bearing symbols transmitted over a communication channel having multiple inputs and multiple outputs. This problem is of *fundamental* importance for modern high-throughput digital communications. Rigorously, the MIMO detection problem arises *if and only if* the multiple inputs are *not* orthogonal to each other, and hence there exists interference between the outputs. As a *generic* mathematical model, the MIMO detection problem underpins numerous relevant applications, and the physical meaning of the inputs and outputs herein may vary in different contexts. For instance, in single-user SDM-MIMO systems equipped with multiple transmit and receive antennas [101–103], the inputs refer to the vector of modulated symbols that are transmitted from multiple *colocated* transmit antennas, while the outputs refer to the vector of received signals recorded at multiple *colocated* receive antennas, as shown in Fig. 1.5. This is indeed a canonical scenario of investigating MIMO detection algorithms [104]. A second example is the uplink of multiuser multiple-antenna systems [105, 106], where the inputs may be multiple transmitted symbols belonging to a cluster of geographically *distributed* single-antenna mobile stations (MSs),

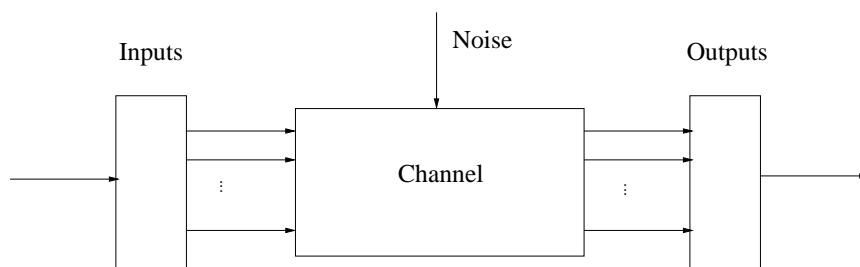


FIGURE 1.5: Point-to-point MIMO channel.

and the outputs may be the signals received at the serving base station (BS) equipped with multiple *colocated* antennas, as shown in Fig. 1.6. This is actually the so-called SDMA system [21, 36, 87–93]. Yet another important example represented by Fig. 1.6 is the uplink of CDMA systems [50–53], where the inputs are the transmitted symbols of distributed single-antenna MSs, and the outputs are typically generated by filtering the signal received

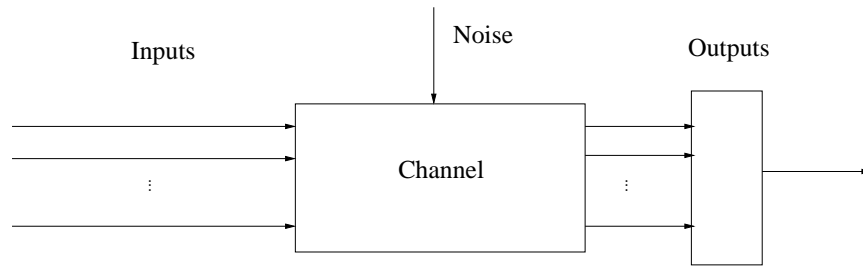


FIGURE 1.6: MIMO multiple-access channel.

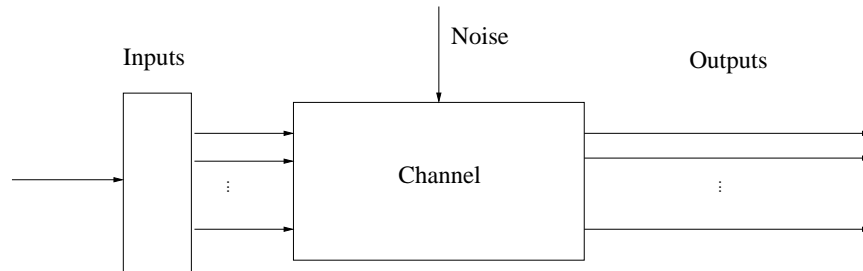


FIGURE 1.7: MIMO broadcast channel.

at the single-antenna BS with a bank of matched filters (MFs), whose impulse responses are matched to a set of *a priori* known user-signature waveforms.

Here, it should be emphasized that whether the multiple inputs and/or the multiple outputs are “colocated” or not is extremely important in determining the signal processing techniques to be used. If multiple inputs/outputs are colocated, the cooperative joint encoding/decoding of the inputs/outputs can be conducted [21, 36, 93, 107–113], which renders joint MIMO transmission/detection feasible. For example, the single-user MIMO system shown in Fig. 1.5 has both its transmit and receive antennas colocated, hence it enjoys the privilege of performing both joint encoding and joint decoding. As a benefit, both simultaneous transmission and simultaneous reception can be attained relatively simply. By contrast, the multiple-access MIMO system of Fig. 1.6 is typically not capable of joint encoding at the user side, hence the uplink transmissions of both CDMA and SDMA systems are *asynchronous* by nature.

Additionally, as far as the downlink of multiuser MIMO systems, namely the multiuser MIMO broadcast channel of Fig. 1.7 is concerned, typically most of the sophisticated signal processing tasks are conducted in the form of transmit preprocessing (i.e. precoding) at the BS, where colocated inputs are available for cooperative joint encoding [114–119]. As a result, detection at the user becomes *less* challenging. Since the investigation of MIMO transmit preprocessing techniques is beyond the scope of this thesis, they will not be discussed in detail.

Finally, when both the transmitters and the receivers are geographically distributed, the MIMO channel turns into an *interference channel* [120–128], which is shown in Fig. 1.8.

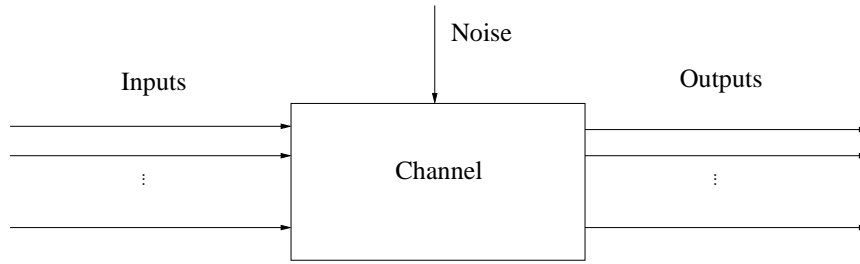


FIGURE 1.8: MIMO interference channel.

An interference channel characterizes such a situation where each transmitter, potentially equipped with multiple antennas, only wants to communicate with its dedicated receiver, and each receiver, possibly equipped with multiple antennas as well, only cares about the information arriving from the corresponding transmitter. There is a strict one-to-one correspondence between the multiple transmitters and the multiple receivers. Therefore, each transmission link interferes with the others. The *distributed nature* of transmitters and receivers makes the signal processing required for mitigating the detrimental effects of the MIMO interference channel far more challenging compared to the single-user MIMO channel. In fact, the capacity analysis and the signal processing techniques for MIMO interference channel still constitute a largely open field, and most of existing efforts have aimed for transforming the MIMO interference channel so that cooperation at the transmitter/receiver side can be exploited to some degree, at least in some specific scenarios. For example, in multicell systems, *BS cooperation* [42, 43, 117, 129–137], also known as *joint multicell processing* [24, 117], has been advocated for the sake of transforming the MIMO interference channel to a number of cooperative multiuser MIMO channels, as will be discussed in Chapter 6 of this thesis. Additionally, the recent advances in the capacity evaluation of the MIMO interference channel have stimulated significant interests in *interference alignment* [138–145], which is essentially constituted by a family of precoding techniques for the MIMO interference channel. The problems related to interference alignment are also beyond the scope of this thesis and will not be discussed in detail.

1.3 Formal Definition of the MIMO Detection Problem

Despite the fact that similar problems have been known for a while [38, 52, 53, 146–181], the term “MIMO detection” became widespread mainly with the advent of multiple-antenna techniques since during the late 1990s [87–91, 101–103, 182–189]. As a result, in the narrow sense, MIMO detection usually refers to the symbol detection problem encountered in narrow-band SDM based multiple-antenna systems, such as the vertical Bell Laboratories layered space-time (VBLAST) system [101–103]. However, we emphasize that as a family of important signal processing techniques, MIMO detection should be interpreted based on a generic mathematical model, as detailed below.

In the generic sense, the MIMO detection problem can be defined for a system having N_I *non-orthogonal* inputs and N_O outputs contaminated by additive random noise, which does not necessarily follow the Gaussian distribution. The multiple inputs can be denoted as a vector \mathbf{s} , which is randomly drawn from the set \mathbb{A}^{N_I} composed by N_I -element vectors, whose components are from a finite set $\mathbb{A} = \{a_m | m = 1, \dots, M\}$ and the *a priori* probability of selecting each vector from \mathbb{A}^{N_I} is identical. The set \mathbb{A} is usually referred to as the constellation alphabet, whose elements can take either real or complex values. Additionally, $\underline{\mathbf{s}}_n$, $n = 1, \dots, M^{N_I}$, represents the realizations of \mathbf{s} , hence they are the elements of \mathbb{A}^{N_I} . Then the relationship between the inputs and the outputs of this system can be characterized by

$$\mathbf{y} = \mathbf{H}\mathbf{s} + \mathbf{n}, \quad (1.1)$$

where $\mathbf{y} \in \mathbb{F}^{N_O}$ is the received signal vector, $\mathbf{H} \in \mathbb{F}^{N_O \times N_I}$ is the channel matrix of the system, and $\mathbf{n} \in \mathbb{F}^{N_O}$ represents the additive random noise vector. Depending on the specific considered applications, \mathbb{F} can be either the field of real numbers, \mathbb{R} , or the field of complex numbers, \mathbb{C} . Concisely speaking, any system having multiple inputs, multiple outputs and subject to additive random noise can be regarded as a MIMO system, but the MIMO detection problem considered herein is only confronted in MIMO systems that have non-orthogonal inputs. It is worth noting that the constellation alphabet \mathbb{A} , the number of inputs N_I , and the number of outputs N_O are typically regarded as constant values for a given system. Hence, they are assumed to be known by default, although this will not be explicitly emphasized, unless necessary.

Based on the generic mathematical model of (1.1), *the basic task of MIMO detection is to estimate the input vector \mathbf{s} relying on the knowledge of the received signal vector \mathbf{y} and the channel matrix \mathbf{H}* . Note that for \mathbf{y} , typically its exact value has to be known, while for \mathbf{H} , sometimes the knowledge of its statistical parameters is sufficient. To elaborate a little further, if the *instantaneous* value of \mathbf{H} is known from *explicit* channel estimation, the detection of \mathbf{s} is said to rely on *coherent* detection. By contrast, if the explicit estimation of the instantaneous channel state is avoided, the detection of \mathbf{s} belongs to the family of *non-coherent* detection schemes. In the latter case, the channel estimation is either performed implicitly in signal detection, or it is completely avoided, whereas typically the statistical knowledge of the channel matrix \mathbf{H} is invoked for supporting signal detection. Additionally, the noncoherent MIMO detection schemes typically require that the input symbols are subject to some form of differential encoding, which imposes correlation on the input symbols, and as a result, a block-by-block based sequence detection has to be employed. This so-called multiple-symbol detection typically leads to higher computational complexity than the symbol-by-symbol based detectors of coherent MIMO systems. Moreover, the noncoherent detectors typically exhibit degraded power efficiency, which results in an inherent performance loss compared to their coherent counterparts. In this thesis, we focus our attention on coherent MIMO detection. Then, from the perspective of mathematical

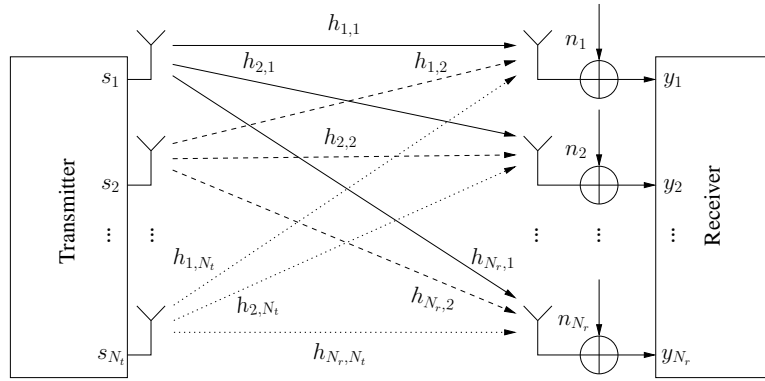


FIGURE 1.9: Schematic of VBLAST-style SDM-MIMO systems.

mapping, a coherent MIMO detector is defined as:

$$\hat{\mathbf{s}} = \mathfrak{D}(\mathbf{y}, \mathbf{H}) : \mathbb{F}^{N_O} \times \mathbb{F}^{N_O \times N_I} \mapsto \mathbb{A}^{N_I}, \quad (1.2)$$

where $\hat{\mathbf{s}}$ is the estimate of \mathbf{s} .

1.4 MIMO System Model for Linear Memoryless Channels

Bearing in mind specific applications, the system model of (1.1) may be established either in the time domain or in the frequency domain, and may be applied to both memoryless channels and dispersive channels exhibiting memory [21, 36, 52, 53, 93, 181]. With respect to linear memoryless MIMO channel, a canonical example is the narrowband synchronous VBLAST-style SDM-MIMO system [101–103] communicating over flat fading channels, as shown in Fig. 1.9. Because the system's outputs at the current time interval are independent of the system's inputs at previous time intervals, its baseband equivalent discrete-time (i.e. sampled) system model, representing an instance of the generic model (1.1), can be written as

$$\begin{bmatrix} y_1 \\ y_2 \\ \vdots \\ y_{N_r} \end{bmatrix} = \begin{bmatrix} h_{1,1} & h_{1,2} & \cdots & h_{1,N_t} \\ h_{2,1} & h_{2,2} & \cdots & h_{2,N_t} \\ \vdots & \vdots & \ddots & \vdots \\ h_{N_r,1} & h_{N_r,2} & \cdots & h_{N_r,N_t} \end{bmatrix} \begin{bmatrix} s_1 \\ s_2 \\ \vdots \\ s_{N_t} \end{bmatrix} + \begin{bmatrix} n_1 \\ n_2 \\ \vdots \\ n_{N_r} \end{bmatrix}. \quad (1.3)$$

In this specific application, we have $N_t = N_I$ and $N_r = N_O$, which represent the number of transmit and receive antennas, respectively. Furthermore, $h_{j,i}$ denotes the impulse response between the i th transmit antenna and the j th receive antenna, with $i = 1, 2, \dots, N_t$ and $j = 1, 2, \dots, N_r$. For this memoryless MIMO channel, the *one-shot detection* which relies only on a single received signal vector $\mathbf{y} = [y_1, y_2, \dots, y_{N_r}]^T$ is sufficient.

1.5 MIMO System Model for Dispersive Channels Exhibiting Memory

On the other hand, when considering the wideband VBLAST system communicating over frequency-selective MIMO channels [190–194], the link between each input-output pair may be modelled by a linear finite impulse response (FIR) dispersive channel, whose sampled version can be denoted as the (possibly complex-valued) vector $\mathbf{h}_{j,i} = (h_{j,i}^0, h_{j,i}^1, \dots, h_{j,i}^{L-1})^T$. Here L is the maximum number of multipath components in each link, and it is also known as the channel memory length. In this case, the *one-shot detection* which utilizes a single N_r -element received signal vector is not optimal. Instead, the *sequence detection* using multiple N_r -element received vectors has to be used.

We assume that a block-based transmission structure relying on zero-padding for eliminating the interblock interference is used, which is beneficial for alleviating the performance degradation imposed by noise enhancement or error propagation [195]. Following zero-padding, a transmission block becomes a frame which occupies $K = N + P$ sampling intervals, where N is the number of sampling intervals occupied by information-bearing symbol vectors in the frame, while $P \geq L - 1$ represents the number of sampling intervals during which P consecutive N_t -element zero vectors are inserted at the tail of the frame. Here we set $P = L - 1$. Given the above-mentioned transmitted frame, the entire received signal vector may be generated by a concatenation of K noise-contaminated sampled received signal vectors, namely, $\mathbf{y} = (\mathbf{y}^T[0], \mathbf{y}^T[1], \dots, \mathbf{y}^T[K - 1])^T$, where $\mathbf{y}[k] = (y_1[k], y_2[k], \dots, y_{N_r}[k])^T$ represents the N_r outputs at the k th sampling instant, $k = 0, 1, \dots, K - 1$. Then, the baseband signal received by the j th receive antenna at the k th sampling instant is given by

$$y_j[k] = \sum_{i=1}^{N_t} \sum_{l=0}^{L-1} h_{j,i}^l s_i[k-l] + n_j[k], \quad (1.4)$$

where $h_{j,i}^l$, the l th element of $\mathbf{h}_{j,i}$, $l = 0, 1, \dots, L - 1$, denotes the channel gain of the l th path between the i th transmit antenna and the j th receive antenna. Furthermore, $s_i[k]$ is the symbol transmitted from the i th transmit antenna at the k th sampling instant, and $n_j[k]$ represents the noise imposed on the j th receive antenna at the k th sampling instant. Similar to $\mathbf{y}[k]$, we define $\mathbf{s}[k] = (s_1[k], s_2[k], \dots, s_{N_t}[k])^T$ and $\mathbf{n}[k] = (n_1[k], n_2[k], \dots, n_{N_r}[k])^T$. Additionally, similar to \mathbf{y} , we may construct $\mathbf{s} = (\mathbf{s}^T[0], \mathbf{s}^T[1], \dots, \mathbf{s}^T[N - 1])^T$ and $\mathbf{n} = (\mathbf{n}^T[0], \mathbf{n}^T[1], \dots, \mathbf{n}^T[K - 1])^T$. Then, the received signal corresponding to a transmitted frame can also be written following the matrix notation of (1.1), where the size of \mathbf{y} and \mathbf{n} is $N_O = KN_r = (N + L - 1)N_r$, while that of \mathbf{s} is $N_I = NN_t$, and the MIMO channel

matrix \mathbf{H} exhibits the banded Toeplitz structure [195] of:

$$\mathbf{H} = \begin{bmatrix} \mathbf{H}^0 & \mathbf{0} & \cdots & \mathbf{0} \\ \vdots & \mathbf{H}^0 & \ddots & \vdots \\ \mathbf{H}^{L-1} & \vdots & \ddots & \mathbf{0} \\ \mathbf{0} & \mathbf{H}^{L-1} & \ddots & \mathbf{H}^0 \\ \vdots & \vdots & \ddots & \vdots \\ \mathbf{0} & \mathbf{0} & \cdots & \mathbf{H}^{L-1} \end{bmatrix}, \quad (1.5)$$

whose dimension is $(KN_r \times NN_t)$, and each entry \mathbf{H}^l of (1.5) is an $(N_r \times N_t)$ -element matrix containing the channel gains between all pairs of transmit and receive antennas for the l th path, i.e. we have

$$\mathbf{H}^l = \begin{bmatrix} h_{1,1}^l & h_{1,2}^l & \cdots & h_{1,N_t}^l \\ h_{2,1}^l & h_{2,2}^l & \cdots & h_{2,N_t}^l \\ \vdots & \vdots & \ddots & \vdots \\ h_{N_r,1}^l & h_{N_r,2}^l & \cdots & h_{N_r,N_t}^l \end{bmatrix}. \quad (1.6)$$

It is worth noting that the linear memoryless MIMO model and the linear MIMO model exhibiting memory may also be used for characterizing the family of *synchronous* and *asynchronous* CDMA systems, respectively. Additionally, the asynchronous CDMA systems can also be characterized by (1.1) in the z domain [52].

1.6 Complex-Valued versus Real-Valued MIMO System Model

As we mentioned in Section 1.3, the generic MIMO system model of (1.1) can be defined both in the field of real numbers, \mathbb{R} , and in the field of complex numbers, \mathbb{C} . Since the complex-valued modulation constellations, such as quadrature amplitude modulation (QAM), are often employed in digital communications, the complex-valued MIMO system model is typically a natural and more concise choice for the formulation and performance analysis of the algorithms considered. However, naturally the complex-valued system model requires the handling of complex-valued variables, which might result in more complex hardware implementations or reduce the manipulation freedom in signal processing. For example, the tree-search based MIMO detectors, which will be introduced in Section 1.8.4, are typically in favor of the real-valued MIMO system model from a hardware implementation perspective.

Fortunately, the complex-valued and the real-valued MIMO system models are often mutually convertible. More specifically, if we assume that the generic MIMO system model of (1.1) is defined in \mathbb{C} , and assume that the real part and the imaginary part of \mathbf{H} , \mathbf{s} and \mathbf{n} ,

and hence of \mathbf{y} , are mutually independent,² then the complex-valued MIMO system model of (1.1) can be transformed to an equivalent real-valued system model of

$$\tilde{\mathbf{y}} = \tilde{\mathbf{H}}\tilde{\mathbf{s}} + \tilde{\mathbf{n}}, \quad (1.7)$$

$$\text{where } \tilde{\mathbf{y}} = \begin{bmatrix} \Re(\mathbf{y}) \\ \Im(\mathbf{y}) \end{bmatrix}, \tilde{\mathbf{s}} = \begin{bmatrix} \Re(\mathbf{s}) \\ \Im(\mathbf{s}) \end{bmatrix}, \tilde{\mathbf{n}} = \begin{bmatrix} \Re(\mathbf{n}) \\ \Im(\mathbf{n}) \end{bmatrix}, \text{ and } \tilde{\mathbf{H}} = \begin{bmatrix} \Re(\mathbf{H}) & -\Im(\mathbf{H}) \\ \Im(\mathbf{H}) & \Re(\mathbf{H}) \end{bmatrix}.$$

Note that as expected, in most cases signal processing algorithms based on the complex-valued model of (1.1) and the real-valued MIMO system model of (1.7) deliver an equivalent performance. For example, [185] showed the equivalence between the complex-valued and the real-valued MIMO system models in the derivation of the optimal ML detector and the MIMO channel capacity. However, this equivalence does not always hold. For example, it was shown in [196] that the real-valued VBLAST detector outperforms its complex-valued counterpart, owing to its additional freedom in selecting the optimum detection ordering. Hence a beneficial performance gain may be gleaned from transforming the complex-valued system model to the dimension-doubled real-valued system model. More generally, for all MIMO detection algorithms whose performance is related to detection ordering, the real-valued system model based formulation may provide a better performance than its complex-valued counterpart.

Finally, it is worth noting that the real-valued formulation of the complex-valued MIMO system model is not unique. For example, a pairwise real-valued MIMO system model was used in [197, 198], which was shown to result in a reduced complexity compared to the conventional real-valued MIMO system model of (1.7). A more comprehensive investigation of the complex-valued versus real-valued MIMO detectors was presented in [199].

1.7 An Introductory Example of SDM-MIMO Systems

For the convenience of later exposition, let us consider a (2×2) -element SDM-MIMO system employing 4-QAM as our introductory example, which complies with (1.3), and is given by

$$\begin{bmatrix} y_1 \\ y_2 \end{bmatrix} = \begin{bmatrix} h_{1,1} & h_{1,2} \\ h_{2,1} & h_{2,2} \end{bmatrix} \begin{bmatrix} s_1 \\ s_2 \end{bmatrix} + \begin{bmatrix} n_1 \\ n_2 \end{bmatrix}, \quad (1.8)$$

where s_i assumes values from $\mathbb{A} = [1 + i, 1 - i, -1 - i, -1 + i]$, and $\mathcal{E}(|n_i|^2) = N_0 = 0.01$, $i = 1, 2$. Since our main goal of using this introductory example is to illuminate the operation of MIMO detection algorithms, the energy normalization of $\mathcal{E}(s_i) = 1$ or $\mathcal{E}(\mathbf{s}) = 1$ is not imposed on the transmitted symbols. Considering a specific channel use, we assume

²This independence assumption is almost always adopted for ease of decoding, even in single-input single-output systems.

that $\begin{bmatrix} h_{1,1} & h_{1,2} \\ h_{2,1} & h_{2,2} \end{bmatrix} = \begin{bmatrix} 5 + 2i & -2 - i \\ 3 - 2i & 4 + 3i \end{bmatrix}$, $\begin{bmatrix} s_1 \\ s_2 \end{bmatrix} = \begin{bmatrix} 1 + i \\ -1 + i \end{bmatrix}$, $\begin{bmatrix} n_1 \\ n_2 \end{bmatrix} = \begin{bmatrix} 0.5 + 0.4i \\ 0.2 - 0.6i \end{bmatrix}$.

Then we have $\begin{bmatrix} y_1 \\ y_2 \end{bmatrix} = \begin{bmatrix} 6.5 + 6.4i \\ -1.8 + 1.4i \end{bmatrix}$. This example will be revisited from time to time for explaining the principles of the advanced MIMO detectors considered.

1.8 History and State-of-the-Art of MIMO detection

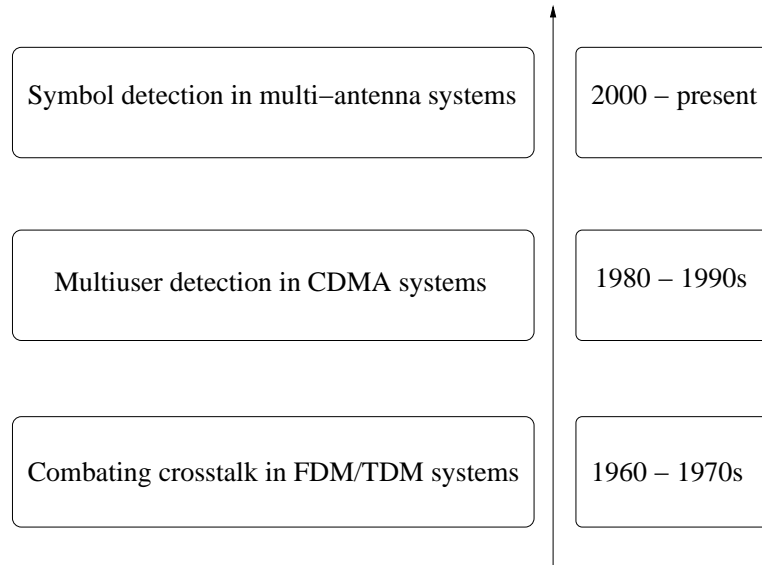


FIGURE 1.10: Development of MIMO detection.

The research of MIMO detection is a broad and vibrant area. Its embryonic concept dates back to the 1960s [146]. The earliest contribution on MIMO detection [146] was sparked off by the classic *Nyquist's problem* [200], which aims for the joint optimization of the transmitter and receiver for the sake of combating the ISI when communicating over a conventional single-input single-output channel. Since then, it has been studied in the context of diverse applications and under possibly different names. This half-century history can be roughly divided into three periods, as seen in Fig. 1.10, namely the period of combating crosstalk in the context of the early single-user FDM/TDM systems (1960s – 1970s) [146–149, 152], the period of multiuser detection (MUD) during the prevalence of CDM/CDMA systems (1980s – 1990s) [38, 52, 53, 150, 151, 153–181], and the period of joint symbol detection in the cutting-edge multiple-antenna systems (2000s – present) [54, 55, 58–65, 69–73, 81, 83, 102, 103, 181, 193, 201–257]. Diverse MIMO detectors have been proposed for meeting the requirements imposed by a multiplicity of applications. These MIMO detectors can be categorised from various perspectives, such as optimum/suboptimum, linear/non-linear, sequential/one-shot, adaptive/non-adaptive, hard-decision/soft-decision, blind/non-blind, iterative/non-iterative, synchronous/asynchronous, coded/uncoded etc. The repre-

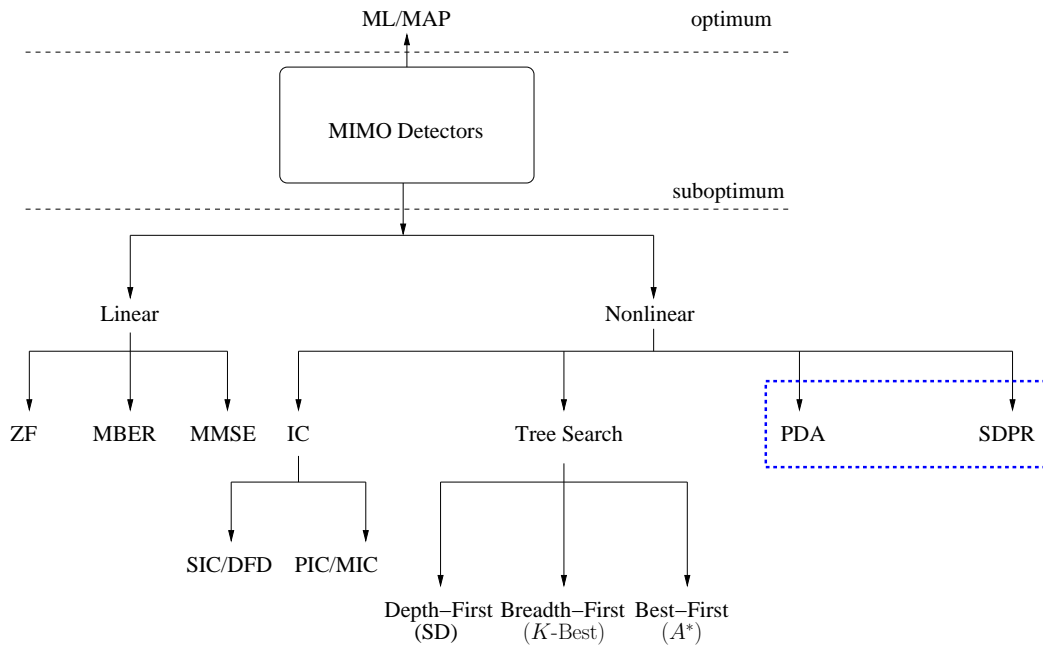


FIGURE 1.11: Overview of representative MIMO detectors considered in this thesis. The novel contributions of this thesis are focused on the PDA and the SDPR detectors.

representative MIMO detectors considered in this thesis are summarized in Fig. 1.11.

Owing to the similarities between the classic equalization problem encountered in channels imposing ISI and the *generic* MIMO detection problem defined by (1.1) and (1.2), it is not surprising that the techniques, which were found to be effective in combating ISI were also often extended to the context of MIMO detection problems [258]. Some of the equalization algorithms which have been adapted for MIMO detection include, but not limited to, the ML sequence estimation (Viterbi algorithm) [259–263] based equalization, linear ZF equalization [96], linear MMSE equalization [96], ZF/MMSE aided decision-feedback equalization [96], adaptive equalization [264, 265], blind equalization [266, 267] etc, as detailed below.

1.8.1 Optimum MIMO Detector

The earliest work on *optimum* MIMO detectors dates back to 1976, when van Etten [149] derived an ML sequence estimation based receiver for combating both ISI and interchannel interference (ICI) in multiple-channel transmission systems. Explicitly, he demonstrated that under certain conditions, the performance of the ML receiver asymptotically approaches that of the optimum receiver of the idealized system which is free from both ISI and ICI. The significance of this work was not widely recognized until the research interests in commercial CDMA systems and multiple-antenna systems intensified.

Although it is widely recognized at the time of writing that MIMO detection provides significant performance gains compared to conventional single-stream detection, there was

a widespread misconception until the early 1980s that the MUI can be accurately modelled as a white Gaussian random process, and thus the conventional single-user MF (SUMF) based detector was believed to be essentially optimum. In 1983, this conventional wisdom was explicitly proven wrong by Verdú [155, 156] with the introduction of the optimal MUD in the context of asynchronous/synchronous Gaussian multiple-access channels shared by K users. The full analysis and derivation of the optimum MUD was reported later in [157, 268], demonstrating that there is, in general, a substantial gap between the performance of the conventional SUMF and the optimal MUD performance. Additionally, upon identifying the non-Gaussian nature of the MUI, Poor and Verdú [269] also designed nonlinear single-user detectors for CDMA systems operating in diverse scenarios such as weak interferers, high spreading gains and high signal-to-noise ratio (SNR).

There does exist some situations where a *bona fide* application of the central limit theorem is feasible and hence the MUI can be rigorously proven to be asymptotically Gaussian.³ However, even if the MUI may be accurately modelled as a Gaussian variable, the SUMF is still not the optimal receiver. This is because the output of the MF for the desired user does not constitute a *sufficient statistic* in the presence of MUI [270]. In other words, the SUMF is optimal only in the context of the single-user channel contaminated by additive white Gaussian noise (AWGN). By contrast, in multiple-access systems, unless the multiplexed signals are orthogonal, the outputs of the MFs corresponding to the interfering users contain valuable information which may be exploited for the detection of the symbol of interest, and hence more intelligent joint detection strategies capable of exploiting all MFs' outputs are required for achieving better detection performance.

In general, the optimum decision criterion is the maximum *a posteriori* (MAP) criterion. When considering the MIMO system model of (1.1), the MAP criterion based MIMO detector is formulated as

$$\mathfrak{D}_{\text{MAP}} : \hat{\mathbf{s}} = \max_{\mathbf{s} \in \mathbb{A}^{N_I}} \Pr(\mathbf{s}|\mathbf{y}). \quad (1.9)$$

Using Bayes' rule, the *a posteriori* probability (APP) in (1.9) may be expressed as

$$\Pr(\mathbf{s}|\mathbf{y}) = \frac{p(\mathbf{y}|\mathbf{s}) \Pr(\mathbf{s})}{p(\mathbf{y})} = \frac{p(\mathbf{y}|\mathbf{s}) \Pr(\mathbf{s})}{\sum_{\mathbf{s} \in \mathbb{A}^{N_I}} p(\mathbf{y}|\mathbf{s}) \Pr(\mathbf{s})}, \quad (1.10)$$

where $\Pr(\mathbf{s})$ is the *a priori* probability of \mathbf{s} , and $p(\mathbf{y}|\mathbf{s})$ is the conditional probability density function (PDF) of the observed signal vector \mathbf{y} given \mathbf{s} . The MAP criterion can be simplified when each vector in \mathbb{A}^{N_I} has an identical *a priori* probability, i.e. we have $\Pr(\mathbf{s}) = 1/|\mathbb{A}|^{N_I}$ for all realizations of \mathbf{s} , where $|\mathbb{A}|$ represents the number of elements, i.e. the cardinality of the constellation alphabet \mathbb{A} . Furthermore, considering the fact that $p(\mathbf{y})$ is independent

³A specific example of such a situation is that an infinite-population multiuser signal model with the individual amplitudes going to zero at the appropriate speed – in other words, when the overall interference power is fixed and the number of equal-power interferers tends to infinity [270].

of which particular signal vector is transmitted, then the MAP detector of (1.9) becomes equivalent to the ML detector of

$$\mathcal{D}_{\text{ML}} : \hat{\mathbf{s}} = \max_{\mathbf{s} \in \mathbb{A}^{N_I}} p(\mathbf{y}|\mathbf{s}). \quad (1.11)$$

Therefore, the MAP criterion is usually used in the iterative detection and decoding (IDD) aided receiver of forward-error-correction (FEC)-coded systems, where the *a priori* probabilities of the transmitted symbols, $\Pr(\mathbf{s})$, may be obtained with the aid of a backward-and-forward oriented iterative information exchange between the signal detector and the channel decoder. By contrast, the ML criterion is usually used in FEC-uncoded systems, where the *a priori* probabilities of the transmitted symbols cannot be made available by the channel decoder. If \mathbf{n} is AWGN, then we have

$$p(\mathbf{y}|\mathbf{s}) \propto \exp(-\|\mathbf{y} - \mathbf{H}\mathbf{s}\|_2^2), \quad (1.12)$$

where the symbol \propto represents the relationship “is proportional to”. Consequently, we have

$$\max_{\mathbf{s} \in \mathbb{A}^{N_I}} p(\mathbf{y}|\mathbf{s}) \Leftrightarrow \min_{\mathbf{s} \in \mathbb{A}^{N_I}} \|\mathbf{y} - \mathbf{H}\mathbf{s}\|_2^2, \quad (1.13)$$

where the symbol \Leftrightarrow represents the relationship “is equivalent to”. Therefore, the ML detection problem for the system model of (1.1) can be reformulated as the finite-set constrained least-squares (LS) optimization problem of

$$\hat{\mathbf{s}}_{\text{ML}} = \arg \min_{\mathbf{s} \in \mathbb{A}^{N_I}} \|\mathbf{y} - \mathbf{H}\mathbf{s}\|_2^2, \quad (1.14)$$

which can also be interpreted as the *minimum Euclidean distance criterion*. The optimization problem of (1.14) can be solved by “brute-force” search over \mathbb{A}^{N_I} , resulting in an exponentially increasing computational complexity of $|\mathbb{A}|^{N_I}$.

To elaborate a little further, let us consider the example shown in Fig. 1.12, where binary phase-shift keying (BPSK) modulation ($M = 2$) and $N_I = 2$ are employed. Hence, there are a total of $M^{N_I} = 4$ possible realizations for the transmitted symbol vector \mathbf{s} , and they are denoted as $\underline{\mathbf{s}}_1 = [1, 1]^T$, $\underline{\mathbf{s}}_2 = [1, -1]^T$, $\underline{\mathbf{s}}_3 = [-1, -1]^T$, $\underline{\mathbf{s}}_4 = [-1, 1]^T$.

As a beneficial implementation of the optimum MIMO detector formulated in (1.11), the optimum MUD proposed in [157] for asynchronous CDMA systems consists of a bank of MFs followed by a dynamic programming algorithm of the forward (Viterbi) type [259–263] (for ML criterion based detection) or of the backward-forward type [271–275] (for minimum error probability criterion based detection). As mentioned in Section 1.5, asynchronous CDMA systems can be modelled relying on the MIMO system model given in Section 1.5 for transmission over linear dispersive channels exhibiting memory. Therefore, the optimum MUD conceived for asynchronous CDMA constitutes a *sequence* detector, while the optimum

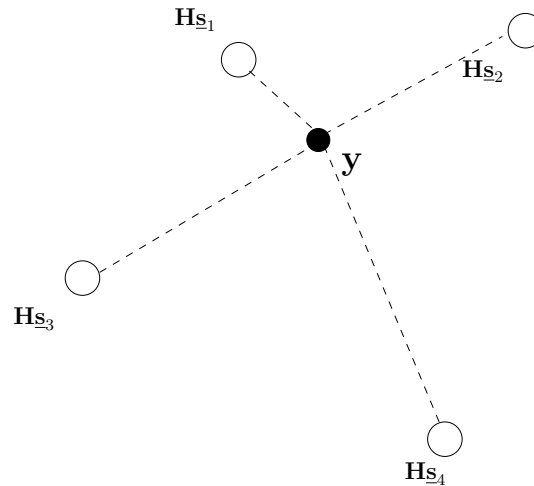


FIGURE 1.12: Example of the optimal ML based MIMO detector in the context of $N_I = 2$ and BPSK modulation.

MUD of synchronous CDMA is a *one-shot* detector, and as such it is a special case of the asynchronous optimum MUD. Additionally, the optimum MUD relying on brute-force search [157] requires that the transmitted energies of each user were known to the receiver. More critically, the time-complexity of the optimum decision algorithms suggested in [157,274,275] increases exponentially with the number of active users, i.e. it is on the order of $O(2^K)$ per bit for asynchronous transmission and $O(2^K/K)$ per bit for synchronous transmission, where K is the number of active users. This is because the optimum MUD of both the synchronous and asynchronous CDMA scenarios was proven by Verdú⁴ to be an NP-hard and a nondeterministic polynomial-time complete (NP-complete) problem [38,268]. Thus, *all known algorithms* designed for solving this problem optimally exhibit an exponentially increasing time-complexity in the number of decision variables. Therefore, the optimum MUD becomes computationally intractable for a large number of active users. It should be noted that this problem would only have a polynomially increasing complexity *if and only if* a polynomial-time solution could be found for any NP-complete problem, such as the famous *travelling salesman problem* and the *integer linear programming problem* which have been so far widely believed insolvable within polynomial time. However, the question of whether there exists a polynomial-time solution for NP-complete problems has not been answered by a rigorous proof to date. It is widely recognized that in computational complexity theory, the complexity class of “P” represents one of the most fundamental complexity classes, and it contains all decision problems that can be solved by a deterministic Turing machine using a polynomially increasing amount of computation time, which is conventionally abbreviated to the parlance of “polynomial-time” for convenience. In fact, the most important open question in computational complexity theory [276,277] has been the formal proof of “Is P =

⁴In fact, the optimum MIMO detection problem of (1.14) constitutes an instance of the general *closest lattice-point search (CLPS)* problem, whose complexity had been analyzed by Boas [37] in 1981, showing that this problem is NP-hard. Additionally, Micciancio [39] provided a simpler proof for the hardness of the CLPS problem in 2001.

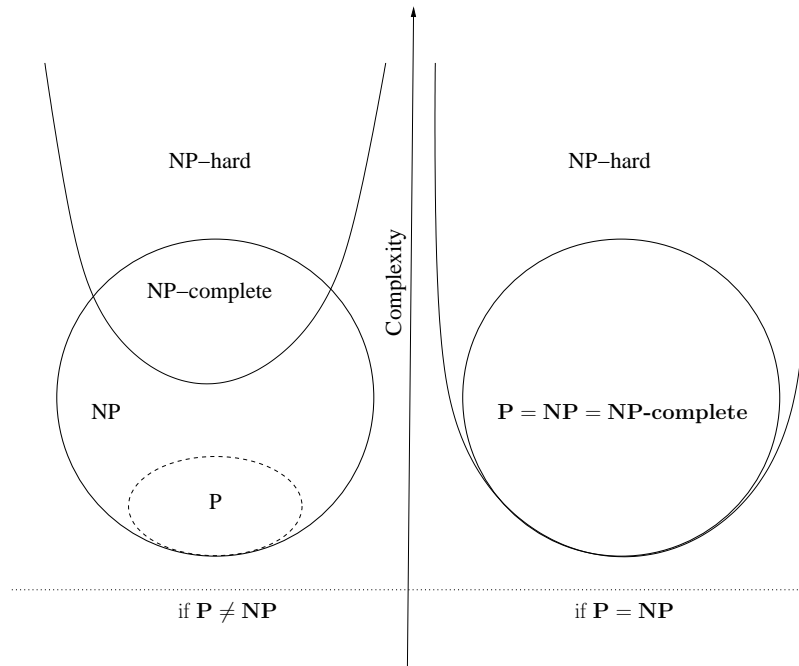


FIGURE 1.13: Euler digram for P, NP, NP-complete, NP-hard set of problems under both $P \neq NP$ and $P = NP$ assumptions [276, 277].

NP?”), which explicitly poses the dilemma whether polynomial-time algorithms actually do exist for NP-complete problems, and by corollary, for all NP problems. Fig. 1.13 concisely depicts the Euler digram characterizing the relationships amongst the P, NP, NP-complete, and NP-hard set of problems under both the $P \neq NP$ and $P = NP$ assumptions.

For the sake of clarity, the main contributions to the development of the optimum MIMO detector are summarized in Table 1.1. The substantial performance and complexity differences between the optimum MIMO detector and the conventional SUMF detector stimulated a lot of interests in the development of suboptimum MIMO detection algorithms that are capable of achieving good performance at a low computational cost. Some representative classes of suboptimum MIMO detectors include the linear detectors, the interference cancellation (IC) aided detectors, the tree-search based detectors, the PDA based detectors, and the SDPR based detectors etc., as detailed below.

1.8.2 Linear MIMO Detectors

The linear MIMO detectors of Fig. 1.11 are based on a linear transformation of the output signal vector \mathbf{y} . In general, they are known for their appealingly low complexity, but suffer from a considerable performance loss in comparison to the ML detector. More explicitly, the decision statistics of linear MIMO detectors may be expressed as

$$\mathbf{d} = \mathbf{T}\mathbf{y}, \quad (1.15)$$

TABLE 1.1: Milestones in the development of the optimal MIMO detector

Year	Authors	Contributions
1976	van Etten [149]	Derived an ML sequence estimation based receiver for combating both the ISI and ICI in multiple-channel transmission systems and demonstrated that under certain conditions, the performance of the ML receiver is asymptotically as good as if both the ISI and ICI were absent.
1981	Boas [37]	Analyzed the complexity of the generic problem of “closest point search in an N_I -dimensional lattice”, which is identical to the optimum MIMO detection problem, as a function of the dimension N_I of the decision-variable vector, and proved that this problem is NP-hard. Thus, all known algorithms conceived for solving the generic MIMO detection problem optimally have an exponentially increasing time-complexity.
1983 - 1986	Verdú [155–157, 268]	First presented a full derivation and analysis of the ML based multiuser detector for asynchronous/synchronous CDMA systems; showed that there is, in general, a huge gap between the performance of the conventional SUMF and the optimal attainable performance; showed that the infamous near-far problem was not an inherent flaw of CDMA but a consequence of the inability of the SUMF to exploit the structure of the MUI; introduced the performance measure of multiuser asymptotic efficiency, which was later widely used in the asymptotic analysis of multiuser detectors at the high-SNR region.
1984 - 1989	Verdú [38, 268]	Independently proved that the optimum MUD problem in CDMA systems is NP-hard and NP-complete.
2001	Micciancio [39]	Presented a simpler proof of the NP-hardness of the problem of closest point search in an N_I -dimensional lattice.

where \mathbf{T} is the linear transformation (or filtering) matrix to be designed using various criteria.

For the sake of illuminating the philosophy of linear MIMO detectors, let us consider (1.3) as an example. Assuming that the noise vector is zero, (1.3) becomes a system of linear equations, and the MIMO detection problem becomes equivalent to “finding the solution for N_t unknown variables subject to N_r linear equations”. Therefore, if \mathbf{H} is a square matrix (i.e. $N_r = N_t$) and of full rank, the solution of this system of linear equations is given by $\mathbf{s} = \mathbf{H}^{-1}\mathbf{y}$. To generalize this problem a little further, if the matrix \mathbf{H} satisfies $N_r > N_t$ and has a full column rank of N_t , we have $\mathbf{s} = \mathbf{H}^\dagger\mathbf{y}$, where $\mathbf{H}^\dagger = (\mathbf{H}^H\mathbf{H})^{-1}\mathbf{H}^H$ is the left-multiplying Moore-Penrose pseudoinverse of \mathbf{H} . This example actually conveys the essential idea of the ZF criterion based MIMO detector, for which the linear transformation matrix is given by

$$\mathbf{T}_{\text{ZF}} = \mathbf{H}^\dagger, \quad (1.16)$$

and if \mathbf{H} is invertible, the left-multiplying pseudoinverse \mathbf{H}^\dagger and the inverse coincides, i.e. we have $\mathbf{H}^\dagger = \mathbf{H}^{-1}$. Upon using the ZF detector, we have $\mathbf{d} = \mathbf{s} + \mathbf{H}^\dagger\mathbf{n}$, which indicates that the interference amongst the multiple inputs is completely eliminated, albeit the noise power is augmented.

The ZF criterion based linear MIMO detector of Fig. 1.11 was first proposed by van Etten

[148] in 1975 for a multiple-channel multiplexing transmission system subjected to both ISI and ICI. As far as CDMA systems are concerned, this solution was first proposed by Schneider [151] in 1979 for synchronous CDMA systems transmitting equal-energy multiuser signals, where he sought to minimize the probability of bit error, but erroneously arrived at the ZF detector. From 1986 to 1990, Lupas and Verdú systematically investigated this detector in the context of both synchronous [159, 278] and asynchronous [160, 279] CDMA systems. They referred to it as the linear decorrelating multiuser detector. It was shown that if the transmitted energies of each user are unknown to the receiver, then both the ML amplitude estimates and the ML decisions on the transmitted bits are obtained by the ZF detector, regardless of the values of the received energies of each user. As a beneficial result, the ZF detector achieves the same degree of resistance to the infamous near-far problem as the optimum ML detector, despite its significantly computational complexity. The insight that the near-far problem was not an inherent flaw of CDMA but a consequence of the SUMF's inability to exploit the non-Gaussian structure of the MUI [157], and the fact that the joint detection based MUDs, including its linear versions, achieve a significantly better near-far resistance [159, 160, 278, 279] became another major incentive for the subsequent research activities dedicated to MUD in CDMA. With the advent of the multiple-antenna technologies since during the late 1990s, the ZF detector was first studied by Wolniansky, Golden, Foschini and Valenzuela in the SDM-based VBLAST systems [102, 103].

As seen in Fig. 1.11, the linear transformation matrix \mathbf{T} of (1.15) can also be designed according to the MMSE criterion, which minimises the mean-square error between the actual transmitted data and the channel's output data after using the linear transformation matrix \mathbf{T} . To be more specific, \mathbf{T} is obtained by solving the optimization problem of

$$\mathbf{T}_{\text{MMSE}} = \arg \min_{\mathbf{T}} \mathcal{E} \left(\|\mathbf{s} - \mathbf{T}\mathbf{y}\|_2^2 \right). \quad (1.17)$$

Using the *orthogonality principle* [280], we have

$$\mathcal{E}[(\mathbf{s} - \mathbf{T}\mathbf{y})\mathbf{y}^H] = \mathbf{0}, \quad (1.18)$$

then \mathbf{T}_{MMSE} may be derived as

$$\mathbf{T}_{\text{MMSE}} = (\mathbf{H}^H \mathbf{H} + 2\sigma^2 \mathbf{I})^{-1} \mathbf{H}^H, \quad (1.19)$$

where σ^2 is the noise power per real dimension. Compared to the linear ZF detector, the linear MMSE detector achieves a better balance between the MUI elimination and noise enhancement by jointly minimizing the total error imposed by both the MUI and the noise. Hence, the linear MMSE detector achieves a better performance at low SNRs than the ZF detector.

The MMSE criterion based linear MIMO detector was first proposed by Shnidman [146]

in 1967, and hence it is the oldest MIMO detector found in the literature. Shnidman formulated a *generalized Nyquist criterion* first pointing out that the ISI and crosstalk⁵ between multiplexed signals essentially represent identical phenomena. Then, relying on this insight, he proposed a linear receiver that is optimal in the sense of the MMSE criterion for combating both the ISI and crosstalk in single-channel multiple-waveform-multiplexed pulse-amplitude modulation (PAM) systems. In 1970, Kaye and George [147] explicitly extended the MMSE receiver of [146] to the family of general multiple-channel systems transmitting multiplexed PAM signals and/or providing diversity. The MMSE criterion based linear detector designed for CDMA systems was proposed by Xie, Rushforth and Short in 1989 [173, 281]. A decade later, it was also revisited by Wolniansky, Golden, Foschini and Valenzuela in the context of SDM-based multi-antenna systems [102, 103]. The probability of error experienced at the output of the linear MMSE detector was analyzed by Poor and Verdú [282] in 1997.

As observed in the family-tree of Fig. 1.11, there are a range of other criteria for designing the linear transformation matrix \mathbf{T} .

- For example, in [159, 278], Lupas and Verdú also proposed a maximum asymptotic-multiuser-efficiency (MAME) based linear detector, which is capable of minimizing the probability of bit errors in the limit as the noise approaches zero. In other words, the asymptotic-multiuser-efficiency (AME) metric [38] characterizes the detector's performance in the high-SNR region. The linear MAME detector was designed by exploiting the assumption that the individual transmitted energies of all the users are fixed and known to the receiver. By contrast, the ZF detector does *not* require the knowledge of the transmitted energies of the users.
- Additionally, since a common disadvantage of the ZF and the MMSE detectors is that their estimates of the transmitted symbols are biased, Xie, Rushforth and Short [173, 281] proposed the so-called weighted least-squares (WLS) linear detector, which is capable of providing an unbiased estimate of the transmitted symbols. It is worth pointing out that except for the linear ZF detector, other linear MIMO detectors – including the linear MMSE detector, the linear MAME detector and the linear WLS detector – were typically derived under the assumption that the system parameters such as the signal's phase, power and delay are known. As a result, in practice these parameters must be estimated and the receiver's structure has to be regularly modified to reflect the updated estimates.
- Another important class of linear MIMO detectors are constituted by the family of minimum bit-error rate (MBER) criterion based linear MIMO detectors. The linear MBER detector is capable of outperforming the linear MMSE detector when either the signature cross-correlation is high or the background noise is non-Gaussian [287]. The MBER based MIMO detector was first considered by van Etten [148] in 1975 in the context

⁵Crosstalk may be interpreted as a special case of ICI. For example, in [146], crosstalk means the interference between the multiplexed different waveforms.

TABLE 1.2: Milestones in the development of linear MIMO detectors

Year	Authors	Contributions
1967	Shnidman [146]	First formulated a generalized Nyquist criterion, which pointed out that the ISI and crosstalk between multiplexed signals are essentially identical phenomena; he then proposed a linear MMSE receiver for combating both ISI and crosstalk in single-channel multiple-waveform-multiplexed PAM systems.
1970	Kaye <i>et al.</i> [147]	Extended the MMSE receiver of [146] to the general multiple-channel systems transmitting multiplexed PAM signals and/or providing diversity.
1975	van Etten [148]	Developed linear receivers based on both the ZF criterion and the minimum error probability criterion for a multiple-channel transmission system similar to that of [147]; these two detectors heralded the linear ZF and the linear MBER multiuser detectors of CDMA systems.
1975	Horwood <i>et al.</i> [150]	Proposed two linear signal-correlation based detectors for synchronous digital multiple-access systems; one of them assumes that each user only knows its own signature, while the other assumes that each user knows all users' signatures; this is the first attempt in multiple-access systems to exploit the structure of the signals simultaneously sent, which is the key idea of MUD in CDMA systems.
1979	Schneider [151]	First made an attempt to conceive MUD for CDMA systems; he proposed the linear decorrelating detector, namely the linear ZF detector, which represents one of the mainstream MUD approaches conceived for CDMA systems; this detector was also extended to the scenario of combating crosstalk in M -ary multiplexed transmission systems in 1980 [152].
1986-1990	Lupas <i>et al.</i> [159, 160, 278, 279]	Systematically investigated the linear ZF MUD in the context of both synchronous [159, 278] and asynchronous [160, 279] CDMA systems; they showed that the ZF detector achieves exactly the same degree of resistance to the infamous near-far problem as the optimum ML detector, despite its much lower computational and implementation complexity; they also first proposed a linear MAME MUD, which is capable of equivalently minimizing the probability of bit error in the limit as the noise approaches zero.
1989 - 1990	Xie <i>et al.</i> [173, 281]	First proposed the MMSE criterion based linear MUD, the modified linear equalizer based MUD, and the WLS linear MUD for CDMA systems. In contrast to the linear ZF detector, to the linear MMSE detector, and to the modified linear equalizer based detector, the linear WLS detector is capable of providing an unbiased estimate of the transmitted symbols.
1993 - 1997	Mandayam <i>et al.</i> [283–286]	First proposed the MBER criterion based linear MIMO detectors for CDMA systems; the linear MBER detector is capable of outperforming the linear MMSE detector when either the signature cross-correlation is high or the background noise is non-Gaussian.
1999	Wolniansky <i>et al.</i> [102, 103]	First discussed the application of linear ZF/MMSE detectors in multiple-antenna aided SDM-MIMO systems.
2006	Chen <i>et al.</i> [204]	Proposed the MBER criterion based linear detector for multi-antenna aided MIMO systems.

of a multiple-channel multiplexing transmission system subjected to both ISI and ICI. This MBER criterion was later studied in the context of CDMA systems [283–292] and multi-antenna systems [204, 205].

- Finally, we would like to mention that the linear MIMO detector can also be designed from the perspective of a linear equalizer [173, 281], since the mathematical models of the MIMO detection problem and of the equalization problem are similar [258]. To elaborate a little further, in MIMO systems each symbol’s interfering signal may be interpreted as though it is a specific tap of the dispersive channel impulse response (CIR).

The main contributions to the development of linear MIMO detectors are summarized in Table 1.2.

1.8.3 Interference Cancellation Aided MIMO Detectors

Another important class of suboptimum MIMO detectors portrayed in Fig. 1.11 are constituted by the *interference cancellation* based MIMO detectors, which are *nonlinear* and generally achieve a better performance than linear MIMO detectors. The concept of interference cancellation was first studied in 1974 by Bergmans and Cover [293, 294], as well as by Carleial [120] in 1975, in their information-theoretic studies of broadcast channels and of interference channels, respectively. In the context of CDMA and multi-antenna systems, this class of MIMO detectors have numerous variants due to the associated design flexibility, including the SIC detector [102, 103, 171, 295], the parallel interference cancellation (PIC) detector [161, 168, 214], the multistage interference cancellation (MIC) detector [154, 164, 165, 296], and the decision-feedback detector (DFD) [173, 175, 176, 178] etc. The interference cancellation based MIMO detectors are typically capable of providing a significantly better performance than their linear counterparts at the expense of a higher complexity, especially in the absence of channel coding [180], albeit this is not necessarily always the case. In practice, a common drawback of the interference cancellation based MIMO detectors is that they often suffer from error propagation. Hence their performance only approaches that of the optimum ML based MUD when the interfering users have a much stronger signal strength than the desired user. From this perspective, the weakest user benefits most from the employment of the interference cancellation detector.

- *SIC*: In the most popular SIC based MIMO detector, a single symbol s_i is detected at a time. Then the interference imposed by this particular symbol on the other symbols $\{s_k\}_{k \neq i}$ yet to be detected is subtracted after recreating the interference upon generating the modulated signal corresponding to this symbol. In this scheme, it is most important to cancel the effect of the strongest interfering signal before detecting the weaker signals. Therefore, the specific symbol detection ordering, which can be designed according to various criteria, is quite critical for the SIC detector’s performance. Some of the

typical ordering criteria for ordered SIC (OSIC) include the decreasing signal-to-noise ratio (DSNR) criterion [206, 207], the greatest signal-to-noise ratio (GSNR) criterion [208], the increasing mean-square error (IMSE) criterion [207], and the least mean-square error (LMSE) criterion [209–211]. The SIC method performs well when there is a substantial difference in the received signal strength of the multiple simultaneously transmitted symbols. However, this condition is not always satisfied in practical applications, which renders the SIC detector potentially sensitive to decision error propagation. Therefore, the SIC detector is well-suited for multiple-access systems suffering from the near-far problem, such as the family of CDMA or SDMA systems. In the SIC detector, there is a need for detection reordering at each iteration of the SIC detector, and the number of detection iterations increases linearly with the number of symbols in \mathbf{s} . Therefore, for a system which has a high-dimensional transmitted symbol vector \mathbf{s} , the SIC technique imposes a substantial complexity, which ultimately increases the processing delay. The SIC detector designed for CDMA systems was first proposed by Viterbi [171]. Later it was studied extensively in [177, 179, 295, 297–302]. In the context of multi-antenna based SDM systems, the SIC scheme was first studied by Wolniansky, Golden, Foschini and Valenzuela in [102, 103], and it was later studied more comprehensively by numerous other researchers in [201–203]. Among these schemes, Viterbi [171] proposed an SIC scheme for a convolutionally coded direct-sequence CDMA (DS-CDMA) system and revealed that with the aid of the SIC based receiver, the aggregate data rate of all simultaneous users may approach the Shannon capacity of the Gaussian channel. It should be emphasized that although theoretically the SIC method achieves the Shannon capacity in the multiple-access channel by assuming perfectly error-free detection (hence avoiding decision error propagation), this is not necessarily true in practice, because the SIC method is sensitive to decision error propagation, and hence MIMO detectors that are more robust to decision error propagation might outperform the SIC detector in practice. Another fact worth mentioning is that the performance degradation imposed by error propagation in the SIC detector can be mitigated by accurate power control [303].

- *PIC*: Alternatively, in the PIC based MIMO detector, all symbols are detected simultaneously. For each symbol, the coarse initial estimate of the interfering symbols can be used for regenerating the interference and then for deducting it from each of the composite received signals. Then this PIC detection process may be repeated for several iterations. Therefore, sometimes the PIC detection is also regarded as a MIC technique, or vice versa. Compared to the SIC detector, the PIC detector has lower processing delay, and is more robust to inter-stream error propagation. However, its near-far resistance is inferior to that of the SIC detector, because some users might have much weaker received signal strength than others. Hence, the PIC is suitable for similar-power signals, while the SIC performs better for different-power streams. In the context of CDMA systems, the earliest contribution to PIC may be attributed to Kohno *et al.* [161–163]. Later significant contributions to PIC were also attributed to Yoon [167, 304], Divsalar [168], Buehrer [305]

and Guo [306] *et al.*. In the context of multi-antenna MIMO systems, the PIC detector was studied mainly in [212–214].

- *MIC*: In the MIC based MIMO detector, the first stage can be the conventional SUMF detector, the linear detector, the SIC detector or any other suboptimum detector. *The decisions made for all symbols \mathbf{s} by the $(n - 1)$ th stage are employed as the input of the n th stage for the sake of cancelling the MUI.* Note that historically, the MIC detector was developed independently of the PIC, although they share similar concepts. The MIC detector was first proposed by Timor for frequency-hopped CDMA (FH-CDMA) systems [153, 154]. Then, it was extensively studied in the context of both *asynchronous DS-CDMA* systems [164, 307] and *synchronous DS-CDMA* systems [165, 296, 308]. An analytical framework was proposed for adaptive MIC in [169].
- *DFD*: The concept of DFD is based on the same premise as that of the family of decision-feedback equalizers [311, 312]. Although DFD also relies on the SIC idea, its emphasis is on the receiver filter’s optimization, which consists of a feedforward filter and a feedback filter) optimization. The first DFD scheme was proposed by Xie *et al.* [173, 281] for *asynchronous DS-CDMA systems*. Other major contributors of the subject of DFD include Duel-Hallen [175, 176, 309, 310], who comprehensively investigated decision-feedback MUDs designed for both synchronous [175, 309] and asynchronous [176, 310] CDMA systems. Furthermore, Varanasi [178] analyzed the performance of a general class of DFDs using a new performance metric constituted by the probability that at least one user is detected erroneously, and also proposed algorithms for determining the most beneficial detection ordering.

The main contributions to the development of the interference cancellation based MIMO detectors are summarized in Table 1.3. A more comprehensive exposition of the above-mentioned MIMO detectors developed in the context of CDMA systems can be found in [50–53, 181, 313].

1.8.4 Tree-Search MIMO Detectors

The tree-search based MIMO detectors are arguably the most popular detectors investigated in the era of multi-antenna MIMO systems. This is because 1) the introduction of the powerful SD algorithm happened to coincide with the development of multi-antenna MIMO techniques; 2) some profound research results on the CLPS problem showed that the tree-search MIMO detectors enjoy significant design flexibility in terms of striking an attractive tradeoff between approaching the optimum ML performance and reducing the computational complexity.

Indeed, some tree-search based MUDs had been reported earlier in the context of CDMA systems [172, 174, 314–316]. For example, the so-called (depth-first) stack sequential detection

TABLE 1.3: Milestones in the development of interference cancellation MIMO detectors

Year	Authors	Contributions
1974 - 1975	Bergmans and Cover [293, 294]	First demonstrated the effectiveness of the SIC concept from an information-theoretic perspective for broadcast channels.
1975	Carleial [120]	First characterized the effectiveness of the SIC principle from an information-theoretic perspective for interference channels.
1980-1981	Timor [153, 154]	First proposed a two-stage [153] MUD and a multistage [154] MUD for FH-CDMA systems employing multiple frequency-shift keying (MFSK) modulation; showed that the mutual interference between the users of a FH-CDMA system may be significantly reduced by making use of the well-defined algebraic structure of the users' signature waveforms, and that introducing an extra stage of interference cancellation may further improve the detector's performance.
1990	Viterbi [171]	First conceived an SIC scheme for a convolutionally coded DS-CDMA system, and revealed that with the aid of the SIC based receiver the aggregate data rate of all simultaneous users can approach the Shannon capacity of the Gaussian channel.
1983 - 1990	Kohno <i>et al.</i> [161–163]	First proposed a PIC based MUD for CDMA systems.
1988 - 1991	Varanasi <i>et al.</i> [164, 165, 307, 308]	Designed and systematically characterized the MIC MUDs for both asynchronous and synchronous CDMA systems.
1989 - 1990	Xie <i>et al.</i> [173, 281]	First proposed a DFD based MUD for <i>asynchronous DS-CDMA systems</i> .
1991 - 1995	Duel-Hallen <i>et al.</i> [175, 176, 309, 310]	Systematically investigated DFD MUDs conceived for both synchronous [175, 309] and asynchronous [176, 310] CDMA systems from a receiver filter optimization perspective.
1999	Wolniansky <i>et al.</i> [102, 103]	First discussed the ZF based SIC detector conceived for multiple-antenna aided SDM-MIMO systems.
2002	Chin <i>et al.</i> [212]	Extended the PIC detector to the multiple-antenna aided SDM-MIMO systems.
2003	Wübben <i>et al.</i> [206]	Proposed a QR-decomposition based MMSE-SIC detector for multiple-antenna aided SDM-MIMO systems.
2011	Stuber <i>et al.</i> [214]	Reported an application-specific integrated circuit (ASIC) implementation of a soft-input soft-output (SISO) MMSE based PIC detector for multiple-antenna aided SDM-MIMO systems.

was proposed by Xie in [172, 314], while the (breadth-first) K -best tree-search detection was proposed, again, by Xie in [174, 315], which was then further studied by Wei *et al.* in [316]. Looking back to the earlier history, because of the convertability between the trellis structure and the tree structure, the tree-search detection methods proposed for CDMA systems, including the classic M -algorithm [317, 318] and T -algorithm [319–322], were actually extensions of their counterparts used in trellis decoding [317–330]. However, these tree-search based detectors did not attract as much attention as the linear detectors and the interference cancellation aided detectors in the era of CDMA systems.

The research interests related to tree-search based MIMO detectors were largely stimulated by the seminal work of Viterbo *et al.* [54, 215], who first applied the depth-first SD algorithm

to the ML detection of multidimensional constellations transmitted over single-antenna fading channels. Note that before it was applied in digital communications, the SD algorithm, also known as the Fincke-Pohst algorithm, had been reported in [331, 332]. Later, Agrell *et al.* [55] proposed to employ the Schnorr-Euchner (SE) refinement [333] of the Fincke-Pohst algorithm [331, 332] for solving the *CLPS problem*, and they concluded that the SE enumeration is more efficient than the Viterbo-Boutros (VB) implementation [54] of the SD algorithm. More recently, Damen *et al.* [58] proposed two improved SD algorithms for finding the closest lattice point, both of which were shown to offer a significant complexity reduction compared to the VB-SD [54] and to the SE-SD [55], respectively. There exist a number of other variants of the tree-search based MIMO detectors, which mainly fall into three categories: the depth-first tree-search detector [54, 55, 58–62, 215], the breadth-first tree-search detector [63–65, 81, 83, 216] and the best-first tree-search detector [69–73, 217, 218].

The major momentum which propels the enormous research activities on tree-search based MIMO detectors is that they were shown to be capable of achieving near-ML performance, or even exact ML performance at the expense of significantly reduced complexity [59, 60, 334–336]. However, we would like to emphasize that this claim is shown not true in general [61, 337]. More specifically, Hassibi and Vikalo [59, 60, 334–336] first studied the expected complexity, averaged over the noise and over the lattice, of the Fincke-Pohst SD based MIMO detectors. It was claimed that although the worst-case complexity of the SD algorithm is exponential, the expected complexity of the SD algorithm is polynomial, in fact, often roughly cubic, for a wide range of SNRs and number of antennas. Contrary to this claim, Jaldén and Ottersten [61, 337] demonstrated that the expected complexity of SD based MIMO detectors is given by $O(M^{\beta N_t})$, where $\beta \in (0, 1]$ is a small factor depending on the value of SNR. In other words, the expected complexity of the SD algorithm is still exponential for fixed SNR values. Therefore, in general the tree-search based MIMO detectors are not efficient for MIMO systems which operate under low-SNR condition and/or have a large number of inputs. Notably, in order to avoid the varying-complexity characteristic of tree-search based MIMO detectors, recently a K -best algorithm based suboptimal fixed-complexity SD (FCSD) was proposed for MIMO systems [81]. It was shown that the FCSD achieves a near-ML performance with a complexity of $O(M^{\sqrt{N_t}})$ [83] regardless of the specific SNR encountered, which represents an attractive solution of facilitating an efficient hardware implementation compared to the conventional exponential-complexity SD. The main contributions in the development of the depth-first tree-search MIMO detectors, the breadth-first tree-search MIMO detectors and the best-first tree-search MIMO detectors are summarized in Table 1.4, Table 1.5 and Table 1.6, respectively.

TABLE 1.4: Milestones in the development of the tree-search MIMO detectors: Depth-first type

Year	Authors	Contributions
1981 - 1985	Pohst and Fincke [331, 332]	First proposed the SD algorithm, which is hence known as the Fincke-Pohst algorithm, for calculating vectors of short length in a lattice at a reduced complexity; this work laid the mathematical foundation of applying the SD algorithm to the MIMO detection problem.
1988 - 1990	Xie <i>et al.</i> [172, 314]	First proposed a stack sequential decoding based MUD for asynchronous CDMA systems; this detector is essentially a depth-first tree-search MIMO detector.
1993 - 1999	Viterbo <i>et al.</i> [54, 215]	Applied the depth-first SD algorithm to the ML detection of multidimensional constellations transmitted over single-antenna fading channels, which largely stimulated the research interests of tree-search based MIMO detectors.
1994	Schnorr and Euchner [333]	Proposed a more efficient variation, known as SE refinement, of the Fincke-Pohst SD algorithm; the SE-SD algorithm was based on the lattice basis reduction philosophy and represents a popular solution to the MIMO detection problem.
2001 - 2003	Hochwald <i>et al.</i> [75, 338]	Proposed a complex-valued SD and the list-SD (LSD) for a FEC-coded MIMO using IDD receiver, showing that a near-capacity performance can be achieved with the aid of a soft-SD based IDD receiver.
2002	Agrell <i>et al.</i> [55]	First proposed to use the SE refinement [333] of the Fincke-Pohst SD algorithm [331, 332] to the <i>CLPS problem</i> , and concluded that the SE enumeration technique is more efficient than the VB implementation [54] of the SD algorithm designed for MIMO detection.
2003	Damen <i>et al.</i> [58]	Proposed a pair of improved SD algorithms for finding the closest lattice point, both of which were shown to offer a significant complexity reduction compared to the VB-SD of [54] and to the SE-SD of [55].
2001 - 2005	Hassibi and Vikalo [59, 60, 334–336]	Analyzed the expected complexity of the SD algorithm, and concluded that the expected complexity of SD algorithm is dependent on both the problem size and the SNR; showed that when the SNR is high, the expected complexity of SD can be approximated by a polynomial function for a small problem size.
2004 - 2005	Jaldén and Ottersten [61, 337]	Further analyzed the expected complexity of the SD algorithm, and demonstrated that the expected complexity of the SD algorithm increases exponentially for a fixed SNR with a search-space, which contradicts previous claims; therefore, strictly speaking, the SD algorithm has an exponential lower bound in terms of both the expected complexity as well as the worst-case complexity, although it can be efficient at high SNRs and for problems of moderate size.
2005	Burg <i>et al.</i> [62]	First reported a very-large-scale integration (VLSI) implementation of the depth-first SD based MIMO detector.

TABLE 1.5: Milestones in the development of the tree-search MIMO detectors: Breadth-first type

Year	Authors	Contributions
1990 - 1993	Xie <i>et al.</i> [174,315,316]	First conceived a breadth-first K -best tree search MUD for asynchronous CDMA systems; proposed a joint signal detection and parameter estimation scheme based on their breadth-first tree search MUD.
1997	Wei <i>et al.</i> [316]	Studied both the M -algorithm and the T -algorithm based breath-first tree-search MUD in the context of CDMA systems operating in fading channels.
2002	Wong <i>et al.</i> [63]	Proposed and implemented a breadth-first K -best tree-search MIMO detector using a VLSI architecture, which is capable of achieving a decoding throughput of 10 Mb/s at 100 MHz clock frequency in a 16-QAM aided (4×4) -element SDM-MIMO system.
2006	Guo <i>et al.</i> [64]	Proposed and implemented both hard and soft SE-strategy based K -best tree-search MIMO detectors, which are capable of supporting up to 53.3 Mb/s throughput at 100 MHz clock frequency for a 16-QAM aided (4×4) -element SDM-MIMO system.
2007	Chen <i>et al.</i> [65]	Reported a VLSI implementation of a soft-output breadth-first tree search aided MIMO detector for a (4×4) -element MIMO system employing 64-QAM, which is capable of achieving a throughput of above 100 Mb/s.
2006 - 2008	Barbero <i>et al.</i> [81,339]	Proposed a noise-level independent fixed-complexity K -best tree-search MIMO detector, which overcomes the two main limitations of the SD from an implementation point of view: its variable complexity and its sequential nature.
2009	Jaldén <i>et al.</i> [83]	Presented analytical study of the error probability of the fixed-complexity SD in MIMO systems having an arbitrary number of antennas, proving that it achieves the same diversity order as the ML detector, regardless of the constellation size used.

TABLE 1.6: Milestones in the development of the tree-search MIMO detectors: best-first type

Year	Authors	Contributions
2004	Fukatani <i>et al.</i> [217]	Applied Dijkstra's algorithm [340] for reducing the complexity of the SD based MIMO detector at the expense of an increased storage size.
2004	Xu <i>et al.</i> [341]	Applied the stack algorithm [326] to the best-first tree search based MIMO detector.
2006	Murugan <i>et al.</i> [67]	Proposed a unified framework for tree search decoding, which encompasses all existing SDs as special cases, hence unifying the depth-first search, the breadth-first search and the best-first search based on the proposed framework.
2012	Chang <i>et al.</i> [73]	A generalization of Dijkstra's algorithm was developed as a unified tree-search detection framework; the proposed framework incorporates a parameter triplet that allows the configuration of the memory usage, detection complexity and the sorting dynamic associated with the tree-search algorithm; by tuning the different parameters, beneficial performance-complexity tradeoffs are attained and a fixed-complexity version can be conceived.
2012	Chang <i>et al.</i> [72]	First applied the A* algorithm to the best-first tree-search based MIMO detection problem.

1.8.5 Probabilistic Data Association Based Detector

The PDA filter technique is a statistical approach originally invented by Bar-Shalom [342] in 1975 for the problem of target tracking and surveillance in a cluttered environment, where measurements are unlabelled and may be spurious. To elaborate a little further, it was developed for solving the problem of *plot-to-track association* in a radar tracker, in which all of the potential candidates for association to a specific track are combined into a single statistically most likely update, taking account of the statistical distributions of both the tracking errors and the clutter, while assuming that only one of the candidates is the desired target with the rest of them representing false alarms. A major extension of the PDA filter is the joint probabilistic data association (JPDA) filter [343, 344], which takes account of the situation that multiple targets are present out of all the potential candidates, and hence seeks to compute the joint decision probabilities for the multiple targets. In addition to their wide applications in radar, sonar, electro-optical sensor networks and navigation systems [342–356], the PDA techniques have also been applied in the field of computer vision for solving the visual target tracking problem [357–360].

The PDA approach may also be applied for solving challenging problems in digital communications. For example, it may be developed as a reduced-complexity design alternative to the optimal soft-decision aided MAP detectors/equalizers of MIMO channels [193, 219–242], and it is also applicable to channel estimation of MIMO systems [361, 362]. Since we mainly focus on MIMO detection in this thesis, a more detailed discussion of the PDA-based MIMO channel estimation will not be included in the sequel. As far as the PDA-based MIMO detection is concerned, it is Luo *et al.* [219] who first applied the PDA approach to the MUD problem of BPSK-modulated synchronous CDMA systems in 2001, showing a near-optimum performance at a significantly lower computational complexity than the ML detector. Thereafter, the PDA-based detector was naturally extended to the scenario of BPSK-modulated asynchronous CDMA systems [221, 222]. Recently, it was also extended to the symbol detection of QAM-aided SDM-MIMO systems [193, 226, 227, 230, 234], striking an attractive tradeoff between the attainable performance and the complexity imposed. More specifically, in [226] a real-valued PDA (RPDA) was formulated for M -QAM constellations, which is based on the equivalent real-valued MIMO signal model previously discussed in Section 1.6. Additionally, in [193] an approximate complex-valued PDA (A-CPDA) detector was proposed, in which the complex-valued Gaussian distribution is approximately characterized by a matched mean and a matched covariance only. Furthermore, the pseudo-covariance, as defined by Neeser and Massey in [363], was employed in [234] to fully characterize the complex-valued Gaussian distribution, and the resultant formulation of complex-valued PDA (CPDA) [234] was shown to outperform both the RPDA [226] and the A-CPDA [193].

In these PDA-based MIMO detectors/equalizers, the probabilities of the potential candidate symbols serve as the soft input/output information and are typically estimated relying on

TABLE 1.7: Milestones in the development of the PDA-based MIMO detectors

Year	Authors	Contributions
2001	Luo <i>et al.</i> [219]	First applied the PDA filter technique to the MUD problem of synchronous CDMA systems, showing a near-optimum performance at a significantly reduced complexity.
2002	Pham <i>et al.</i> [221]	Proposed a PDA-Kalman MUD approach for asynchronous CDMA systems.
2003	Luo <i>et al.</i> [222]	Conceived a sliding-window PDA based MUD approach for asynchronous CDMA systems.
2003	Tan <i>et al.</i> [223]	Designed a PDA-based IDD receiver for a coded CDMA system using BPSK modulation.
2004	Pham <i>et al.</i> [226]	Extended the PDA detector to SDM-MIMO systems based on a real-valued signal model.
2004	Liu <i>et al.</i> [193]	Proposed a PDA-based soft equalization scheme for frequency-selective MIMO channels.
2005	Liu <i>et al.</i> [227]	Extended the PDA-Kalman MUD approach of [221] to the soft equalization of frequency-selective MIMO channels.
2005	Latsoudas <i>et al.</i> [228]	Proposed a hybrid MIMO detector that combined the SD and the PDA detectors.
2005	Fricke <i>et al.</i> [230]	Studied the impact of Gaussian approximation on the performance of the PDA based MIMO detector.
2006	Jia <i>et al.</i> [234]	Proposed a complex-valued PDA detector which takes the pseudo-covariance into account during the derivation of the complex-valued PDA detector.
2008	Kim <i>et al.</i> [240]	Applied the PDA method as a component of an iterative receiver designed for non-coherent MIMO systems.
2009	Mohammed <i>et al.</i> [241]	Applied the PDA algorithm to the problem of decoding large non-orthogonal spacetime block codes (STBC).

a self-iterative process. The key operation in this process is the iterative approximation of the interference-plus-noise term obeying a *multimodal Gaussian mixture* distribution by an *ever-updated* multivariate Gaussian distribution [193, 219, 226, 227, 242]. The advantages of the PDA based detectors are as follows.

- First, it may achieve a near-optimal detection performance in certain circumstances, for example in the context of FEC-uncoded CDMA systems [219–222].
- Second, it has a low complexity that increases no faster than $O(N_I^3)$ per symbol vector, where N_I represents either the number of users in CDMA [219–222], or the number of transmit antennas in multi-antenna aided MIMO systems [193, 226, 234].
- Third, it is inherently an SISO algorithm, which is eminently applicable in combination with FEC codes such as convolutional codes, turbo codes [364, 365] or low-density parity-

check (LDPC) codes [366, 367].

- Furthermore, the higher the number of transmit antennas or users, the better its performance, provided that the channel is not rank-deficient [230]. However, due to its nature of approximation and iteration, the PDA based MIMO detector has not been well-understood compared to other mature MIMO detectors. For the sake of prominent exposition, the main contributions to the development of the PDA based MIMO detectors are summarized in Table 1.7.

1.8.6 Semidefinite Programming Relaxation Based Detector

In contrast to other MIMO detectors, the SDPR approach relies on a relaxation of the optimum MIMO detection problem to the mathematical model of semidefinite programming (SDP) [243, 244, 368], which is a subfield of convex optimization theory [369]. The SDPR based MIMO detectors have recently received substantial research attention [245–257]. The most attractive characteristic of the SDPR-aided detectors is that they guarantee a so-called polynomial-time⁶ worst-case computational complexity, while achieving a high performance in certain circumstances.

Most of the existing SDPR detectors are dependent on the specific modulation constellation. To elaborate a little further, SDPR was first proposed for a BPSK-modulated CDMA system [245, 246, 370–373], and then it was extended to quadrature phase-shift keying (QPSK) [247]. Simulation results showed that the SDPR detector is capable of achieving a near-ML BER performance, when using BPSK [245] and QPSK [247]. The numerical and analytical results of [248, 249] confirmed that the SDPR detector achieves the maximum possible diversity order, when using BPSK for transmission over a real-valued fading MIMO channel. The SDPR approach was also further developed for high-order modulation schemes, such as for M -ary phase-shift keying (PSK) scenario in [250, 251], and for high-order rectangular QAM in [252–256]. As for the high-order QAM scenario, it was recently shown in [257] that the so-called polynomial-inspired SDPR (PI-SDPR) [252], the bound-constrained SDPR (BC-SDPR) [254] and the virtually antipodal SDPR (VA-SDPR) [256] are actually equivalent in the sense that they obtain the same symbol decisions, and hence they exhibit an identical symbol error rate (SER) performance.⁷ It should be noted, however, that for high-order modulation scenarios, we will show in Chapter 3 that the performance of the SDPR detectors is not quite promising compared to that of the BPSK/QPSK scenario. Therefore, there is a need to further improve the performance of the SDPR based MIMO detector designed for high-order QAM constellations, while maintaining its appealingly low

⁶The computational complexity increases as a polynomial function of N_t .

⁷More specifically, the solution equivalence of the PI-SDPR and BC-SDPR schemes holds for 16-QAM and 64-QAM, while that between the BC-SDPR and VA-SDPR techniques holds for any 4^q -QAM scheme, where q is a positive integer. The SDPR QAM detector of [255] exhibits a better performance than that of [252, 254, 256], but has a much higher complexity.

computational complexity. The main contributions to the development of the SDPR based MIMO detectors are summarized in Table 1.8.

1.9 Organization and Novel Contributions of the Thesis

Having reviewed the literature of MIMO detection methods, let us now highlight the organization and the novel contributions of this thesis.

1.9.1 Organization

For the sake of clarity, the organization of the remaining part of this thesis and the logical connections between all chapters are shown in Fig. 1.14. To be more specific, the remaining chapters mainly focus on the PDA and the SDPR based MIMO detection methods, which are systematically investigated in both the FEC-uncoded and FEC-coded point-to-point SDM-MIMO systems, as well as in the base station cooperation aided multiuser multicell network-MIMO systems.

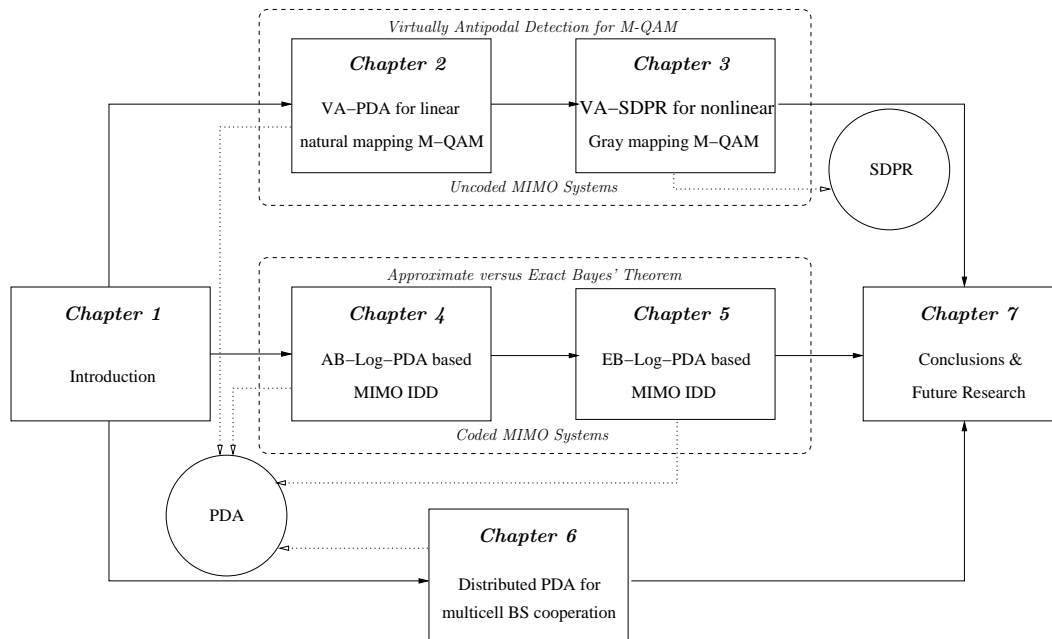


FIGURE 1.14: Organization of the thesis.

- **Chapter 2:** In Chapter 2, we investigate the PDA detector for SDM-MIMO systems which employ high-order rectangular QAM constellations. In particular, the proposed PDA detector performs in a virtually antipodal (VA) manner, which means, the PDA-based symbol detection of rectangular QAM constellations is realized in a BPSK-like

TABLE 1.8: Milestones in the development of the SDPR-based MIMO detectors

Year	Authors	Contributions
2001 -2003	Tan <i>et al.</i> [245, 370], Ma <i>et al.</i> [246, 371], and Wang <i>et al.</i> [372, 373]	These authors independently proposed a SDPR based MUD for BPSK-modulated synchronous CDMA systems; the eigen-decomposition based method of [245, 370, 372, 373] and the randomization method of [246, 371] were proposed for converting the continuous-valued solution of the SDP problem into the binary decision output. Additionally, a cutting plane method was introduced for further improving the performance of the SDPR detector for systems supporting a large number of users [245, 370]; it was shown that the classic MUDs, such as the linear ZF/MMSE detector, can be interpreted as degenerate forms of the SDPR based MUD [246, 371].
2003	Steingrimsson <i>et al.</i> [374]	Proposed a soft SDPR detector for an IDD receiver of QPSK-aided MIMO systems employing LDPC codes.
2004	Ma <i>et al.</i> [247]	Conceived a SDPR based MUD for BPSK/QPSK aided asynchronous CDMA systems with multiple receive antennas in frequency-selective fading environments; based on a flexible block alternating likelihood maximization (BALM) principle, the large-scale ML detection problem was decomposed into smaller subproblems, and each subproblem was solved by the SDPR detector.
2003 -2004	Luo <i>et al.</i> [250] and Ma <i>et al.</i> [251]	Proposed SDPR detectors for general M -PSK aided synchronous CDMA systems.
2005	Kisialiou <i>et al.</i> [248]	Provided the first analytical study of the SDPR detector for BPSK-aided MIMO systems; it was shown that the SDPR detector is capable of achieving the same BER performance as that of the ML detector in high-SNR scenarios, while at the low SNR region, the SDPR detector serves as a constant factor approximation to the ML detector in large systems.
2005	Wiesel <i>et al.</i> [252]	Designed a PI-SDPR detector for 16-QAM aided MIMO systems, which can be extended to high-order M -QAM scenarios.
2006	Sidiropoulos <i>et al.</i> [254]	Advocated a BC-SDPR detector for employment in high-order M -QAM aided MIMO systems.
2007	Mao <i>et al.</i> [256]	Proposed a VA-SDPR detector for M -QAM aided multicarrier CDMA(MC-CDMA) systems; the method can directly operate at the bit-level in the context of linear mapping based M -QAM.
2007	Mobasher <i>et al.</i> [255]	Studied several variants of the SDPR detectors, and showed that it is possible to further improve the SDPR detector's performance by increasing their complexity.
2008	Jaldén <i>et al.</i> [249]	Analytically demonstrated that the SDPR based detector is capable of achieving full receive diversity order in BPSK-aided real-valued MIMO channels.
2009	Ma <i>et al.</i> [257]	Demonstrated that the PI-SDPR of [252], the BC-SDPR of [254], and the VA-SDPR of [256] are actually equivalent in the sense that they obtain the same symbol decisions, and hence exhibit an identical SER performance.

bit-by-bit detection style. The mathematical foundation based on which the symbol-based processing is transformed to bit-based processing is systematically investigated for both the linear natural mapping and the nonlinear Gray mapping based rectangular QAM constellations. However, the resultant bit-based PDA (**B-PDA**) detector, which may be interchangeably called VA-PDA detector, is not practical in the latter case due to the nonlinearity of Gray mapping, and hence the B-PDA detector obtained for the Gray mapping scenario serves only as a theoretic performance bound for the linear natural mapping based B-PDA. The BER/SER performance and the computational complexity of the proposed B-PDA detector are compared with that of the benchmarking ML, MMSE-OSIC, and the symbol-based CPDA [234] detectors, which corroborates the benefits of the proposed B-PDA detector over the conventional symbol-based PDA detector.

- **Chapter 3:** Further to Chapter 2, in Chapter 3, the practically feasible method of transforming symbol-based MIMO detection to bit-based MIMO detection for Gray mapping based rectangular M -QAM is further investigated. Based on these results, we propose a generalized computationally efficient direct-bit-based VA-SDPR (**DVA-SDPR**) detector which is practically feasible for direct bitwise detection of Gray mapping based rectangular M -QAM. For improving the numerical accuracy of solving the associated SDP problem, a modified interior point algorithm (**IPA**) is presented. Additionally, the VA processing facilitates the exploitation of the unequal error protection (**UEP**) property of QAM bits, and consequently a simple but effective bit-flipping technique is shown capable of further improving the performance of the DVA-SDPR detector at the expense of trivial extra complexity. Finally, both the performance and the computational complexity of the proposed DVA-SDPR detector are extensively evaluated and compared to those of other relevant benchmarking MIMO detectors.
- **Chapter 4:** Having dealt with the PDA and the SDPR based MIMO detection for FEC-uncoded SDM-MIMO systems in Chapter 2 and Chapter 3, respectively, in Chapter 4, our attention is drawn to addressing the issue of designing a low-complexity PDA method based IDD receiver for FEC-coded SDM-MIMO systems using the memoryless M -ary modulation. More specifically, the distribution of the interference-plus-noise term encountered in the PDA method is analyzed, and the mathematical property of the output symbol decision probabilities of the conventional PDA detectors is investigated. Consequently, we develop an IDD receiver relying on the approximate Bayes' theorem based logarithmic-domain PDA (**AB-Log-PDA**). Furthermore, the method of calculating extrinsic logarithmic likelihood ratio (**LLR**) relying on the output symbol decision probabilities of the AB-Log-PDA is discussed, which results in a irregular IDD receiver architecture. Finally, the impact of various design parameters on the performance and the complexity of the AB-Log-PDA based IDD receiver is comprehensively investigated.
- **Chapter 5:** Further to the AB-Log-PDA based IDD receiver proposed in Chapter 4, in Chapter 5, another type of PDA-based IDD receiver, namely the exact Bayes' theorem based logarithmic domain PDA (**EB-Log-PDA**) based IDD receiver, is proposed for FEC-

coded SDM-MIMO systems employing the memoryless M -ary modulation. Because the mathematical property of the output symbol decision probabilities of the EB-Log-PDA is different from that of the AB-Log-PDA, the classic IDD receiver architecture, which does not fit into the AB-Log-PDA based IDD receiver, is readily applicable to the EB-Log-PDA based IDD receiver. Furthermore, a comparative study of the AB-Log-PDA and the EB-Log-PDA based IDD receivers is conducted from various aspects, including the relationship between the output bitwise extrinsic LLRs of both the AB-Log-PDA and the EB-Log-PDA, the impact of inner PDA iterations on the performance of the two IDD receivers, as well as the computational complexity of the two PDA-based IDD receivers relying on the decoupled and non-decoupled signal models.

- **Chapter 6:** Having investigated the MIMO detection problem in the context of point-to-point FEC-uncoded/-coded SDM-MIMO systems from Chapter 2 to Chapter 5, in Chapter 6, we investigate the MIMO detection problem in the context of the uplink of multiuser multicell networks. More specifically, we extend the PDA algorithm to a distributed soft-reception scheme conceived for reducing the prohibitive computational complexity and the huge amount of backhaul traffic encountered by multicell multiuser MIMO systems employing BS cooperation. A realistic 19-cell hexagonal cellular MIMO-aided network model relying on either perfect or imperfect channel estimation is considered, and a simple but effective soft combining (SC) technique is used at each BS for generating the final soft-decision information. Additionally, we investigate the impact of quantization on both the backhaul traffic and the performance of the proposed scheme. We also considered challenging rank-deficient scenarios, where the number of transmitters is higher than that of the receivers.
- **Chapter 7:** Finally, in Chapter 7 we summarized the main findings of this thesis, and outline a range of suggestions concerning the MIMO detection problem for future research.

1.9.2 Novel Contributions

In summary, the novel contributions of this thesis focus on the PDA and the SDPR based MIMO detectors, because the initiative of developing these two methods in digital communications is known relatively recently to the research community and hence they are not well-investigated compared to other suboptimum MIMO detectors. For the sake of clarity, the theories underpinning these novel contributions, as well as the relationship amongst these contributions is shown in Fig. 1.15. Both algorithm optimizations and their novel applications are covered, which are elaborated on in more detail as follows.

- The mathematical description of the mapping process between the transmit bit vector and the corresponding transmit symbol vector in high-order rectangular M -QAM aided SDM-MIMO systems is systematically studied, and unified modulation matrix is explicitly obtained for the cases of both linear natural mapping [40,41] and nonlinear binary reflected

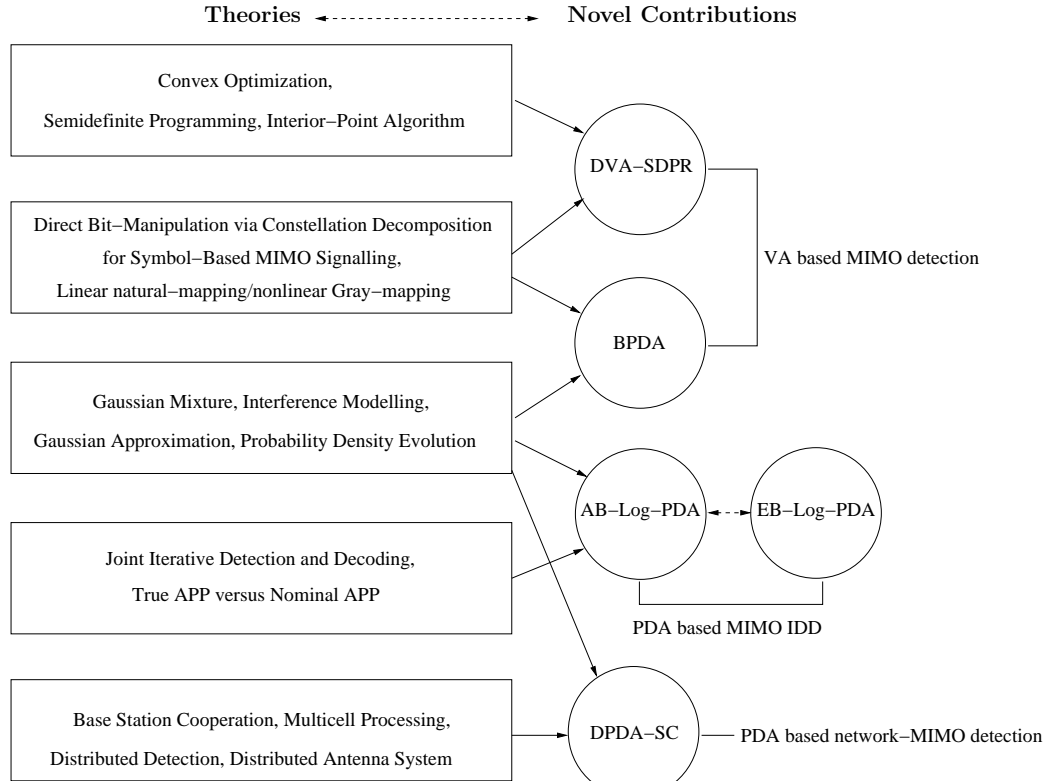


FIGURE 1.15: The framework of novel contributions of the thesis.

Gray mapping [48, 49], which includes BPSK modulation as a special case. As a universal benefit, it becomes convenient to directly manipulate the bits modulated by rectangular M -QAM symbols in MIMO systems.

- A virtually antipodal detection based B-PDA detector [40, 41], which is practically applicable to linear natural mapping scenario, is proposed for high-order rectangular M -QAM aided SDM-MIMO systems. In contrast to the conventional symbol-based PDA MIMO detectors, the linear natural mapping based B-PDA transforms the symbol-based QAM detection problem to a BPSK-like binary scenario in MIMO systems, thus eliminating symbol-based decisions, and hence directly operating at the bit-level. In addition to its remarkable complexity reduction, the linear natural mapping based B-PDA has an improved performance in comparison to the conventional symbol-based PDA in most scenarios considered. Furthermore, it is found that the binary reflected Gray mapping is not the best choice of labelling scheme for B-PDA. In fact it is preferable to use the simpler and more practicable linear natural mapping for the B-PDA detector in the context of the uncoded SDM-MIMO systems.
- A virtually antipodal detection based SDPR detector [48, 49], which is dubbed DVA-SDPR and is practically applicable to the ubiquitous nonlinear binary reflected Gray mapping scenario, is proposed for high-order rectangular M -QAM aided SDM-MIMO systems. The DVA-SDPR detector is also capable of directly deciding on the transmit information bits without invoking the conventional symbol-based decisions, which is a

benefit more challenging to achieve than the scenario of linear natural mapping. The DVA-SDPR detector converts the classic nonlinear Gray-mapping aided M -QAM symbol detection problem to a Boolean quadratic programming (BQP) problem. Furthermore, when combined with low-complexity bit-flipping based “hill climbing”, the DVA-SDPR detector achieves the best BER performance among the known SDPR-based MIMO detectors in the context considered, while still maintaining a polynomial-time worst-case complexity order as low as $O[(M_c N_t + 1)^{3.5}]$.

- In the context of FEC-coded SDM-MIMO systems using general M -ary memoryless modulation, we demonstrate that the classic candidate-search-aided bit-wise extrinsic LLR calculation method is not applicable to the family of existing PDA-based detectors. Additionally, we reveal that in contrast to the interpretation in the existing literature, the output symbol probabilities of existing PDA algorithms are not the true APPs, but rather the normalized symbol likelihoods. Therefore, the classic relationship, where the extrinsic LLRs are given by subtracting the *a priori* LLRs from the *a posteriori* LLRs, does not hold for the existing PDA-based detectors. Motivated by these revelations, we conceive a novel AB-Log-PDA method and unveil the technique of calculating bit-wise extrinsic LLRs for the AB-Log-PDA [44, 45], which facilitates the employment of the AB-Log-PDA in an irregular IDD receiver structure. Additionally, we demonstrate that it is preferable to dispense with inner iterations within the AB-Log-PDA in the context of IDD receivers, and that the proposed AB-Log-PDA-based IDD scheme is capable of achieving a performance comparable to that of the optimal MAP-detector-based IDD receiver, while imposing a significantly lower computational complexity in the scenarios considered.
- An EB-Log-PDA approach based IDD receiver is proposed for FEC-coded MIMO systems using arbitrary M -ary modulation [46, 47]. As opposed to that of the existing PDAs based on an approximate version of the Bayes’ theorem, the estimated symbol-wise output probabilities of the EB-Log-PDA exhibit similar characteristics to the true APPs. Hence the bit-wise extrinsic LLRs delivered by the proposed EB-Log-PDA to the outer FEC decoder may be calculated simply by subtracting the bit-wise *a priori* LLRs from the bit-wise *a posteriori* LLRs. Furthermore, we investigate the relationship between the EB-Log-PDA based IDD scheme and the AB-Log-PDA based IDD scheme proposed in [44, 45]. We demonstrate that the two schemes achieve a similar near-optimum performance when dispensing with inner iterations within the PDAs. However, our analysis of the cumulative distribution functions (CDFs) and the PDFs concerning the *differences* between the two types of extrinsic LLR values output by the EB-Log-PDA and the AB-Log-PDA reveal that these two types of extrinsic LLRs are different, even though they might be similar in certain scenarios. Additionally, we compare the impact of the inner iterations within the PDAs on the achievable performance of the EB-Log-PDA and the AB-Log-PDA based IDD schemes. We demonstrate that, similar to that of the AB-Log-PDA based IDD scheme, the performance of the EB-Log-PDA based IDD scheme is also degraded when inner iterations of the EB-Log-PDA are invoked. However, their specific performance

degradation profile is slightly different.

- The PDA algorithm is extended into a distributed soft-reception scheme for mitigating the prohibitive computational complexity and the huge amount of backhaul traffic faced by multicell multiuser network-MIMO systems employing BS cooperation [42, 43]. The fundamental philosophy of the proposed DPDA-SC scheme is not that of the conventional “interference cancellation” but “knowledge sharing and data fusion”. Since in practice only the index of the possible discrete value of the converged soft information has to be exchanged for SC operation, the proposed DPDA-SC scheme is relatively robust to the quantization errors of the soft information exchanged, which dramatically reduces the backhaul traffic at the cost of a negligible performance degradation. Despite its significant performance gain over the conventional non-cooperative MUD schemes, the proposed DPDA-SC approach imposes a modest complexity. Specifically, it obeys a cubically increasing function of the number of streams processed, while maintaining a low backhaul traffic. Its low complexity is achieved as a benefit of the PDA’s rapid convergence, since only the converged soft-information is exchanged amongst the BSs of the specific cooperative BS-cluster, requiring a single action.

Unified Bit-Based PDA Aided MIMO Detection for High-Order QAM Constellations

2.1 Introduction

IN Chapter 1, we discussed the essence of the MIMO detection problem from a generalized physical-layer CCI management perspective and provided a comprehensive overview of both the history as well as the state-of-the-art in the field of MIMO detectors. We have seen that the MIMO detection problem defined by (1.1) and (1.2) is of fundamental importance for both contemporary and future spectrum-/energy-efficient communication systems. However, the known algorithms conceived for optimally solving the MIMO detection problem based on the MAP [see (1.9), (1.10)] and the ML [see (1.11)-(1.14)] criteria impose an exponentially increasing complexity upon increasing the number of jointly detected symbols N_I . This potentially excessive complexity generally precludes the application of the MAP and the ML based detection algorithms in high-dimensional MIMO systems that has a large N_I . Therefore, substantial research efforts have been invested in developing suboptimum MIMO detectors which strike an attractive performance/complexity tradeoff in the context of diverse practical applications.

In this chapter, our attention is focused on the PDA-based MIMO detector, because it is less well-understood compared to other suboptimum MIMO detectors, such as the linear MIMO detectors, the interference cancellation MIMO detectors and the tree-search based MIMO detectors of Fig. 1.10, as discussed in Chapter 1. More specifically, we aim for improving the PDA detector's own performance/complexity tradeoff in the context of high-order rectangular QAM aided SDM-MIMO systems without accessing external resources.

Therefore, no FEC codec is integrated into the SDM-MIMO system model considered in this chapter, which facilitates our investigations of the PDA detector's performance without the ameliorating influence of the FEC decoder's error correction. However, we will further elaborate on the interplay of the PDA detector and the FEC decoder in Chapter 4 and 5.

The particular motivation for addressing this specific problem arises from the following observations.

Firstly, high-order QAM aided high-throughput SDM-MIMO¹ transmission techniques will play a pivotal role in next-generation wireless systems. For example, the Third Generation Partnership Project (3GPP) Long-Term Evolution (LTE)-Advanced initiative [375] and the Institute of Electrical and Electronics Engineers (IEEE) 802.16m standard [Worldwide Interoperability for Microwave Access (WiMAX) Release 2] [376, 377] based systems will use up to (8×8) -element SDM-MIMO combined with 128-QAM. Therefore, there is a need for developing low-complexity MIMO detectors that are appropriate for high-order QAM aided SDM-MIMO systems.

Secondly, the mathematical description of QAM constellations is a fundamental problem in digital communications. Conventionally, the bit-to-symbol mapping process is implemented by either a look-up table using a programmable memory device, or as the superposition of a number of PSK signals [378]. However, both of them conceal the specific mathematical characteristics of the bit-to-symbol mapping process to a certain extent.

More importantly, as we mentioned in Section 1.8.5, the PDA detector was shown to achieve a near-optimal performance in CDMA systems [219], [221] at a low computational complexity, which was on the order of $O(L^3)$ per transmitted symbol vector, where L is the number of active users. However, the performance of the conventional symbol-based PDA detectors designed for SDM-MIMO systems [193, 226, 227, 230, 234] was shown to be less impressive than that of their counterparts employed in CDMA systems [219, 221]. According to the results of [230], one of the reasons accounting for this performance loss is that the number of transmit antennas in a MIMO system is typically lower than that of the users in CDMA. For example, the number of transmit antennas considered in SDM-MIMO systems is typically less than ten [193, 226, 227, 230, 234], while the number of users considered in CDMA systems is often much higher than ten, e.g. $L = 29$ in [219] and $L = 25$ in [221]. A second reason is that in MIMO systems typically QAM is used [193, 226, 227, 230, 234], whereas some CDMA systems are based on BPSK modulation scheme [219, 221]². Additionally, the "equivalent channel matrix" of CDMA systems is more likely to be well-conditioned than the channel matrix of MIMO systems. More specifically, the "equivalent channel matrix" in CDMA systems is constituted by the matrix product of the cross-correlation matrix of the well-

¹The throughput is defined as " $N_t \log_2 M$ bits/channel use" for FEC-uncoded SDM-MIMO systems.

²Having said this, the CDMA based high speed packet access (HSPA) system employs QAM having as many as 64 constellation points.

designed spreading codes and the diagonal matrix containing the signal amplitudes of the corresponding users. This “equivalent channel matrix” is typically well-conditioned. However, in MIMO systems it is possible that the channel matrix becomes rather ill-conditioned for some realizations.

According to the central limit theorem, in MIMO systems the fewer independent random channel vectors which are either resulted from the ill-conditioned channel matrix or are corresponding to the lower number of transmit antennas, may result in poor Gaussian approximations. As a result, the performance of the PDA detector may suffer. To expound a little further, as argued in [219], a key feature of PDA is the repeated approximation of a *multimodal* Gaussian mixture distribution by a single *multivariate* Gaussian distribution having carefully matched moments. For convenience, this approximation process is simply referred to as Gaussian approximation. Hence, the accuracy of the Gaussian approximation dominates the attainable performance of PDA based MIMO detectors. In fact, it has been demonstrated in [230] that the quality of the Gaussian approximation in PDA improves for a large number of transmit antennas and a low number of modulation constellation points. Therefore, the performance of the symbol-based PDA detectors significantly degrades for high-order QAM constellations compared to that of the ML/MAP detector, despite the fact that its complexity substantially increases owing to the increased number of symbol probabilities to be computed.

With the above-mentioned motivation, in this chapter we aim for developing an *efficient* PDA-based MIMO detector for high-order rectangular QAM constellations. Inspired by the conclusions of [230], we intend to find a method that may *equivalently* increase the dimension of the effective transmitted signal vector and/or reduce the effective constellation size for PDA-based MIMO detectors. Our main contributions in this chapter are given as follows.

- 1) We present an explicit UMR of both linear natural mapping [256,379] and nonlinear binary reflected Gray-mapping based rectangular QAM employed in MIMO systems, including BPSK modulation as a special case.
- 2) Based on the UMR, we first propose a B-PDA detector for MIMO systems using high-order rectangular QAM. In contrast to the conventional symbol-based PDA MIMO detectors of [193, 226, 227, 230, 234], the B-PDA transforms the symbol-based QAM detection of MIMO systems to a BPSK-like binary scenario, thus eliminating symbol-based decisions, and directly operates at the bit-level. While a similar mathematical representation of the linear-natural-mapping-based rectangular QAM was also used in the context of the SDPR technique of [256] and in the multilevel bit-interleaved coded modulation (BICM) scheme of [379], its extension to the nonlinear binary reflected Gray mapping and its application to improving the PDA-based MIMO detectors have not been suggested before.
- 3) We investigate the complexity of the proposed B-PDA MIMO detector both analytically

and by simulations. It is demonstrated that the linear-natural-mapping-based B-PDA substantially reduces the computational complexity, compared with the conventional symbol-based PDA MIMO detector in FEC-uncoded VBLAST systems using high-order QAM.

4) In addition to a beneficial complexity reduction, the simulation results show that the linear-natural-mapping-based B-PDA has a slightly improved performance in comparison with the conventional symbol-based PDA. Furthermore, it approaches the lower bound performance provided by the binary reflected Gray-mapping-based B-PDA under the idealized perfect modulation matrix estimation assumption.

5) Considering the additional complexity and the potential performance degradation entailed by the modulation matrix estimation for binary reflected Gray-mapping-based B-PDA, we argue that the binary reflected Gray mapping is not the best choice of labeling scheme for B-PDA. In fact, it is preferable to use the simpler and more practicable linear natural mapping for the B-PDA detector in the context of the FEC-uncoded VBLAST system considered.

The rest of this chapter is organized as follows. Section 2.2 describes the system model and the basic task of PDA-based MIMO detectors. Section 2.3 derives the UMR for SDM-MIMO systems employing linear natural mapping based high-order rectangular QAM constellations. In Section 2.4, the UMR for the nonlinear Gray mapping scenario is derived. Then, in Section 2.5, we propose a bit-based PDA-aided MIMO detector using UMR, and present the corresponding complexity analysis. The achievable BER and SER performance, as well as the convergence properties of both the conventional CPDA and the proposed B-PDA, are characterized with the aid of simulations and further remarks in Section 2.6. The summary and conclusions drawn in this chapter are given in Section 2.7.

2.2 Problem Statement

Consider a SDM-MIMO system with N_t transmit and N_r receive antennas, as shown in Fig. 1.9. The received baseband signal at each symbol instant is thus given by (1.3), and can be written in vector form as

$$\mathbf{y} = \mathbf{H}\mathbf{s} + \mathbf{n}, \quad (2.1)$$

where \mathbf{H} is the $(N_r \times N_t)$ -element complex-valued channel matrix, \mathbf{s} is the size- N_t vector of transmitted symbols taken from a rectangular QAM constellation $\mathbb{A} = \{a_1, a_2, \dots, a_M\}$ with cardinality M , and \mathbf{n} represents the size- N_r complex-valued circularly symmetric Gaussian noise vector with zero mean and a covariance matrix of $N_0\mathbf{I}_{N_r}$, where \mathbf{I}_{N_r} is an $(N_r \times N_r)$ -element identity matrix.

Assume that the components of the transmitted symbol vector \mathbf{s} are obtained using the bit-to-symbol mapping function $s_j = \text{map}(\mathbf{d}_j)$, $j = 1, 2, \dots, N_t$, where $\mathbf{d}_j = [d_{j,1}, d_{j,2}, \dots, d_{j,M_c}]^T$

$\in \{+1, -1\}^{M_c}$ is the vector of data bits, and $M_c = \log_2 M$ is the number of bits per M -QAM symbol. The vector of bits corresponding to \mathbf{s} is denoted as \mathbf{b} , which satisfies $\mathbf{s} = \text{map}(\mathbf{b})$ and is formed by concatenating the N_t antennas' bits $\mathbf{d}_1, \mathbf{d}_2, \dots, \mathbf{d}_{N_t}$, yielding $\mathbf{b} = [b_1, b_2, \dots, b_k, \dots, b_{M_c N_t}]^T = [\mathbf{d}_1^T, \mathbf{d}_2^T, \dots, \mathbf{d}_{N_t}^T]^T \in \{+1, -1\}^{M_c N_t}$.

At the receiver of the SDM-MIMO system, the task of the conventional symbol-based PDA detector is to seek a small BER or SER by *estimating* the symbol APPs $P(s_j = a_m | \mathbf{y}) = P_m(s_j | \mathbf{y})$, without an exhaustive search in the space of all possible N_t -dimensional symbol vectors consisting of M -QAM symbol combinations. By contrast, in this chapter our goal is to attain a high detection performance by estimating the bit APPs $P(d_{j,q} = \pm 1 | \mathbf{y})$, $q = 1, 2, \dots, M_c$. Here, we would like to emphasize that the PDA detector provides the estimate of APPs, rather than the accurate APPs themselves.

2.3 UMR of QAM: Linear Natural Bit-to-Symbol Mapping

TABLE 2.1: Look-up table for Gray constellation mapping of 4-QAM

Bit Tuple	Constellation Symbol
$\{-1, -1\}$	$a_1 = -1 - i$
$\{-1, +1\}$	$a_2 = -1 + i$
$\{+1, +1\}$	$a_3 = +1 + i$
$\{+1, -1\}$	$a_4 = +1 - i$

Let us first review the conventional description of the bit-to-symbol mapping process of QAM [378]. Considering 4-QAM as an example,³ we have $\mathbb{A} = \{-1 - i, -1 + i, 1 + i, 1 - i\}$. Conventionally, each of the 2-bit tuples $(-1, -1)$, $(-1, +1)$, $(+1, +1)$ and $(+1, -1)$ is assigned an appropriate constellation symbol in the set \mathbb{A} according to the specific mapping rules; in other words, the bit-to-symbol mapping process is based on a look-up table method. To some extent, this method conceals the mathematical characteristic of a specific bit-to-symbol mapping process.

In MIMO systems, the mapping from bits to symbols may be compactly formulated by a unified transformation to be outlined below. Note that QAM signals are two-dimensional, i.e. we have $a_m = x + iy$, $\forall m \in \{1, 2, \dots, M\}$ where x and y are taken from the real alphabets \mathbb{A}^{real} and \mathbb{A}^{imag} , respectively. For simplicity, we assume that each transmit antenna uses the same modulation scheme of $\mathbb{A}^{\text{real}} = \mathbb{A}^{\text{imag}} = \underline{\mathbb{A}} = \{\alpha_1, \alpha_2, \dots, \alpha_{\sqrt{M}}\}$ for even-throughput rectangular QAM, although our approach may be generalized to different alphabets for the real and imaginary parts. Below We will expound the procedure of formulating the unified matrix representation (UMR) of the linear natural bit-to-symbol mapping based rectangular

³In practice, the symbol energy may be normalized by multiplying $\frac{1}{\sqrt{2}}$, $\frac{1}{\sqrt{10}}$, or $\frac{1}{\sqrt{42}}$ for 4-QAM, 16-QAM, 64-QAM, respectively.

QAM in Section 2.3 and the nonlinear binary reflected Gray mapping⁴ based rectangular QAM in Section 2.4, respectively.

Let us now consider the bit-to-symbol mapping function $s_j = \text{map}(\mathbf{d}_j)$ defined in Section 2.2, and rewrite this function as

$$s_j = s_j^{\Re} + i s_j^{\Im} = \text{map}\left(d_{j,1}^{\Re}, d_{j,2}^{\Re}, \dots, d_{j,M_c/2}^{\Re}, d_{j,M_c/2+1}^{\Im}, d_{j,M_c/2+2}^{\Im}, \dots, d_{j,M_c}^{\Im}\right), \quad (2.2)$$

where \Re and \Im indicate real and imaginary parts of s_j , respectively, and $s_j^{\Re}, s_j^{\Im} \in \underline{\mathbb{A}}$.

Since square QAM constellations having symmetric real and imaginary parts are considered here, it is sufficient to consider the real part only in the following derivation of the matrix representation without any loss of generality.

Let us assume that the elements of $\underline{\mathbb{A}}$ are placed in ascending order for constructing the vector $\mathbf{a} = [\alpha_1, \alpha_2, \dots, \alpha_{\sqrt{M}}]^T$ and denote the corresponding bit strings as the $(\sqrt{M} \times \frac{M_c}{2})$ -element matrix \mathbf{B} , in which the k th row is the bit string corresponding to α_k , $k = 1, 2, \dots, \sqrt{M}$. Then the bit-to-symbol mapping rule is described as

$$\mathbf{B}\mathbf{x} = \mathbf{a}, \quad (2.3)$$

where we would like to express \mathbf{x} , namely the “sub-generating unit”, which maps the bits to the real part of a QAM symbol. Furthermore, the vector $\mathbf{g} = [\mathbf{x}^T, i\mathbf{x}^T]$ is defined as the “generating unit” of M -QAM and it maps the bits to a QAM symbol.

2.3.1 Even-Throughput Rectangular QAM

2.3.1.1 4-QAM

Here we consider the linear natural mapping rules of Table 2.1, where $(-1, -1) \rightarrow a_1 = -1 - i$, $(-1, +1) \rightarrow a_2 = -1 + i$, $(+1, +1) \rightarrow a_3 = 1 + i$ and $(+1, -1) \rightarrow a_4 = 1 - i$. Thus the alphabet $\underline{\mathbb{A}}$ is given by $\underline{\mathbb{A}}_{4\text{-QAM}} = \{-1, +1\}$, $M_c = 2$, $\mathbf{B} = [-1; +1]$ (the different rows in \mathbf{B} are distinguished by “;”), and $\mathbf{a} = [-1, +1]^T$, hence $\mathbf{x} = 1$ according to Eq. (2.3).

For simplicity, let us use $N_t = 2$ as an example. Then the modulation matrix of 4-QAM is

$$\mathbf{W}_{4\text{-QAM}}^{N_t=2} = \begin{bmatrix} 1 & i & 0 & 0 \\ 0 & 0 & 1 & i \end{bmatrix}, \quad (2.4)$$

⁴Although there may be distinct Gray labellings that result in different bit-error probability, especially in high-order constellations, the binary reflected Gray mapping has been shown to give the lowest possible average probability of bit errors for conventional symbol-based detection under certain assumptions on the channel [380]. We will simply use “Gray mapping” to refer to the “binary reflected Gray mapping” in the rest of the chapter.

where $i = \sqrt{-1}$.

The above matrix may be readily generalized for 4-QAM in conjunction with an arbitrary N_t value as

$$\mathbf{W}_{4\text{-QAM}} = \begin{bmatrix} \mathbf{g}_{4\text{-QAM}} & \cdots & \mathbf{0} \\ \vdots & \ddots & \vdots \\ \mathbf{0} & \cdots & \mathbf{g}_{4\text{-QAM}} \end{bmatrix}_{N_t \times 2N_t}, \quad (2.5)$$

where the vector $\mathbf{g}_{4\text{-QAM}} = [1, i]$ represents the generating unit of 4-QAM.

It should be pointed out that the linear natural mapping presented here is the same as Gray mapping for 4-QAM. This observation will be beneficial for understanding the implications behind the matrix representation of Gray mapping based rectangular QAM in Section 2.4.

2.3.1.2 16-QAM

The alphabet $\underline{\mathbb{A}}$ is described by $\underline{\mathbb{A}}_{16\text{-QAM}} = \{-3, -1, +1, +3\}$, $M_c = 4$, $\mathbf{B} = [-1, -1; -1, +1; +1, -1; +1, +1]$, and $\mathbf{a} = [-3, -1, +1, +3]^T$, hence we have $\mathbf{x} = [2, 1]^T$ based on Eq. (2.3). Similarly to 4-QAM, the modulation matrix for $N_t = 2$ and for an arbitrary N_t value is given by

$$\mathbf{W}_{16\text{-QAM}}^{N_t=2} = \begin{bmatrix} 2 & 1 & 2i & i & 0 & 0 & 0 & 0 \\ 0 & 0 & 0 & 0 & 2 & 1 & 2i & i \end{bmatrix} \quad (2.6)$$

and

$$\mathbf{W}_{16\text{-QAM}} = \begin{bmatrix} \mathbf{g}_{16\text{-QAM}} & \cdots & \mathbf{0} \\ \vdots & \ddots & \vdots \\ \mathbf{0} & \cdots & \mathbf{g}_{16\text{-QAM}} \end{bmatrix}_{N_t \times 4N_t}, \quad (2.7)$$

respectively, where we have $\mathbf{g}_{16\text{-QAM}} = [2, 1, 2i, i]$.

It is observed that the linear natural mapping considered here is no longer the same as Gray mapping for 16-QAM. In this case, some neighboring labels have a Hamming distance of 1, while some have 2. For example, the labels $(-1, +1, -1, +1)$ and $(+1, -1, -1, +1)$ are assigned to adjacent constellation points.

2.3.1.3 64-QAM

The alphabet $\underline{\mathbb{A}}$ is given by $\underline{\mathbb{A}}_{64\text{-QAM}} = \{-7, -5, -3, -1, +1, +3, +5, +7\}$, $M_c = 6$, $\mathbf{B} = [-1, -1, -1; -1, -1, +1; -1, +1, -1; -1, +1, +1; +1, -1, -1; +1, -1, +1; +1, +1, -1; +1, +1, +1]$, and $\mathbf{a} = [-7, -5, -3, -1, +1, +3, +5, +7]^T$, thus we have $\mathbf{x} = [4, 2, 1]^T$ in the light of Eq. (2.3). Analogously, the modulation matrix for $N_t = 2$ and for an arbitrary N_t value is

formulated as

$$\mathbf{W}_{64\text{-QAM}}^{N_t=2} = \begin{bmatrix} 4 & 2 & 1 & 4i & 2i & i & 0 & 0 & 0 & 0 & 0 & 0 \\ 0 & 0 & 0 & 0 & 0 & 0 & 4 & 2 & 1 & 4i & 2i & i \end{bmatrix} \quad (2.8)$$

and

$$\mathbf{W}_{64\text{-QAM}} = \begin{bmatrix} \mathbf{g}_{64\text{-QAM}} & \cdots & \mathbf{0} \\ \vdots & \ddots & \vdots \\ \mathbf{0} & \cdots & \mathbf{g}_{64\text{-QAM}} \end{bmatrix}_{N_t \times 6N_t}, \quad (2.9)$$

respectively, where $\mathbf{g}_{64\text{-QAM}} = [4, 2, 1, 4i, 2i, i]$. The Hamming distances between neighboring constellation points in this case are still either 1 or 2, similarly to 16-QAM.

2.3.2 Odd-Throughput Rectangular QAM

The constellation size of the odd-throughput rectangular QAM is 2^{M_c} , $M_c = 2n + 1$, $n \in \{0, 1, 2, \dots\}$, while its even-throughput rectangular counterpart is 2^{M_c+1} -QAM. The former is essentially a subset of the latter, under the constraint of $\mathbb{A}_{2^{M_c}\text{-QAM}}^{\text{real(imag)}} = \mathbb{A}_{2^{M_c+1}\text{-QAM}}^{\text{real(imag)}}$, $\mathbb{A}_{2^{M_c}\text{-QAM}}^{\text{imag(real)}} = \text{Half}_{\text{sml-abs}} \left(\mathbb{A}_{2^{M_c+1}\text{-QAM}}^{\text{imag(real)}} \right)$, where $\text{Half}_{\text{sml-abs}}(\cdot)$ represents the half components of a set with the smallest absolute values. Therefore, it may be readily inferred that the maximum Hamming distance between the adjacent labels of the odd-throughput rectangular QAM is equal to 2 as well.

2.3.2.1 BPSK

Although the BPSK signal is not two-dimensional, it is reasonable to regard BPSK as a special case of an odd-throughput rectangular QAM signal with its imaginary part being 0. Since the BPSK constellation is $\{-1, +1\}$, with $M_c = 1$, its even-throughput rectangular QAM counterpart is 4-QAM, and the BPSK signal may be obtained by setting the imaginary part of 4-QAM to 0. Then the modulation matrix of BPSK for $N_t = 2$ and for an arbitrary N_t is

$$\mathbf{W}_{\text{BPSK}}^{N_t=2} = \begin{bmatrix} 1 & 0 \\ 0 & 1 \end{bmatrix} \quad (2.10)$$

and

$$\mathbf{W}_{\text{BPSK}} = \begin{bmatrix} \mathbf{g}_{\text{BPSK}} & \cdots & \mathbf{0} \\ \vdots & \ddots & \vdots \\ \mathbf{0} & \cdots & \mathbf{g}_{\text{BPSK}} \end{bmatrix}_{N_t \times N_t}, \quad (2.11)$$

respectively, where $\mathbf{g}_{\text{BPSK}} = 1$.

2.3.2.2 8-QAM

The alphabet is $\mathbb{A}_{8\text{-QAM}}^{\text{real}} = \{-3, -1, +1, +3\}$, $\mathbb{A}_{8\text{-QAM}}^{\text{imag}} = \{-1, +1\}$ for the real and imaginary parts of 8-QAM signals, respectively, and $M_c = 3$. Based on the modulation matrix of 16-QAM, the modulation matrix of 8-QAM when we have $N_t = 2$ or an arbitrary N_t value is

$$\mathbf{W}_{8\text{-QAM}}^{N_t=2} = \begin{bmatrix} 2 & 1 & i & 0 & 0 & 0 \\ 0 & 0 & 0 & 2 & 1 & i \end{bmatrix} \quad (2.12)$$

or

$$\mathbf{W}_{8\text{-QAM}} = \begin{bmatrix} \mathbf{g}_{8\text{-QAM}} & \cdots & \mathbf{0} \\ \vdots & \ddots & \vdots \\ \mathbf{0} & \cdots & \mathbf{g}_{8\text{-QAM}} \end{bmatrix}_{N_t \times 3N_t}, \quad (2.13)$$

respectively, where $\mathbf{g}_{8\text{-QAM}} = (2, 1, i)$.

2.3.2.3 32-QAM

The alphabet is $\mathbb{A}_{32\text{-QAM}}^{\text{real}} = \{-7, -5, -3, -1, +1, +3, +5, +7\}$, $\mathbb{A}_{32\text{-QAM}}^{\text{imag}} = \{-3, -1, +1, +3\}$, and $M_c = 5$. Based on the modulation matrix of 64-QAM, the modulation matrix of 32-QAM for $N_t = 2$ and for an arbitrary N_t value is

$$\mathbf{W}_{32\text{-QAM}}^{N_t=2} = \begin{bmatrix} 4 & 2 & 1 & 2i & i & 0 & 0 & 0 & 0 & 0 \\ 0 & 0 & 0 & 0 & 0 & 4 & 2 & 1 & 2i & i \end{bmatrix} \quad (2.14)$$

and

$$\mathbf{W}_{32\text{-QAM}} = \begin{bmatrix} \mathbf{g}_{32\text{-QAM}} & \cdots & \mathbf{0} \\ \vdots & \ddots & \vdots \\ \mathbf{0} & \cdots & \mathbf{g}_{32\text{-QAM}} \end{bmatrix}_{N_t \times 5N_t}, \quad (2.15)$$

respectively, where $\mathbf{g}_{32\text{-QAM}} = (4, 2, 1, 2i, i)$.

2.3.3 General M -QAM

From the above derivations for 4-QAM, 16-QAM and 64-QAM, we find that the “generating unit” \mathbf{g} of each considered constellation is determined by the largest element value of its alphabet. The specific value of \mathbf{g} is given by the exponential expansion of the largest value in the alphabet, such as for instance, $7 = 2^2 + 2^1 + 2^0 = 4 + 2 + 1$ for 64-QAM, $3 = 2^1 + 2^0 = 2 + 1$ for 16-QAM, $1 = 2^0 = 1$ for 4-QAM. Therefore, we can infer that for

general even-throughput rectangular QAM, the modulation matrix is given by

$$\mathbf{W}_{\text{even-QAM}} = \begin{bmatrix} \mathbf{g}_{\text{even-QAM}} & \cdots & \mathbf{0} \\ \vdots & \ddots & \vdots \\ \mathbf{0} & \cdots & \mathbf{g}_{\text{even-QAM}} \end{bmatrix}_{N_t \times M_c N_t}, \quad (2.16)$$

where $\mathbf{g}_{\text{even-QAM}} = [2^{\frac{M_c}{2}-1}, 2^{\frac{M_c}{2}-2}, \dots, 1, 2^{\frac{M_c}{2}-1}i, 2^{\frac{M_c}{2}-2}i, \dots, i]$. for even-throughput rectangular QAM.

On the other hand, assuming that the real alphabet of 2^{M_c} -QAM is the same as that of 2^{M_c+1} -QAM, $M_c = 2n + 1, n \in \{0, 1, 2, \dots\}$, we may similarly conclude from the modulation matrices of BPSK, 8-QAM, 32-QAM given in equations (2.11), (2.13), and (2.15) that the general modulation matrix of the odd-throughput rectangular QAM is given by

$$\mathbf{W}_{\text{odd-QAM}} = \begin{bmatrix} \mathbf{g}_{\text{odd-QAM}} & \cdots & \mathbf{0} \\ \vdots & \ddots & \vdots \\ \mathbf{0} & \cdots & \mathbf{g}_{\text{odd-QAM}} \end{bmatrix}_{N_t \times M_c N_t}, \quad (2.17)$$

where $\mathbf{g}_{\text{odd-QAM}} = [2^{\frac{M_c-1}{2}}, 2^{\frac{M_c-1}{2}-1}, \dots, 1, 2^{\frac{M_c-1}{2}-1}i, \dots, i]$, including BPSK as a special case of an odd-throughput rectangular QAM signal with its imaginary part being 0.

When the imaginary alphabet of 2^{M_c} -QAM is assumed to be the same as that of 2^{M_c+1} -QAM, $M_c = 2n + 1, n \in \{0, 1, 2, \dots\}$, the $\mathbf{g}_{\text{odd-QAM}} = [2^{\frac{M_c-1}{2}-1}, \dots, 1, 2^{\frac{M_c-1}{2}}i, 2^{\frac{M_c-1}{2}-1}i, \dots, i]$. Therefore, the general modulation matrix of the odd-throughput rectangular QAM is a modified version of the general modulation matrix of the even-throughput rectangular QAM,

Consequently the mapping function $\mathbf{s} = \text{map}(\mathbf{b})$ in Section 2.2 may be characterized by $\mathbf{s} = \mathbf{W}\mathbf{b}$ for MIMO systems using the linear natural mapping based rectangular QAM.

Specifically, the first row of the matrix \mathbf{W} maps the first M_c bits of the $M_c N_t$ -bit vector \mathbf{b} to the transmitted symbol of the first antenna, while the second row maps the second M_c bits to the transmitted symbol of the second antenna. The functionality of the other rows may be deduced by analogy.

2.4 UMR of QAM: Nonlinear Gray Bit-to-Symbol Mapping

In Section 2.3, we presented a UMR of general rectangular QAM constellations using linear natural mapping for MIMO systems. The limitation of this matrix representation is, however, that it did not provide the nonlinear Gray mapping for rectangular QAM constellations having cardinality larger than 4 (for 4-QAM, the linear natural and the Gray bit-to-symbol mappings are identical). Consequently, since the binary reflected Gray mapping was shown

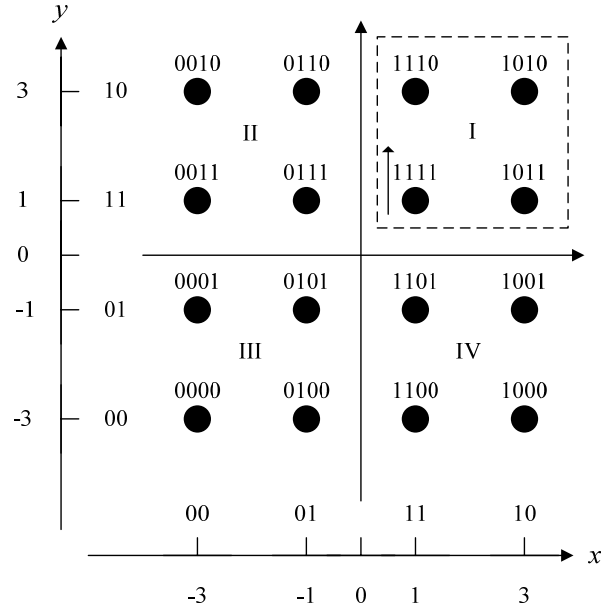


FIGURE 2.1: Signal space diagram for 16-QAM under Gray mapping.

to be the optimal labelling scheme [380], two interesting questions arise: 1) Would the linear natural mapping based B-PDA detector's performance degrade for high-order QAM owing to the lack of Gray mapping in the context of FEC-uncoded systems? 2) Is the Gray mapping still the best labelling scheme for the B-PDA MIMO detector?⁵ In order to answer these questions, in this section, we extend the previous linear natural mapping based results to the nonlinear Gray mapping case. In contrast to the linear natural bit-to-symbol mapping scenario, the matrix representation of Gray mapping depends on the bits to be transmitted, as detailed below.

2.4.1 16-QAM

According to Eq. (2.3) and to the Gray mapping rule of Fig. 2.1, we have $\mathbf{a} = [-3, -1, +1, +3]^T$, $\mathbf{x} = [a, b]^T$, and the original Gray mapping based bits 00, 01, 11, 10 are converted into the bipolar representation of $\mathbf{B} = [-1, -1; -1, +1; +1, +1; +1, -1]$ under the rule of $2b_i - 1$, where b_i , $i = 1, 2$, is a binary digit of 0 or 1. Upon substituting \mathbf{a} , \mathbf{B} and \mathbf{x} into Eq. (2.3), we find that \mathbf{x} does not have a unique solution owing to the nonlinear nature of Gray mapping. However, each of the following two sub-systems of equations has a unique solution:

$$\begin{cases} -a - b = -3 \\ -a + b = -1 \end{cases} \Rightarrow a = 2, b = 1, \quad (2.18)$$

⁵For coded system using iterative joint detection and decoding, Gray mapping is generally the most unfavorable one, because it has an almost horizontal extrinsic information transfer (EXIT) function, see [381].

TABLE 2.2: Generating units of 16-QAM using Gray mapping

Index	Generating Unit	Bit Sequence	Symbol	Quadrant	Index	Generating Unit	Bit Sequence	Symbol	Quadrant
1	$2 - 1 - 2i - i$	-1 -1 -1 -1	$-3 - 3i$	III	9	$2 - 1 - 2i - i$	1 1 -1 -1	$1 - 3i$	IV
2	$2 - 1 - 2i - i$	-1 -1 -1 1	$-3 - i$		10	$2 - 1 - 2i - i$	1 1 -1 1	$1 - i$	
3	$2 - 1 - 2i - i$	-1 -1 1 1	$-3 + i$	II	11	$2 - 1 - 2i - i$	1 1 1 1	$1 + i$	I
4	$2 - 1 - 2i - i$	-1 -1 1 -1	$-3 + 3i$		12	$2 - 1 - 2i - i$	1 1 1 -1	$1 + 3i$	
5	$2 - 1 - 2i - i$	-1 1 1 -1	$-1 + 3i$		13	$2 - 1 - 2i - i$	1 -1 1 -1	$3 + 3i$	
6	$2 - 1 - 2i - i$	-1 1 1 1	$-1 + i$		14	$2 - 1 - 2i - i$	1 -1 1 1	$3 + i$	
7	$2 - 1 - 2i - i$	-1 1 -1 1	$-1 - i$	III	15	$2 - 1 - 2i - i$	1 -1 -1 1	$3 - i$	IV
8	$2 - 1 - 2i - i$	-1 1 -1 -1	$-1 - 3i$		16	$2 - 1 - 2i - i$	1 -1 -1 -1	$3 - 3i$	

$$\begin{cases} a + b = +1 \\ a - b = +3 \end{cases} \Rightarrow a = 2, b = -1. \quad (2.19)$$

We can observe that there are only two possible solution vectors i.e. $\mathbf{x}_1 = [2, 1]^T$ and $\mathbf{x}_2 = [2, -1]^T$ for Eq. (2.18) and Eq. (2.19) in which -1 and $+1$ are the first bit, respectively. Therefore in practice the choice of the generating unit depends on the first bit of each consecutive 2-bit tuple. For example, if the 2-bit tuple is $(-1, x)$, then the corresponding sub-generating unit is $(a = 2, b = 1)$, and if the 2-bit tuple is $(1, x)$ then $(a = 2, b = -1)$, where x is -1 or 1 . The complete generating units derived for every 4-bit tuple are seen in Table 2.2 and detailed as follows.

By jointly considering Fig. 2.1 and Table 2.2, we may infer several pieces of useful information for 16-QAM. 1) Firstly, the component having the largest modulus in the generating unit remains the same as that of its counterpart in linear natural mapping, but the signs of the smaller components may change. 2) Secondly, the constellation points which are in the same quadrant share the same generating unit, as exemplified by the dash box in Fig. 2.1. 3) Thirdly, the constellation points in the same half plane of Fig. 2.1 are explicitly described by one sub-system of equations, i.e. (2.18) describes the left half plane, while (2.19) describes the right half plane.

2.4.2 64-QAM

According to Eq. (2.3) and to the Gray mapping rule shown in Fig. 2.2, we have $\mathbf{a} = [-7, -5, -3, -1, +1, +3 + 5, +7]^T$, $\mathbf{x} = [a, b, c]^T$, and the original Gray mapping based bits 000, 001, 011, 010, 110, 111, 101, 100 are converted into the bipolar representation of $\mathbf{B} = [-1, -1, -1; -1, -1, +1; -1, +1, +1; -1, +1, -1; +1, +1, -1; +1, +1, +1; +1, -1, +1; +1, -1, -1]$ under the rule of $2b_i - 1$, where b_i , $i = 1, 2$, is a binary digit of 0 or 1. Substituting \mathbf{a} , \mathbf{B} and \mathbf{x} into Eq. (2.3), again, owing to the non-linearity of Gray mapping, \mathbf{x} does not have a

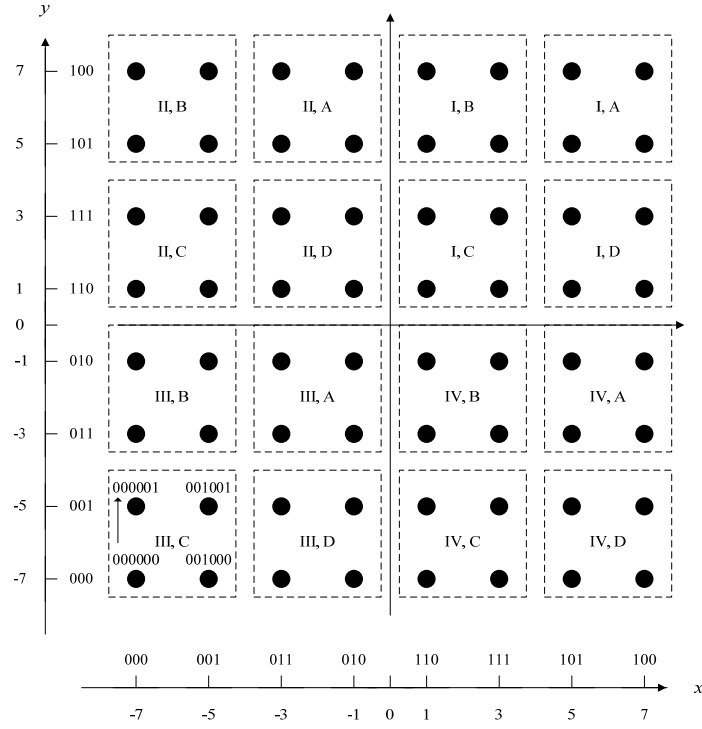


FIGURE 2.2: Signal space diagram for 64-QAM under Gray mapping.

unique solution. However, each of the following four sub-systems of equations has a unique solution:

$$\left\{ \begin{array}{l} i) \begin{cases} -a - b - c = -7 \\ -a - b + c = -5 \end{cases} \Rightarrow a = 4, b = 2, c = 1 \\ ii) \begin{cases} -a + b + c = -3 \\ -a + b - c = -1 \end{cases} \Rightarrow a = 4, b = 2, c = -1 \end{array} \right. \quad (2.20)$$

$$\left\{ \begin{array}{l} iii) \begin{cases} a + b - c = 1 \\ a + b + c = 3 \end{cases} \Rightarrow a = 4, b = -2, c = 1 \\ iv) \begin{cases} a - b + c = 5 \\ a - b - c = 7 \end{cases} \Rightarrow a = 4, b = -2, c = -1 \end{array} \right. \quad (2.21)$$

We can observe in Eq. (2.20) and Eq. (2.21) that there are four possible solution vectors, i.e. $\mathbf{x}_1 = [4, 2, 1]^T$, $\mathbf{x}_2 = [4, 2, -1]^T$, $\mathbf{x}_3 = [4, -2, 1]^T$ and $\mathbf{x}_4 = [4, -2, -1]^T$ corresponding to four 3-bit tuples (every three adjacent bits as a unit) in which $(-1, -1)$, $(-1, 1)$, $(1, 1)$ and $(1, -1)$ are the first two bits, respectively. Hence for Gray mapping, the sub-generating unit has the above-mentioned four legitimate values of (a, b, c) . For example, if the 3-bit tuple to be transmitted is $(-1, -1, x)$, then its corresponding sub-generating unit is $(a = 4, b = 2, c = 1)$,

and if the 3-bit tuple is $(1, -1, x)$, then we have $(a = 4, b = -2, c = -1)$, where x is -1 or 1 . The complete set of generating units for 64-QAM is shown in Table 2.3 and discussed below.

Again, we jointly consider Fig. 2.2 and Table 2.3. We find that Conclusion 1) drawn for 16-QAM still holds for 64-QAM. Conclusion 2) derived for 16-QAM, however, should be refined to state that it is the set of constellation points, which dwell in the same four-point-block within the dashed box of Fig. 2.2 that share the same generating unit, rather than all within the entire quadrant, which was the case for 16-QAM. Nonetheless, we observe that 16-QAM is divided into 4 four-point-blocks and has 4 different generating units made of 2 different sub-generating units, while 64-QAM is divided into 16 four-point-blocks and has 16 different generating units constructed by 4 different sub-generating units.

Furthermore, the constellation points in the same half plane are still described by Eq. (2.20) (the left half plane) and Eq. (2.21) (the right half plane), each of which is composed by two further sets of equations, as seen in i), ii), iii) and iv) of Eq. (2.20) and Eq. (2.21), respectively. In addition, it is plausible that the solution of (a, b, c) for each of i), ii), iii) and iv) is unique under the constraint that i) and ii) constituting the left half plane share the same values of (a, b) , and so do iii) and iv) constituting the right half plane.

2.4.3 General M -QAM

Based on the above insights drawn from 16-QAM and 64-QAM, the UMR of the most commonly used Gray mapping may be obtained by appropriately alternating the sign of certain entries in the above static UMR of the linear natural mapping based QAM, which in fact serves as the basis matrix for Gray mapping aided QAM and may be prestored for access. The corresponding procedures are summarized as follows.

- 1) Generate the UMR of the linear natural bit mapping, i.e. \mathbf{W} according to Eq. (2.16), which serves as the base matrix of the UMR of Gray mapping.
- 2) Check the sign of the bipolar bits in \mathbf{b} , and adjust the sign of the corresponding entries in \mathbf{W} accordingly. The sign of the first element of the real and imaginary part in \mathbf{g} is always positive, while the signs of the remaining elements should be changed according to the various combinations of the residue bits. When taking into account the symmetry of the real and imaginary parts of the QAM constellation points and excluding the specific combination where each element is positive, the number of additional different cases—the number of additional sub-generating units is $2^{\frac{M_c}{2}-1} - 1$ for the square QAM and $2^{\frac{M_c-1}{2}} - 1$ for the odd rectangular QAM. The selection of the appropriate generating unit is illuminated using 16-QAM and 64-QAM as our examples in Table 2.4. For ease of exposition, Matlab-style pseudo-code is used.

TABLE 2.3: Generating units of 64-QAM using Gray mapping

Index	Generating Unit	Bit Sequence	Symbol	Quadrant	Index	Generating Unit	Bit Sequence	Symbol	Quadrant
1	$4 2 1 4i 2i i$	-1 -1 -1 -1 -1 -1	$-7 - 7i$	III, C	33	$4 -2 1 4i 2i i$	1 1 -1 -1 -1 -1	$1 - 7i$	IV, C
2	$4 2 1 4i 2i i$	-1 -1 -1 -1 -1 1	$-7 - 5i$		34	$4 -2 1 4i 2i i$	1 1 -1 -1 -1 1	$1 - 5i$	
3	$4 2 1 4i 2i -i$	-1 -1 -1 -1 1 1	$-7 - 3i$	III, B	35	$4 -2 1 4i 2i -i$	1 1 -1 -1 1 1	$1 - 3i$	IV, B
4	$4 2 1 4i 2i -i$	-1 -1 -1 -1 1 -1	$-7 - i$		36	$4 -2 1 4i 2i -i$	1 1 -1 -1 1 -1	$1 - i$	
5	$4 2 1 4i -2i i$	-1 -1 -1 1 1 -1	$-7 + i$	II, C	37	$4 -2 1 4i -2i i$	1 1 -1 1 1 -1	$1 + i$	I, C
6	$4 2 1 4i -2i i$	-1 -1 -1 1 1 1	$-7 + 3i$		38	$4 -2 1 4i -2i i$	1 1 -1 1 1 1	$1 + 3i$	
7	$4 2 1 4i -2i -i$	-1 -1 -1 1 -1 1	$-7 + 5i$	II, B	39	$4 -2 1 4i -2i -i$	1 1 -1 1 -1 1	$1 + 5i$	I, B
8	$4 2 1 4i -2i -i$	-1 -1 -1 1 -1 -1	$-7 + 7i$		40	$4 -2 1 4i -2i -i$	1 1 -1 1 -1 -1	$1 + 7i$	
9	$4 2 1 4i -2i -i$	-1 -1 1 1 -1 -1	$-5 + 7i$		41	$4 -2 1 4i -2i -i$	1 1 1 1 -1 -1	$3 + 7i$	
10	$4 2 1 4i -2i -i$	-1 -1 1 1 -1 1	$-5 + 5i$		42	$4 -2 1 4i -2i -i$	1 1 1 1 -1 1	$3 + 5i$	
11	$4 2 1 4i -2i i$	-1 -1 1 1 1 1	$-5 + 3i$	II, C	43	$4 -2 1 4i -2i i$	1 1 1 1 1 1	$3 + 3i$	I, C
12	$4 2 1 4i -2i i$	-1 -1 1 1 1 -1	$-5 + i$		44	$4 -2 1 4i -2i i$	1 1 1 1 1 -1	$3 + i$	
13	$4 2 1 4i 2i -i$	-1 -1 1 -1 1 -1	$-5 - i$	III, B	45	$4 -2 1 4i 2i -i$	1 1 1 -1 1 -1	$3 - i$	IV, B
14	$4 2 1 4i 2i -i$	-1 -1 1 -1 1 1	$-5 - 3i$		46	$4 -2 1 4i 2i -i$	1 1 1 -1 1 1	$3 - 3i$	
15	$4 2 1 4i 2i i$	-1 -1 1 -1 -1 1	$-5 - 5i$	III, C	47	$4 -2 1 4i 2i i$	1 1 1 -1 -1 1	$3 - 5i$	IV, C
16	$4 2 1 4i 2i i$	-1 -1 1 -1 -1 -1	$-5 - 7i$		48	$4 -2 1 4i 2i i$	1 1 1 -1 -1 -1	$3 - 7i$	
17	$4 2 -1 4i 2i i$	-1 1 1 -1 -1 -1	$-3 - 7i$	III, D	49	$4 -2 -1 4i 2i i$	1 -1 1 -1 -1 -1	$5 - 7i$	IV, D
18	$4 2 -1 4i 2i i$	-1 1 1 -1 -1 1	$-3 - 5i$		50	$4 -2 -1 4i 2i i$	1 -1 1 -1 -1 1	$5 - 5i$	
19	$4 2 -1 4i 2i -i$	-1 1 1 -1 1 1	$-3 - 3i$	III, A	51	$4 -2 -1 4i 2i -i$	1 -1 1 -1 1 1	$5 - 3i$	IV, A
20	$4 2 -1 4i 2i -i$	-1 1 1 -1 1 -1	$-3 - i$		52	$4 -2 -1 4i 2i -i$	1 -1 1 -1 1 -1	$5 - i$	
21	$4 2 -1 4i -2i i$	-1 1 1 1 1 -1	$-3 + i$	II, D	53	$4 -2 -1 4i -2i i$	1 -1 1 1 1 -1	$5 + i$	I, D
22	$4 2 -1 4i -2i i$	-1 1 1 1 1 1	$-3 + 3i$		54	$4 -2 -1 4i -2i i$	1 -1 1 1 1 1	$5 + 3i$	
23	$4 2 -1 4i -2i -i$	-1 1 1 1 -1 1	$-3 + 5i$	II, A	55	$4 -2 -1 4i -2i -i$	1 -1 1 1 -1 1	$5 + 5i$	I, A
24	$4 2 -1 4i -2i -i$	-1 1 1 1 -1 -1	$-3 + 7i$		56	$4 -2 -1 4i -2i -i$	1 -1 1 1 -1 -1	$5 + 7i$	
25	$4 2 -1 4i -2i -i$	-1 1 -1 1 -1 -1	$-1 + 7i$		57	$4 -2 -1 4i -2i -i$	1 -1 -1 1 -1 -1	$7 + 7i$	
26	$4 2 -1 4i -2i -i$	-1 1 -1 1 -1 1	$-1 + 5i$		58	$4 -2 -1 4i -2i -i$	1 -1 -1 1 -1 1	$7 + 5i$	
27	$4 2 -1 4i -2i i$	-1 1 -1 1 1 1	$-1 + 3i$	II, D	59	$4 -2 -1 4i -2i i$	1 -1 -1 1 1 1	$7 + 3i$	I, D
28	$4 2 -1 4i -2i i$	-1 1 -1 1 1 -1	$-1 + i$		60	$4 -2 -1 4i -2i i$	1 -1 -1 1 1 -1	$7 + i$	
29	$4 2 -1 4i 2i -i$	-1 1 -1 -1 1 -1	$-1 - i$	III, A	61	$4 -2 -1 4i 2i -i$	1 -1 -1 -1 1 -1	$7 - i$	IV, A
30	$4 2 -1 4i 2i -i$	-1 1 -1 -1 1 1	$-1 - 3i$		62	$4 -2 -1 4i 2i -i$	1 -1 -1 -1 1 1	$7 - 3i$	
31	$4 2 -1 4i 2i i$	-1 1 -1 -1 -1 1	$-1 - 5i$	III, D	63	$4 -2 -1 4i 2i i$	1 -1 -1 -1 -1 1	$7 - 5i$	IV, D
32	$4 2 -1 4i 2i i$	-1 1 -1 -1 -1 -1	$-1 - 7i$		64	$4 -2 -1 4i 2i i$	1 -1 -1 -1 -1 -1	$7 - 7i$	

TABLE 2.4: UMR rule of Gray mapping

16-QAM ($M_c = 4$)	64-QAM ($M_c = 6$)
for $k = 1: \frac{M_c}{2}: M_c N_t$ for $j = 1: N_t$ if $b_k == 1$ $\mathbf{W}(j, k + 1) = -\mathbf{W}(j, k + 1)$ end end end	for $k = 1: \frac{M_c}{2}: M_c N_t$ for $j = 1: N_t$ if $b_k == 1 \ \&\& \ b_{k+1} == 1$ $\mathbf{W}(j, k + 1) = -\mathbf{W}(j, k + 1)$ elseif $b_k == -1 \ \&\& \ b_{k+1} == 1$ $\mathbf{W}(j, k + 2) = -\mathbf{W}(j, k + 2)$ elseif $b_k == 1 \ \&\& \ b_{k+1} == -1$ $\mathbf{W}(j, k + 1) = -\mathbf{W}(j, k + 1)$ $\mathbf{W}(j, k + 2) = -\mathbf{W}(j, k + 2)$ end end end

Therefore, the mapping function $\mathbf{s} = \text{map}(\mathbf{b})$ in Section 2.2 may be formulated as $\mathbf{s} = \mathbf{W}(\mathbf{b})\mathbf{b}$ for MIMO systems using the nonlinear Gray mapping based rectangular QAM.

In fact, it may be readily shown that not only the natural and Gray mapping, but any regular bit mapping rule devised for rectangular QAM can be represented using the above-mentioned alternating-sign approach based on the linear natural bit mapping UMR.

2.5 B-PDA MIMO Detection based on UMR

We have provided a UMR of the rectangular M -QAM. Given the UMR, diverse MIMO signal processing problems involving high-order rectangular QAM may be simplified to a BPSK scenario, hence potentially reducing the computational complexity. Below we will further develop the conventional symbol-based PDA MIMO detector of [234] to a reduced-complexity bit-based approach.

2.5.1 Basic Detection Algorithm

Based on the UMR of QAM, we have $\mathbf{s} = \mathbf{W}\mathbf{b}$ and $\mathbf{s} = \mathbf{W}(\mathbf{b})\mathbf{b}$ for the linear natural mapping and nonlinear Gray mapping, respectively. For ease of exposition, we will take the linear mapping based rectangular QAM as an example to elaborate on the B-PDA detector. Thus the original system model of (2.1) may be rewritten as

$$\mathbf{y} = \mathbf{H}\mathbf{W}\mathbf{b} + \mathbf{n} = \mathbf{Q}\mathbf{b} + \mathbf{n}, \quad (2.22)$$

where $\mathbf{Q} = \mathbf{H}\mathbf{W}$ captures the combined effect of both the channel matrix and of the bit-to-symbol mapping matrix. We can see from Eq. (2.22) that the original QAM detection problem has been transformed into an equivalent BPSK detection model.

Adopting the non-decorrelated signal model of [230], Eq. (2.22) can be further reformulated as

$$\mathbf{y} = \mathbf{q}_l b_l + \sum_{k \neq l} \mathbf{q}_k b_k + \mathbf{n} \triangleq \mathbf{q}_l b_l + \mathbf{v}_l, \quad (2.23)$$

where \mathbf{q}_l denotes the l th column of \mathbf{Q} , and b_l is the l th bit of \mathbf{b} , while \mathbf{v}_l is the interference-plus-noise term contaminating bit b_l , which will be approximated by a Gaussian random vector, $l, k = 1, 2, \dots, M_c N_t$. Consequently, (2.23) becomes reminiscent of the classic single-input multiple-output transmission model subjected to AWGN. More explicitly, since \mathbf{q}_l is a known vector, the random vector $\mathbf{y}|b_l$ also obeys the Gaussian distribution conditioned on b_l .

For the transmitted bit vector \mathbf{b} , we define an $M_c N_t \times 2$ probability matrix $\mathbf{P}^{(z)}$ whose (l, n) th element $\Pr^{(z)}(b_l = u_n | \mathbf{y})$ is the *estimate* of the APP that $b_l = u_n$ at the z th iteration, where z is a non-negative integer, $n = 1, 2$ and $u_1 = +1$, $u_2 = -1$. The key idea of the PDA algorithm [219] is to iteratively approximate the interference-plus-noise term \mathbf{v}_l as an ever-updated N_r -variate colored Gaussian distributed random variable with a mean of

$$\boldsymbol{\mu}_l \triangleq \mathcal{E}(\mathbf{v}_l) = \sum_{k \neq l} \mathcal{E}(b_k) \mathbf{q}_k, \quad (2.24)$$

covariance of

$$\boldsymbol{\Upsilon}_l \triangleq \mathcal{C}(\mathbf{v}_l) = \sum_{k \neq l} \mathcal{C}(b_k) \mathbf{q}_k \mathbf{q}_k^H + N_0 \mathbf{I}, \quad (2.25)$$

and pseudo-covariance of

$$\boldsymbol{\Omega}_l \triangleq \mathcal{C}_p(\mathbf{v}_l) = \sum_{k \neq l} \mathcal{C}_p(b_k) \mathbf{q}_k \mathbf{q}_k^T, \quad (2.26)$$

where

$$\mathcal{E}(b_k) = \sum_{n=1}^2 u_n \Pr^{(z)}(b_k = u_n | \mathbf{y}), \quad (2.27)$$

$$\mathcal{C}(b_k) = \sum_{n=1}^2 [u_n - \mathcal{E}(b_k)][u_n - \mathcal{E}(b_k)]^* \Pr^{(z)}(b_k = u_n | \mathbf{y}), \quad (2.28)$$

$$\mathcal{C}_p(b_k) = \sum_{n=1}^2 [u_n - \mathcal{E}(b_k)][u_n - \mathcal{E}(b_k)]^T \Pr^{(z)}(b_k = u_n | \mathbf{y}). \quad (2.29)$$

Since b_k has real value, $\mathcal{C}(b_k)$ is identical to $\mathcal{C}_p(b_k)$. Here $\Pr^{(z)}(b_k = u_n | \mathbf{y})$ is initialized as a uniform distribution and will be replaced with an updated bit-probability at the $(z + 1)$ th iteration of the B-PDA detector.

Let

$$\mathbf{w} = \mathbf{y} - b_l \mathbf{q}_l - \boldsymbol{\mu}_l \quad (2.30)$$

and

$$p^{(z+1)}(\mathbf{y}|b_l = u_n) \propto \varphi_n^{(z+1)}(b_l) \triangleq \exp \left(- \begin{pmatrix} \Re(\mathbf{w}) \\ \Im(\mathbf{w}) \end{pmatrix}^T \mathbf{\Lambda}_l^{-1} \begin{pmatrix} \Re(\mathbf{w}) \\ \Im(\mathbf{w}) \end{pmatrix} \right), \quad (2.31)$$

where we have

$$\mathbf{\Lambda}_l \triangleq \begin{pmatrix} \Re(\mathbf{\Upsilon}_l + \mathbf{\Omega}_l) & -\Im(\mathbf{\Upsilon}_l - \mathbf{\Omega}_l) \\ \Im(\mathbf{\Upsilon}_l + \mathbf{\Omega}_l) & \Re(\mathbf{\Upsilon}_l - \mathbf{\Omega}_l) \end{pmatrix}, \quad (2.32)$$

while $\Re(\cdot)$ and $\Im(\cdot)$ represent the real and imaginary part of a complex variable, respectively.

Since there is no external source of *a priori* probabilities for the transmitted bits, the bitwise APP is approximated as

$$\Pr^{(z+1)}(b_l = u_n|\mathbf{y}) \approx \frac{p^{(z+1)}(\mathbf{y}|b_l = u_n)}{\sum_{n=1}^2 p^{(z+1)}(\mathbf{y}|b_l = u_n)} = \frac{\varphi_n^{(z+1)}(b_l)}{\sum_{n=1}^2 \varphi_n^{(z+1)}(b_l)}. \quad (2.33)$$

In summary, according to Fig. 2.3, the B-PDA algorithm proceeds as follows.

Step 1: Initialization: set the iteration counter to $z = 0$; set the initial value of $\mathbf{P}^{(z)}$, i.e. the initial values of the bit probabilities $\Pr^{(z)}(b_l = u_n|\mathbf{y})$ using a uniform distribution, $\forall l = 1, 2, \dots, M_c N_t, \forall n = 1, 2$, i.e. $\Pr^{(0)}(b_l = u_n|\mathbf{y}) = 0.5$.

Step 2: Set the bit index to $l = 1$.

Step 3: Based on the current values of $\{\mathbf{P}^{(z)}(k, :)\}_{k \neq l}$, compute $\Pr^{(z+1)}(b_l = u_n|\mathbf{y})$ for $\mathbf{P}^{(z+1)}$ using (2.24) - (2.33), which represents an updated value corresponding to the (l, n) th element of $\mathbf{P}^{(z)}$. Here $\mathbf{P}^{(z)}(k, :)$ represents the k th row of $\mathbf{P}^{(z)}$.

Step 4: If $l \leq M_c N_t$, let $l = l + 1$ and go to step 3). Otherwise, go to step 5).

Step 5: If \mathbf{P} has converged, i.e. $|\mathbf{P}^{(z+1)}(l, n) - \mathbf{P}^{(z)}(l, n)| < \epsilon, \forall l$ and $\forall n$, where ϵ is a small positive real number; or if the iteration index z has reached its maximum z_{\max} , go to step 6). Otherwise, let $z = z + 1$ and return to step 2).

Step 6: For $l = 1, 2, \dots, M_c N_t$, make a decision concerning \hat{b}_l using $\hat{b}_l = u_d, d = \arg \max_{n=1,2} \{\Pr^{(z+1)}(b_l = u_n|\mathbf{y})\}$, yielding $\hat{\mathbf{b}} = \{\hat{b}_l | l = 1, 2, \dots, M_c N_t\}$.

For the sake of clarity, the flow chart of the B-PDA algorithm is given in Fig. 2.3.

2.5.2 Example of the B-PDA

In order to illuminate the operating procedures of the proposed B-PDA detector in a more explicit manner, let us consider the same simple example as in Section 1.7, where we have

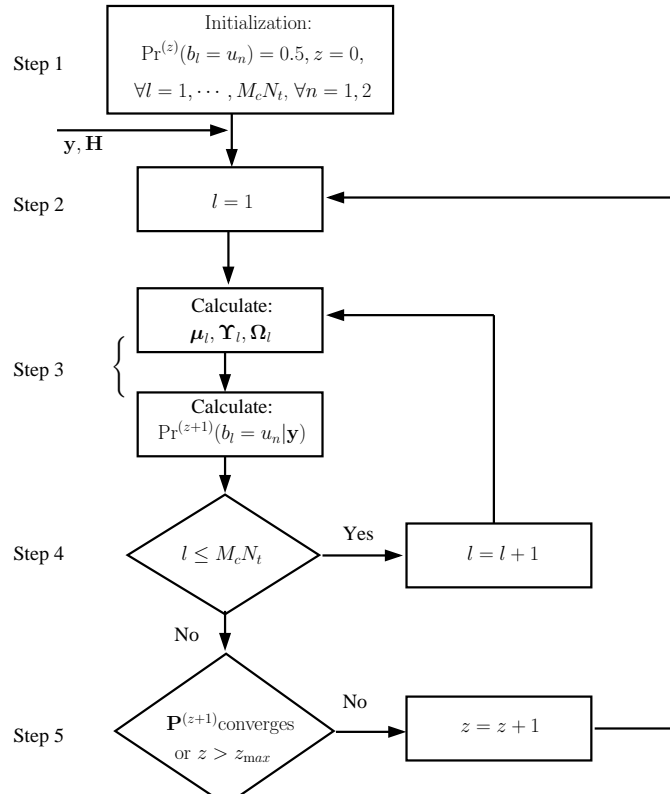


FIGURE 2.3: Flow chart of the B-PDA algorithm.

$N_t = 2$ and 4-QAM. Additionally, we assume that the convergence tolerance $\epsilon = 0.001$ and the maximum iteration number $z_{\max} = 5$ in the B-PDA algorithm. The modulation matrix \mathbf{W} is given by (2.4), and the 4-QAM symbol vector is formulated as

$$\mathbf{s} = \begin{bmatrix} s_1 \\ s_2 \end{bmatrix} = \begin{bmatrix} 1 + i \\ -1 + i \end{bmatrix} = \mathbf{W}\mathbf{b} = \begin{bmatrix} 1 & i & 0 & 0 \\ 0 & 0 & 1 & i \end{bmatrix} \begin{bmatrix} 1 \\ 1 \\ -1 \\ 1 \end{bmatrix}. \quad (2.34)$$

Hence, the “composite channel matrix” \mathbf{Q} of (2.22), which encapsulates both the channel matrix \mathbf{H} and the bit-to-symbol mapping matrix \mathbf{W} , can be expressed as

$$\begin{aligned} \mathbf{Q} = \mathbf{HW} &= \begin{bmatrix} 5 + 2i & -2 - i \\ 3 - 2i & 4 + 3i \end{bmatrix} \begin{bmatrix} 1 & i & 0 & 0 \\ 0 & 0 & 1 & i \end{bmatrix} \\ &= \begin{bmatrix} 5 + 2i & -2 + 5i & -2 - i & 1 - 2i \\ 3 - 2i & 2 + 3i & 4 + 3i & -3 + 4i \end{bmatrix}. \end{aligned} \quad (2.35)$$

Hence the received signal of (1.8) can be reformulated as

$$\begin{aligned}
\mathbf{y} &= \mathbf{Q}\mathbf{b} + \mathbf{n} \\
&= \begin{bmatrix} 5 + 2i & -2 + 5i & -2 - i & 1 - 2i \\ 3 - 2i & 2 + 3i & 4 + 3i & -3 + 4i \end{bmatrix} \begin{bmatrix} 1 \\ 1 \\ -1 \\ 1 \end{bmatrix} + \begin{bmatrix} 0.5 + 0.4i \\ 0.2 - 0.6i \end{bmatrix} \\
&= \begin{bmatrix} 6.5 + 6.4i \\ -1.8 + 1.4i \end{bmatrix}.
\end{aligned} \tag{2.36}$$

Then, according to the B-PDA algorithm procedures described in Fig. 2.3 and at the end of Section 2.5.1, the decision probabilities associated with each bit are calculated as follows.

Step 1: The decision probabilities associated with each bit are uniformly initialized, as shown in Table 2.5(a), where z is initially set to zero.

Step 2: Without loss of generality, set the bit index to $l = 1$, which means we will update the decision probabilities for b_1 . More specifically, let us now start to update Table 2.5(a) from its first row, namely $\mathbf{P}(1, :)$, which represents the current value of $\Pr^{(z)}(b_1 = \pm 1 | \mathbf{y})$. Then, according to (2.23), (2.36) can be further rewritten as

$$\mathbf{y} = \underbrace{\begin{bmatrix} 5 + 2i \\ 3 - 2i \end{bmatrix}}_{\mathbf{q}_1 b_1} + \underbrace{\begin{bmatrix} -2 + 5i \\ 2 + 3i \end{bmatrix}}_{\mathbf{q}_2 b_2} + \underbrace{\begin{bmatrix} 2 + i \\ -4 - 3i \end{bmatrix}}_{\mathbf{q}_3 b_3} + \underbrace{\begin{bmatrix} 1 - 2i \\ -3 + 4i \end{bmatrix}}_{\mathbf{q}_4 b_4} + \underbrace{\begin{bmatrix} 0.5 + 0.4i \\ 0.2 - 0.6i \end{bmatrix}}_{\mathbf{v}_1}, \tag{2.37}$$

where \mathbf{v}_1 is the interference-plus-noise term contaminating b_1 and it is approximated as a Gaussian random vector.

Step 3: In order to obtain an updated value $\Pr^{(1)}(b_1 = \pm 1 | \mathbf{y})$ for $\Pr^{(0)}(b_1 = \pm 1 | \mathbf{y})$ according to (2.33), we have to calculate the three statistics of \mathbf{v}_1 according to (2.24), (2.25) and (2.26), respectively, yielding

$$\boldsymbol{\mu}_1 = \begin{bmatrix} 0 \\ 0 \end{bmatrix}, \tag{2.38}$$

$$\boldsymbol{\Upsilon}_1 = \sum_{k=2}^4 \mathcal{C}(b_k) \mathbf{q}_k \mathbf{q}_k^H + N_0 \mathbf{I} = \begin{bmatrix} 39.01 & -11 + 20i \\ -11 - 20i & 63.01 \end{bmatrix}, \tag{2.39}$$

$$\boldsymbol{\Omega}_1 = \sum_{k=2}^4 \mathcal{C}_p(b_k) \mathbf{q}_k \mathbf{q}_k^T = \begin{bmatrix} -21 - 20i & -19 + 4i \\ -19 + 4i & -5 + 12i \end{bmatrix}. \tag{2.40}$$

Here, $N_0 = 0.01$ is used, which is specified in Section 1.7 and indicates that an instantaneous per-antenna received SNR = $10 \log_{10} \frac{\|\mathbf{H}\mathbf{s}\|^2}{N_r N_0} = 26.021$ dB is assumed. Hence, according to

(2.32), we have

$$\mathbf{\Lambda}_1 = \begin{bmatrix} 18.01 & -30 & -20 & -16 \\ -30 & 58.01 & 24 & 12 \\ -20 & 24 & 60.01 & 8 \\ -16 & 12 & 8 & 68.01 \end{bmatrix}. \quad (2.41)$$

Then, according to (2.30), we arrive at

$$\mathbf{w}_{1,u_1} = \begin{bmatrix} 1.5 + 4.4i \\ -4.8 + 3.4i \end{bmatrix} \quad (2.42)$$

for the hypothesis of $b_1 = +1$ and at

$$\mathbf{w}_{1,u_2} = \begin{bmatrix} 11.5 + 8.4i \\ 1.2 - 0.6i \end{bmatrix} \quad (2.43)$$

for the hypothesis of $b_1 = -1$, respectively. As a result, according to (2.31), we have

$$\varphi_{u_1}^{(1)}(b_1) = \exp(-26.8408) = 2.2038 \times 10^{-12} \quad (2.44)$$

and

$$\varphi_{u_2}^{(1)}(b_1) = \exp(-1.4078 \times 10^4) \approx 0 \quad (2.45)$$

for $\Pr^{(1)}(b_1 = +1|\mathbf{y})$ and $\Pr^{(1)}(b_1 = -1|\mathbf{y})$, respectively. Therefore, we obtain the updated bit decision probabilities of

$$\Pr^{(1)}(b_1 = +1|\mathbf{y}) = \frac{\varphi_{u_1}^{(1)}(b_1)}{\varphi_{u_1}^{(1)}(b_1) + \varphi_{u_2}^{(1)}(b_1)} = 1, \quad (2.46)$$

and

$$\Pr^{(1)}(b_1 = -1|\mathbf{y}) = \frac{\varphi_{u_2}^{(1)}(b_1)}{\varphi_{u_1}^{(1)}(b_1) + \varphi_{u_2}^{(1)}(b_1)} = 0, \quad (2.47)$$

which are shown in Table 2.5(b).

Step 4: Since the current value of l is 1, which is not greater than $N_t = 2$, the operation $l = l + 1$ is carried out, resulting $l = 2$. Therefore, we now start to update the decision probabilities for b_2 , namely the second row of Table 2.5(a) is to be updated, similarly, we have

$$\mathbf{y} = \underbrace{\begin{bmatrix} -2 + 5i \\ 2 + 3i \end{bmatrix}}_{\mathbf{q}_2 b_2} + \underbrace{\begin{bmatrix} 5 + 2i \\ 3 - 2i \end{bmatrix}}_{\mathbf{q}_1 b_1} + \underbrace{\begin{bmatrix} 2 + i \\ -4 - 3i \end{bmatrix}}_{\mathbf{q}_3 b_3} + \underbrace{\begin{bmatrix} 1 - 2i \\ -3 + 4i \end{bmatrix}}_{\mathbf{q}_4 b_4} + \begin{bmatrix} 0.5 + 0.4i \\ 0.2 - 0.6i \end{bmatrix}, \quad (2.48)$$

and the three statistics of \mathbf{v}_2 evaluated from (2.24) to (2.26) are

$$\boldsymbol{\mu}_2 = \begin{bmatrix} 5 + 2i \\ 3 - 2i \end{bmatrix}, \quad (2.49)$$

$$\mathbf{r}_2 = \sum_{k \neq 2} \mathcal{C}(b_k) \mathbf{q}_k \mathbf{q}_k^H + N_0 \mathbf{I} = \begin{bmatrix} 10.01 & -22 + 4i \\ -22 - 4i & 50.01 \end{bmatrix}, \quad (2.50)$$

$$\boldsymbol{\Omega}_2 = \sum_{k \neq 2} \mathcal{C}_p(b_k) \mathbf{q}_k \mathbf{q}_k^T = \begin{bmatrix} 0 & 0 \\ 0 & 0 \end{bmatrix}. \quad (2.51)$$

Hence, according to (2.32), we have

$$\boldsymbol{\Lambda}_2 = \begin{bmatrix} 10.01 & -22 & 0 & -4 \\ -22 & 50.01 & 4 & 0 \\ 0 & 4 & 10.01 & -22 \\ -4 & 0 & -22 & 50.01 \end{bmatrix}, \quad (2.52)$$

Additionally, according to (2.30), we obtain

$$\mathbf{w}_{2,u_1} = \begin{bmatrix} 3.5 - 0.6i \\ -6.8 + 0.4i \end{bmatrix} \quad (2.53)$$

for the hypothesis of $b_2 = +1$ and

$$\mathbf{w}_{2,u_2} = \begin{bmatrix} -0.5 + 9.4i \\ -2.8 + 6.4i \end{bmatrix} \quad (2.54)$$

for the hypothesis of $b_2 = -1$, respectively. Consequently, according to (2.31), we arrive at

$$\varphi_{u_1}^{(1)}(b_2) = \exp(-26.4791) = 3.1643 \times 10^{-12} \quad (2.55)$$

and

$$\varphi_{u_2}^{(1)}(b_2) = \exp(-1.3020 \times 10^4) \approx 0 \quad (2.56)$$

for $\Pr^{(1)}(b_2 = +1|\mathbf{y})$ and $\Pr^{(1)}(b_2 = -1|\mathbf{y})$, respectively. Therefore, we can now generate the updated bit decision probabilities of

$$\Pr^{(1)}(b_2 = +1|\mathbf{y}) = \frac{\varphi_{u_1}^{(1)}(b_2)}{\varphi_{u_1}^{(1)}(b_2) + \varphi_{u_2}^{(1)}(b_2)} = 1, \quad (2.57)$$

and

$$\Pr^{(1)}(b_2 = -1|\mathbf{y}) = \frac{\varphi_{u_2}^{(1)}(b_2)}{\varphi_{u_1}^{(1)}(b_2) + \varphi_{u_2}^{(1)}(b_2)} = 0, \quad (2.58)$$

which are shown in Table 2.5(c).

The remaining rows of Table 2.5(a) can be updated in a similar fashion, as shown in Table 2.5(d) and 2.5(e). In the example considered, this updating process does not stop until we arrive at $l = 5$. Then, the decision probabilities of all the four bits, as shown in Table 2.5(e), have been calculated in the first iteration.

Step 5: Since $|\mathbf{P}^{(1)}(l, n) - \mathbf{P}^0(l, n)| < \epsilon = 0.001$ does not hold for all $l = 1, \dots, 4$ and $n = 1, 2$, which indicates that \mathbf{P} has not converged. Additionally, since $z = 0 > z_{\max} = 5$ does not hold either, we let $z = z + 1$ and return to Step 2. As a result, we obtain the probability table, namely Table 2.5(f) which corresponds to the second iteration as indicated by $z + 1 = 2$.

Step 6: Since $|\mathbf{P}^{(2)}(l, n) - \mathbf{P}^1(l, n)| < \epsilon = 0.001$ holds true, according to Table 2.5(f), we readily obtain the bit decisions $\mathbf{b} = [b_1, b_2, b_3, b_4]^T = [1, 1, -1, 1]^T$, which is seen to be the correct decisions by referring to (2.36).

TABLE 2.5: An example of updating probability table for B-PDA.

(a) $\mathbf{P}^{(0)}$: initialization			(b) $\mathbf{P}^{(1)}$: first row updated			(c) $\mathbf{P}^{(1)}$: second row updated		
	$u_1 = +1$	$u_2 = -1$		$u_1 = +1$	$u_2 = -1$		$u_1 = +1$	$u_2 = -1$
$\mathbf{P}(1, :)$	<u>0.5</u>	<u>0.5</u>	$\mathbf{P}(1, :)$	<u>1</u>	<u>0</u>	$\mathbf{P}(1, :)$	1	0
$\mathbf{P}(2, :)$	0.5	0.5	$\mathbf{P}(2, :)$	0.5	0.5	$\mathbf{P}(2, :)$	<u>1</u>	<u>0</u>
$\mathbf{P}(3, :)$	0.5	0.5	$\mathbf{P}(3, :)$	0.5	0.5	$\mathbf{P}(3, :)$	0.5	0.5
$\mathbf{P}(4, :)$	0.5	0.5	$\mathbf{P}(4, :)$	0.5	0.5	$\mathbf{P}(4, :)$	0.5	0.5
(d) $\mathbf{P}^{(1)}$: third row updated			(e) $\mathbf{P}^{(1)}$: fourth row updated			(f) $\mathbf{P}^{(2)}$: Second iteration		
	$u_1 = +1$	$u_2 = -1$		$u_1 = +1$	$u_2 = -1$		$u_1 = +1$	$u_2 = -1$
$\mathbf{P}(1, :)$	1	0	$\mathbf{P}(1, :)$	1	0	$\mathbf{P}(1, :)$	1	0
$\mathbf{P}(2, :)$	1	0	$\mathbf{P}(2, :)$	1	0	$\mathbf{P}(2, :)$	1	0
$\mathbf{P}(3, :)$	<u>0</u>	<u>1</u>	$\mathbf{P}(3, :)$	0	1	$\mathbf{P}(3, :)$	0	1
$\mathbf{P}(4, :)$	0.5	0.5	$\mathbf{P}(4, :)$	<u>1</u>	<u>0</u>	$\mathbf{P}(4, :)$	1	0

2.5.3 Discussions

2.5.3.1 Positive versus Negative Impact of UMR

From the above procedures we can see that the size of the detected vector is extended from N_t symbols to $M_c N_t$ bits and the number of equivalent constellation points is reduced from $M \geq 4$ to 2. It was demonstrated in [230] that the quality of ‘‘Gaussian approximation’’, and therefore of the soft outputs, is the best for a large number of transmit antennas and a small number of constellation points [230]. In this context the question arises, as to how the UMR of QAM will influence the achievable performance of the proposed B-PDA? This

may not be an easy dilemma to resolve, since the theoretical performance bound of PDA based algorithms is still an open problem, and the UMR transformation may have both a positive and a negative impact on the achievable performance.

On the one hand, based on the observations in [230], we intuitively infer that our approach may be interpreted as virtually increasing the number of transmit antennas, while reducing the QAM constellation to a binary constellation. This approach improves the quality of the Gaussian approximation, and additionally reduces the decision ambiguity concerning the symbols of high-order QAM because it leads to binary decisions. Hence the performance of B-PDA is expected to be enhanced.

On the other hand, the UMR transformation may result into a rank-deficient composite channel of $\mathbf{Q} = \mathbf{H}\mathbf{W}$, which may deteriorate the achievable performance of B-PDA. We will demonstrate that in fact, the composite effect of the UMR is positive, as it will be evidenced in Section 2.6.

For the sake of more explicitly clarifying the fundamental differences between the conventional symbol-based CPDA and the proposed B-PDA, their Gaussian approximation processes are conceptually illustrated in Fig. 2.4 and Fig. 2.5, which are based on a single-variate multimodal (four-modal) Gaussian mixture distribution of $p_M(x) = p_1 \times f_1(x) + p_2 \times f_2(x) + p_3 \times f_3(x) + p_4 \times f_4(x)$ and a single-variate bimodal Gaussian mixture distribution of $p_B(x) = p_1 \times g_1(x) + p_2 \times g_2(x)$, respectively. Here, the ‘‘single variate’’ assumption indicates that only a single interfering symbol, say s_i , exists for the other symbol to be detected. In other words, a (2×2) -element VBLAST system is assumed. More specifically, the four-modal distribution observed in Fig. 2.4 stands for the case of a 4PAM-like scenario, which is a simplified real-valued example for M -QAM. It is constructed by a mixture of four constituent Gaussian distributions $f_1(x)$, $f_2(x)$, $f_3(x)$, $f_4(x)$ having the same variance, but different means of $m_1 = -3$, $m_2 = -1$, $m_3 = +1$, $m_4 = +3$ and different constituent probabilities of p_1 , p_2 , p_3 , p_4 . The four constituent probabilities correspond to the different probabilities that an interfering symbol has the value $s_i = -3$, $s_i = -1$, $s_i = +1$ and $s_i = +3$, respectively. Similarly, the bimodal distribution seen in Fig. 2.5 represents the case of a BPSK-like scenario, which corresponds to the B-PDA. It is constructed by a mixture of two constituent Gaussian distributions $g_1(x)$ and $g_2(x)$ having the same variance, but different means of $m_1 = -1$ and $m_2 = +1$, and different constituent probabilities of p_1 and p_2 . The two constituent probabilities correspond to the different probabilities that an interfering symbol has the value of $s_i = -1$ and $s_i = +1$, respectively. By observing Fig. 2.4 and Fig. 2.5, it becomes clear that when the constellation size is lower, the accuracy of approximating the corresponding multimodal Gaussian mixture distribution by a single Gaussian distribution is higher. This intuitive conclusion is also confirmed by the analysis of [230].

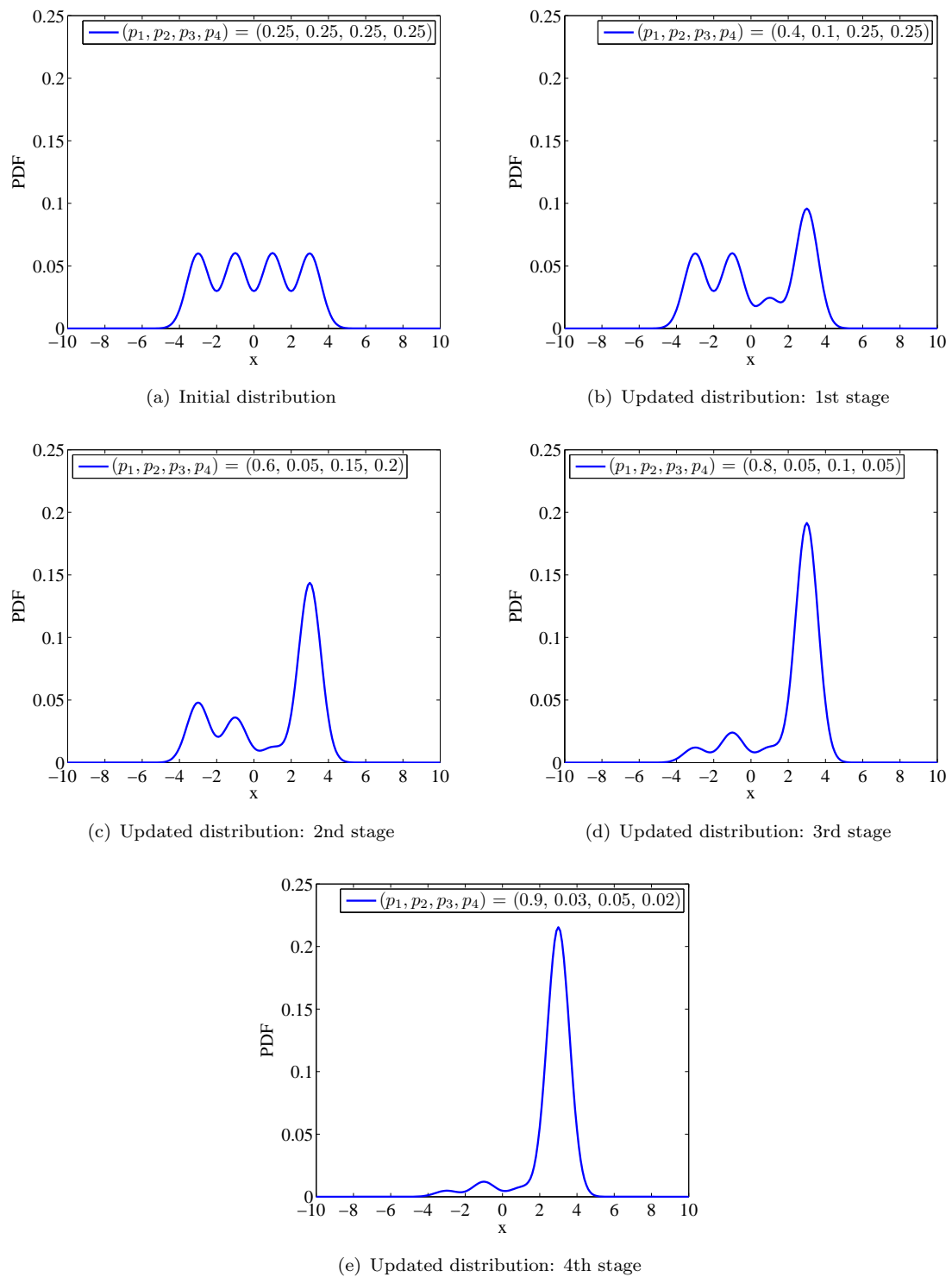


FIGURE 2.4: The process of approximating a single-variate four-modal Gaussian mixture distribution by a single Gaussian distribution.

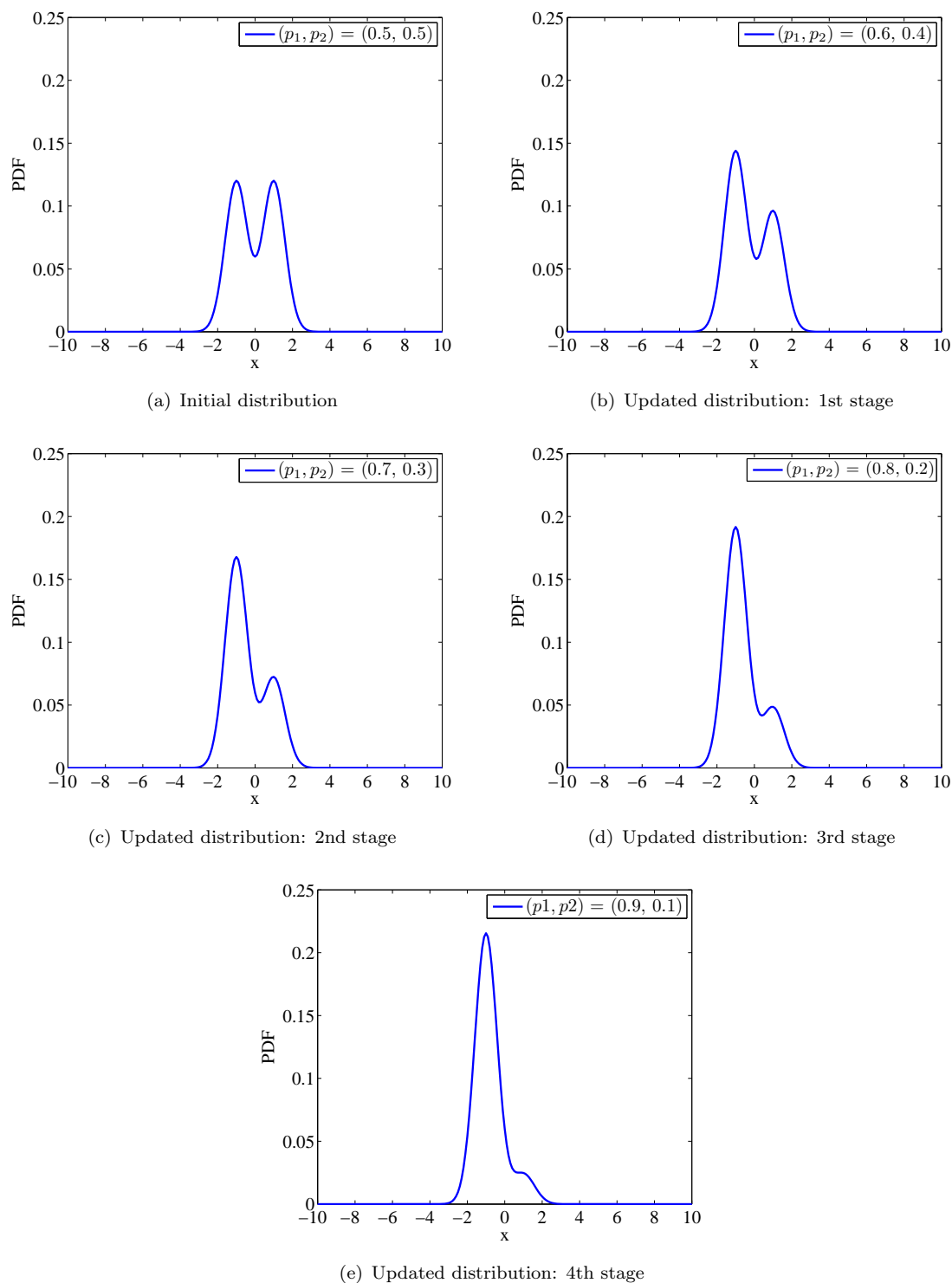


FIGURE 2.5: The process of approximating a single-variate bimodal Gaussian mixture distribution by a single Gaussian distribution.

2.5.3.2 Impact of Constellation Labelling on BER/SER Performance

The design and choice of constellation labelling may have a significant impact on the BER performance of symbol-based detectors. This explains why the Gray mapping is generally regarded as the optimal labelling scheme. However, the specific bit assignment within a symbol does not affect the SER performance, because the SER performance is determined by the minimum Euclidean distance of the constellation employed. However, since the proposed B-PDA skips the symbol-detection stage and directly operates at the bit-level, where the bits are treated separately and independently, the correlation between bits may not affect the achievable BER performance, as seen from the simulation results in Section 2.6.

2.5.3.3 Practical Feasibility of UMR for Gray Mapping

Note that if Gray mapping based rectangular QAM is used in the above B-PDA aided MIMO systems, it may be difficult to perfectly determine in advance the specific modulation matrix $\mathbf{W}(\mathbf{b})$ used at the receiver, because the modulation matrix depends on the transmitted bit vector. This implies that either a realistic detector should be used to first estimate $\mathbf{W}(\mathbf{b})$ at the receiver, or a flag containing the index of the modulation matrix used should be sent to the receiver via the signaling channel. Beside the additional complexity, there would be a performance degradation, which is determined by the quality of the corresponding estimation algorithm. However, in order to provide a lower bound performance for the linear natural mapping based B-PDA, we assume that the modulation matrix $\mathbf{W}(\mathbf{b})$ of the Gray mapping scenario is perfectly known at the receiver in the simulations of Section 2.6. In fact, observe in Fig. 2.9 to Fig. 2.12 that the linear natural mapping based B-PDA achieves almost the same performance as the Gray mapping based B-PDA under the idealized perfect modulation matrix estimation assumption.

2.5.4 Computational Complexity Analysis

It was shown in [234] that the conventional symbol-based CPDA detector has to update an $(M \times N_t)$ -element probability-matrix at each iteration, until all the entries in the matrix converge or the maximum iteration index is reached. For the sake of compactness, these probabilities are given in Table 2.6. Consequently, the number of probabilities to be computed may be as high as MN_tN_{it} for each symbol vector \mathbf{s} , where N_{it} is the average number of iterations required for convergence in the process of detecting each N_t -symbol vector containing M -QAM symbols.

By comparison, it may be readily observed from the above B-PDA procedures that provided the UMR of QAM is employed, the corresponding probability-matrix for B-PDA has M_cN_t

TABLE 2.6: Probabilities computed in one iteration of conventional symbol-based CPDA

	1	2	...	m	...	M
$\mathbf{P}(1, :)$	$\Pr(s_1 = a_1 \mathbf{y})$	$\Pr(s_1 = a_2 \mathbf{y})$...	$\Pr(s_1 = a_m \mathbf{y})$...	$\Pr(s_1 = a_M \mathbf{y})$
$\mathbf{P}(2, :)$	$\Pr(s_2 = a_1 \mathbf{y})$	$\Pr(s_2 = a_2 \mathbf{y})$...	$\Pr(s_2 = a_m \mathbf{y})$...	$\Pr(s_2 = a_M \mathbf{y})$
\vdots	\vdots	\vdots	...	\vdots	...	\vdots
$\mathbf{P}(j, :)$	$\Pr(s_j = a_1 \mathbf{y})$	$\Pr(s_j = a_2 \mathbf{y})$...	$\Pr(s_j = a_m \mathbf{y})$...	$\Pr(s_j = a_M \mathbf{y})$
\vdots	\vdots	\vdots	...	\vdots	...	\vdots
$\mathbf{P}(N_t, :)$	$\Pr(s_{N_t} = a_1 \mathbf{y})$	$\Pr(s_{N_t} = a_2 \mathbf{y})$...	$\Pr(s_{N_t} = a_m \mathbf{y})$...	$\Pr(s_{N_t} = a_M \mathbf{y})$

TABLE 2.7: Probabilities computed in one iteration for B-PDA

	1	2
$\mathbf{P}(1, :)$	$\Pr(b_1 = u_1 \mathbf{y})$	$\Pr(b_1 = u_2 \mathbf{y})$
$\mathbf{P}(2, :)$	$\Pr(b_2 = u_1 \mathbf{y})$	$\Pr(b_2 = u_2 \mathbf{y})$
\vdots	\vdots	\vdots
$\mathbf{P}(l, :)$	$\Pr(b_l = u_1 \mathbf{y})$	$\Pr(b_l = u_2 \mathbf{y})$
\vdots	\vdots	\vdots
$\mathbf{P}(M_c N_t, :)$	$\Pr(b_{M_c N_t} = u_1 \mathbf{y})$	$\Pr(b_{M_c N_t} = u_2 \mathbf{y})$

rows and two columns, thus the number of probabilities to be computed reduces to $2M_c N_t$ at each iteration. Hence the total number of probabilities to be computed becomes $2M_c N_t N'_{it}$, where N'_{it} is the average number of iterations required for detecting each corresponding bit vector. Additionally, the complexity imposed by computing a single probability is denoted as C_p and C'_p for CPDA and B-PDA, respectively.

Then, the achievable complexity ratio of the B-PDA detector over the conventional CPDA detector required for decoding a single N_t -symbol vector becomes

$$R_c(M) = \frac{2M_c N_t N'_{it} C'_p}{M N_t N_{it} C_p} = \frac{2 \log_2(M)}{M} \cdot \frac{N'_{it}}{N_{it}} \cdot \frac{C'_p(M)}{C_p(M)}, \quad (2.59)$$

where $2 \log_2(M) C'_p(M)$ and $M C_p(M)$ are the per-iteration-complexity for B-PDA and CPDA, respectively, while $2 \log_2(M) N'_{it} C'_p(M)$ and $M N_{it} C_p(M)$ are the complexity per symbol vector for B-PDA and CPDA, respectively. Eq. (2.59) is a monotonically decreasing function of the modulation order M , because the ratio of the number of iterations $\frac{N'_{it}}{N_{it}}$ is typically close to 1, whereas $\frac{C'_p(M)}{C_p(M)}$ is less than 1 and decreases upon increasing M , as it will be demonstrated in Fig. 2.6.⁶ Consequently, we have $R_c(M) \ll 1$ for $M \gg 4$. We provide a demonstrative example in Fig. 2.6 for the complexity comparison between the conventional

⁶The average number of iterations of the conventional PDA MIMO detector is typically 3 - 5 as seen in [219] [226] and also in Fig. 2.6 and Fig. 2.8. In addition, the computational cost in terms of floating point operations (FLOPs) for estimating the APP of a BPSK-like signal is lower than that of a complex-valued multilevel QAM signal.

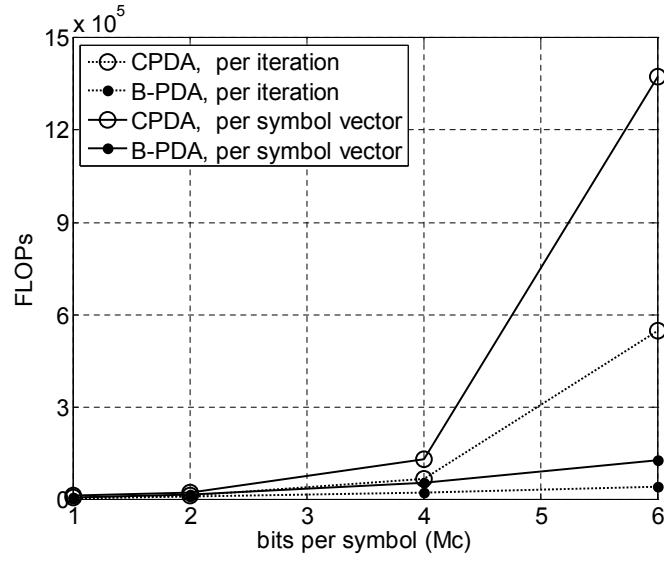


FIGURE 2.6: Complexity comparison in terms of FLOPs per iteration and per symbol vector for B-PDA with natural bit mapping and CPDA with Gray bit mapping. BPSK ($M_c = 1$), 4-QAM ($M_c = 2$), 16-QAM ($M_c = 4$), and 64-QAM ($M_c = 6$) are considered, SNR = 20dB, and $N_t = N_r = 2$.

CPDA and the proposed B-PDA quantified in terms of the number of FLOPs per iteration and per symbol vector for different QAM constellations. It may be readily seen in Fig. 2.6 that the complexity of B-PDA using the linear natural bit mapping is reduced by about 80% for the system configuration of 64-QAM, $N_t = N_r = 2$, SNR = 20dB.

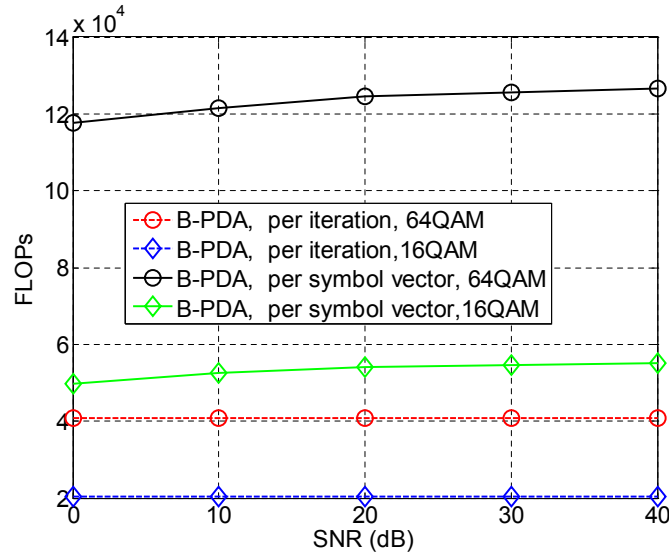


FIGURE 2.7: Computational complexity of B-PDA under different SNR values for 16-QAM and 64-QAM, $N_t = N_r = 2$.

On the other hand, Fig. 2.7 evaluates the complexity of the proposed B-PDA detector under different SNR values, for which both the rectangular 16-QAM and 64-QAM are considered

in a (2×2) -element VBLAST system. It can be seen from Fig. 2.7 that the per-iteration-complexity of the proposed B-PDA detector is almost constant, regardless of the SNR values, although the per-vector-complexity recorded for relatively high SNR values is a little higher than that of the low SNR values. This is because the AWGN plays a more significant role at low SNR values than it does at high SNR values. In other words, the B-PDA has a near-constant complexity for different SNR values. This property is also consistent with our complexity analysis of Section 2.5.4, where again, the complexity does not depend on the SNR value. This near-constant complexity property may be regarded as another merit of the B-PDA detector, especially in the context of circuits implementation. By comparison, some other reduced-complexity MIMO detectors, for example the tree-search based methods, typically have a complexity that is quite sensitive to the SNR values encountered.

2.6 Simulation Results

In this section, we characterize the achievable performance of the B-PDA algorithm using Monte Carlo simulations in the context of the VBLAST system [102] as a function of the average SNR per receive antenna $[\text{SNR} \triangleq 10 \log_{10} (\mathcal{E} \{ \|\mathbf{H}\mathbf{s}\|^2 \} / \mathcal{E} \{ \|\mathbf{n}\|^2 \}) = 10 \log_{10} (N_t/N_0)]$ for transmission over flat Rayleigh fading channels, where the entries of the MIMO channel are independent and identically distributed (i.i.d.), zero mean, unit-variance complex-valued Gaussian random variables. A new independent channel realization is drawn for each transmitted symbol vector. The noise vector \mathbf{n} is i.i.d. $\mathcal{CN}(0, N_0)$. No optimal ordering of the bits is performed before detection in the following PDA related simulations for the sake of fair comparison with the results of [234]. The convergence threshold is set to $|\mathbf{P}^{(z+1)}(r, c) - \mathbf{P}^{(z)}(r, c)| \leq \varepsilon = 0.001$, where $\mathbf{P}^{(z)}(r, c)$ represents the (r, c) th value of the probability-matrix of CPDA or B-PDA at the z th iteration.

In order to choose the appropriate number of iterations for the PDA-aided MIMO detectors, Fig. 2.8 evaluates the impact of the number of iterations both on the performance of the conventional symbol-based CPDA of [234] using Gray mapping based 16-QAM and on the proposed B-PDA using linear natural mapping based 16-QAM in the context of (2×2) -antenna aided VBLAST systems. The maximum number of iterations I_{max} is set to 1, 3, and 5, respectively. It can be seen from Fig. 2.8 that both the CPDA and B-PDA exhibit quite a good convergence, since the performance loss is modest even when the maximum number of iterations is set to be as low as $I_{max} = 3$.

Based on the above observation, we set the maximum number of iterations to $I_{max} = 5$ in the following investigations, where B-PDA is compared to the conventional symbol-based CPDA, MMSE-OSIC and ML, while using both the linear natural bit mapping and the nonlinear Gray mapping. Note that we treat the matrix \mathbf{W} as being perfectly known at the receiver, which is merely an idealized assumption for the nonlinear Gray mapping based

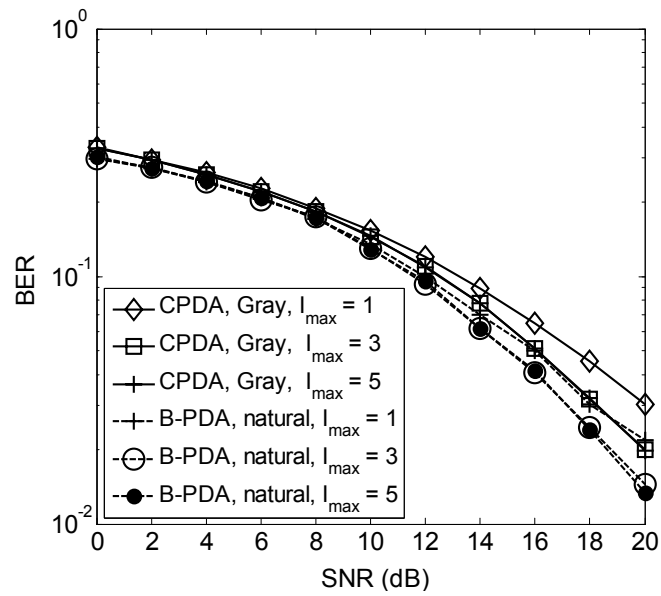


FIGURE 2.8: Impact of the number of iterations on the achievable performance of CPDA and B-PDA in VBLAST using 16-QAM, $N_t = N_r = 2$.

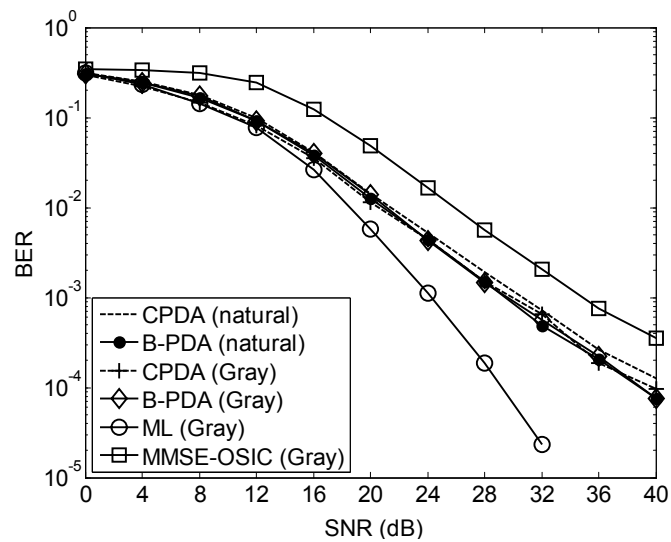


FIGURE 2.9: BER comparison of B-PDA and CPDA, MMSE-OSIC, ML in VBLAST with 16-QAM, $I_{max} = 5$, $N_t = N_r = 2$.

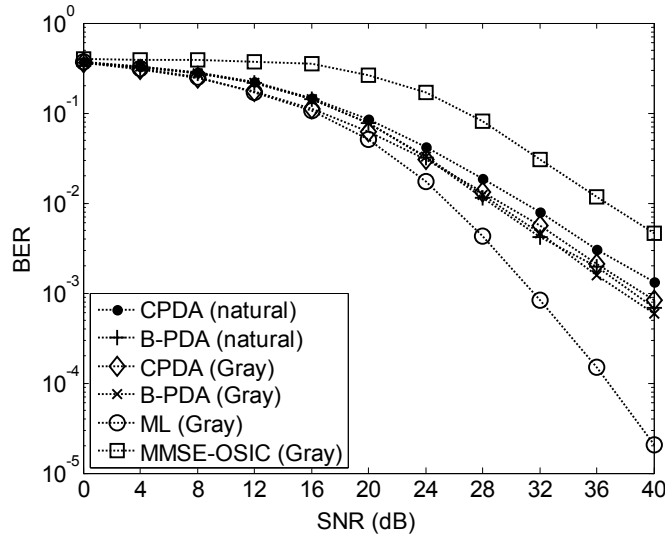


FIGURE 2.10: BER comparison of B-PDA and CPDA, MMSE-OSIC, ML in VBLAST with 64-QAM, $I_{max}=5$, $N_t = N_r = 2$.

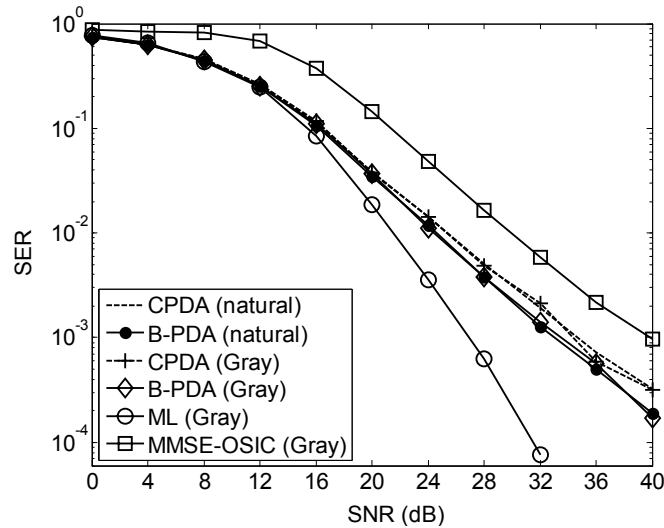


FIGURE 2.11: SER comparison of B-PDA and CPDA, MMSE-OSIC, ML in VBLAST with 16-QAM, $I_{max}=5$, $N_t = N_r = 2$.

B-PDA. Based on this assumption, the performance curve of the B-PDA plotted for the Gray mapping scenario serves as a lower bound of the B-PDA performance in the linear natural mapping case. The pairs of Fig. 2.9 - Fig. 2.10 and Fig. 2.11 - Fig. 2.12 evaluate the attainable BER and SER performance, respectively, for both 16-QAM and 64-QAM constellations.⁷ In general, the performance of B-PDA is superior to that of CPDA, and the attainable gain is more substantial in terms of SER. For the linear natural mapping based

⁷For high-order modulation, multiple bit errors occurring close to each other will probably create only one symbol error. In this situation, SER is a useful metric and widely adopted in literature regarding the high-order M -ary signaling detection in MIMO systems, as seen in [256], [255] and [226].

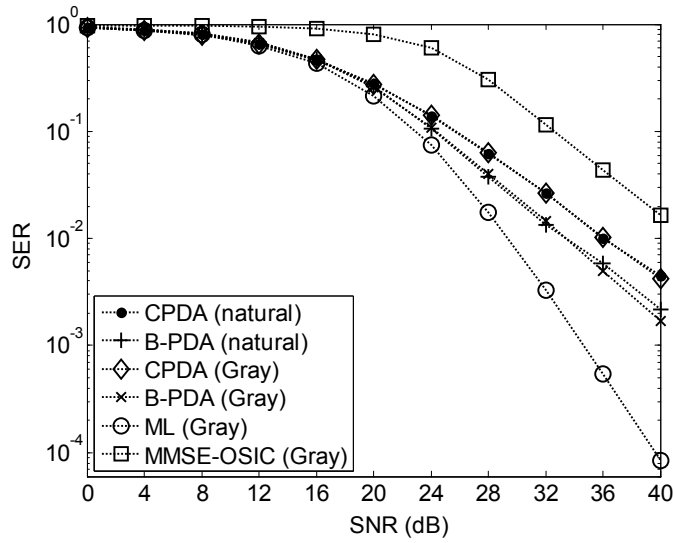


FIGURE 2.12: SER comparison of B-PDA and CPDA, MMSE-OSIC, ML in VBLAST with 64-QAM, $I_{max}=5$, $N_t = N_r = 2$.

16-QAM, B-PDA outperforms CPDA by approximately 2 dB at both $BER = 10^{-3}$ and $SER = 10^{-3}$. Similarly, for the linear natural bit mapping based 64-QAM, the corresponding gains are up to 3dB at $BER = 10^{-2}$ and $SER = 10^{-2}$. When the conventional symbol-based CPDA uses the nonlinear Gray mapping, it can be seen by comparing the results of Fig. 2.9 and Fig. 2.10 to those of Fig. 2.11 and Fig. 2.12 that the BER performance of the linear natural mapping B-PDA erodes slightly at low SNRs, but still has an advantage over that of CPDA at high SNRs. Furthermore, observe from the SER curves of Fig. 2.11 and Fig. 2.12 that the SNR gain of the linear natural mapping based B-PDA remains superior to that of CPDA at all the SNR values considered. This is because Gray mapping is efficient in terms of reducing the BER through the binary labelling gain, but it is unable to improve the SER, since the SER is determined by the minimum Euclidean distance of the constellation points (a single constellation may have various labelling schemes). It is also interesting to observe that the performance of the linear natural mapping aided QAM approaches that of the Gray mapping aided QAM for the proposed B-PDA, while the latter represents a lower bound performance valid under the assumption of perfect knowledge of \mathbf{W} at the receiver. In other words, B-PDA is insensitive to the specific mapping rule, as long as the matrix \mathbf{W} is known at the receiver. This is because it operates directly on the basis of the separate bits, namely in a bit-by-bit fashion which treats each bit independently and remains unaffected by the specific correlation between the bits within a symbol. By comparison, the conventional PDA generally makes the decision at the symbol-level using the estimated symbolwise APPs, and if necessary, the bits are recovered according to the inverse bit-to-symbol mapping, which retains the better BER of Gray mapping but has no advantage in SER. Therefore, it may be concluded that it is not necessary to design complex bit-to-symbol mapping rules for the proposed B-PDA, because it is capable of approaching the lower bound performance provided

by the Gray mapping based B-PDA in ideal conditions even upon using the simplest linear natural bit-to-symbol mapping.

It can also be seen from Fig. 2.9 to Fig. 2.12 that the linear natural mapping based B-PDA significantly outperforms MMSE-OSIC, but remains inferior in comparison to the ML detector. This indicates that the proposed B-PDA may not be able to achieve the full diversity in the specific context considered. Some other reduced complexity MIMO detectors, such as for example the FCSD and the SDPR detector derived for binary signaling have been shown to be capable of achieving the full diversity [382], [249] under certain conditions, while the partial equalization (PE) approach of [383] achieves a diversity order between that of the ML and ZF solutions. To the best of our knowledge, the theoretical performance analysis and the diversity order analysis of the PDA algorithm in the MIMO detection context still remain open questions. The challenge is that it proceeds in an iterative fashion and the accuracy of approximating a multimodal Gaussian mixture probability structure with the aid of a single multivariate Gaussian distribution in PDA-based detectors may not always guarantee that the global optimum is achieved. We will investigate this issue in our future research.

2.7 Chapter Summary and Conclusions

We proposed a unified B-PDA detection scheme for VBLAST-style SDM-MIMO systems. Based on the UMR of rectangular QAM, the B-PDA transforms the symbol detection process of QAM to that of a BPSK scenario with the aid of a composite channel matrix combining the effect of modulation and of the original channel matrix. Simulations and complexity analysis demonstrate that the proposed B-PDA outperforms the conventional CPDA, despite it dramatically reduces complexity, especially in the context of high-order QAM constellations. In addition, the simulation results show that the linear natural mapping based B-PDA is insensitive to the choice of labelling scheme, and almost achieves the lower bound performance provided by the Gray mapping based B-PDA with perfect modulation matrix assumption. Finally, we concluded that it is preferable to use the simpler and more practicable linear natural bit-to-symbol mapping rather than Gray mapping for the B-PDA aided MIMO detector in the FEC-uncoded VBLAST-style systems considered.

Semidefinite Programming Relaxation Based Virtually Antipodal MIMO Detection for Gray-Coded High-Order QAM

3.1 Introduction

THE MIMO detection problem formulated in Chapter 1 can be solved at a reduced complexity, but in suboptimum manner relying on diverse mathematical perspectives. In Chapter 2, this problem has been investigated from an iterative probabilistic approximation perspective, which essentially aims for performing interference-modelling using a density evolution based approximation process. To elaborate a little further, corresponding to each transmitted symbol, the interference-plus-noise term which obeys a multimodal Gaussian mixture distribution is iteratively approximated by a gradually updated multivariate Gaussian distribution, as portrayed in Fig. 2.4 and Fig. 2.5 of Section 2.5.3. In particular, the B-PDA detector of Fig. 2.3 was designed for MIMO systems that use rectangular M -QAM constellations. Compared to the conventional PDA detector of [193, 226, 227, 230, 234], which carries out the MIMO detection on a symbol-by-symbol basis, the proposed B-PDA detector of Fig. 2.3 operates in a bit-by-bit manner. By identifying the matrix transformation relationship between the transmitted symbol vector and the transmitted bit vector of rectangular M -QAM constellations, the B-PDA detector may be viewed as a solution which increases the dimension of the *effective* transmitted signal vector while at the same time reducing the *effective* constellation size in the context of PDA-based MIMO detectors. As a beneficial result, we demonstrated in Fig. 2.6 - Fig. 2.12 that the

B-PDA typically achieves a superior performance, despite imposing a significantly reduced complexity compared to the conventional symbol-based PDA detectors.

As another beneficial design alternative, in this chapter, we intend to investigate the MIMO detection problem from a convex optimization [244, 369] perspective. In particular, we will propose a bit-based VA-SDPR detector, which is capable of making *direct* binary decisions concerning the transmitted information bits of SDM-MIMO systems employing Gray-coded high-order rectangular QAM constellations. The specific rationale and motivation of this initiative is detailed as follows.

First of all, as mentioned in Section 1.8.6, the SDPR detectors are capable of achieving a near-optimal performance in several practical applications, such as BPSK/QPSK-modulated MIMO systems, at a guaranteed polynomial-time worst-case computational complexity which increases as a polynomial function of N_t . This is opposed to the optimum ML detector which exhibits an exponentially increasing computational complexity. However, in high-order modulation scenarios the performance of the SDPR detectors is less promising compared to that of the BPSK/QPSK scenario. Hence, we embark on further improving the performance of the SDPR based MIMO detector in the context of high-order QAM constellations, while maintaining a low computational complexity.

Secondly, although in Chapter 2 we have considered both the linear natural-mapping and the nonlinear Gray-mapping for bit-based detection of rectangular M -QAM, the transformation matrices proposed in Section 2.4 for Gray-coded rectangular QAM are dependent on the transmitted bit vector owing to the nonlinear nature of Gray-mapping. Therefore, in practice these data-dependent transform matrices cannot be readily invoked at the receiver. Hence, the performance of the B-PDA detector designed for Gray-coded QAM was only used as a theoretical benchmarker in Chapter 2.

Finally, in the family of existing SDPR based MIMO detectors developed for high-order QAM [252–256], the specific VA-SDPR detector, which converts the associated non-binary integer programming problem into a binary integer programming problem, is of particular interest to us. This is because the VA-SDPR detector may be shown to have a strong connection with the SDPR detector designed for BPSK, where the SDPR attains near-optimal performance. However, in the index-bit-based VA-SDPR (*I*VA-SDPR) detector of [256], the binary decisions are made as regards to the so-called “index bits”, rather than on the original “information bits”, as we will detail in Section 3.3. These two types of bits are in general different from each other [256], except for the linear natural-mapping¹ aided rectangular QAM considered in Chapter 2. More specifically, the Gray-mapping based bit-to-symbol conversion of rectangular M -QAM is nonlinear for $M > 4$. Therefore, as shown in Section 2.4, in contrast to the scenario of linear natural-mapping aided rectangular QAM, for Gray-mapping the relationship between the transmitted symbol vector \mathbf{s} and the associated

¹The linear natural mapping is defined as the mapping which satisfies eq.(2.3).

antipodal information bit vector \mathbf{b} *cannot* be characterized by a compact linear matrix transformation of the form $\mathbf{s} = \mathbf{W}\mathbf{b}$, where \mathbf{W} is the constellation-specific modulation matrix known to both the transmitter and receiver. Consequently, when the ubiquitous Gray-mapping aided high-order rectangular QAM is used, the VA-SDPR detector of [256] still has to obtain its symbol decisions first relying on the decided “index bits”, before making correct decisions of the information bits.

Against this background, the major contributions of this chapter are as follows.

1) We propose a novel model transformation method for MIMO systems using Gray-coded high-order rectangular QAM, which allows us to reformulate the classic symbol-based MIMO detection model as a simpler bit-based detection model. Gray-mapping is known to be non-linear, and hence has made direct bit manipulation difficult to many detection methods. Our method is established by exploiting the structural regularity of Gray-coded high-order rectangular QAM with the aid of a strikingly simple linear matrix representation (LMR) of 4-QAM. As an appealing benefit, the conventional three-step “signal-to-symbols-to-bits” decision process can be replaced by a simpler “signal-to-bits” decision process for the classic Gray-mapping aided high-order rectangular QAM, and hence any bit-based detection method becomes potentially applicable.

2) Based on the above model transformation method, we propose a new DVA-SDPR detector for the ubiquitous Gray-mapping aided high-order rectangular QAM, which is capable of directly deciding on the information bits for transmission over fading MIMO channels. To elaborate a little further, our approach firstly transforms the original Gray-coded M -QAM aided $(N_t \times N_r)$ -element MIMO system to a virtual 4-QAM aided $(2N_t \times N_r)$ -element MIMO system. Since we have shown in Chapter 2 that the modulation matrix of 4-QAM is identical for both the natural-mapping and the Gray-mapping, the proposed DVA-SDPR detector finally converts the classic nonlinear Gray-mapping aided M -QAM symbol detection problem to a BQP problem [369]. When relying on this technique, we can directly carry out the information-bit decisions without first invoking conventional symbol decisions for the nonlinear Gray-mapping aided rectangular M -QAM scheme.

3) The proposed model transformation method facilitates the exploitation of the unequal error protection (UEP) property of high-order QAM with the aid of the low-complexity bit-flipping based “hill climbing” method. As a beneficial result, the proposed DVA-SDPR detector achieves the best BER performance among the known SDPR-based MIMO detectors in the context considered, while still maintaining the lowest-possible polynomial-time worst-case complexity order of $O[(N_t \log_2 M + 1)^{3.5}]$.

4) Finally, a modified primal-dual interior point algorithm is employed for solving the SDP problem considered. Additionally, the performance versus complexity tradeoff of the modified primal-dual interior-point algorithm with respect to its convergence accuracy is investi-

gated, and the advantage of the proposed SDPR-based MIMO detector over the SD in the context of the emerging “massive” MIMO systems [384, 385] is elaborated on.

The remainder of the chapter is organized as follows. In Section 3.2, the basics of convex optimization and semidefinite programming are briefly provided. In Section 3.3, our system model and the problem considered are presented. In Section 3.4, the structure of Gray-coded high-order rectangular QAM constellations is scrutinized by considering both Gray-coded 16-QAM and 64-QAM as examples, and the insights obtained therein are generalized to the M -QAM scenario. As a result, the inherent relationship between the information bits of a QAM symbol is unveiled. Then, in Section 3.5 the proposed DVA-SDPR detector is detailed from various perspectives, while our numerical results and discussions are presented in Section 3.6. Finally, our conclusions are offered in Section 3.7.

3.2 Basics of Convex Optimization and Semidefinite Programming

3.2.1 Convex Optimization

Consider a generic mathematical optimization problem in the standard minimization form²

$$\begin{aligned} \min \quad & f_0(\mathbf{x}) \\ \text{s. t.} \quad & f_i(\mathbf{x}) \leq 0, i = 1, 2, \dots, N_1, \\ & h_j(\mathbf{x}) = 0, j = 1, 2, \dots, N_2, \\ & \mathbf{x} \in \mathbb{K}^N, \end{aligned} \tag{3.1}$$

where f_0 is known as the *objective function*, while $\{f_i\}_{i=1}^{N_1}$ and $\{h_j\}_{j=1}^{N_2}$ are known as the inequality and equality *constraint functions*, respectively. Additionally, $\mathbb{K}^N \subset \mathbb{R}^N$ is referred to as the *constraint set*, while \mathbf{x} is called the *optimization variable*, which facilitates the minimization of the objective function $f_0(\mathbf{x})$. The variable \mathbf{x} is regarded as being feasible, i.e. as a potentially legitimate solution, if we have $\mathbf{x} \in \mathbb{K}^N$ and it satisfies all the inequality and equality constraints of (3.1). A feasible solution \mathbf{x}^* is said to be globally optimal, if we have $f_0(\mathbf{x}^*) \leq f_0(\mathbf{x})$ for all feasible \mathbf{x} .

Convex optimization constitutes a subfield of the generic mathematical optimization problem of (3.1). It studies the minimization of a *convex objective function* over *convex sets*. Therefore, the terms *convex set* and *convex function* represent two basic concepts in convex optimization, which are briefly highlighted below for the sake of a self-contained treatment.

²In diverse subfields of mathematical optimization, the corresponding standard forms are usually needed, because 1) for a particular class of optimization problems, a unified model facilitates the study of both the theory and the methods regarding this class of optimization problems; 2) the software packages developed for solving mathematical optimization problems are usually only available in standard forms.

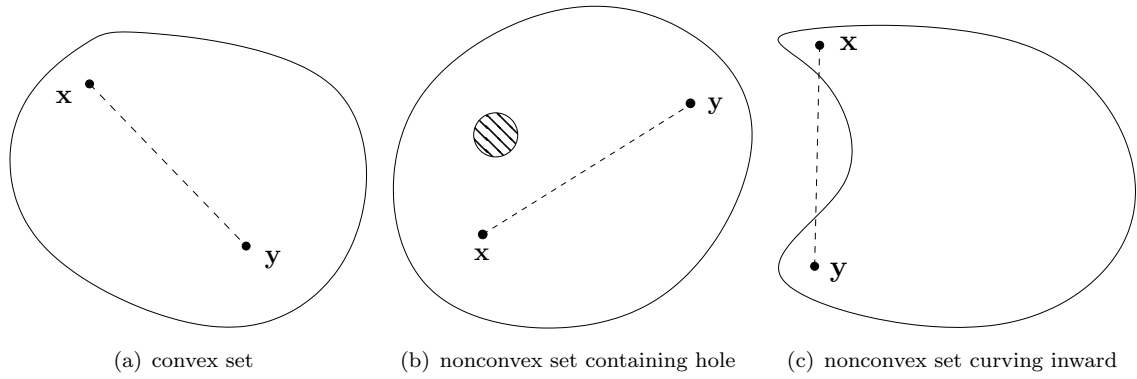


FIGURE 3.1: Convex set versus nonconvex set.

1) *Convex Set*: A set $\mathbb{K}^N \subset \mathbb{R}^N$ is said to be convex if any two points $\mathbf{x}, \mathbf{y} \in \mathbb{K}^N$ satisfy

$$\alpha \mathbf{x} + (1 - \alpha) \mathbf{y} \in \mathbb{K}^N, \quad \forall \alpha \in [0, 1]. \quad (3.2)$$

As seen in Fig. 3.1(a), from a tangible geometric perspective this implies that the line segment joining \mathbf{x} and \mathbf{y} also lies within the set \mathbb{K}^N . Therefore, in general, the geometric region represented by a convex set must not encompass holes *and* its boundary must always curve outward. By contrast, the geometric region represented by a nonconvex set either contains a hole, or its boundary curves inward, as seen in Fig. 3.1(b) and 3.1(c). An important property of convex sets is that the intersection of any number of convex sets remains a convex set. Apart from using the definition of a convex set, this “intersection property” is often used as another way of determining whether a specific set is convex or not, which constitutes a key step in identifying a convex problem. Note, however, that the union of convex sets is typically not a convex set.

2) *Convex Function*: A real-valued function defined as $f(\mathbf{x}) : \mathbb{K}^N \rightarrow \mathbb{R}$ is said to be a convex function, if any two points $\mathbf{x}, \mathbf{y} \in \mathbb{K}^N \subset \mathbb{R}^N$ satisfy

$$f[\alpha \mathbf{x} + (1 - \alpha) \mathbf{y}] \leq \alpha f(\mathbf{x}) + (1 - \alpha) f(\mathbf{y}), \quad \forall \alpha \in [0, 1]. \quad (3.3)$$

The geometric interpretation of the inequality (3.3) is illustrated in Fig. 3.2. To elaborate a little further, the right-hand side of (3.3) represents the line segment joining the pair of points $[\mathbf{x}, f(\mathbf{x})]$ and $[\mathbf{y}, f(\mathbf{y})]$, namely the dashed line segment joining the two points $[x_1, f(x_1)]$ and $[x_2, f(x_2)]$ in Fig. 3.2. Additionally, the left-hand side of (3.3) represents the segment of the curve $f(\mathbf{x})$ corresponding to the interval defined by the line segment $\alpha \mathbf{x} + (1 - \alpha) \mathbf{y}$, namely the curve segment below the dashed line segment seen in Fig. 3.2. Therefore, we can simply infer that a convex function $f(\mathbf{x})$ always curves downward and it is said to be dominated by the line segment joining any two points of its curve. By contrast, $f(\mathbf{x})$ is said to be concave if $-f(\mathbf{x})$ is convex. Obviously, the convex/concave functions represent merely a special class of the more generic class of functions defined as $f(\mathbf{x}) : \mathbb{R}^N \rightarrow \mathbb{R}$, and there

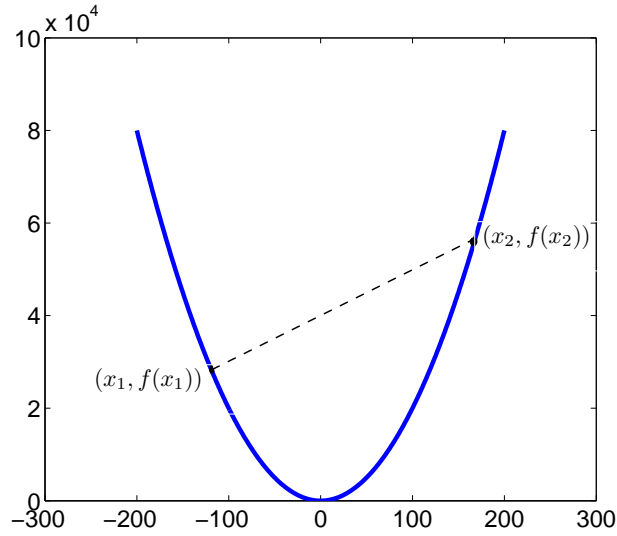


FIGURE 3.2: Example of a convex function.

are numerous functions which are neither convex nor concave. For example, the function $\sin(x)$ is concave over $[0, \pi]$ but convex over $[\pi, 2\pi]$.

In general, there are three ways of determining whether a function is convex or not.

- **Definition test:** The most conceptually straightforward technique, which is not necessarily easy in practical terms, is to test $f(\mathbf{x})$ against the definition of a convex function as characterized by (3.3).
- **Differentiability based methods:** The second family of methods invoke the differentiability test of the function $f(\mathbf{x})$, including both the first-order derivative test and second-order derivative test. More explicitly, if the function $f(\mathbf{x})$ is continuously differentiable and its domain is convex, then the convexity of $f(\mathbf{x})$ is equivalent to

$$f(\mathbf{y}) \geq f(\mathbf{x}) + \nabla f(\mathbf{x})^T (\mathbf{y} - \mathbf{x}), \quad \forall \mathbf{x}, \mathbf{y} \in \mathbb{K}^N, \quad (3.4)$$

which is the first-order derivative test. In physically tangible terms this implies that the function $f(\mathbf{x})$ is lower-bounded by its first-order Taylor series expansion, or that the function $f(\mathbf{x})$ lies above all of its tangents.

Furthermore, if $f(\mathbf{x})$ is twice differentiable, then $f(\mathbf{x})$ is convex if and only if its domain is convex and its Hessian matrix $\nabla^2 f(\mathbf{x})$ is positive semidefinite (PSD), i.e. we have $\nabla^2 f(\mathbf{x}) \succeq 0, \forall \mathbf{x} \in \mathbb{K}^N$. For the sake of clarity, a more detailed exposure of the concept of a PSD matrix is provided in Section 3.2.2, bearing in mind that the Hessian matrix of

$f(\mathbf{x}) = f(x_1, x_2, \dots, x_N)$ is defined as

$$H(f) = \begin{bmatrix} \frac{\partial^2 f}{\partial x_1^2} & \frac{\partial^2 f}{\partial x_1 \partial x_2} & \cdots & \frac{\partial^2 f}{\partial x_1 \partial x_N} \\ \frac{\partial^2 f}{\partial x_2 \partial x_1} & \frac{\partial^2 f}{\partial x_2^2} & \cdots & \frac{\partial^2 f}{\partial x_2 \partial x_N} \\ \vdots & \vdots & \ddots & \vdots \\ \frac{\partial^2 f}{\partial x_N \partial x_1} & \frac{\partial^2 f}{\partial x_N \partial x_2} & \cdots & \frac{\partial^2 f}{\partial x_N^2} \end{bmatrix}. \quad (3.5)$$

Several classic methods of linear algebra can be used for determining that $H(f)$ is a PSD matrix. To elaborate a little further, for an $(N \times N)$ -element symmetric matrix \mathbf{A} the following statements are equivalent: i) $\mathbf{A} \succeq \mathbf{0}$; ii) all eigenvalues of \mathbf{A} are nonnegative; iii) all its *principal minors*³ are nonnegative; iv) the Cholesky decomposition is applicable to \mathbf{A} , yielding $\mathbf{A} = \mathbf{C}^T \mathbf{C}$, where we have $\mathbf{C} \in \mathbb{R}^{L \times N}$. The Hessian matrix based PSD testing method is a second-order derivative test, and it reduces to $f''(x) \geq 0$ for $x \in \mathbb{R}$. As seen from Fig. 3.2, this implies that the first-order derivative of $f(x)$ is monotonically non-decreasing.

- **Convex function calculus:** There are several operations which preserve the convexity of convex functions. Briefly, convex functions are closed under summation, nonnegative scaling and the pointwise maximum operations. This property is important, because in many cases $f(\mathbf{x})$ might be complicated, which makes it difficult to directly use the above-mentioned “definition” and “differentiability” based methods for determining its convexity. Even if the “definition” and “differentiability” based methods are directly applicable to $f(\mathbf{x})$, it might still be beneficial to first decompose $f(\mathbf{x})$ into several simpler constituent functions, and then invoke the relevant convexity-preserving properties for determining the convexity of $f(\mathbf{x})$. For clarity, the major operations which preserve convexity are summarized as follows.

1. If $f(\mathbf{x})$ and $g(\mathbf{x})$ are convex functions, then $h(\mathbf{x}) = \omega_1 f(\mathbf{x}) + \omega_2 g(\mathbf{x})$, $\omega_1, \omega_2 \geq 0$ is convex.
2. If $f(\mathbf{x})$ is convex, while $g(\mathbf{x})$ is convex and non-decreasing, then $h(\mathbf{x}) = g[f(\mathbf{x})]$ is convex. For example, if $f(\mathbf{x})$ is convex, so is $e^{f(\mathbf{x})}$, because e^x is convex and non-decreasing.
3. If $f(\mathbf{x})$ is concave, while $g(\mathbf{x})$ is convex and non-increasing, then $h(\mathbf{x}) = g[f(\mathbf{x})]$ is convex.
4. Convexity is preserved under affine mapping. More specifically, if $f(\mathbf{x})$ is convex, then

³In linear algebra, an order- k minor of an $(M \times N)$ -element matrix \mathbf{A} is the determinant of a $(k \times k)$ -element submatrix formed by deleting $(M - k)$ rows and $(N - k)$ columns of \mathbf{A} , where we have $1 \leq k \leq M$, and $k \leq N$. Furthermore, an order- k minor of \mathbf{A} is said to be *principal* if the submatrix is composed of the rows and columns with the same indices. For instance, to get an order-2 principal minor from a matrix \mathbf{A} , if the row 1 and 3 of \mathbf{A} have been kept, then the column 1 and 3 of \mathbf{A} should also be kept. Additionally, a principal minor is termed as a *leading principal minor*, if the submatrix corresponding to a principal minor is composed by the matrix elements of \mathbf{A} in rows and columns from 1 to k . In other words, a leading principal minor corresponds to a submatrix composed by the top k rows and the left k columns. For an $(N \times N)$ -element square matrix, there are N leading principal minors.

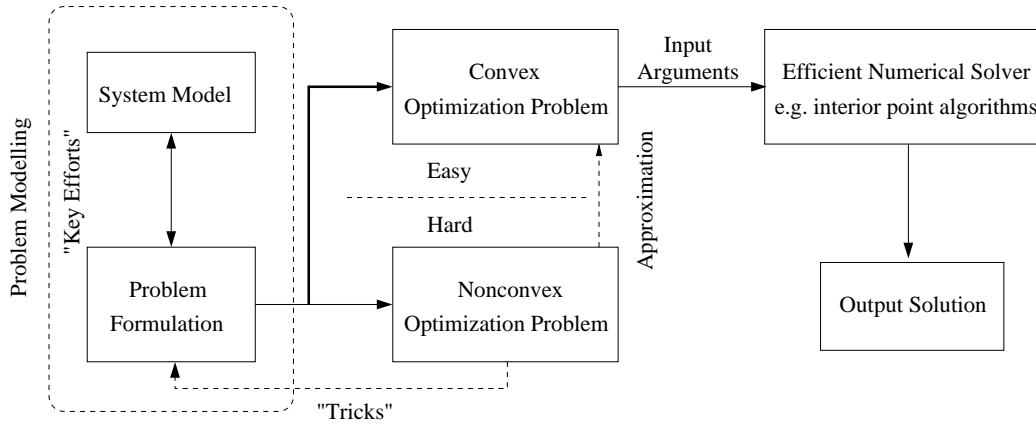


FIGURE 3.3: Framework of solving problems using convex optimization.

$g(\mathbf{x}) = f(\mathbf{A}\mathbf{x} + \mathbf{b})$ is also convex.

5. If $f(\mathbf{x})$ and $g(\mathbf{x})$ are convex functions, then the pointwise maximum $h(\mathbf{x}) = \max\{f(\mathbf{x}), g(\mathbf{x})\}$ is also convex. This property can be extended to the pointwise supremum. More specifically, if for each $\mathbf{y} \in \mathbb{Y}$, $f(\mathbf{x}, \mathbf{y})$ is convex in \mathbf{x} , then the function $g(\mathbf{x}) = \sup_{\mathbf{y} \in \mathbb{Y}} f(\mathbf{x}, \mathbf{y})$ is also convex in \mathbf{x} .
6. The *perspective* operation preserves convexity. More specifically, for a convex function of $f : \mathbb{K}^N \rightarrow \mathbb{R}$, its perspective $g : \mathbb{K}^{N+1} \rightarrow \mathbb{R}$ is defined as $g(\mathbf{x}, t) = tf(\mathbf{x}/t)$, which remains a convex function.

3) *Convex Optimization Problem*: Having reviewed the basic concepts of convex sets, convex functions, as well as the main techniques of identifying a convex function, let us now introduce the concept of convex optimization problems. The problem formulated in (3.1) is said to be a convex optimization problem if all the following conditions are satisfied:

1. the objective function f_0 , and the inequality constraint functions $\{f_i\}_{i=1}^{N_1}$ are convex functions.
2. the equality constraint functions $\{h_j\}_{j=1}^{N_2}$ are affine functions, i.e. h_j can be written in the form of $\mathbf{a}_j^T \mathbf{x} + b_j$ for some $\mathbf{a}_j \in \mathbb{R}^N$ and $b_j \in \mathbb{R}$.
3. \mathbb{K}^N is a convex set.

Fig. 3.3 illustrates the basic framework of solving mathematical optimization problems using convex optimization. If a mathematical optimization problem is identified as a convex optimization problem, it is mathematically regarded as an “easy” problem, because powerful numerical algorithms, such as the interior-point methods [386], exist for efficiently finding the optimal solution of convex problems. Therefore, in mathematical optimization theory, the dividing line between the family of “easy” and “difficult” problems is “convex versus nonconvex”, rather than “linear versus nonlinear”. In other words, convex optimization problems are efficiently solvable, whereas nonconvex optimization problems are generally difficult to solve. Convex optimization has a range of other important properties. For example, in

convex optimization problems, every locally optimal solution constitutes the globally optimal solution, hence there is no risk of being trapped in a local optimum. Additionally, a rigorous optimality condition and a duality theory exist for verifying the optimal nature of a solution in convex optimization problems. For more details of convex optimization, please refer to [244, 369].

3.2.2 Semidefinite Programming

Semidefinite programming (SDP) [243, 368] is a relatively new subfield of convex optimization. It has attracted growing interest, because it unifies several standard optimization techniques such as linear and quadratic programming, whilst imposing only a polynomially rather than exponentially increasing worst-case computational complexity for finding the solution of many engineering and combinatorial optimization problems. Some preliminary mathematical concepts and definitions involved in SDP are briefly introduced as follows.

If \mathbf{X} is a *symmetric* ($N \times N$)-element real-valued matrix, then \mathbf{X} is said to be a PSD matrix, provided that we have

$$\mathbf{v}^T \mathbf{X} \mathbf{v} \geq 0 \quad (3.6)$$

for any vector $\mathbf{v} \in \mathbb{R}^N$. More generally, an ($N \times N$)-element complex-valued matrix \mathbf{X} is said to be a PSD matrix, if

$$\mathbf{v}^H \mathbf{X} \mathbf{v} \geq 0 \quad (3.7)$$

is satisfied for any vector $\mathbf{v} \in \mathbb{C}^N$, where \mathbf{X} becomes a Hermitian matrix. Let $\mathbb{S}^{N \times N}$ and $\mathbb{S}_+^{N \times N}$ denote the set of ($N \times N$)-element symmetric matrices and the set of ($N \times N$)-element PSD symmetric matrices, respectively. Then the expression of “ $\mathbf{X} \succeq 0$ ”, which is a generalized inequality, is conventionally used for indicating that $\mathbf{X} \in \mathbb{S}_+^{N \times N}$. Note that the set of PSD matrices, $\mathbb{S}_+^{N \times N} = \{\mathbf{X} \in \mathbb{S}^{N \times N} | \mathbf{X} \succeq 0\}$, is a convex cone.⁴

3.2.2.1 Several Widely Used Forms of SDP

- **Inequality form:** A SDP problem aims for minimizing a *linear function* of a variable $\mathbf{x} \in \mathbb{R}^N$ subject to the *linear matrix inequality (LMI)* constraint of

$$F(\mathbf{x}) \triangleq \mathbf{F}_0 + \sum_{i=1}^N x_i \mathbf{F}_i \succeq 0, \quad (3.8)$$

where we have $F_0, F_1, \dots, \dots, F_N \in \mathbb{S}^{P \times P}$.

⁴A convex cone is a special type of convex set which is closed under positive scaling.

More specifically, the *inequality form* of a SDP problem is defined as [368]

$$\begin{aligned} \min \quad & \mathbf{c}^T \mathbf{x} \\ \text{s. t.} \quad & F(\mathbf{x}) \succeq 0. \end{aligned} \quad (3.9)$$

The *problem data* of (3.9), namely the coefficients of the objective and constraint functions, are represented by the vector $\mathbf{c} \in \mathbb{R}^N$ and by $(N+1)$ real-valued symmetric matrices F_0, F_1, \dots, F_N , which are all constants known *a priori*.

- **LMI standard form (with equality constraints):** The SDP problem of (3.9) may also be formulated in other widely used forms. In the *LMI standard form (with equality constraints)*, a set of linear equality constraints are introduced in addition to the LMI constraints, which results in the following formulation:

$$\begin{aligned} \min \quad & \mathbf{c}^T \mathbf{x} \\ \text{s. t.} \quad & F(\mathbf{x}) \succeq 0, \\ & \mathbf{A}\mathbf{x} = \mathbf{b}, \end{aligned} \quad (3.10)$$

where the matrices $\mathbf{A} \in \mathbb{R}^{K \times N}$, and the vector $\mathbf{b} \in \mathbb{R}^K$ constitute additional *problem data*. It is worth pointing out that (3.10) may also be converted to the form of (3.9). To elaborate a little further, let us rewrite $\mathbf{A}\mathbf{x} = \mathbf{b}$ as

$$\mathbf{a}_i^T \mathbf{x} = b_i, \quad i = 1, \dots, K, \quad (3.11)$$

where \mathbf{a}_i^T is the i th row of \mathbf{A} , and b_i is the i th element of \mathbf{b} . Furthermore, (3.11) can be rewritten as

$$\mathbf{a}_i^T \mathbf{x} \leq b_i, \quad \mathbf{a}_i^T \mathbf{x} \geq b_i, \quad i = 1, \dots, K, \quad (3.12)$$

which is equivalent to the LMI of

$$\mathbf{G}(\mathbf{x}) = \text{diag}(b_1 - \mathbf{a}_1^T \mathbf{x}, \dots, b_K - \mathbf{a}_K^T \mathbf{x}, \mathbf{a}_1^T \mathbf{x} - b_1, \dots, \mathbf{a}_K^T \mathbf{x} - b_K) \succeq 0. \quad (3.13)$$

As a result, the SDP problem of (3.10) relies on two LMIs, which may however be combined into a single LMI with the aid of the block diagonal operation of $\text{blkdiag}\{\mathbf{F}(\mathbf{x}), \mathbf{G}(\mathbf{x})\}$. Therefore, we can say that SDP essentially represents a family of optimization problems relying on a linear objective function subject to an LMI constraint, as exemplified in (3.9). From a convex geometry based perspective, the SDP problem may also be interpreted as the minimization of a linear objective function over the space created by the intersection of the convex cone $\mathbb{S}_+^{N \times N}$ with an affine space. This geometric object resulted from the intersection is also referred to as a *spectrahedron*, which is essentially a shape defined by an LMI as characterized by (3.8).

- **Standard form:** Alternatively, upon defining a linear function of $\mathbf{X} \in \mathbb{S}_+^{N \times N}$ as

$$\mathbf{C} \bullet \mathbf{X} = \sum_{i=1}^N \sum_{j=1}^N c_{ij} x_{ij} = \text{Trace}(\mathbf{C}\mathbf{X}^T) = \text{Trace}(\mathbf{C}\mathbf{X}), \quad (3.14)$$

the *standard form* of SDP may also be further formulated from (3.10) as

$$\begin{aligned} \min \quad & \mathbf{C} \bullet \mathbf{X} \\ \text{s. t.} \quad & \mathbf{A}_i \bullet \mathbf{X} = b_i, \quad i = 1, \dots, K, \\ & \mathbf{X} \succeq 0, \end{aligned} \quad (3.15)$$

where “ \bullet ” represents the *inner product* of two matrices, and we have $\mathbf{C}, \mathbf{A}_1, \dots, \mathbf{A}_K \in \mathbb{S}^{N \times N}$. Note that because \mathbf{X} is a symmetric matrix, namely we have $x_{ij} = x_{ji}$, hence there are only $\frac{N(N+1)}{2}$ rather than N^2 distinct scalar optimization variables in (3.15).

3.2.2.2 Example of SDP

For the sake of explicit clarity, an example of the SDP problem is given as follows. Considering the standard SDP form of (3.15), let us set $\mathbf{X} = \begin{bmatrix} x_{11} & x_{12} \\ x_{12} & x_{22} \end{bmatrix}$, $\mathbf{C} = \begin{bmatrix} -1 & -2 \\ -2 & -5 \end{bmatrix}$, $\mathbf{A}_1 = \begin{bmatrix} 2 & 1.5 \\ 1.5 & 1 \end{bmatrix}$, $\mathbf{A}_2 = \begin{bmatrix} 1 & 0.5 \\ 0.5 & 0 \end{bmatrix}$, and $\mathbf{b} = \begin{bmatrix} 7 \\ 11 \end{bmatrix}$, then the SDP problem considered can be written as

$$\begin{aligned} \min \quad & -x_{11} - 4x_{12} - 5x_{22} \\ \text{s. t.} \quad & 2x_{11} + 3x_{12} + x_{22} = 7 \\ & x_{11} + x_{12} = 11, \\ & \begin{bmatrix} x_{11} & x_{12} \\ x_{12} & x_{22} \end{bmatrix} \succeq 0, \end{aligned} \quad (3.16)$$

where the last constraint is equivalent to “ $x_{11} \geq 0$, $x_{22} \geq 0$, and $x_{11}x_{22} - x_{12}^2 \geq 0$ ” according to the principal minors method introduced in Section 3.2.1 for determining a PSD matrix. It is worth pointing out that the SDP problem of (3.16), which is a standard form SDP, can also be converted to the LMI standard form that has equality constraints, i.e. to the form of (3.10). More specifically, let us write \mathbf{X} as

$$\mathbf{X} = \sum_{1 \leq i < j \leq \frac{N(N+1)}{2}} x_{ij} \mathbf{E}_{ij}, \quad (3.17)$$

where \mathbf{E}_{ij} is the $\frac{N(N+1)}{2} \times \frac{N(N+1)}{2}$ basis matrix with 1 being the (i, j) th and the (j, i) th elements (i.e. at the symmetric positions determined by (i, j) and (j, i)), and 0 elsewhere.

For example, when considering (3.16), we have

$$\begin{bmatrix} x_{11} & x_{12} \\ x_{12} & x_{22} \end{bmatrix} = \mathbf{F}(\mathbf{x}) = x_{11} \underbrace{\begin{bmatrix} 1 & 0 \\ 0 & 0 \end{bmatrix}}_{\mathbf{E}_{11}} + x_{22} \underbrace{\begin{bmatrix} 0 & 0 \\ 0 & 1 \end{bmatrix}}_{\mathbf{E}_{22}} + x_{12} \underbrace{\begin{bmatrix} 0 & 1 \\ 1 & 0 \end{bmatrix}}_{\mathbf{E}_{12}} + \mathbf{F}_0 \succeq 0, \quad (3.18)$$

with \mathbf{F}_0 being a zero matrix. Similarly, if \mathbf{X} is a 3×3 symmetric matrix, then we have

$$\begin{bmatrix} x_{11} & x_{12} & x_{13} \\ x_{12} & x_{22} & x_{23} \\ x_{13} & x_{23} & x_{33} \end{bmatrix} = x_{11} \begin{bmatrix} 1 & 0 & 0 \\ 0 & 0 & 0 \\ 0 & 0 & 0 \end{bmatrix} + x_{22} \begin{bmatrix} 0 & 0 & 0 \\ 0 & 1 & 0 \\ 0 & 0 & 0 \end{bmatrix} + x_{33} \begin{bmatrix} 0 & 0 & 0 \\ 0 & 0 & 0 \\ 0 & 0 & 1 \end{bmatrix} \\ + x_{12} \begin{bmatrix} 0 & 1 & 0 \\ 1 & 0 & 0 \\ 0 & 0 & 0 \end{bmatrix} + x_{13} \begin{bmatrix} 0 & 0 & 1 \\ 0 & 0 & 0 \\ 1 & 0 & 0 \end{bmatrix} + x_{23} \begin{bmatrix} 0 & 0 & 0 \\ 0 & 0 & 1 \\ 0 & 1 & 0 \end{bmatrix}. \quad (3.19)$$

Finally, the *Lagrangian dual problem* of the standard form SDP of (3.15) is given by

$$\begin{aligned} \max \quad & \mathbf{b}^T \mathbf{y} \\ \text{s. t.} \quad & \sum_{i=1}^K \mathbf{A}_i^T y_i + \mathbf{S} = \mathbf{C} \\ & \mathbf{S} \succeq 0, \end{aligned} \quad (3.20)$$

which also constitutes a SDP problem characterized by the LMI inequality form of (3.9), because the constraint is equivalent to $\mathbf{C} - \sum_{i=1}^K \mathbf{A}_i^T y_i \succeq 0$.

3.3 System Model and Problem Statement

Having introduced the basics of both convex optimization and SDP, let us now focus our attention on the specific MIMO detection problem to be dealt with in this chapter. Similar to Chapter 2, again we consider a symbol-synchronized memoryless SDM-MIMO system having N_t transmit and N_r receive antennas, as shown in Fig. 1.9. The baseband equivalent system model is written as

$$\mathbf{y} = \mathbf{H}\mathbf{s} + \mathbf{n}, \quad (3.21)$$

where \mathbf{y} is the N_r -element received signal vector, \mathbf{s} is the N_t -element transmitted symbol vector, whose elements are from the Gray-coded rectangular M -QAM constellation $\mathbb{A} = \{a_1, a_2, \dots, a_M\}$. Additionally, \mathbf{H} is the $(N_r \times N_t)$ -element complex-valued channel matrix, and \mathbf{n} is the N_r -element complex Gaussian noise vector with a zero mean and covariance matrix of $2\sigma^2 \mathbf{I}_{N_r}$, where $\sigma^2 = N_0/2$.

As mentioned in Section 1.8.1, the ML detection problem of the MIMO system of (3.21) may be formulated as the following constrained discrete LS optimization problem

$$\hat{\mathbf{s}}_{\text{ML}} = \arg \min_{\mathbf{s} \in \mathbb{A}^{N_t}} \|\mathbf{y} - \mathbf{H}\mathbf{s}\|_2^2, \quad (3.22)$$

where \mathbb{A}^{N_t} represents the set of all legitimate N_t -element transmit symbol vectors composed of Gray-coded M -QAM symbols taken from the constellation \mathbb{A} .

In [256], (3.22) was further formulated as⁵

$$\hat{\mathbf{d}}_{\text{ML}} = \arg \min_{\mathbf{d} \in \{+1, -1\}^{M_c N_t}} \left\| \tilde{\mathbf{y}} - \tilde{\mathbf{H}}\mathbf{T}\mathbf{d} \right\|_2^2, \quad (3.23)$$

where $M_c = \log_2 M$ denotes the number of bits per symbol, and \mathbf{d} represents the vector of “index bits” [256]⁶, which are different from the (antipodal) information-bit vector \mathbf{b} [256]. $\tilde{\mathbf{H}}$ and $\tilde{\mathbf{y}}$ are the real-valued versions of \mathbf{H} and \mathbf{y} in (3.22) respectively, while \mathbf{T} is the real-valued transformation matrix, which is fixed for a specific constellation, similar to the complex-valued modulation matrix \mathbf{W} of Chapter 2. After obtaining $\hat{\mathbf{d}}_{\text{ML}}$, the original real-valued symbol vector corresponding to the real-valued system model is estimated as

$$\hat{\mathbf{s}}_{\text{ML}} = \mathbf{T}\hat{\mathbf{d}}_{\text{ML}}. \quad (3.24)$$

In contrast to this solution, the problem of interest to us is — how can we develop a VA-SDPR detector that directly estimates the (antipodal) information bit vector \mathbf{b} without having to estimate the symbol vector \mathbf{s} first?

3.4 Revisiting Gray-Mapping Aided M-QAM

Assume that the j th component of the transmitted M -QAM symbol vector \mathbf{s} is obtained using the bit-to-symbol mapping function $s_j = \text{map}(\mathbf{u}_j)$, $j = 1, 2, \dots, N_t$, where $\mathbf{u}_j = [u_{j,1}, u_{j,2}, \dots, u_{j,M_c}]^T$ is the vector of information bits with each element being 1 or 0. The vector of information bits corresponding to \mathbf{s} is denoted as \mathbf{u} , which satisfies $\mathbf{s} = \text{map}(\mathbf{u})$ and is formed by concatenating the N_t antennas’ information bits $\mathbf{u}_1, \mathbf{u}_2, \dots, \mathbf{u}_{N_t}$, yielding $\mathbf{u} = [u_1, u_2, \dots, u_k, \dots, u_{M_c N_t}]^T = [\mathbf{u}_1^T, \mathbf{u}_2^T, \dots, \mathbf{u}_{N_t}^T]^T \in \{1, 0\}^{M_c N_t}$. The antipodal information bits are obtained from the original information bits of logical 1 or 0 using $b_k = 2u_k - 1$, where $b_k \in \{+1, -1\}$.

As shown in Chapter 2, the nonlinear Gray-mapping aided M -QAM scheme may be formu-

⁵The real-valued model is used in [256], whereas we use the more general complex-valued model here. The relationship between the real-valued and complex-valued MIMO system models is detailed in Section 1.6.

⁶In general, the (real-valued) Gray-coded QAM symbol vector $\tilde{\mathbf{s}}$ *cannot* be represented as a linear transformation of $\tilde{\mathbf{s}} = \mathbf{T}\mathbf{b}$, as shown in Chapter 2. However, it was formulated as $\tilde{\mathbf{s}} = \mathbf{T}\mathbf{d}$ in [256], where \mathbf{d} was termed as “index bits”.

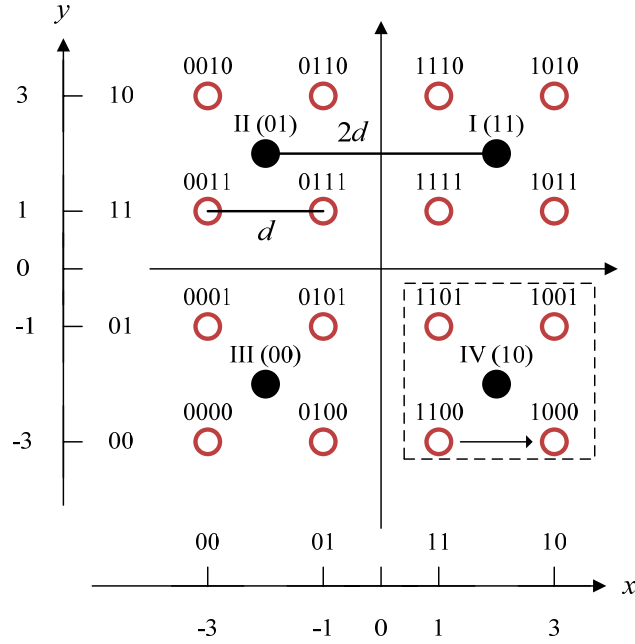


FIGURE 3.4: Constellation decomposition of the Gray-mapping aided 16-QAM.

lated as $\mathbf{s} = \mathbf{W}(\mathbf{b})\mathbf{b}$, where the structure of the modulation matrix $\mathbf{W}(\mathbf{b})$ exhibits multiple forms, depending on the antipodal information bit vector \mathbf{b} . Hence $\mathbf{W}(\mathbf{b})$ is not readily available at the receiver side. Although it may be possible to estimate the modulation matrix $\mathbf{W}(\mathbf{b})$ at the receiver, the estimation error will inevitably degrade the achievable performance.

As an instance, let us revisit the “generating units” of the Gray-mapping aided 16-QAM scheme shown in Table 2.2. Since the four constellation points in the same quadrant share the same generating units, without loss of generality, we will consider the constellation points in Quadrant IV of Fig. 3.4 as an example.

The legitimate original information-bit sequences $[u_1 \ u_2 \ u_3 \ u_4]$ are⁷

$$[1 \ \underline{1} \ 0 \ \underline{0}] \quad [1 \ \underline{0} \ 0 \ \underline{0}] \quad [1 \ \underline{0} \ 0 \ \underline{1}] \quad [1 \ \underline{1} \ 0 \ \underline{1}]. \quad (3.25)$$

The above-mentioned generating units $[g_1 \ g_2 \ g_3 \ g_4]$ corresponding to $[u_1 \ u_2 \ u_3 \ u_4]$ are

$$[2 \ \underline{-1} \ 2i \ \underline{i}] \quad [2 \ \underline{-1} \ 2i \ \underline{i}] \quad [2 \ \underline{-1} \ 2i \ \underline{i}] \quad [2 \ \underline{-1} \ 2i \ \underline{i}]. \quad (3.26)$$

Observing (3.25) and (3.26), two remarks can be made. Firstly, the bits u_1 and u_3 of the four information-bit sequences that are mapped to the specific constellation points dwelling in the

⁷Here the underline is used for dividing the four elements of a vector into two groups.

same quadrant are identical. Secondly, the first and the third components of the generating units are $[g_1 \ g_3] = [2 \ 2i]$, which indicates that the bits u_1 and u_3 of each information-bit sequence are mapped to a 4-QAM constellation, whose amplitude is doubled⁸. Therefore, the Gray-mapping aided 16-QAM symbols of Quadrant IV can be formulated as

$$\begin{aligned} s &= \text{map}_{16\text{-QAM}}(u_1 \ u_2 \ u_3 \ u_4) \\ &= 2 \times \text{map}_{4\text{-QAM}}(u_1 \ u_3) + \text{map}_x(u_2 \ u_4) \\ &= 2s^{(1)} + s^{(2)}. \end{aligned} \quad (3.27)$$

To elucidate the notation of $\text{map}_x(u_2 \ u_4)$ further, let us observe

$$[u_2 \ u_4] : \quad [1 \ 0] \quad [0 \ 0] \quad [0 \ 1] \quad [1 \ 1], \quad (3.28)$$

$$[g_2 \ g_4] : \quad [-1 \ i] \quad [-1 \ i] \quad [-1 \ i] \quad [-1 \ i], \quad (3.29)$$

$$s^{(2)} : \quad -1 - i \quad 1 - i \quad 1 + i \quad -1 + i, \quad (3.30)$$

where we have $s^{(2)} = (2[u_2 \ u_4] - 1) \times [g_2 \ g_4]^T$. Note that $s^{(2)}$ may also be obtained by mapping the bits

$$[\tilde{u}_2 \ \tilde{u}_4] : \quad [0 \ 0] \quad [1 \ 0] \quad [1 \ 1] \quad [0 \ 1] \quad (3.31)$$

to 4-QAM, where $s^{(2)} = (2[\tilde{u}_2 \ \tilde{u}_4] - 1) \times [1 \ i]^T$.

Therefore, (3.27) may be reformulated as

$$s = 2 \times \text{map}_{4\text{-QAM}}(u_1 \ u_3) + \text{map}_{4\text{-QAM}}(\tilde{u}_2 \ \tilde{u}_4). \quad (3.32)$$

On the other hand, we notice that $[\tilde{u}_2 \ \tilde{u}_4]$ may be given by

$$\begin{aligned} 00 &= (\underline{1} \oplus 1)(\underline{0} \oplus 0), \\ 10 &= (\underline{0} \oplus 1)(\underline{0} \oplus 0), \\ 11 &= (\underline{0} \oplus 1)(\underline{1} \oplus 0), \\ 01 &= (\underline{1} \oplus 1)(\underline{1} \oplus 0), \end{aligned} \quad (3.33)$$

where \oplus represents the “exclusive or” (XOR) operation. Eq. (3.33) may be rewritten in a more compact manner as

$$[\tilde{u}_2 \ \tilde{u}_4] = (u_2 \oplus u_1)(u_4 \oplus u_3) = [u_2 \ u_4] \boxplus [u_1 \ u_3], \quad (3.34)$$

⁸As shown in Chapter 2, the natural-mapping and the Gray-mapping are identical for 4-QAM.

TABLE 3.1: Gray-mapping based QAM transformation

16-QAM	$s = 2 \times \text{map}_{4\text{-QAM}}(u_1 u_3) + \text{map}_{4\text{-QAM}}(\tilde{u}_2 \tilde{u}_4),$ where $[\tilde{u}_2 \tilde{u}_4] = (u_1 \oplus u_2)(u_3 \oplus u_4)$
64-QAM	$s = 4 \times \text{map}_{4\text{-QAM}}(u_1 u_4) + 2 \times \text{map}_{4\text{-QAM}}(\tilde{u}_2 \tilde{u}_5) + \text{map}_{4\text{-QAM}}(\tilde{u}_3 \tilde{u}_6),$ where $[\tilde{u}_2 \tilde{u}_5] = (u_1 \oplus u_2)(u_4 \oplus u_5),$ $[\tilde{u}_3 \tilde{u}_6] = (u_1 \oplus u_2 \oplus u_3)(u_4 \oplus u_5 \oplus u_6)$
256-QAM	$s = 8 \times \text{map}_{4\text{-QAM}}(u_1 u_5) + 4 \times \text{map}_{4\text{-QAM}}(\tilde{u}_2 \tilde{u}_6) + 2 \times \text{map}_{4\text{-QAM}}(\tilde{u}_3 \tilde{u}_7) + \text{map}_{4\text{-QAM}}(\tilde{u}_4 \tilde{u}_8),$ where $[\tilde{u}_2 \tilde{u}_6] = (u_1 \oplus u_2)(u_5 \oplus u_6),$ $[\tilde{u}_3 \tilde{u}_7] = (u_1 \oplus u_2 \oplus u_3)(u_5 \oplus u_6 \oplus u_7),$ $[\tilde{u}_4 \tilde{u}_8] = (u_1 \oplus u_2 \oplus u_3 \oplus u_4)(u_5 \oplus u_6 \oplus u_7 \oplus u_8),$
4^q -QAM	$s = 2^{q-1} \times \text{map}_{4\text{-QAM}}(u_1 u_{q+1}) + 2^{q-2} \times \text{map}_{4\text{-QAM}}(\tilde{u}_2 \tilde{u}_{q+2}) + \cdots + 2 \times \text{map}_{4\text{-QAM}}(\tilde{u}_{q-1} \tilde{u}_{2q-1})$ $+ \text{map}_{4\text{-QAM}}(\tilde{u}_q \tilde{u}_{2q}),$ where $\tilde{u}_2 \tilde{u}_{q+2} = (u_1 \oplus u_2)(u_{q+1} \oplus u_{q+2}),$ \vdots $[\tilde{u}_{q-1} \tilde{u}_{2q-1}] = (u_1 \oplus u_2 \oplus \cdots \oplus u_{q-1})(u_{q+1} \oplus u_{q+2} \oplus \cdots \oplus u_{2q-1})$ $[\tilde{u}_q \tilde{u}_{2q}] = (u_1 \oplus u_2 \oplus \cdots \oplus u_q)(u_{q+1} \oplus u_{q+2} \oplus \cdots \oplus u_{2q})$

hence we have

$$[u_2 u_4] = [u_1 u_3] \boxplus [\tilde{u}_2 \tilde{u}_4], \quad (3.35)$$

where \boxplus is the element-wise XOR operator. It may be readily shown that (3.34) and (3.35) also hold for the other three quadrants.

Similarly, the Gray-mapping aided 64-QAM symbols shown in Fig. 2.2 may be derived as

$$\begin{aligned}
 s &= \text{map}_{64\text{-QAM}}(u_1 u_2 u_3 u_4 u_5 u_6) \\
 &= 2 \times \text{map}_{16\text{-QAM}}(u_1 u_2 u_4 u_5) + \text{map}_{4\text{-QAM}}(\tilde{u}_3 \tilde{u}_6) \\
 &= 4 \times \text{map}_{4\text{-QAM}}(u_1 u_4) + 2 \times \text{map}_{4\text{-QAM}}(\tilde{u}_2 \tilde{u}_5) \\
 &\quad + \text{map}_{4\text{-QAM}}(\tilde{u}_3 \tilde{u}_6) \\
 &= 4s^{(1)} + 2s^{(2)} + s^{(3)}.
 \end{aligned} \quad (3.36)$$

where

$$[\tilde{u}_2 \tilde{u}_5] = [u_1 u_4] \boxplus [u_2 u_5], \quad (3.37)$$

and

$$[\tilde{u}_3 \tilde{u}_6] = (u_1 \oplus u_2 \oplus u_3)(u_4 \oplus u_5 \oplus u_6). \quad (3.38)$$

Hence we have

$$[u_2 u_5] = [u_1 u_4] \boxplus [\tilde{u}_2 \tilde{u}_5], \quad (3.39)$$

and

$$[u_3 u_6] = (u_1 \oplus u_2 \oplus \tilde{u}_3)(u_4 \oplus u_5 \oplus \tilde{u}_6). \quad (3.40)$$

The above transformation method can be extended to even higher-order rectangular QAM constellations. For clarity, we summarize their transformation formulae in Table 3.1.

3.5 DVA-SDPR Detector

3.5.1 DVA-SDPR Formulation

For the sake of simplicity, below we will consider 16-QAM as an example to formulate the proposed DVA-SDPR detector. Based on (3.32), the system model (3.21) can be rewritten as

$$\begin{aligned} \mathbf{y} &= [\mathbf{h}_1, \mathbf{h}_2, \dots, \mathbf{h}_{N_t}] \begin{bmatrix} 2s_1^{(1)} + s_1^{(2)} \\ 2s_2^{(1)} + s_2^{(2)} \\ \vdots \\ 2s_{N_t}^{(1)} + s_{N_t}^{(2)} \end{bmatrix} + \mathbf{n} \\ &= [2\mathbf{H} \ \mathbf{H}]\mathbf{x} + \mathbf{n}, \end{aligned} \quad (3.41)$$

where \mathbf{h}_j is the j th column of \mathbf{H} , $\mathbf{x} = [s_1^{(1)}, s_2^{(1)}, \dots, s_{N_t}^{(1)}, s_1^{(2)}, s_2^{(2)}, \dots, s_{N_t}^{(2)}]^T$ with each element being a standard 4-QAM symbol. At this stage, (3.41) may be regarded as a virtual 4-QAM aided $(2N_t \times N_r)$ -element MIMO system⁹.

According to the modulation matrix of 4-QAM given in (2.5), (3.41) can be further reformulated as

$$\mathbf{y} = [2\mathbf{H} \ \mathbf{H}]\mathbf{W}\mathbf{p} + \mathbf{n} = \mathbf{G}\mathbf{p} + \mathbf{n}, \quad (3.42)$$

where \mathbf{G} is the ‘‘composite channel matrix’’, $\mathbf{p} \in \{-1, +1\}^{M_c N_t}$, and

$$\mathbf{W} = \begin{bmatrix} 1 & i & 0 & 0 & \cdots & 0 & 0 \\ 0 & 0 & 1 & i & \cdots & 0 & 0 \\ 0 & 0 & 0 & 0 & \ddots & 0 & 0 \\ 0 & 0 & 0 & 0 & \cdots & 1 & i \end{bmatrix}_{\frac{M_c N_t}{2} \times M_c N_t} \quad (3.43)$$

is the modulation matrix of 4-QAM for both natural-mapping and Gray-mapping. Hence the original Gray-coded 16-QAM $(N_t \times N_r)$ -element MIMO channel has been converted to a virtual $(M_c N_t \times N_r)$ -element MIMO channel relying on binary signaling, where we have $M_c = 4$.

Therefore, the original ML detection related constrained discrete LS optimization problem

⁹This virtual MIMO system is not exactly equivalent to a real $(2N_t \times N_r)$ -element MIMO system, because the left half and the right half of the virtual channel matrix $[2\mathbf{H} \ \mathbf{H}]$ are fully correlated, both relying on \mathbf{H} .

of (3.22) may be reformulated as

$$\hat{\mathbf{p}}_{\text{ML}} = \arg \min_{\mathbf{p} \in \{+1, -1\}^{M_c N_t}} \|\mathbf{y} - \mathbf{G}\mathbf{p}\|_2^2, \quad (3.44)$$

which is shown to be equivalent to the following BQP problem [369]

$$\begin{aligned} \max \quad & 2\mathbf{y}^H \mathbf{G}\mathbf{p} - \mathbf{p}^T \mathbf{G}^H \mathbf{G}\mathbf{p} \\ \text{s. t.} \quad & \mathbf{p} \in \{+1, -1\}^{M_c N_t}, \end{aligned} \quad (3.45)$$

which is difficult to solve due to the non-convex constraints of $p_i^2 = 1$.

In order to cast the objective function of (3.45) into a homogeneous quadratic form, we introduce a redundant scalar $t \in \{+1, -1\}$. Since $t\mathbf{p} \in \{+1, -1\}^{M_c N_t}$ for any $\mathbf{p} \in \{+1, -1\}^{M_c N_t}$, (3.45) may also be formulated as

$$\begin{aligned} \max \quad & [\mathbf{p}^T \ t] \Re\{\mathbf{Q}_c\} [\mathbf{p}^T \ t]^T \\ \text{s. t.} \quad & [\mathbf{p}^T \ t] \in \{+1, -1\}^{M_c N_t + 1}, \end{aligned} \quad (3.46)$$

where $\Re\{\mathbf{Q}_c\}$ represents the real part of the Hermitian matrix

$$\mathbf{Q}_c \triangleq \begin{bmatrix} -\mathbf{G}^H \mathbf{G} & \mathbf{G}^H \mathbf{y} \\ \mathbf{y}^H \mathbf{G} & 0 \end{bmatrix}. \quad (3.47)$$

Upon defining $\mathbf{x} \triangleq [\mathbf{p}^T \ t]^T$ and $\mathbf{Q} \triangleq \Re\{\mathbf{Q}_c\}$, (3.46) may be written in the following homogeneous quadratic form

$$\begin{aligned} \max \quad & \mathbf{x}^T \mathbf{Q} \mathbf{x} \\ \text{s. t.} \quad & \mathbf{x} \in \{+1, -1\}^{M_c N_t + 1}, \end{aligned} \quad (3.48)$$

where \mathbf{Q} is a symmetric matrix. Since we have $\mathbf{x}^T \mathbf{Q} \mathbf{x} = \text{Trace}(\mathbf{Q} \mathbf{x} \mathbf{x}^T) = \text{Trace}(\mathbf{x} \mathbf{x}^T \mathbf{Q})$, the problem of (3.48) may be equivalently rewritten as

$$\begin{aligned} \max \quad & \text{Trace}(\mathbf{X} \mathbf{Q}) \\ \text{s. t.} \quad & \mathbf{X} \succeq 0, \\ & \text{rank}(\mathbf{X}) = 1, \\ & \text{diag}(\mathbf{X}) = \mathbf{e}_{M_c N_t + 1}, \end{aligned} \quad (3.49)$$

where $\mathbf{X} = \mathbf{x} \mathbf{x}^T$, $\mathbf{x} \in \{+1, -1\}^{M_c N_t + 1}$, $\text{diag}(\mathbf{X})$ is the vector composed by the diagonal elements of \mathbf{X} , $\mathbf{e}_{M_c N_t + 1}$ is the ‘‘all-ones’’ vector of size $M_c N_t + 1$, and $\mathbf{X} \succeq 0$ indicates that \mathbf{X} is a symmetric and PSD matrix. Due to the constraint of $\text{rank}(\mathbf{X}) = 1$, the problem (3.49) is non-convex, hence it is difficult to solve. However, by dropping the constraint of

$\text{rank}(\mathbf{X}) = 1$, the problem of (3.49) may be *relaxed* to

$$\begin{aligned} \max \quad & \text{Trace}(\mathbf{X}\mathbf{Q}) \\ \text{s. t.} \quad & \mathbf{X} \succeq 0, \\ & \text{diag}(\mathbf{X}) = \mathbf{e}_{M_c N_t + 1}. \end{aligned} \quad (3.50)$$

The problem of (3.50) is known as an instance of SDP [368], which constitutes a more general class of optimization techniques than linear programming¹⁰. Additionally, since SDP is a subclass of convex optimization, it does not suffer from getting trapped in local minima¹¹.

3.5.2 DVA-SDPR Solving Method

The SDP problem of (3.50) is solved using a modified version of the efficient primal-dual interior-point algorithm (PD-IPA) of [386] with arbitrarily high convergence accuracy, which guarantees a polynomial-time¹² worst-case complexity. The Lagrange dual problem associated with (3.50) is formulated as [245]

$$\begin{aligned} \min \quad & \mathbf{e}_{M_c N_t + 1}^T \mathbf{v} \\ \text{s. t.} \quad & \mathbf{Z} = \text{Diag}(\mathbf{v}) - \mathbf{Q} \succeq 0, \end{aligned} \quad (3.51)$$

where $\text{Diag}(\mathbf{v})$ represents a diagonal matrix with its diagonal elements being \mathbf{v} .

When the objective function values of the primal problem (3.50) and of its dual problem (3.51) satisfy

$$\mathbf{e}_{M_c N_t + 1}^T \mathbf{v} - \text{Trace}(\mathbf{X}\mathbf{Q}) \leq \max[1.0, \text{abs}(\mathbf{e}_{M_c N_t + 1}^T \mathbf{v})] \times \epsilon, \quad (3.52)$$

the PD-IPA is deemed to have converged, where the so-called convergence tolerance $\epsilon = 10^{-k}$ associated with an integer $k \geq 1$, controls the accuracy of convergence. The procedure of the modified version¹³ of the PD-IPA is detailed as follows.

Input: the cost matrix \mathbf{Q} , the required convergence accuracy $\epsilon = 10^{-k}$, $k \in \mathbb{Z}^+$ and the singularity threshold $\tau = 10^{-n}$, $n \in \mathbb{Z}^+$.

Step 1: Initialization—Set the initial value of the number of iterations to $l = 0$; select a starting point $(\mathbf{X}_0, \mathbf{v}_0, \mathbf{Z}_0)$ so that it is in the interior of the feasible sets of both (3.50) and (3.51). For

¹⁰Several standard optimization problems, such as linear and quadratic programming can be unified under the framework of SDP [368].

¹¹This does not mean that the SDPR detector is always capable of achieving the optimal ML performance, because the problem of (3.50) is a relaxed version of the original ML optimization problem of (3.45).

¹²The complexity increases as a polynomial function of the problem size, which is determined by the number of rows (or columns) of the symmetric cost matrix \mathbf{Q} of (3.50) in the considered context. Here \mathbf{Q} is the input argument of the PD-IPA employed.

¹³For details of the modifications we have made regarding the original PD-IPA, please refer to the Remark following Step 2.4.

example, $\mathbf{X}_0 = \text{Diag}(\mathbf{e}_{M_c N_t + 1}) \succ 0$, $\mathbf{v}_0 = \text{abs}(\mathbf{Q}) \times \mathbf{e}_{M_c N_t + 1} \times 1.1$, $\mathbf{Z}_0 = \text{Diag}(\mathbf{v}_0) - \mathbf{Q} \succ 0$, where $\text{abs}(\cdot)$ represents the element-wise absolute value function.

Set the initial value of the primal and dual costs to $C_0^p = \text{Trace}(\mathbf{X}_0 \mathbf{Q})$ and to $C_0^d = \mathbf{e}_{M_c N_t + 1}^T \mathbf{v}_0$, respectively.

Set the initial value of the penalty parameter to $\mu_0 = \frac{0.5 \times \text{Trace}(\mathbf{X}_0 \mathbf{Z}_0)}{M_c N_t + 1}$.

Set the initial value of the positive definiteness indicator of \mathbf{Z}_0 to $f_0^{pd} = 1$.

Step 2: Search loop—while both $(C_l^d - C_l^p > \max([1.0, \text{abs}(C_l^d)] \times \epsilon))$ and $(f_l^{pd} = 1)$ hold true:

Step 2.1: Compute $(\Delta \mathbf{X}, \Delta \mathbf{v}, \Delta \mathbf{Z})$, which determines the search direction using

$$\Delta \mathbf{v} = \left((\mathbf{Z}_l^{-1} \otimes \mathbf{X}_l)^{-1} \right) \times \mu_l \text{diag}(\mathbf{Z}_l^{-1}) - \mathbf{e}_{M_c N_t + 1}, \quad (3.53)$$

$$\Delta \mathbf{Z} = \text{Diag}(\Delta \mathbf{v}), \quad (3.54)$$

$$\Delta \hat{\mathbf{X}} = \mu_l \mathbf{Z}_l^{-1} - \mathbf{X}_l - \mathbf{Z}_l^{-1} \Delta \mathbf{Z} \mathbf{X}_l, \quad (3.55)$$

$$\Delta \mathbf{X} = 0.5 \times \left(\Delta \hat{\mathbf{X}} + \Delta \hat{\mathbf{X}}^T \right), \quad (3.56)$$

where \otimes represents the element-wise multiplication operation.

Step 2.2: Execute line search on the primal problem (resp. the dual problem), and update \mathbf{X}_l (resp. \mathbf{v}_l and \mathbf{Z}_l) and μ_l :

Set the initial step size to $\alpha_p = 1.0$ (resp. $\alpha_d = 1.0$), then invoke Cholesky decomposition to determine whether $\mathbf{X}_l + \alpha_p \Delta \mathbf{X}$ (resp. $\mathbf{Z}_l + \alpha_d \Delta \mathbf{Z}$) is positive-definite or not. If $\mathbf{X}_l + \alpha_p \Delta \mathbf{X} \succ 0$ (resp. $\mathbf{Z}_l + \alpha_d \Delta \mathbf{Z} \succ 0$), let $\mathbf{X}_{l+1} = \mathbf{X}_l + \alpha_p \Delta \mathbf{X}$ (resp. $\mathbf{v}_{l+1} = \mathbf{v}_l + \alpha_d \Delta \mathbf{v}$ and $\mathbf{Z}_{l+1} = \mathbf{Z}_l + \alpha_d \Delta \mathbf{Z}$).

Otherwise, reduce the step size to $\alpha'_p = \eta \alpha_p$ (resp. $\alpha'_d = \eta \alpha_d$), where $\eta \in (0, 1)$, e.g. $\eta = 0.8$, until $\mathbf{X}_l + \alpha'_p \Delta \mathbf{X} \succ 0$ (resp. $\mathbf{Z}_l + \alpha'_d \Delta \mathbf{Z} \succ 0$) holds; then set $\alpha''_p = \gamma \alpha'_p$ (resp. $\alpha''_d = \gamma \alpha'_d$), where $\eta < \gamma < 1.0$ holds true, e.g. $\gamma = 0.95$, so that the currently selected interim point is not on the boundary but in the interior of the corresponding feasible region, and let $\mathbf{X}_{l+1} = \mathbf{X}_l + \alpha''_p \Delta \mathbf{X}$ (resp. $\mathbf{v}_{l+1} = \mathbf{v}_l + \alpha''_d \Delta \mathbf{v}$ and $\mathbf{Z}_{l+1} = \mathbf{Z}_l + \alpha''_d \Delta \mathbf{Z}$).

Subsequently, update the penalty parameter using $\mu_{l+1} = \frac{0.5 \times \text{Trace}(\mathbf{X}_{l+1} \mathbf{Z}_{l+1})}{M_c N_t + 1}$, and if $\alpha''_p + \alpha''_d > 1.8$ (or initially, $\alpha_p + \alpha_d > 1.8$), the current value of μ_{l+1} should be further reduced to $0.5 \mu_{l+1}$.

Step 2.3: Update the value of the primal and dual costs using $C_{l+1}^p = \text{Trace}(\mathbf{X}_{l+1} \mathbf{Q})$ and $C_{l+1}^d = \mathbf{e}_{M_c N_t + 1}^T \mathbf{v}_{l+1}$, respectively.

Step 2.4: Calculate the eigenvalues λ_i of the matrix \mathbf{Z}_{l+1} , $i = 1, 2, \dots, M_c N_t + 1$. If $\exists \text{abs}(\lambda_i) < \tau$, let the positive definiteness indicator of \mathbf{Z}_{l+1} be $f_{l+1}^{pd} = 0$, and terminate the search loop in advance. Otherwise, let $f_{l+1}^{pd} = 1$ and $l = l + 1$, and if the condition $(C_l^d - C_l^p > \max([1.0, \text{abs}(C_l^d)] \times \epsilon))$ holds true as well, repeat Step 2 until the stopping criteria of the search loop are satisfied, and return the solution matrix $\mathbf{X}^* = \mathbf{X}_l$ as the output.

Remark: Note that as μ_l approaches zero, \mathbf{Z}_l tends to be nearly singular, which potentially leads to a degraded numerical stability of the PD-IPA algorithm considered, because

the computation of \mathbf{Z}_l^{-1} is explicitly involved. In order to circumvent this problem, the eigenvalues of \mathbf{Z}^{-1} are examined in Step 2.4 to ensure that the matrix \mathbf{Z}_l employed in the modified PD-IPA always remains positive-definite, and hence the accuracy of the output solution matrix \mathbf{X}^* is not affected. Additionally, the search loop can be curtailed whenever \mathbf{Z}_l is deemed to be singular, because the value of the positive definiteness indicator f_0^{pd} of \mathbf{Z}_l is introduced as another condition for allowing the search loop to proceed. As a result, the potentially unnecessary computations are avoided. ■

After obtaining the solution matrix \mathbf{X}^* of the problem (3.50), the solution vector \mathbf{p}^* of the problem (3.45) may be derived with the aid of several post-processing techniques [252], among which the simplest one is

$$\mathbf{p}^* = \text{sgn}(\mathbf{X}_{1:M_c N_t, M_c N_t + 1}), \quad (3.57)$$

with $\mathbf{X}_{1:M_c N_t, M_c N_t + 1}$ denoting the first $M_c N_t$ elements of the last column of \mathbf{X} . For 16-QAM, as shown by (3.32), the vector $\hat{\mathbf{u}} = (\mathbf{p}^* + \mathbf{e}_{M_c N_t})/2$ contains half of the original information bit vector \mathbf{u}^* . The remaining half of \mathbf{u}^* may be obtained from $\hat{\mathbf{u}}$ with the aid of the element-wise XOR operations of (3.35). On the other hand, for 64-QAM, (3.36) indicates that the vector $\hat{\mathbf{u}} = (\mathbf{p}^* + \mathbf{e}_{M_c N_t})/2$ contains two original information bits, namely u_1 and u_4 , and the remaining four information bits may be obtained from $\hat{\mathbf{u}}$ by using the element-wise XOR operations of (3.39) and (3.40).

3.5.3 Performance Refinement Using Bit-Flipping

The proposed DVA-SDPR detector exhibits the UEP property for the bits in different positions of a single M -QAM symbol¹⁴. This may be explained with the aid of, for example (3.32), where the bits u_1 and u_3 are mapped to a 4-QAM constellation having a doubled amplitude. Inspired by this observation, corresponding to (3.42), each time we may flip the sign of the i th bit p_i^* of \mathbf{p}^* , $i = \frac{M_c N_t}{2} + 1, \dots, M_c N_t$, to obtain a modified solution vector $\tilde{\mathbf{p}}_i^*$. There will be a total of $\frac{M_c N_t}{2}$ modified solution vectors. The final solution vector is chosen as the one, which minimizes $\|\mathbf{y} - \mathbf{G}\mathbf{p}\|_2^2$, when considering \mathbf{p}^* and $\tilde{\mathbf{p}}_i^*$. For 64-QAM, a similar bit-flipping technique may be used corresponding to (3.36).

3.5.4 Computational Complexity Analysis

The SDP problem of (3.50) involves a matrix variable \mathbf{X} of size $(M_c N_t + 1) \times (M_c N_t + 1)$, which entails a computational complexity of $O\left[(M_c N_t + 1)^{3.5}\right]$, when employing the above-mentioned modified version of the PD-IPA of [386]. The complexity of the $\text{sgn}(\cdot)$ operations of (3.57), the XOR operations of for example (3.35), (3.39) and (3.40), the operations of

¹⁴Please refer to the description of Fig. 3.7 in Section 3.6.

the bit-flipping as well as the related Euclidean distance computations do not affect the complexity order. Hence the overall complexity of recovering the original information bit vector is on the order of $O\left[(M_c N_t + 1)^{3.5}\right]$.

3.6 Simulation Results and Discussions

In this section, without loss of generality, we characterize the proposed DVA-SDPR MIMO detector's achievable performance versus the computational complexity in the scenario of the classic Gray-mapping aided 16-QAM using Monte Carlo simulations. The average SNR per receive antenna is defined as

$$\begin{aligned} \text{SNR} &\triangleq 10 \log_{10} \left(\mathcal{E} \left\{ \frac{\|\mathbf{H}\mathbf{s}\|^2}{N_r} \right\} / 2\sigma^2 \right) \\ &= 10 \log_{10} (N_t / 2\sigma^2). \end{aligned} \quad (3.58)$$

The computational complexity is quantified in terms of the number of “equivalent additions”, denoted as N_{add} , required for decoding a single transmitted MIMO symbol vector. More explicitly, we have $N_{\text{add}} \triangleq \mathcal{E}\{T_{\text{tot}}\} / \mathcal{E}\{T_{\text{add}}\}$, where T_{tot} is the average “execution time” required for decoding a MIMO symbol vector, while T_{add} is the average execution time per addition operation.¹⁵ Compared to the absolute “execution-time” metric used in [254], this complexity metric has the advantage of being independent of different simulation platforms.¹⁶ An (8×8) -element flat Rayleigh fading MIMO channel is considered, where the MIMO channel-matrix entries are chosen as independent and identically distributed (i.i.d.), zero mean, unit-variance complex-valued Gaussian random variables. Hence the system's total throughput is $8 \times 4 = 32$ bits/MIMO symbol vector. A new realization of the channel matrix is drawn for each transmitted symbol vector. Each element of the noise vector \mathbf{n} is i.i.d. and $\mathcal{CN}(0, 2\sigma^2)$. Since it has been shown that the SDPR detectors of [252], [254] and [256] are equivalent in performance, below we will consider the IVA-SDPR of [256] as one of the benchmarks.

3.6.1 Simulation Results

Fig. 3.5 quantified the impact of the convergence tolerance ϵ on the performance of the DVA-SDPR MIMO detector. We can observe from Fig. 3.5 that for ϵ being represented by $k = 8$

¹⁵Note that the notion of “equivalent additions” does *not* mean that the proposed DVA-SDPR detector only entails the operation of “real additions”. In fact, it is a metric converting all other operations, like multiplication and inversion etc, to an amount of additions which require the same execution time. To elaborate a little further, in order to get a good estimate of the execution time of a single real addition on a particular computer platform, we can use a single loop performing a large amount of, say 10^9 real additions, and then obtain the execution time of a single real addition by averaging over 10^9 samples.

¹⁶For a given algorithm, both T_{tot} and T_{add} should be measured in the same simulation platform, where T_{add} serves as a normalizing unit.

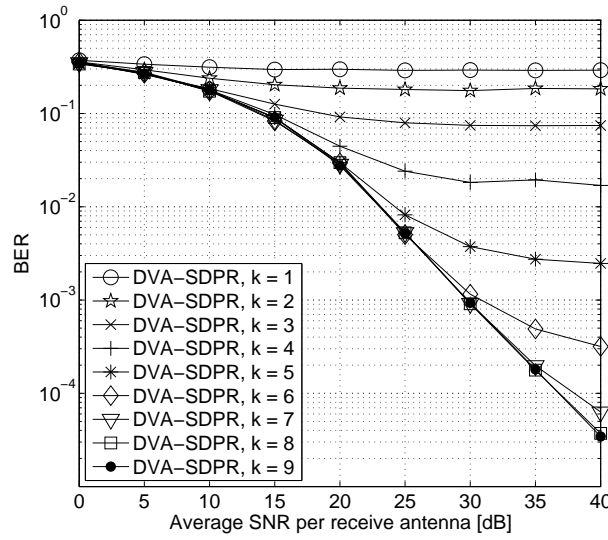


FIGURE 3.5: Impact of the convergence tolerance $\epsilon = 10^{-k}$ on the performance of the DVA-SDPR for 16-QAM aided (8×8) -element MIMO over uncorrelated flat Rayleigh fading channels.

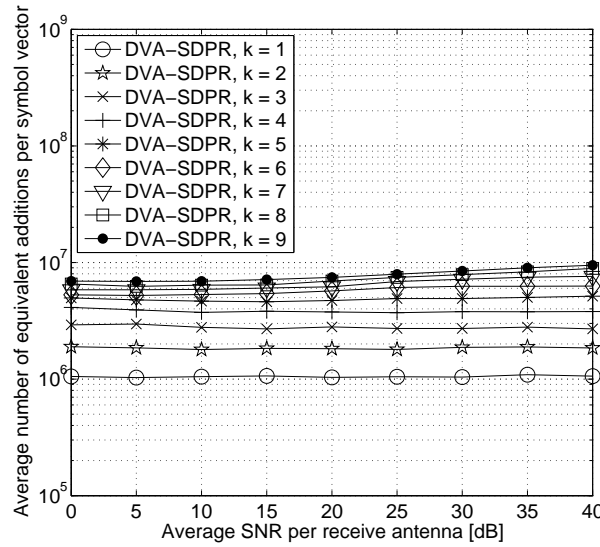


FIGURE 3.6: Impact of the convergence tolerance $\epsilon = 10^{-k}$ on the complexity of the DVA-SDPR for 16-QAM aided (8×8) -element MIMO over uncorrelated flat Rayleigh fading channels.

and $k = 9$ decimal digit accuracy, the DVA-SDPR detector achieved an almost identical performance. By contrast, Fig. 3.6 represents the impact of the convergence tolerance ϵ on the computational complexity of the DVA-SDPR detector. It can be observed that the complexity of the DVA-SDPR detector increased almost linearly upon increasing the number of digits. Based on these observations, we use $\epsilon = 10^{-9}$ in the following numerical experiments related to the DVA-SDPR detector.

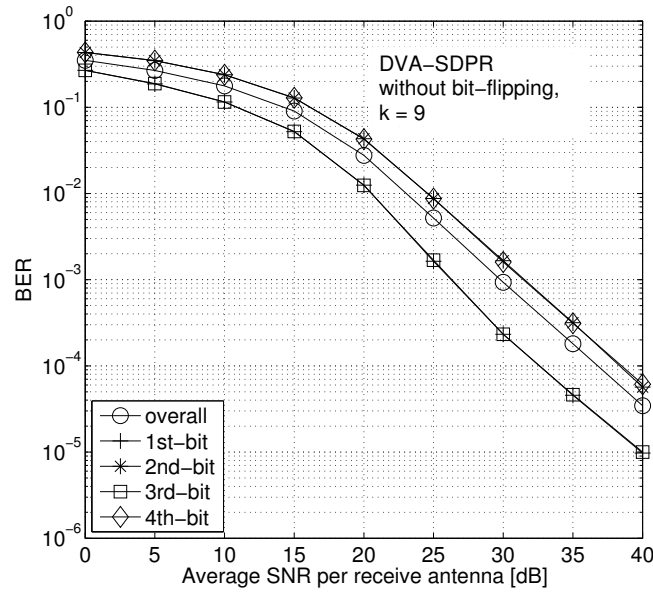


FIGURE 3.7: UEP effect of the DVA-SDPR for Gray-coded 16-QAM aided (8×8) -element MIMO over uncorrelated flat Rayleigh fading channels, with the convergence tolerance $\epsilon = 10^{-9}$.

Fig. 3.7 provided an insight into the UEP characteristics of the proposed DVA-SDPR detector. Observe in the figure that the first and the third bits (resp. the second and the fourth bits), namely u_1 and u_3 (resp. u_2 and u_4) of a single 16-QAM symbol exhibit an identical BER performance, which is better (resp. worse) than the overall BER performance.

In Fig. 3.8, we contrasted the BER performance of the proposed DVA-SDPR (with or without bit-flipping) to that of these benchmarkers, namely to that of the IVA-SDPR of [256], of the MMSE-OSIC, and of the SD relying on an adaptive sphere radius for the sake of achieving the exact ML performance¹⁷. Observe in Fig. 3.8 that the proposed DVA-SDPR detector operating without bit-flipping achieves a BER performance identical to that of the IVA-SDPR benchmarker. By contrast, the bit-flipping aided DVA-SDPR outperforms the IVA-SDPR by about 2dB at $\text{BER} = 10^{-3}$ and $\text{BER} = 10^{-4}$. As expected, all the SDPR detectors considered exhibit a superior BER performance compared to the MMSE-OSIC detector. However, unlike in the BPSK scenario, where the SDPR detector achieves the maximum attainable diversity [249], in the 16-QAM scenario considered, the DVA-SDPR and IVA-SDPR detectors suffer from a considerable performance degradation in the high SNR region compared to the SD. This indicates that the SDPR detectors considered might not be able to achieve full diversity for the Gray-coded 16-QAM aided (8×8) -element MIMO fading channel.

¹⁷This SD is based on the classic SD of [54], and the minimum sphere radius was set to 2.

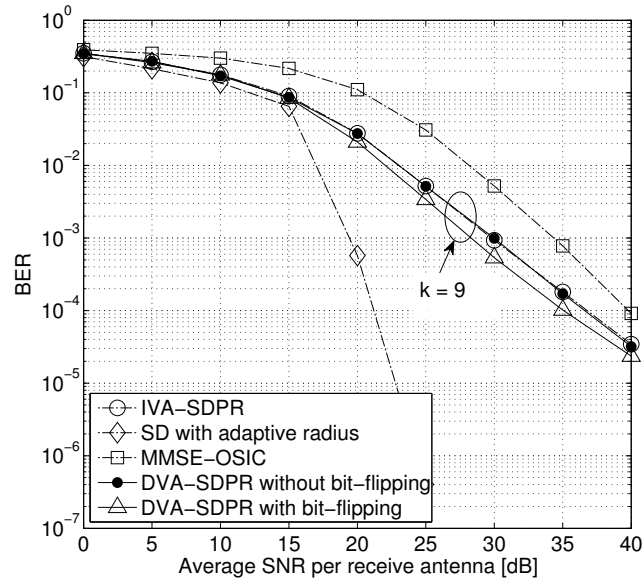


FIGURE 3.8: Performance comparison of the DVA-SDPR, IVA-SDPR, SD and MMSE-OSIC detectors for 16-QAM aided (8×8) -element MIMO over uncorrelated flat Rayleigh fading channels.

In Fig. 3.9, we compared the complexity of the detectors considered in Fig. 3.8. It is readily seen that the SD imposed a significantly higher computational complexity in the low-SNR region than in the high-SNR region, which is consistent with the theoretical results of [61]. By comparison, the computational complexities of both the proposed DVA-SDPR detectors operating with and without bit-flipping as well as the IVA-SDPR detector are near-constant. More specifically, the DVA-SDPR dispensing with bit-flipping has a slightly lower complexity than the IVA-SDPR benchmarker, since the IVA-SDPR detector requires the computation of Eq. (3.24) plus the computation of 16 Euclidean distances for deciding upon each transmitted 16-QAM symbol, before proceeding to the information-bit decisions. On the other hand, the DVA-SDPR using bit-flipping imposes a computational complexity near-identical to that of the IVA-SDPR. Furthermore, the complexity of both the IVA-SDPR and the DVA-SDPR detectors is considerably lower than that of the SD detector. For example, the complexity of the SD at $\text{SNR} = 0$ dB is over 1000 times higher than that of the DVA-SDPR, and is still about 7 times higher than that of the DVA-SDPR in the high-SNR region. Nonetheless, as expected, the complexity of the SDPR based detectors is still higher than that of the MMSE-OSIC detector.

Finally, in Fig. 3.10 we compared the complexity of the DVA-SDPR, the classic SD as well as the FCSD detectors in the context of “massive” MIMOs [384, 385], where the number of transmit antennas can be very high. Indeed, the employment of “massive” MIMOs becomes potentially important in the emerging heterogeneous wireless communication systems using the millimeter-wave band. This is because at millimetric wavelength hundreds of low-cost

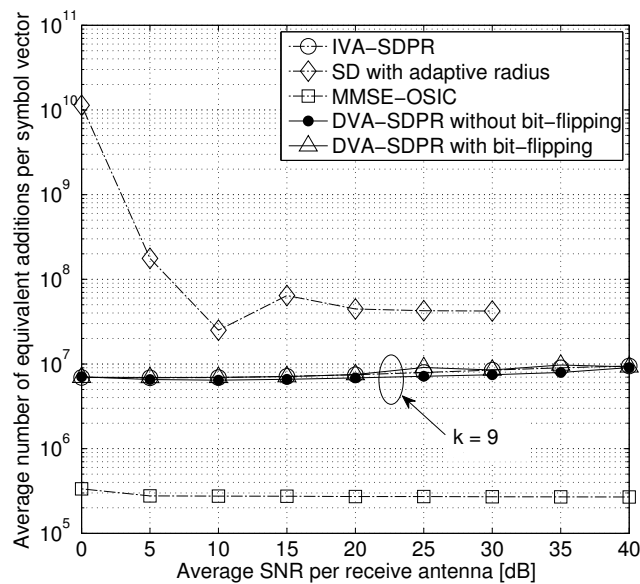


FIGURE 3.9: Complexity comparison of the DVA-SDPR, IVA-SDPR, SD and MMSE-OSIC detectors for 16-QAM aided (8×8) -element MIMO.

antenna-elements may be integrated into the backplane of laptops and mobile phones for the sake of compensating for the increased pathloss [385]. It is observed in Fig. 3.10 that the DVA-SDPR detector has a significantly lower computational complexity compared to the SD, especially when N_t is high. Additionally, the FCSD also shows a dramatically reduced complexity compared to the SD, but it still has a higher complexity than the DVA-SDPR detector, when N_t is very high. This implies that although the SD based detectors are competitive at the time of writing in the relatively low-throughput MIMO systems associated with moderate values of N_t , it might be difficult to use them in the “massive” MIMO systems of the near future [384, 385], where the DVA-SDPR detector might be more promising.

3.6.2 Discussions

1) To the best of our knowledge, in the uncoded Gray-mapping aided 16-QAM (8×8) -element MIMO scenario considered, the DVA-SDPR using bit-flipping achieves the best BER performance result among the known SDPR-aided MIMO detectors, while still maintaining a polynomially increasing worst-case complexity order of $O[(M_c N_t + 1)^{3.5}]$. Additionally, since the proposed DVA-SDPR detector directly generates the information-bit decisions without first making symbol decisions, it may reduce the hardware cost in practical applications. In general, the DVA-SDPR, the IVA-SDPR and the MMSE-OSIC detectors may serve as efficient alternatives for the SD in the low-SNR region, say below about 15dB in the context considered. The SDPR detectors achieve full-diversity in a BPSK scenario, hence

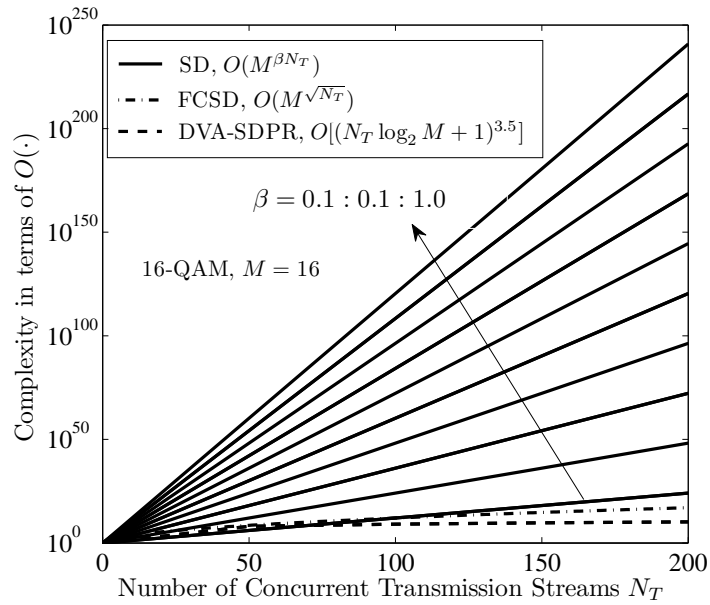


FIGURE 3.10: Complexity comparison of the DVA-SDPR and the SD based detectors for 16-QAM aided massive MIMO where the value of N_t can be very high.

an interesting problem for future research is to conceive efficient SDPR detectors that can approach the ML performance for high-order QAM.

2) In practical MIMO systems, typically channel coding is applied and a powerful iterative detection and decoding based receiver is employed. In order to facilitate its application in coded systems, the SDP based MIMO detector has to output soft information. Indeed, there have been some efforts dedicated to extending the SDP based detection to the soft-input soft-output scenario. However, because most of the existing SDP based hard MIMO detectors are dependent on the specific modulation constellation, most of the available *soft* SDP detectors are only capable of estimating unknown binary variables. For example, the soft SDP-based MIMO detectors proposed in [374, 387] are only applicable to BPSK and QPSK (since a QPSK symbol can be treated equivalently to two BPSK symbols). As a further effort, the authors of [388] proposed a soft SDP based MIMO detector for 16-QAM, which is not applicable to other high-order QAM constellations. Since the DVA-SDPR detector proposed in this chapter transforms the symbol detection of the general rectangular M -QAM constellations to BPSK-like detection, the existing soft SDP detectors devised for estimating unknown binary variables are expected to be immediately applicable to facilitating the soft-detection in MIMO systems relying on high-order rectangular QAM. However, because the soft SDP detection is beyond the scope of this chapter, it may be investigated in our future work.

3) Although the empirical results found in both the open literature and in this chapter imply that the SDP based MIMO-QAM detectors experience a considerable performance

loss, so far little has been known about the theoretical performance of the SDP based MIMO-QAM detector¹⁸. Indeed, the theoretical performance of the SDP based MIMO detector is relatively well-understood in the case of a BPSK scenario. More specifically, it was shown that the SDP based MIMO detector achieves the maximum possible receiver diversity order in the high-SNR region, as the ML detector does, when assuming a real-valued channel matrix [249].

Unfortunately, the performance analysis provided in [249] *cannot* be extended to the scenario of QAM constellations, because the analysis presented in [249] depends crucially on the structure of the channel matrix. More specifically, in the scenario of a channel matrix having real-valued elements corresponding to BPSK modulation, the rotational symmetry of the distribution of the channel matrix is explicitly exploited for proving that the SDP based MIMO detector is capable of achieving the maximum attainable diversity order. However, for the scenario of a channel matrix having complex-valued elements corresponding to QAM constellations, the rotational symmetry of the channel matrix is lost, even when the channel matrix is i.i.d. circularly symmetric zero-mean complex Gaussian [249]. It was shown in [249] that the SDP based MIMO detector appears to experience a modest loss in diversity gain even for 4-QAM, although the complex-valued channel matrix has been rewritten in an equivalent real-valued form.

In this chapter, the SDP based MIMO-QAM detector is reformulated as a virtually BPSK-like MIMO detector, which facilitates the employment of bit-flipping for improving the SDP based MIMO-QAM detector's performance. Additionally, this transformation might be helpful for analyzing the SDP based MIMO-QAM detector's performance, because it has a close connection to the SDP based MIMO-BPSK detector. To elaborate a little further, due to the transformation presented in this chapter, it has become possible to invoke the analytical results previously obtained for the SDP based MIMO-BPSK detector for the sake of assisting the performance analysis of the SDP based MIMO-QAM detectors. For instance, we can now infer that the structure of the "equivalent" channel matrix in our BPSK-like signal model is responsible for the diversity-order loss experienced by high-order QAM constellations. The more rigorous and comprehensive theoretical performance analysis of the SDP based MIMO-QAM detectors is an interesting problem to tackle in our future work.

3.7 Chapter Summary and Conclusions

In contrast to the existing IVA-SDPR detector, the proposed DVA-SDPR detector bypasses symbol-decisions and directly generates the information bits of classic Gray-mapping aided

¹⁸There is only one paper investigating the SDP based MIMO detector's diversity-order performance to date, but it is limited to BPSK scenario, as seen in [249].

M -QAM by employing a simple linear matrix representation of 4-QAM. Based on this contribution, the MIMO detector and constellation demapper modules of high-order rectangular QAM using either linear natural mapping or nonlinear Gray mapping may be replaced by a single DVA-SDPR detector, which performs detection and demapping jointly. Furthermore, when combined with low-complexity bit-flipping based “hill climbing” method, the proposed DVA-SDPR detector achieves the best BER performance among the known SDPR-based detectors in the context considered, while still maintaining the lowest-possible polynomial-time worst-case complexity order of $O[(N_t \log_2 M + 1)^{3.5}]$.

Approximate Bayes' Theorem Based PDA for Iterative MIMO Detection and Channel Decoding

4.1 Introduction

IN Chapter 2 and Chapter 3, we investigated the PDA and the SDPR based virtually antipodal detectors in the context of *uncoded* MIMO systems, respectively. One of the major benefits of using MIMO techniques is that they are capable of significantly improving the capacity of a wireless communication system. When conceiving more advanced wireless systems that use both MIMO techniques [101, 186] and near-capacity FEC codes, such as turbo codes [364, 365, 389] and LDPC codes [366, 367] to simultaneously achieve a high throughput and an infinitesimally low error rate, a significant challenge is that the computational complexity of the receivers becomes even more prohibitive than that of their uncoded counterparts.

More specifically, when uncoded MIMO systems are considered, the transmitted bits are usually assumed to be equiprobable and independent. Consequently, it remains optimal for the ML detector to operate solely on each individual received signal vector \mathbf{s} , as shown in Fig. 4.1. We have pointed out in Section 1.8.1 that this vector-by-vector based detection strategy imposes an exponentially increasing complexity of $O(2^{M_b N_t})$, where M_b is the number of bits per constellation symbol and N_t is the number of transmit antennas.

By comparison, if the bit vector \mathbf{b} mapped to the symbol vector \mathbf{s} is the output of an FEC encoder having a coding rate of $R \leq 1$ that introduces redundancy and correlation between the entries of \mathbf{b} , it is suboptimal for the signal detector and FEC decoder to

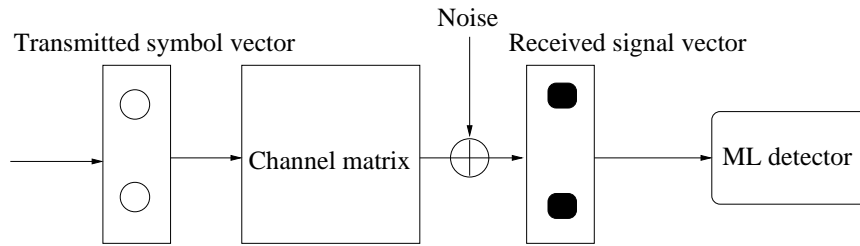


FIGURE 4.1: The optimal vector-by-vector based detection strategy for uncoded MIMO systems.

operate separately and only on individual vectors of \mathbf{s} or \mathbf{b} . As opposed to this conventional receiver architecture, the optimal receiver conceived for FEC-coded MIMO systems has to *jointly* optimize the MIMO detector and the FEC decoder, which implies that the signal detector should make decisions jointly on all the symbol vectors using the knowledge of the *correlation* across these symbol vectors introduced by the FEC code, and the FEC decoder should decode using likelihood information on all the bit vectors obtained from the signal detector. This optimal joint detection-and-decoding strategy is illustrated in Fig. 4.2. For example, in an analogous BPSK-modulated convolutionally coded CDMA system, the maximum-likelihood sequence estimator (MLSE) based optimal joint detector/decoder performs both the functions of MUD and FEC decoding together, which was shown to impose a complexity that is on the order of $\mathcal{O}(2^{KL})$ per bit [390], where K is the number of users and L is the code's constraint length. This result may be readily extended to FEC-coded MIMO scenarios, yielding a complexity of $\mathcal{O}(2^{M_b N_t L})$ per bit, where M_b is the number of bits per modulated symbol and N_t is the number of transmit antennas. Regrettably, this computational complexity is excessive even for a low-throughput system.

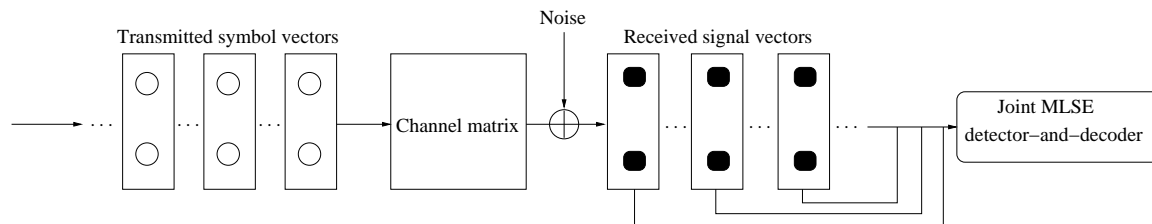


FIGURE 4.2: The optimal MLSE based joint detection-and-decoding strategy conceived for FEC-coded MIMO systems.

Alternatively, the iterative detection and decoding (IDD) [75, 391, 392], which was inspired by decoding of concatenated codes [364, 365, 393, 394], is capable of closely approximating the performance of the MLSE based optimal joint detector/decoder suggested in [390]. A conceptual illustration of the IDD strategy is provided in Fig. 4.3. When exploiting the “turbo principle” [391], the individual decoding modules must be capable of both accepting and generating probabilities or soft values, where the so-called extrinsic part of the soft output of one decoder is delivered to the other decoder as its *a priori* information. As a benefit, a good IDD design is capable of achieving a near-optimum performance at a

significantly lower complexity than the optimal joint detector/decoder [75, 392]. Even so, the computational complexity imposed by the IDD might remain the limiting factor in practical applications.

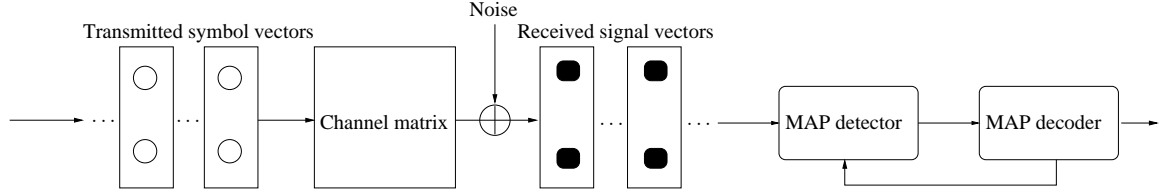


FIGURE 4.3: The near-optimal MAP based iterative detection and decoding strategy designed for FEC-coded MIMO systems.

As mentioned in Section 1.8.5 and shown in Chapter 2, the PDA technique inherently constitutes a SISO algorithm, hence it is expected to be eminently applicable in combination with soft-decodable FEC codes, such as convolutional codes, turbo codes and LDPC codes. Because the key feature of PDA is the repeated conversion of a multimodal Gaussian mixture distribution to a single multivariate Gaussian distribution, the accuracy of the Gaussian approximation dominates the attainable performance. We have shown in Chapter 2 that in the context of uncoded MIMO systems using rectangular M -QAM, the quality of the Gaussian approximation in PDA may be improved by transforming the symbol-based model into a bit-based model, which in effect increases the length of the *effective transmitted signal vector* from N_t to $N_t \log_2 M$, and reduces the *effective constellation* to a binary constellation. With regard to improving the quality of the Gaussian approximation in FEC-coded MIMO systems, we benefit from having an increased exploitable degree of freedom. For example, the soft information gleaned from the output of the FEC decoder tends to be more reliable than the output symbol probabilities of the PDA detector itself. Therefore the FEC decoder's soft output would facilitate a more accurate modelling of the interantenna interference (IAI). In this chapter, our aim is to design a low complexity PDA-based IDD receiver for FEC-coded MIMO systems using arbitrary memoryless M -ary modulation.

Note that there are other alternative SISO MIMO detection algorithms, which include, but are not limited to the high-complexity MAP algorithm, the family of soft interference cancellation algorithms [392, 395], and the list sphere decoding (LSD) algorithm [75]. More explicitly, the MAP algorithm achieves the best performance, but its computational complexity increases exponentially with the number of transmit antennas. Compared with the MAP algorithm, the LSD has a reduced complexity but a suboptimal performance. However, the size of the LSD's candidate list is determined by the SNR-dependent sphere radius, which still results in an excessive complexity for the scenario of low-SNR and/or high-throughput MIMO systems [61], especially in the vicinity of the "turbo-cliff". The soft interference cancellation algorithm has a substantially lower computational complexity than the MAP and the LSD algorithms, but its achievable performance is also less attractive. Since the

PDA algorithm was shown to achieve a near-optimal performance at a low computational complexity in *uncoded* systems [219], it is interesting to investigate its potential in *coded* MIMO systems.

However, there are several particular challenges that render the IDD design using PDA less straightforward than it seems to be.

- *Firstly*, to the best of our knowledge, all the existing PDA detectors conceived for uncoded systems operate purely in the probability-domain [41, 43, 193, 219, 226, 234], which results in a poor numerical stability in IDD scenarios, hence potentially leading to a degraded performance.
- *Secondly*, it is unclear how to produce the *correct* bit-based extrinsic log-likelihood ratios (LLRs) required by the concatenated outer FEC decoder. Conventionally, the output symbol probabilities of the existing PDA algorithms were interpreted as the APPs [193, 219, 226, 234]. Hence, one may assume that a natural way of generating the bit-based extrinsic LLRs is to subtract the bit-based *a priori* LLRs from the bit-based *a posteriori* LLRs generated from the output probabilities of the PDA algorithms. However, we will show that this classic relationship no longer holds if we still treat the output symbol probabilities of the existing PDA algorithms as APPs in the context of IDD receivers.
- *Thirdly*, the existing PDA algorithms [41, 43, 193, 219, 226, 234] have an inherently self-iterative structure, where the estimated symbol probabilities are delivered to the next *inner iteration* after the current inner iteration is completed. Then, the question of how to deal with the inner iterations of the existing PDAs in the context of IDD receivers arises.

Against this backdrop, the main contributions of this chapter are as follows.

- 1) We present an analysis of the interference-plus-noise distribution for the MIMO signal model, which sheds light on the fundamental principles of the PDA algorithms from a new perspective.
- 2) We propose an approximate Bayes' theorem based logarithmic-domain PDA (AB-Log-PDA) MIMO detector for IDD aided MIMO systems employing arbitrary M -ary modulations, which has not been reported before. The proposed AB-Log-PDA enjoys better numerical stability and accuracy, hence it is better suited for iterative detection than the existing probability-domain PDA detectors conceived for uncoded systems [41, 43, 193, 219, 226, 234].
- 3) In contrast to the conventional interpretations of the mathematical properties of the estimated output symbol probabilities of the PDA algorithms, we will demonstrate that these probabilities do *not* constitute the true symbol APPs, they rather constitute the normalized symbol likelihoods. We note however that these output symbol probabilities were treated as APPs without causing any problems in the uncoded systems considered in [41, 43, 193, 219, 226, 234]. The differences between these symbol probabilities and the

true APPs have never been reported before, because the calculation of the extrinsic LLRs is not required in the context of uncoded systems. Owing to this misinterpretation, it is flawed to produce the bit-based extrinsic LLRs from the output symbol probabilities of the PDA algorithms by using the classic relationship, where the extrinsic LLRs are given by subtracting the *a priori* LLRs from the *a posteriori* LLRs. We demonstrate furthermore that the classic candidate-search aided bit-based extrinsic LLRs calculation method, which is used for example by the MAP detector and the list sphere decoder, is not applicable to any PDA-based detector. In order to circumvent the above-mentioned problems, we conceive a new technique of producing the bit-based extrinsic LLRs for the proposed AB-Log-PDA, which results in a simplified IDD structure, where the extrinsic LLRs of the AB-Log-PDA are generated by directly transforming the output symbol probabilities into bit-based LLRs, without subtracting the *a priori* LLRs.

4) We reveal that introducing inner iterations into the AB-Log-PDA actually degrades the achievable performance of the IDD receiver, which is in contrast to the impact of the inner iterations within the FEC-decoder of other types of iterative receivers. The reasons as to why the inner PDA iterations fail to provide BER improvement are investigated and discussed in detail. Notably, we show that the proposed AB-Log-PDA based IDD scheme invoking no inner iterations within the AB-Log-PDA strikes an attractive performance versus complexity tradeoff, which compares favorably to that of the optimal MAP based IDD scheme in both *perfect and imperfect* channel-estimation scenarios, when communicating over Nakagami- m fading channels. For example, in some scenarios the performance of the proposed AB-Log-PDA based IDD scheme approaches that of the MAP-based IDD scheme within 0.5 dB, while imposing a significantly lower computational complexity.

The remainder of this chapter is organized as follows. In Section 4.2, our FEC-coded MIMO system model is introduced, while in Section 4.3, we present our analysis of the interference-plus-noise distribution for our MIMO signal model, which sheds light on the fundamental principles of the PDA from a new perspective. In Section 4.4, the proposed AB-Log-PDA is presented, which relies on the *a priori* soft information feedback gleaned from the FEC decoder. Then, in Section 4.5 the extrinsic LLR calculation of the AB-Log-PDA is detailed, while our simulation results and discussions are presented in Section 4.6. Finally, this chapter is concluded in Section 4.7.

4.2 System Model

We consider the FEC-coded SDM-MIMO system that employs an IDD receiver, as shown in Fig. 4.3. IDD receivers have numerous design variants. As far as SDM-MIMO systems are concerned, the classic IDD receiver architecture is depicted in Fig. 4.4, which is the most frequently encountered implementation of the generic IDD receiver of Fig. 4.3. At

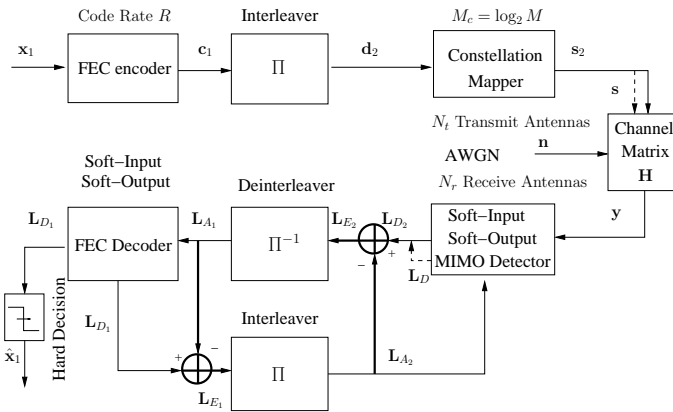


FIGURE 4.4: The FEC-coded MIMO system with the classic IDD receiver architecture, where we have both $\mathbf{L}_{E_1} = \mathbf{L}_{D_1} - \mathbf{L}_{A_1}$ and $\mathbf{L}_{E_2} = \mathbf{L}_{D_2} - \mathbf{L}_{A_2}$, as indicated by the two highlighted addresses. This architecture is the most frequently encountered implementation of the generic IDD receiver of Fig. 4.3. The subscript “1” denotes the processing modules associated with the outer FEC encoder/decoder, and the subscript “2” denotes the processing modules that are connected to the inner space-time mapper/detector. The arrow with dashed line indicates that \mathbf{s} and \mathbf{L}_D are the subvectors of \mathbf{s}_2 and \mathbf{L}_{D_2} , respectively. The closed loop of $\mathbf{L}_{E_2} \rightarrow \mathbf{L}_{A_1} \rightarrow \mathbf{L}_{E_1} \rightarrow \mathbf{L}_{A_2} \rightarrow \mathbf{L}_{E_2}$ represents a global/outer iteration, while the local/inner iterations take place within the soft FEC decoder and/or the soft MIMO detector.

the transmitter, the $(L_f \times 1)$ -bit source frame \mathbf{x}_1 is firstly encoded by a rate $R < 1$ FEC encoder (typically a convolutional code, a turbo code or an LDPC code) into the $(\frac{L_f}{R} \times 1)$ -bit coded frame \mathbf{c}_1 . In order to guard against bursty fading, \mathbf{c}_1 is then passed through a bit-interleaver. Then the $(\frac{L_f}{R} \times 1)$ -bit interleaver’s output frame \mathbf{d}_2 is mapped to the $(\frac{L_f}{RM_b} \times 1)$ -element symbol frame \mathbf{s}_2 , with each symbol taken from the M -ary modulation constellation $\mathbb{A} = \{a_1, a_2, \dots, a_M\}$, where $M_b = \log_2 M$ is the number of bits per constellation symbol. Finally, \mathbf{s}_2 is transmitted in the form of the $(N_t \times 1)$ -element *symbol vector* \mathbf{s} using $N_t \geq 1$ transmit antennas per channel use, and \mathbf{s} does not contain any additional space-time coding. This indicates that a single FEC-coded bit frame \mathbf{c}_1 is transmitted by $\frac{L_f}{RM_b N_t}$ channel uses.

At the output of the fading channel \mathbf{H} , the received $(N_r \times 1)$ -element complex-valued base-band signal vector per channel use is represented by

$$\mathbf{y} = \mathbf{H}\mathbf{s} + \mathbf{n}, \quad (4.1)$$

where $\mathbf{s} = [s_1, s_2, \dots, s_{N_t}]^T$ is normalized by the component-wise energy constraint $\mathcal{E}(|s_i|^2) = E_s/N_t$ in order to maintain a total transmit power E_s per channel use; and \mathbf{n} is the $(N_r \times 1)$ -element zero-mean complex-valued Gaussian noise vector with a covariance matrix of $2\sigma^2 \mathbf{I}_{N_r}$ where \mathbf{I}_{N_r} represents an $(N_r \times N_r)$ -element identity matrix; and \mathbf{H} is an $(N_r \times N_t)$ -element complex-valued matrix with entries of h_{ji} , which are perfectly known to the receiver, $j = 1, \dots, N_r$, $i = 1, \dots, N_t$. In this chapter, we assume that

$$h_{ji} = r \exp(j\theta) \quad (4.2)$$

is independent and identically distributed (i.i.d), where the phase θ is uniformly distributed and independent of the envelope r , while r obeys the Nakagami- m distribution with the probability density function (PDF) of [396]

$$p(r) = \frac{2}{\Gamma(m)} \left(\frac{m}{\Omega}\right)^m r^{2m-1} \exp(-mr^2/\Omega), \quad r \geq 0, \quad (4.3)$$

where $\Gamma(\cdot)$ represents the Gamma function, $\Omega \triangleq \mathcal{E}(r^2)$, and the Nakagami *fading parameter* is $m \triangleq \Omega^2/\mathcal{E}[(r^2 - \Omega)^2]$, $m \geq 0.5$.

Note that the Nakagami- m fading model captures a wide range of realistic fading environments, encompassing the most frequently used Rayleigh fading model as a special case and often serving as a good approximation to the Rician fading model. More specifically, the parameter m indicates the severity of the fading. As m becomes smaller, the fading effects become more severe. For example, when m decreases to 0.5, Eq. (4.3) approaches the one-sided Gaussian distribution; when $m = 1$, Eq. (4.3) reduces to a Rayleigh PDF, and as $m \rightarrow \infty$, Eq. (4.3) reduces to a δ -distribution located at $r = 1$, which corresponds to imposing no fading on the amplitude of the transmitted signal, but only a “pure random phase” obeying a uniform distribution on the circle of radius $\sqrt{\Omega}$. The Rician and the Nakagami- m models may be deemed to behave similarly near their mean value. Hence, for the sake of analytical simplicity, the Nakagami- m model is often advocated in the literature as an approximation of the Rician model. This approximation is more accurate if the main lobe of the Rician model’s PDF is concerned, but it becomes inaccurate for the tail of the Rician model’s PDF. Since bit errors or outages mainly occur during deep fades, these performance measures are typically governed by the tail of the PDF, which represents the probability of receiving a low power. As a result, for deep fades, modeling a Rician fading signal by a Nakagami distribution of the amplitude leads to overly optimistic results. In addition to its generalized nature, the Nakagami- m fading model was shown to fit the experimental propagation data better than the Rayleigh, Rician and Lognormal distributions [397].

4.3 Interference-Plus-Noise Distribution Analysis

In order to provide more insight on the fundamental principle underlying the PDA method, an interference-plus-noise distribution analysis is carried out in this section.

The received signal model of (4.1) may be rewritten as

$$\mathbf{y} = s_i \mathbf{h}_i + \underbrace{\sum_{k \neq i} s_k \mathbf{h}_k}_{\mathbf{u}_i} + \mathbf{n} \triangleq s_i \mathbf{h}_i + \underbrace{\mathbf{u}_i}_{\mathbf{v}_i} + \mathbf{n}, \quad (4.4)$$

where \mathbf{h}_i denotes the i th column of \mathbf{H} , and s_i is the i th symbol of \mathbf{s} , while \mathbf{u}_i is the sum

of $(N_t - 1)$ IAI components contaminating the symbol s_i , $i, k = 1, 2, \dots, N_t$, and \mathbf{v}_i is the interference-plus-noise term for s_i .

Note that if \mathbf{u}_i vanishes, Eq. (4.4) reduces to the classic single-input-multiple-output interference-free broadcast channel having a receive diversity order of N_r . Similarly, if we know exactly the distribution of \mathbf{u}_i or s_k , potentially the adverse effects of the IAI may be mitigated. This is because \mathbf{h}_k is assumed to be perfectly known to the receiver, hence it can be regarded deterministic per channel use, as mentioned in Section 4.2. However, unfortunately, the distribution of \mathbf{u}_i is generally unknown. A notable exception is, when the number of independent IAI components is sufficiently high, \mathbf{u}_i approaches a multivariate Gaussian distribution according to the central limit theorem,

On the other hand, we observe that the interference term \mathbf{u}_i has a total of M^{N_t-1} possible interference patterns. Then, the n th legitimate interference pattern imposed by a given sample of

$$\underline{\mathbf{s}}_n = [\underline{s}_{1,n}, \dots, \underline{s}_{k,n}, \dots, \underline{s}_{N_t,n}]_{k \neq i}^T \quad (4.5)$$

is defined as

$$\underline{\mathbf{u}}_{i,n} \triangleq \sum_{k \neq i} \underline{s}_{k,n} \mathbf{h}_k, \quad (4.6)$$

while the corresponding interference-plus-noise pattern is defined as

$$\underline{\mathbf{v}}_{i,n} \triangleq \underline{\mathbf{u}}_{i,n} + \mathbf{n}, \quad (4.7)$$

where $\underline{s}_{k,n} = a_m \in \mathbb{A}$, $n = 1, 2, \dots, M^{N_t-1}$. We observe that $\underline{\mathbf{v}}_{i,n}$ obeys a multivariate Gaussian distribution with a mean of $\sum_{k \neq i} \underline{s}_{k,n} \mathbf{h}_k$ and a covariance of $2\sigma^2 \mathbf{I}_{N_r}$ for complex-valued noise, hence the PDF of $\underline{\mathbf{v}}_{i,n}$ is formulated as

$$f(\underline{\mathbf{v}}_{i,n}) = c \exp \left(- \frac{\|\underline{\mathbf{v}}_{i,n} - \sum_{k \neq i} \underline{s}_{k,n} \mathbf{h}_k\|^2}{2\sigma^2} \right), \quad (4.8)$$

where

$$c = \frac{1}{\pi^{N_r} \det(2\sigma^2 \mathbf{I})} = \frac{1}{(2\pi\sigma^2)^{N_r}}. \quad (4.9)$$

If we assume that the probability of encountering the n th interference pattern caused by $\underline{\mathbf{s}}_n$ is P_n , then upon jointly considering the distribution of $\underline{\mathbf{s}}_n$ and that of $\underline{\mathbf{v}}_{i,n}$, the distribution of \mathbf{v}_i may be characterized by the multimodal Gaussian mixture distribution of

$$p(\mathbf{v}_i) = \sum_{n=1}^{M^{N_t-1}} P_n f(\underline{\mathbf{v}}_{i,n}), \quad (4.10)$$

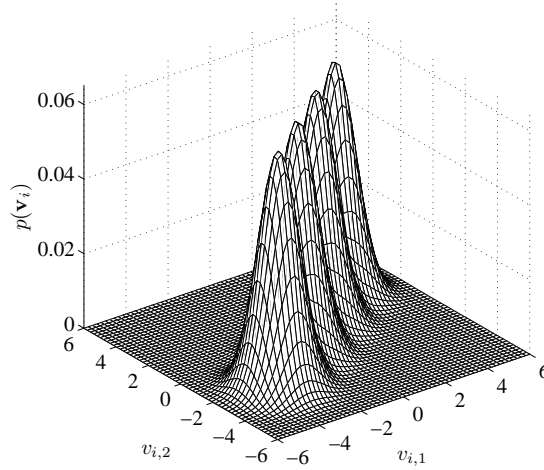


FIGURE 4.5: The multimodal Gaussian mixture PDF of $\mathbf{v}_i = [v_{i,1}, v_{i,2}]^T$ for a $N_t = N_r = 2$ MIMO system. For visualization purpose, the real-valued 4-PAM modulation with constellation $\mathbb{A} = \{-3, -1, 1, 3\}$ is used. s_1 is assumed to be detected, s_2 is the interference signal to s_1 , and the real-valued Gaussian channel vectors $\mathbf{h}_1 = [0.8884, -1.1471]^T$, $\mathbf{h}_2 = [-1.0689, -0.8095]^T$. The possible interference patterns are $\mathbf{u}_{1,1} = [3.2066, 2.4285]^T$, $\mathbf{u}_{1,2} = [1.0689, 0.8095]^T$, $\mathbf{u}_{1,3} = [-1.0689, -0.8095]^T$, $\mathbf{u}_{1,4} = [-3.2066, -2.4285]^T$, and a given *a priori* probability vector $\mathbf{P}_n = [0.25, 0.25, 0.25, 0.25]$ is used for the possible interference patterns. The means of the four component Gaussian distributions are $\mathbf{u}_{1,1}$, $\mathbf{u}_{1,2}$, $\mathbf{u}_{1,3}$, $\mathbf{u}_{1,4}$, respectively, and the covariance matrices of the four component Gaussian distributions are all $\sigma^2 \mathbf{I}$ where $\sigma^2 = 0.631$.

where we have $\sum_{n=1}^{M^{N_t-1}} P_n = 1$. Eq. (4.10) indicates that the true distribution of \mathbf{v}_i is a weighted average of a set of component multivariate Gaussian distributions. Note that Eq. (4.10) is *not* the PDF used by the classic optimal MAP detection. Since P_n is not known beforehand, and the complexity of computing $p(\mathbf{v}_i)$ increases at an exponential rate of $\mathcal{O}(M^{N_t-1})$, it is infeasible to carry out symbol detection directly relying on Eq. (4.10) for large-dimensional MIMO systems. Instead, we can resort to the PDA method to simplify the MIMO detection.

An example of a four-modal Gaussian mixture distribution is shown in Fig. 4.5 and Fig. 4.6 in order to illustrate the fundamental principle of the PDA, which was first alluded to in Fig. 2.4 and Fig. 2.5 for the scenario where the interference-plus-noise term \mathbf{v}_i has only a single element. This scenario corresponds to a system that has a single receive antenna, hence the PDF of \mathbf{v}_i may be visualized in a 2-D coordinate system. By contrast, in Fig. 4.5 and Fig. 4.6, we consider a MIMO system that has two receive antennas, hence \mathbf{v}_i is a two-element vector and its PDF may be plotted as a 3-D figure. However, for a MIMO system having more than two receive antennas, the PDF of \mathbf{v}_i cannot be readily visualized. More specifically, Fig. 4.5 represents the initial distribution of the interference-plus-noise term \mathbf{v}_i , when we have no *a priori* knowledge about the interference symbols $\{s_k\}_{k \neq i}$ before performing symbol detection, and Fig. 4.6 represents the distribution of \mathbf{v}_i after performing

the PDA based detection, when we have a relatively strong belief about the correct value of s_i among all legitimate constellation symbols a_m . Note that in Fig. 4.6 the *a priori* probability vector \mathbf{P}_n is set to $[0.1, 0.1, 0.7, 0.1]$, which is for convenience of conceptual visualization. The actual maximum value of the elements of the probability vector after performing the PDA detection is typically near to 1.0, which makes the other smaller peaks corresponding to the less probable constellation symbols almost vanish.

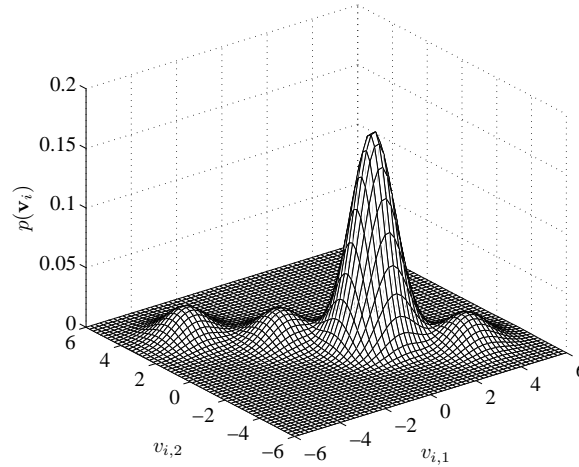


FIGURE 4.6: The multimodal Gaussian mixture PDF of $\mathbf{v}_i = [v_{i,1}, v_{i,2}]^T$ for a $N_t = N_r = 2$ MIMO system after iteration. For visualization purpose, the real-valued 4PAM modulation with constellation $\mathbb{A} = \{-3, -1, 1, 3\}$ is used. s_1 is assumed to be detected, s_2 is the interference signal to s_1 , and the real-valued Gaussian channel vectors $\mathbf{h}_1 = [-3.0292, -0.4570]^T$, $\mathbf{h}_2 = [1.2424, -1.0667]^T$. The possible interference patterns are $\mathbf{u}_{1,1} = [-3.7273, 3.2001]^T$, $\mathbf{u}_{1,2} = [-1.2424, 1.0667]^T$, $\mathbf{u}_{1,3} = [1.2424, -1.0667]^T$, $\mathbf{u}_{1,4} = [3.7273, -3.2001]^T$, and a given *a priori* probability vector $\mathbf{P}_n = [0.1, 0.1, 0.7, 0.1]$ is used for the possible interference patterns. The means of the four component Gaussian distributions are $\mathbf{u}_{1,1}$, $\mathbf{u}_{1,2}$, $\mathbf{u}_{1,3}$, $\mathbf{u}_{1,4}$, respectively, and the covariance matrices of the four component Gaussian distributions are all $\sigma^2 \mathbf{I}$ where $\sigma^2 = 0.631$.

4.4 AB-Log-PDA Relying on *A Priori* Soft Feedback From the FEC Decoder

Based on the interference-plus-noise distribution analysis of Section 4.3, below we will elaborate on the proposed low-complexity AB-Log-PDA algorithm. This algorithm uses the received signal \mathbf{y} , the channel matrix \mathbf{H} , as well as the *a priori* soft feedback gleaned from the FEC decoder, representing the soft estimates of the transmitted symbols $\{s_i\}_{i=1, \dots, N_t}$, as its input parameters, and generates the estimated decision probabilities for $\{s_i\}_{i=1, \dots, N_t}$ as its output.

As mentioned in Section 4.3, each symbol s_i to be detected in Eq. (4.4) is contaminated by both the noise \mathbf{n} and the interfering signal \mathbf{u}_i . The noise is generally undesirable, but

the interference might potentially become a useful signal, which is only not desired at some specific instant. Hence, if we can estimate the distribution of the interfering symbols $\{s_k\}_{k \neq i}$, the performance degradation imposed by \mathbf{u}_i may be mitigated. Although initially we do not have any *a priori* knowledge about the distribution of $\{s_k\}_{k \neq i}$, we know exactly the distribution of the noise \mathbf{n} and we are also aware of the legitimate values of $\{s_k\}_{k \neq i}$. Hence it is feasible to generate a coarse estimate of $\{s_i\}_{i=1, \dots, N_t}$ relying solely on the knowledge of the noise distribution and the modulation constellation \mathbb{A} at the beginning. Based on these observations, we may assume that the interference-plus-noise term \mathbf{v}_i obeys a single N_r -variate Gaussian distribution. Although this approximation is more accurate when N_t becomes larger, it is competent to produce a coarse estimate of $\{s_i\}_{i=1, \dots, N_t}$. In order to fully characterize the complex random vector \mathbf{v}_i , which is not necessarily *proper*,¹ we specify the mean as

$$\boldsymbol{\mu}_i \triangleq \mathcal{E}(\mathbf{v}_i) = \sum_{k \neq i} \mathcal{E}(s_k) \mathbf{h}_k, \quad (4.11)$$

the covariance as

$$\boldsymbol{\Upsilon}_i \triangleq \mathcal{C}(\mathbf{v}_i) = \sum_{k \neq i} \mathcal{C}(s_k) \mathbf{h}_k \mathbf{h}_k^H + 2\sigma^2 \mathbf{I}_{N_r}, \quad (4.12)$$

and the pseudo-covariance as

$$\boldsymbol{\Omega}_i \triangleq \mathcal{C}_p(\mathbf{v}_i) = \sum_{k \neq i} \mathcal{C}_p(s_k) \mathbf{h}_k \mathbf{h}_k^T. \quad (4.13)$$

We define an $(N_t \times M)$ -element probability matrix $\mathbf{P}^{(z, z')}$, whose (i, m) th element $P_m^{(z, z')}(s_i | \mathbf{y}) \triangleq P^{(z, z')}(s_i = a_m | \mathbf{y})$ is the estimate of the probability that we have $s_i = a_m$ at the (z, z') th iteration, for $i = 1, \dots, N_t$ and $m = 1, \dots, M$. More specifically, the integer $z' \geq 0$ denotes the inner iteration index of the AB-Log-PDA, while the integer $z \geq 0$ is the index of the outer iteration between the AB-Log-PDA and the soft FEC decoder of Fig. 4.4. Then, the $\mathcal{E}(s_k)$, $\mathcal{C}(s_k)$ and $\mathcal{C}_p(s_k)$ in (4.11), (4.12) and (4.13) are given by

$$\mathcal{E}(s_k) = \sum_{m=1}^M a_m P^{(z, z')}(s_k = a_m | \mathbf{y}), \quad (4.14)$$

$$\mathcal{C}(s_k) = \sum_{m=1}^M [a_m - \mathcal{E}(s_k)][a_m - \mathcal{E}(s_k)]^* P^{(z, z')}(s_k = a_m | \mathbf{y}), \quad (4.15)$$

¹The pseudo-covariance of a complex random vector \mathbf{x} is defined as $\mathcal{C}_p(\mathbf{x}) \triangleq \mathcal{E} \{ [\mathbf{x} - \mathcal{E}(\mathbf{x})] [\mathbf{x} - \mathcal{E}(\mathbf{x})]^T \}$. For a *proper* complex random variable, its pseudo-covariance vanishes, and it is sufficient to describe a proper complex Gaussian distribution using only the mean and the covariance [363, 398, 399]. However, for a coded system the in-phase and quadrature components of the complex modulated signal s_i might be correlated, especially when the coding block-length is not long enough. In this case, it is necessary to take into account an additional second-order statistics, i.e. the pseudo-covariance [363], to fully specify the *improper* complex Gaussian distribution in a generalized manner.

and

$$C_p(s_k) = \sum_{m=1}^M [a_m - \mathcal{E}(s_k)]^2 P^{(z,z')}(s_k = a_m | \mathbf{y}), \quad (4.16)$$

respectively.

Note that Eq. (4.11) - Eq. (4.16) effectively use $(N_t - 1)$ probability vectors $\{\mathbf{P}^{(z,z')}(k, :)\}_{k \neq i}$ associated with the interfering signal $\{s_k\}_{k \neq i}$ to model \mathbf{v}_i . Since we do not have any *a priori* knowledge about the distribution of $s_i | \mathbf{y}$ at the beginning, an all-zero LLR vector will be provided as the input to the AB-Log-PDA, which is equivalent to initializing $P^{(z,z')}(s_i = a_m | \mathbf{y})$ with a uniform distribution, i.e.

$$P^{(0,0)}(s_i = a_m | \mathbf{y}) = \frac{1}{M}, \quad (4.17)$$

$\forall i = 1, \dots, N_t$ and $\forall m = 1, \dots, M$.

Based on the assumption that \mathbf{v}_i obeys the Gaussian distribution, $\mathbf{y} | s_i$ is also Gaussian distributed. Let us now define

$$\mathbf{w} \triangleq \mathbf{y} - s_i \mathbf{h}_i - \sum_{k \neq i} \mathcal{E}(s_k) \mathbf{h}_k \quad (4.18)$$

and

$$\beta_{m,i}^{(z,z'+1)} \triangleq - \begin{bmatrix} \Re(\mathbf{w}) \\ \Im(\mathbf{w}) \end{bmatrix}^T \mathbf{\Lambda}_i^{-1} \begin{bmatrix} \Re(\mathbf{w}) \\ \Im(\mathbf{w}) \end{bmatrix}, \quad (4.19)$$

in which the *composite* covariance matrix $\mathbf{\Lambda}_i$ is defined as [234]

$$\mathbf{\Lambda}_i \triangleq \begin{bmatrix} \Re(\mathbf{\Upsilon}_i + \mathbf{\Omega}_i) & -\Im(\mathbf{\Upsilon}_i - \mathbf{\Omega}_i) \\ \Im(\mathbf{\Upsilon}_i + \mathbf{\Omega}_i) & \Re(\mathbf{\Upsilon}_i - \mathbf{\Omega}_i) \end{bmatrix}, \quad (4.20)$$

where $\Re(\cdot)$ and $\Im(\cdot)$ represent the real and imaginary part of a complex variable, respectively. Then the likelihood function of $\mathbf{y} | s_i = a_m$ at the $(z, z' + 1)$ th iteration satisfies

$$p^{(z,z'+1)}(\mathbf{y} | s_i = a_m) \propto \exp\left(\beta_{m,i}^{(z,z'+1)}\right), \quad (4.21)$$

where the symbol “ \propto ” means “proportional to”.

Upon invoking an approximate form of the Bayes' theorem [219, 226], the *estimated* proba-

bility of symbol s_i at the $(z, z' + 1)$ th iteration may be calculated as

$$\begin{aligned}
& P^{(z, z'+1)}(s_i = a_m | \mathbf{y}) \\
& \approx \frac{p^{(z, z'+1)}(\mathbf{y} | s_i = a_m)}{\sum_{m=1}^M p^{(z, z'+1)}(\mathbf{y} | s_i = a_m)} \\
& = \frac{\exp\left(\beta_{m,i}^{(z, z'+1)} - \gamma\right)}{\sum_{m=1}^M \exp\left(\beta_{m,i}^{(z, z'+1)} - \gamma\right)}, \tag{4.22}
\end{aligned}$$

where $\gamma \triangleq \max_{m=1, \dots, M} \beta_{m,i}^{(z, z'+1)}$ is subtracted from $\beta_{m,i}^{(z, z'+1)}$ for enhancing the numerical stability. Note that $P^{(z, z')}(s_i = a_m)$ is ignored in (4.22), since it has been utilized for calculating the likelihood of $\mathbf{y} | s_i = a_m$ at the $(z, z' + 1)$ th iteration — typically the same *a priori* information should not be used multiple times in IDD scenarios.

As a further effort to improve the achievable numerical stability and accuracy, the logarithmic-domain form of (4.22) is formulated as

$$\begin{aligned}
\psi_{m,i}^{(z, z'+1)} & \triangleq \ln \left[P^{(z, z'+1)}(s_i = a_m | \mathbf{y}) \right] \\
& = \tilde{\beta}_{m,i}^{(z, z'+1)} - \ln \left[\sum_{m=1}^M \exp\left(\tilde{\beta}_{m,i}^{(z, z'+1)}\right) \right], \tag{4.23}
\end{aligned}$$

in which we have $\tilde{\beta}_{m,i}^{(z, z'+1)} \triangleq \beta_{m,i}^{(z, z'+1)} - \gamma$, and the second term of the right-hand-side expression may be computed by invoking the ‘‘Jacobian logarithm’’ of [75]. Alternatively, upon employing the Max-log approximation, (4.23) may be further simplified to

$$\psi_{m,i}^{(z, z'+1)} \approx \tilde{\beta}_{m,i}^{(z, z'+1)}. \tag{4.24}$$

As a result, the estimated decision probability of s_i relying on (4.23) and (4.24) is given by

$$P^{(z, z'+1)}(s_i = a_m | \mathbf{y}) \approx e^{\psi_{m,i}^{(z, z'+1)}}, \tag{4.25}$$

which will update the value of $P^{(z, z')}(s_i = a_m | \mathbf{y})$ in the probability matrix $\mathbf{P}^{(z, z')}$. Following the inner iterations within the AB-Log-PDA, *if any*, the updated symbol probabilities have to be converted to the equivalent bit-based LLRs, whose *extrinsic* constituent will be delivered to the outer FEC decoder of Fig. 4.4. In turn, the extrinsic LLRs output by the FEC decoder of Fig. 4.4 will be converted to symbol probabilities in the next outer iteration, before feeding them into the AB-Log-PDA for generating new estimates of the symbol probabilities. Note, however that it is a challenge to calculate the extrinsic LLRs using the output symbol probabilities of the AB-Log-PDA. This challenge will be tackled in Section 4.5. For reasons of explicit clarity, the AB-Log-PDA algorithm relying on the *a*

TABLE 4.1: Summary of the AB-Log-PDA based IDD algorithm

Given the received signal \mathbf{y} , the channel matrix \mathbf{H} and the constellation \mathbb{A} .

Step 1. Set the initial values of the inner iteration index and outer iteration index to $z' = 0$ and $z = 0$, respectively. Initialize the bit-based *a priori* LLRs feedback from the FEC decoder as zeros.

Step 2. Convert the *a priori* LLRs feedback from the FEC decoder to symbol probabilities shown in probability matrix $\mathbf{P}^{(z,z')}$.

Step 3. Using the values of $\left\{ \mathbf{P}^{(z,z')}(k, \cdot) \right\}_{k \neq i}$, calculate $P_m^{(z,z'+1)}(s_i|\mathbf{y})$ by
for $i = 1 : N_t$
 calculate the statistics of the interference-plus-noise term \mathbf{v}_i using
 (4.11) - (4.16), as well as the inverse of $\mathbf{\Lambda}_i$ in (4.20),
 for $m = 1 : M$
 calculate $P_m^{(z,z'+1)}(s_i|\mathbf{y})$ using (4.18), (4.19), (4.23) and (4.25).
 end
end

Step 4. If z' has reached a given number of inner iterations, go to Step 5. Otherwise, let $z' \leftarrow z' + 1$, and return to Step 3.

Step 5. Convert the symbol probabilities $P_m^{(z,z'+1)}(s_i|\mathbf{y})$ to bit-based LLRs, of which the extrinsic parts are delivered to the outer FEC decoder. If z has reach a given number of outer iterations, make hard decisions using the soft output of the FEC decoder. Otherwise, let $z \leftarrow z + 1$, and return to Step 2.

priori soft feedback generated by the FEC decoder of Fig. 4.4 is summarized in Table 4.1.

4.5 Extrinsic LLR Calculation Using the Output of AB-Log-PDA

In order to integrate the AB-Log-PDA into the IDD scheme, the AB-Log-PDA has to output correct extrinsic LLRs for each of the FEC-coded bits, which is however, not quite as straightforward as it seems at first sight, given the fact that the output probabilities of the PDA were misinterpreted² as APPs in [41, 43, 193, 219, 226, 234]. We assume that the components of the transmitted symbol-vector \mathbf{s} are obtained using the bit-to-symbol mapping function of $s_i = \text{map}(\mathbf{b}_i)$, $i = 1, 2, \dots, N_t$, where $\mathbf{b}_i = [b_{i,1}, b_{i,2}, \dots, b_{i,l}, \dots, b_{i,M_b}]^T \in \{+1, -1\}^{M_b}$ is the vector of bits mapped to symbol s_i . Additionally, we denote the vector of bits corresponding to \mathbf{s} as \mathbf{b} , which satisfies $\mathbf{s} = \text{map}(\mathbf{b})$ and is formed by concatenating the N_t antennas' bit vectors $\mathbf{b}_1, \mathbf{b}_2, \dots, \mathbf{b}_{N_t}$, yielding $\mathbf{b} = [\mathbf{b}_1^T, \mathbf{b}_2^T, \dots, \mathbf{b}_{N_t}^T]^T = [b_1, b_2, \dots, b_k, \dots, b_{M_b N_t}]^T \in \{+1, -1\}^{M_b N_t}$. Hence the indices of b_{il} and b_k are related to each other by $k = M_b(i - 1) + l$.

Note that the AB-Log-PDA algorithm finally outputs the *estimated* symbol probabilities

²As we will detail later, despite the fact that the output symbol probability of the existing PDAs was typically interpreted as the symbol APP, it is actually not the true APP, because the true APP ought to be proportional to both the likelihood and the *a priori* probability [400].

of $P(s_i = a_m|\mathbf{y})$, where the iteration indices are omitted without causing any confusion. Additionally, it provides the likelihood functions of $p(\mathbf{y}|s_i = a_m)$ conditioned on s_i as its intermediate output. By contrast, the classic candidate-search based approach outputs the likelihood function of $p(\mathbf{y}|\mathbf{b})$ [or equivalently, $p(\mathbf{y}|\mathbf{s})$] conditioned on the bit vector \mathbf{b} (or symbol vector \mathbf{s}), and calculates the bit-based extrinsic LLRs by using $p(\mathbf{y}|\mathbf{b})$ [or $p(\mathbf{y}|\mathbf{s})$]. Below we will demonstrate that the candidate-search based approach of computing the bit-based extrinsic LLRs is not feasible for the AB-Log-PDA algorithm. In other words, we cannot obtain $p(\mathbf{y}|\mathbf{b})$ or $p(\mathbf{y}|\mathbf{s})$ based on $P(s_i = a_m|\mathbf{y})$ and/or $p(\mathbf{y}|s_i = a_m)$. Instead, we will demonstrate that there exists a simpler method of directly obtaining the bit-based extrinsic LLRs based on the output of the AB-Log-PDA.

4.5.1 Challenges in Calculating Extrinsic LLRs for PDA Based Methods

In principle, for a MIMO system characterized by Eq. (4.1), the classic approach of deriving bit-based extrinsic LLRs is based on the likelihood function of $p(\mathbf{y}|\mathbf{b})$ or $p(\mathbf{y}|\mathbf{s})$. Specifically, the extrinsic LLR of b_{il} (or b_k) is given by [75]

$$\begin{aligned} L_D(b_k|\mathbf{y}) &= \ln \frac{P(b_k = +1|\mathbf{y})}{P(b_k = -1|\mathbf{y})} \\ &= \ln \frac{p(\mathbf{y}|b_k = +1)P(b_k = +1)}{p(\mathbf{y}|b_k = -1)P(b_k = -1)} \end{aligned} \quad (4.26)$$

$$\begin{aligned} &= \ln \frac{\sum_{\forall \mathbf{b} \in \mathbb{B}_k^+} p(\mathbf{y}|\mathbf{b})P(\mathbf{b})}{\sum_{\forall \mathbf{b} \in \mathbb{B}_k^-} p(\mathbf{y}|\mathbf{b})P(\mathbf{b})} + L_A(b_k) \end{aligned} \quad (4.27)$$

$$\begin{aligned} &= \ln \frac{\sum_{\forall \mathbf{s} \in \mathbb{S}_{il}^+} p(\mathbf{y}|\mathbf{s})P(\mathbf{s})}{\sum_{\forall \mathbf{s} \in \mathbb{S}_{il}^-} p(\mathbf{y}|\mathbf{s})P(\mathbf{s})} + L_A(b_k), \end{aligned} \quad (4.28)$$

where

$$L_A(b_k) = \ln \frac{P(b_k = +1)}{P(b_k = -1)} \quad (4.29)$$

and $L_E(b_k|\mathbf{y})$ represents the *a priori* and extrinsic LLRs of b_k , respectively, \mathbb{B}_k^\pm represents the set of $2^{N_t M_b - 1}$ legitimate bit vectors \mathbf{b} having $b_k = \pm 1$, while \mathbb{S}_{il}^\pm denotes the particular set of $2^{N_t M_b - 1}$ legitimate symbol vectors in which the l th bit of symbol s_i is $b_{il} = \pm 1$. Note that Eq. (4.27) is derived from Eq. (4.26) by invoking the Total Probability Theorem [396], yielding

$$P(\mathbf{y}|b_k) = \sum_{\forall \mathbf{b}_{[k]}} P(\mathbf{y}|b_k, \mathbf{b}_{[k]})P(\mathbf{b}_{[k]}) = \sum_{\forall \mathbf{b} \in \mathbb{B}_k^\pm} P(\mathbf{y}|\mathbf{b})P(\mathbf{b}), \quad (4.30)$$

where $\mathbf{b}_{[k]} = [b_1, b_2, \dots, b_j, \dots, b_{N_t M_b}]_{j \neq k}^T$ represents a truncated version of \mathbf{b} excluding b_k . By exploiting the approximate independence between b_j , $j \in \mathbb{J}_k \triangleq \{j | j = 1, \dots, N_t M_b, j \neq k\}$, and the equation of

$$P(b_j) = \frac{\exp\left(\frac{1}{2}L_A(b_j)\right)}{1 + \exp L_A(b_j)} \cdot \exp\left(\frac{b_j}{2}L_A(b_j)\right), \quad (4.31)$$

we can further reformulate $L_E(b_k|\mathbf{y})$ of (4.27) as

$$\begin{aligned} L_E(b_k|\mathbf{y}) &= \ln \frac{\sum_{\forall \mathbf{b} \in \mathbb{B}_k^+} p(\mathbf{y}|\mathbf{b}) \prod_{\forall j \in \mathbb{J}_k} P(b_j)}{\sum_{\forall \mathbf{b} \in \mathbb{B}_k^-} p(\mathbf{y}|\mathbf{b}) \prod_{\forall j \in \mathbb{J}_k} P(b_j)} \\ &= \ln \frac{\sum_{\forall \mathbf{b} \in \mathbb{B}_k^+} p(\mathbf{y}|\mathbf{b}) \prod_{\forall j \in \mathbb{J}_k} \exp\left(\frac{b_j L_A(b_j)}{2}\right)}{\sum_{\forall \mathbf{b} \in \mathbb{B}_k^-} p(\mathbf{y}|\mathbf{b}) \prod_{\forall j \in \mathbb{J}_k} \exp\left(\frac{b_j L_A(b_j)}{2}\right)} \\ &= \ln \frac{\sum_{\forall \mathbf{b} \in \mathbb{B}_k^+} p(\mathbf{y}|\mathbf{b}) \exp\left(\frac{1}{2}\mathbf{b}_{[k]}^T \mathbf{L}_{A,[k]}\right)}{\sum_{\forall \mathbf{b} \in \mathbb{B}_k^-} p(\mathbf{y}|\mathbf{b}) \exp\left(\frac{1}{2}\mathbf{b}_{[k]}^T \mathbf{L}_{A,[k]}\right)}, \end{aligned} \quad (4.32)$$

where \mathbb{B}_k^\pm denotes the set of $2^{N_t M_b - 1}$ legitimate bit vectors \mathbf{b} having $b_k = \pm 1$, and $\mathbf{b}_{[k]} = [b_1, \dots, b_j, \dots, b_{N_t M_b}]_{j \neq k}^T$ represents a truncated version of \mathbf{b} excluding b_k , while $\mathbf{L}_{A,[k]}$ represents the *a priori* LLRs corresponding to $\mathbf{b}_{[k]}$. Eq. (4.32) indicates that $L_E(b_k|\mathbf{y})$ is determined by $p(\mathbf{y}|\mathbf{b})$, and by the *a priori* LLRs of the other bits conveyed by a single symbol vector \mathbf{s} . However, below we will prove that it is infeasible to invoke this approach to calculate bit-based extrinsic LLRs for the family of PDA based algorithms including the AB-Log-PDA.

Proposition 4.1. *For all PDA algorithms which output the probabilities $P(s_i|\mathbf{y})$, or the likelihood functions $p(\mathbf{y}|s_i)$, the bit-based extrinsic LLR $L_E(b_k|\mathbf{y})$ cannot be calculated using the candidate-search method which relies on $p(\mathbf{y}|\mathbf{b})$ or $p(\mathbf{y}|\mathbf{s})$.*

Proof. Define a non-zero random vector $\mathbf{s} = [s_1, s_2, \dots, s_{N_t}]^T$, and a non-zero random vector \mathbf{y} , where s_i and s_j are independent of each other in the absence of *a priori* knowledge, $i \neq j$, $i, j = 1, \dots, N_t$, and assume that \mathbf{y} is associated with \mathbf{s} by the function of $\mathbf{y} = f(\mathbf{s})$. We have

$$\begin{aligned} P(\mathbf{y}|\mathbf{s}) &= P(\mathbf{y}|s_1, s_2, \dots, s_{N_t}) \\ &= \frac{P(\mathbf{y}, s_1, s_2, \dots, s_{N_t})}{P(s_1, s_2, \dots, s_{N_t})} \\ &= \frac{P(s_1|\mathbf{y})P(s_2, \dots, s_{N_t}|\mathbf{y}, s_1)P(\mathbf{y})}{P(s_1)P(s_2) \cdots P(s_{N_t})}, \end{aligned} \quad (4.33)$$

where $P(s_2, \dots, s_{N_t} | \mathbf{y}, s_1)$ can be further expanded as

$$P(s_2 | \mathbf{y}, s_1) P(s_3 | \mathbf{y}, s_1, s_2) \cdots P(s_{N_t} | \mathbf{y}, s_1, s_2, \dots, s_{N_t-1}). \quad (4.34)$$

Note that the conditions s_i associated with each single probability in (4.34) cannot be removed, which implies that it is infeasible to further simplify each probability in (4.34). In other words, we have $P(\mathbf{s} | \mathbf{y}) \neq P(s_1 | \mathbf{y}) P(s_2 | \mathbf{y}) \cdots P(s_{N_t} | \mathbf{y})$, which implies that in a converging connection of the acyclic, directed graph representation of Bayesian Networks, the presence of knowledge as regards to the child-node makes the parent-nodes conditionally dependent. Again, this is a standard result in Bayesian Networks [401]. Therefore, the probability $P(\mathbf{y} | \mathbf{s})$ cannot be exactly expressed as a function of any probabilities of $P(s_i)$, $P(\mathbf{y})$, $P(\mathbf{y} | s_i)$ and/or $P(s_i | \mathbf{y})$. Hence the proof of Proposition 4.1 is established. \square

4.5.2 Calculating Extrinsic LLRs for AB-Log-PDA

Due to Proposition 4.1, the candidate-search based approach of calculating bit-based extrinsic LLRs is not applicable to the family of PDA algorithms. Let \mathbb{A}_l^\pm denote the set of $M/2$ constellation points whose l th bit is ± 1 . Then, alternatively, the extrinsic LLR of b_{il} may be rewritten as³

$$L_E(b_{il} | \mathbf{y}) = \ln \underbrace{\frac{\sum_{\forall a_m \in \mathbb{A}_l^+} P(s_i = a_m | \mathbf{y})}{\sum_{\forall a_m \in \mathbb{A}_l^-} P(s_i = a_m | \mathbf{y})}}_{L_D(b_{il} | \mathbf{y})} - \ln \underbrace{\frac{P(b_{il} = +1)}{P(b_{il} = -1)}}_{L_A(b_{il})}, \quad (4.35)$$

where $L_D(b_{il} | \mathbf{y})$ and $L_A(b_{il})$ denote the *a posteriori* and *a priori* LLRs of b_{il} , respectively. It is noteworthy that (4.35) represents a simple approach of generating the bit-based extrinsic LLR of $L_E(b_{il} | \mathbf{y})$, as long as the *true* symbol APP of $P(s_i = a_m | \mathbf{y})$ can be obtained.

However, although we can directly obtain the estimated symbol probabilities of $P(s_i = a_m | \mathbf{y})$ from the output of the AB-Log-PDA, as shown in (4.22), our study shows that this sort of estimated symbol probabilities, interpreted as symbol APPs in [41, 43, 193, 219, 226, 234], fail to generate the correct bit-based extrinsic LLRs, when invoking (4.35).⁴ Therefore, the

³The relationship of $P(\mathbf{y} | b_{il} = \pm 1) = \sum_{\forall a_m \in \mathbb{A}_l^\pm} P(\mathbf{y} | s_i = a_m) P(s_i = a_m)$ holds only for single-antenna systems. One may argue nonetheless that it also seems to make sense for multiple-antenna systems, because the value of b_{il} is directly determined by the value of the symbol s_i at the i th antenna, rather than by the values of other symbols s_j , $j \neq i$. This line of argument is however, deceptive for the MIMO scenario considered. The rationale is that \mathbf{y} is associated with the symbol vector \mathbf{s} (or bit vector \mathbf{b}), rather than only with the specific symbol of any specific antenna.

⁴In fact, if $L_E(b_{il} | \mathbf{y})$ is calculated by substituting the estimated symbol probabilities of $P(s_i = a_m | \mathbf{y})$, i.e. the output of the AB-Log-PDA, into Eq. (4.35), the slope of the resultant BER curve of the AB-Log-PDA based IDD scheme of Fig. 4.7 remains almost horizontal upon increasing SNR values. This flawed BER curve will be presented in Fig. 5.2.

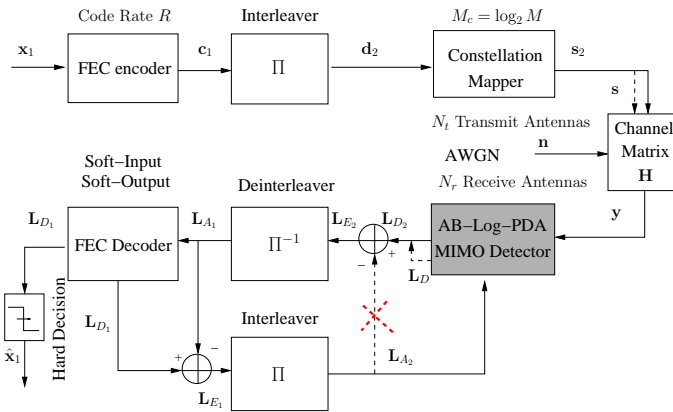


FIGURE 4.7: Schematic of the FEC-coded MIMO system with a simplified structure for the AB-Log-PDA based IDD receiver. In contrast to the classic IDD architecture of Fig. 4.4, where $\mathbf{L}_{E_2} = \mathbf{L}_{D_2} - \mathbf{L}_{A_2}$, we have $\mathbf{L}_{E_2} = \mathbf{L}_{D_2}$ in this simplified IDD architecture. In other words, as far as the AB-Log-PDA based IDD is concerned, the dashed line marked by a cross has to be removed.

results of (4.22) should not be interpreted as symbol APPs satisfying (4.35), but rather as the normalized symbol likelihoods. Based on this insight, the bit-based extrinsic LLRs of the AB-Log-PDA may be obtained by directly employing the approximate Bayes' Theorem based symbol probabilities of (4.22) as follows.

Conjecture 1. The bit-based extrinsic LLR of the AB-Log-PDA algorithm relying on (4.22) is given by

$$L_E(b_{il}|\mathbf{y}) \approx \ln \frac{\sum_{\forall a_m \in \mathbb{A}_l^+} P(s_i = a_m|\mathbf{y})}{\sum_{\forall a_m \in \mathbb{A}_l^-} P(s_i = a_m|\mathbf{y})}, \quad (4.36)$$

where $P(s_i = a_m|\mathbf{y})$ is calculated by invoking (4.25).

The $L_E(b_{il}|\mathbf{y})$ values calculated from (4.36) using the normalized symbol likelihoods are typically not equivalent to $L_E(b_{il}|\mathbf{y})$ calculated from (4.35) using the true symbol APPs, but nonetheless, they constitute a good approximation of the latter without inducing any significant performance loss, as it will be demonstrated by our simulations in Section 4.6. As a result, the classic IDD receiver structure is simplified, as shown in Fig. 4.7, where we have $\mathbf{L}_{E_2} = \mathbf{L}_{D_2}$, rather than $\mathbf{L}_{E_2} = \mathbf{L}_{D_2} - \mathbf{L}_{A_2}$.

4.6 Simulation Results and Discussions

In this section, the performance of the proposed AB-Log-PDA based IDD scheme is characterized with the aid of both the semi-analytical extrinsic information transfer (EXIT) charts [402] and Monte-Carlo simulations. Additionally, the complexity of the proposed AB-Log-PDA based IDD scheme is analyzed, which further confirms the attractive per-

TABLE 4.2: Global simulation parameters

Channel model	Uncorrelated Nakagami- m fading, $m = 0.5, 1.0, 1.5$
Modulation scheme	Gray-coded 4QAM, 16QAM
FEC encoder	parallel concatenated RSC code based Turbo code
Turbo code parameters	coding rate $R = \frac{k}{n} = 1/2$, constraint length $L = 3$, generator polynomials $(7, 5)$ in octal form
Turbo decoder	Approximate-Log-MAP
Interleaver	2400-bit random sequence interleaver
Turbo decoder inner iterations	$it_{tc} = 4$
MIMO arrangement	$(N_t, N_r) = (2 \times 2), (4 \times 4)$

formance versus complexity tradeoff achieved by the proposed AB-Log-PDA based IDD scheme. For the sake of clarity, the global simulation parameters are summarized in Table 4.2. More specifically, the FEC employed is the parallel concatenated recursive systematic convolutional (RSC) code based turbo code having a coding rate⁵ of $R = \frac{k}{n} = 1/2$, constraint length of $L = 3$ and generator polynomials of $(7, 5)$ in octal form. The turbo code is decoded by the Approximate-Log-MAP algorithm using $it_{tc} = 4$ inner iterations. The interleaver employed is the 2400-bit random sequence interleaver. The remaining scenario-dependent simulation parameters are shown in the respective figures, where the MIMO arrangement is represented in form of $(N_t \times N_r)$.

4.6.1 Performance of the AB-Log-PDA based IDD

1) Impact of the inner PDA iterations

In Fig. 4.8, we investigate the impact of the number of inner iterations within the AB-Log-PDA algorithm on the achievable performance of the IDD scheme, which is degraded upon increasing the number of inner iterations of the AB-Log-PDA, despite the fact that the computational complexity increases dramatically. This implies that the optimal number of inner iterations of the AB-Log-PDA conceived for the IDD receiver is $it_i = z' = 0$. It should be noted that for other types of iterative receivers, the inner iterations often refer to the iterations within the FEC-decoder, in which typically the MAP algorithm and its variants are employed. In that context, increasing the number of inner iterations typically improves the iterative receiver's performance, which is in contrast to the impact of the inner PDA detector's iterations, as shown in Fig. 4.8.

The reasons as to why the inner PDA iterations fail to provide BER improvement can be understood from three different perspectives, as detailed below.

i) The PDA method is reconfigurable, and both the inner PDA iterations as well as the

⁵As usual, half of the parity bits generated by each of the two RSC codes are punctured.

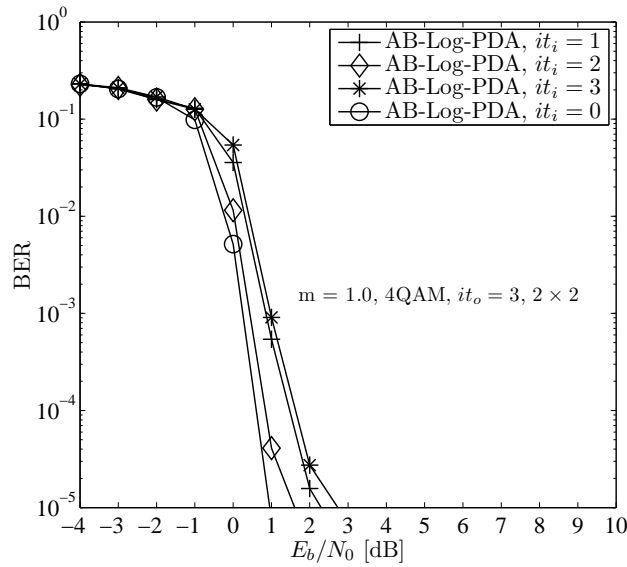


FIGURE 4.8: Impact of the number of inner iterations it_i on the achievable BER of the AB-Log-PDA based IDD scheme of Fig. 4.7. We can see that as it_i increases, the BER tends to be degraded on the whole, except for of $it_i = 2$, which performs better than $it_i = 1$. The scenario-dependent simulation parameters used for obtaining these results are shown in the figure, while other simulation parameters are given in Table 4.2.

outer iterations play a similar *role* with respect to the PDA detector module in our IDD scenario, but the soft information provided by the two sorts of iterations has a different *quality*. Firstly, when the number of IAI components is insufficiently high for the central limit theorem to prevail, there is an inevitable Gaussian approximation error, even if the PDA method has converged to its best possible estimate. This approximation error is more severe, when the soft information provided by the Gaussian approximation in each inner PDA iteration is unreliable, because error propagation will occur during the process of inner PDA iterations. Furthermore, if we look at the PDA detector module in isolation, the inner PDA iterations and the outer iterations play a similar *role* – both of them are responsible for providing the input soft information for the next round of Gaussian approximation. This Gaussian approximation procedure is identical for the two sorts of iterations, while the *quality* of the soft information provided by the two types of iterations is different. Additionally, compared to the scenario of uncoded systems, where the PDA method can only rely on its own knowledge of the transmitted/received signal and its own inner iterations, in FEC-coded systems the Gaussian approximation error can be mitigated more effectively by the improved-reliability soft information fed back by the FEC decoder. In other words, the improved-reliability soft information input provided by the outer FEC decoder is more beneficial for the PDA method than the less reliable soft information input generated by the PDA method relying entirely on its own knowledge. Therefore, the inner PDA iterations can be replaced by the more efficient outer iterations in the IDD scenario considered.

ii) The convergence profile of the PDA method is not monotonic. In engineering/opti-

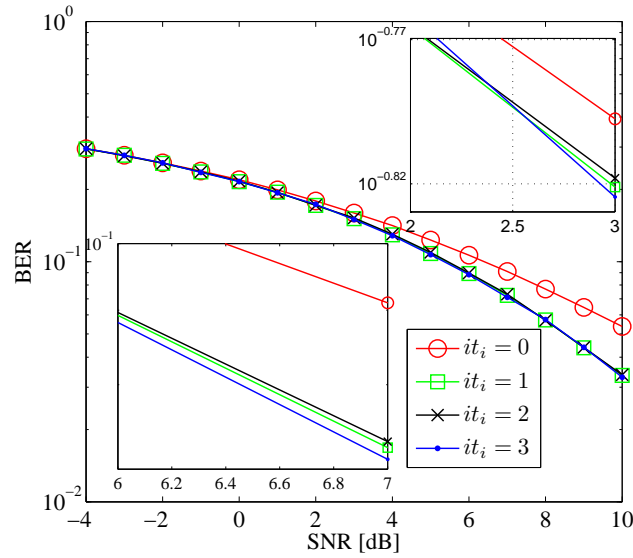


FIGURE 4.9: Observation of the fine details of the impact of inner PDA iterations it_i on the achievable performance of the symbol-based PDA detector of [234] in an uncoded MIMO system, where we have $N_t = N_r = 2$, and 4QAM is used. At first glance, it seems that the BERs of $it_i = 1$, $it_i = 2$, and $it_i = 3$ are almost the same, hence the PDA detector may be regarded converged for $it_i \geq 1$. However, there are indeed slight fluctuations when we compare the fine details of the BERs of $it_i = 1$, $it_i = 2$, and $it_i = 3$.

mization problems two typical types of convergence behaviors may be observed for a function/sequence. Namely, the function/sequence may monotonically approach its optimum, or may fluctuate during the process of approaching its optimum — hopefully without getting trapped in a local optimum. Upon observing Fig. 4.9 as to the fine details of the impact of inner PDA iterations on the achievable performance of the PDA detector in an uncoded MIMO system, we find that the convergence behavior of the PDA method belongs to the second type. This particular convergence behavior of the PDA has not been reported in the open literature, because in uncoded systems hard decisions are made based on the output symbol probabilities of the PDA method. Hence the resultant BER performance fluctuation may remain so trivial that it may be regarded as being unchanged after several inner PDA iterations. However, as we can see from Fig. 4.9, the BER performance of $it_i = 1, 2, 3$ actually exhibits some degree of fluctuations.

These fluctuations can be further confirmed by tracking the changes of a single symbol's probability $P(s_i = a_m | \mathbf{y})$ during the inner PDA iterations, as shown in Fig. 4.10. In uncoded systems, the PDA method is regarded to be converged when the probability changes obey $\Delta P = |P(\text{current iteration}) - P(\text{previous iteration})| < \epsilon$, where the threshold ϵ is a small positive real number. In Fig. 4.10 we show how ΔP changes upon increasing the number of inner PDA iterations in the context of a 4QAM aided uncoded (2×2) -element MIMO system, where we have $\epsilon = 0.001$. Again, although a superficial observation shows that ΔP remains more or less unchanged after two iterations, ΔP actually exhibits a modest

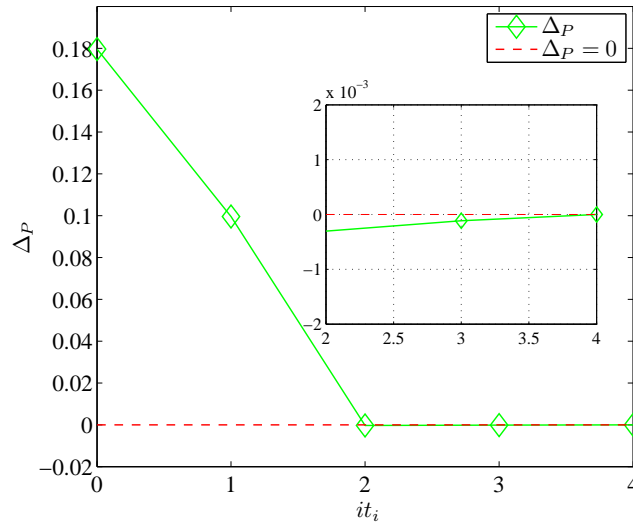


FIGURE 4.10: Observation of the fine details of the convergence profile concerning the symbol probability of the symbol-based PDA detector of [234]: the probability gap ΔP between the previous iteration and the current iteration of a PDA-based detector is measured when we look at a single symbol's probability $P(s_i = a_m | \mathbf{y})$ in an uncoded MIMO system, where we have $N_t = N_r = 2$, and 4QAM is used. We see that ΔP slightly changes upon increasing the number of inner PDA iterations it_i .

fluctuation, because we have both positive and negative values of ΔP during the iterations.

However, the trivial fluctuation at the soft output of the PDA detector module may induce an augmented BER fluctuation at the output of the FEC-coded system. Let us consider for example a symbol probability vector of $\mathbf{p}_1 = [0.35, 0.58, 0.06, 0.01]$, which represents our belief as regards to $s_i = a_1, a_2, a_3, a_4$, respectively. In uncoded systems, what we care about is, which specific probability is the maximum. In this case we will choose $s_i = a_2$, and a modest fluctuation from \mathbf{p}_1 to $\mathbf{p}_2 = [0.38, 0.53, 0.06, 0.01]$ will not lead to a different decision. However, in FEC-coded systems, we care about both the amplitude and the sign of the LLRs. A modest fluctuation in the probability vector \mathbf{p}_1 may alter some of the resultant LLRs that are near zero, so that they fluctuate between positive/negative values and hence might cause more severe decision errors.

iii) The inner PDA iterations degrade the quality of the LLRs output by the AB-Log-PDA. In Fig. 4.11 we show the impact of the inner PDA iterations on the quality of the LLRs at the output of the AB-Log-PDA by testing the so-called consistency condition [403] of these LLRs. As seen from Fig. 4.11, the consistency profile of the LLRs at the output of the AB-Log-PDA is degraded upon increasing the number of inner PDA iterations. This observation provides another perspective, confirming that it may in fact be detrimental to include inner PDA iterations, when a PDA-based IDD receiver is considered in FEC-coded systems. Therefore, we dispense with inner iterations in the AB-Log-PDA and set $it_i = 0$ in our forthcoming simulations.

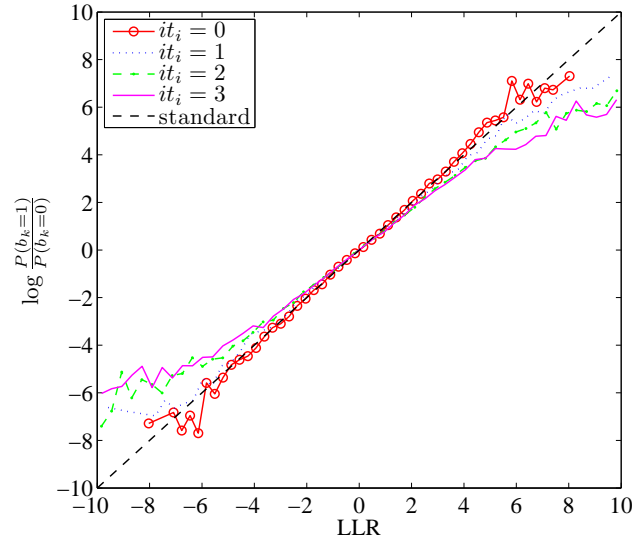


FIGURE 4.11: The impact of inner PDA iterations it_i on the quality of the LLRs output by the AB-Log-PDA of Fig. 4.7. $N_t = N_r = 2$, $m = 1.0$ and 4QAM are used. The LLR quality is indicated by testing the so-called consistency condition [403] of these LLRs. We see that the consistency profile of the LLRs at the output of the AB-Log-PDA is degraded upon increasing it_i .

2) Impact of outer iterations

Fig. 4.12 compares the convergence behavior of the proposed AB-Log-PDA based IDD with $it_i = 0$ and that of the optimal Exact-Log-MAP⁶ based IDD scheme [75] using EXIT chart [402] analysis. Referring to Fig. 4.7, for the inner detector, $I_{A,inner}$ is measured between \mathbf{d}_2 and a corresponding artificially generated Gaussian distributed *a priori* LLR vector, $I_{E,inner}$ is measured between \mathbf{d}_2 and \mathbf{L}_{E_2} ; while for the outer decoder, $I_{A,outer}$ is measured between \mathbf{c}_1 and a corresponding artificially generated Gaussian distributed *a priori* LLR vector, and $I_{E,outer}$ is measured between \mathbf{c}_1 and \mathbf{L}_{E_1} . We can see that the the EXIT curve of the AB-Log-PDA is close to that of the Exact-Log-MAP. For example, when the *a priori* mutual information is $I_{A,inner} = 0$, the extrinsic mutual information of the AB-Log-PDA and of the Exact-Log-MAP is $I_{E,outer} = 0.5332$ and $I_{E,outer} = 0.5596$, respectively. This indicates that the performance of the AB-Log-PDA is close to that of the Exact-Log-MAP in the scenario considered. Additionally, the detection/decoding trajectories indicate that both the AB-Log-PDA and the Exact-Log-MAP based IDD schemes converge after three iterations, although the respective performance improvements achieved at each iteration are different.

The above EXIT chart based performance prediction and the convergence behavior of the IDD schemes considered are also characterized by the BER performance results of Fig. 4.13, where the Nakagami- m fading parameter is set to $m = 1.0$, which corresponds to the

⁶The look-up table based Approximate-Log-MAP detector and the Max-Log-MAP detector are not considered here because they will induce performance-loss to some extent, though often very small.

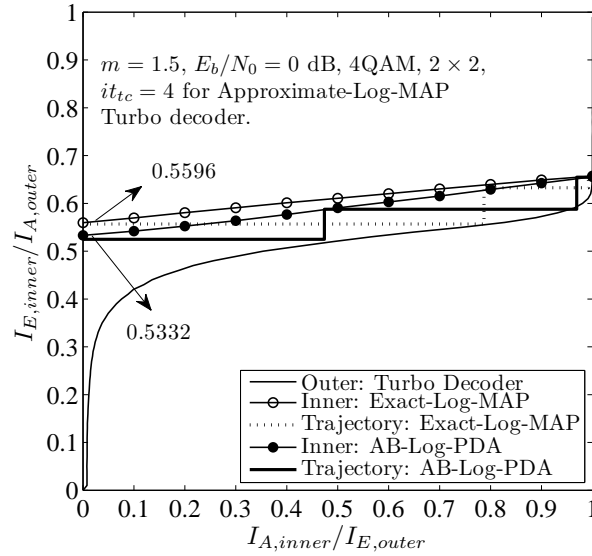


FIGURE 4.12: EXIT chart analysis of the AB-Log-PDA ($it_i = 0$) based IDD scheme of Fig. 4.7 and the Exact-Log-MAP based IDD scheme of [75]. The scenario-dependent simulation parameters used for obtaining these results are shown in the figure, while other simulation parameters are given in Table 4.2. We can see that the the EXIT curve of the AB-Log-PDA is close to that of the Exact-Log-MAP.

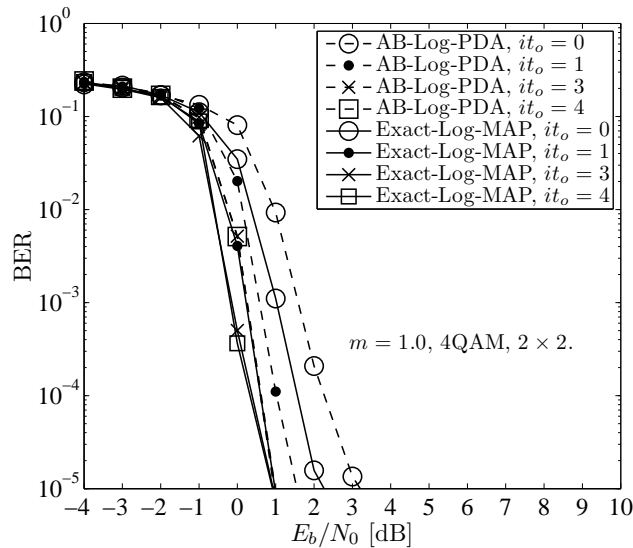


FIGURE 4.13: Impact of the number of outer iterations it_o on the achievable BER of the AB-Log-PDA ($it_i = 0$) based IDD scheme of Fig. 4.7 and the Exact-Log-MAP based IDD scheme of [75]. The scenario-dependent simulation parameters used for obtaining these results are shown in the figure, while other simulation parameters are given in Table 4.2. We see that the performance of both IDD schemes is improved upon increasing it_o , but the attainable improvement gradually becomes smaller and the performance achieved after three outer iterations becomes almost the same as that of four outer iterations.

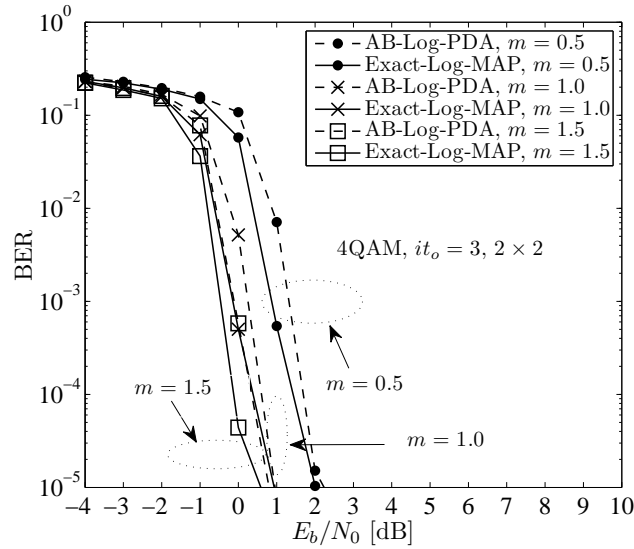


FIGURE 4.14: Impact of Nakagami- m fading parameter m on the achievable BER of the AB-Log-PDA ($it_i = 0$) based IDD scheme of Fig. 4.7 and the Exact-Log-MAP based IDD scheme of [75]. The scenario-dependent simulation parameters used for obtaining these results are shown in the figure, while other simulation parameters are given in Table 4.2. We see that as m decreases, the achievable performance of both IDD schemes considered is degraded, since the fading becomes more severe.

Rayleigh fading channel. Observe from Fig. 4.13 that the performance of the AB-Log-PDA based IDD scheme is improved upon increasing the number of outer iterations it_o , where $it_o = 0$ represents the conventional receiver structure in which the signal detector and the FEC decoder are serially concatenated, but operate without exchanging soft information. However, the attainable improvement gradually becomes smaller and the performance achieved after three outer iterations becomes almost the same as that of four outer iterations. This implies that the AB-Log-PDA based IDD scheme essentially converges after three outer iterations. A similar convergence profile is also observed for the optimal Exact-Log-MAP based IDD, although its performance is always marginally better than that of the corresponding AB-Log-PDA based IDD scheme. Notably, both IDD schemes considered achieve $BER = 10^{-5}$ at about $E_b/N_0 = 1$ dB after three iterations.

3) Impact of Nakagami- m fading parameter m

Fig. 4.14 shows the impact of different m values on the achievable BER performance of the IDD schemes considered. As m decreases, the achievable performance of both the IDD schemes considered is degraded, since the fading becomes more severe. However, the performance gap between the AB-Log-PDA and the Exact-Log-MAP based IDD schemes is marginal for all values of m considered.

4) Impact of modulation order

Additionally, in Fig. 4.15 we investigate the impact of the modulation order on the achiev-

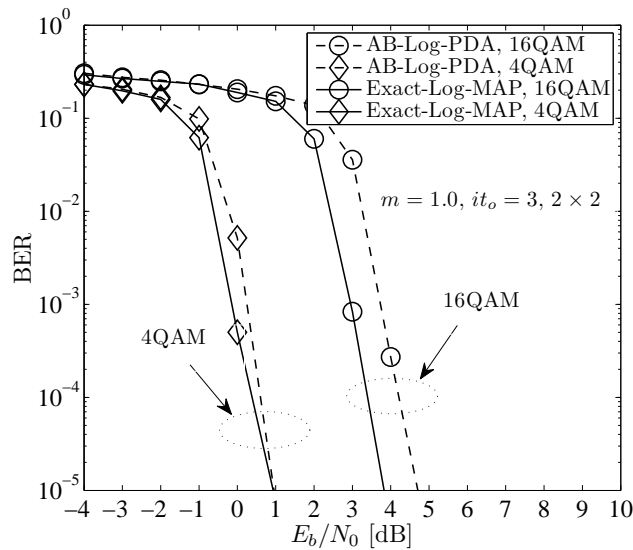


FIGURE 4.15: Impact of the modulation order on the achievable BER of the AB-Log-PDA ($it_i = 0$) based IDD scheme of Fig. 4.7 and the Exact-Log-MAP based IDD scheme of [75]. The scenario-dependent simulation parameters used for obtaining these results are shown in the figure, while other simulation parameters are given in Table 4.2. It is observed that for higher-order modulation, for example, 16QAM, the performance gap between the AB-Log-PDA and the Exact-Log-MAP based IDDs becomes larger. This is because the accuracy of the Gaussian approximation in the PDA method degrades, when the modulation order is increased.

able performance of the AB-Log-PDA based IDD scheme. It is observed that for higher-order modulation, for example, 16QAM, the performance gap between the AB-Log-PDA and the Exact-Log-MAP based IDDs becomes larger. This is because the accuracy of the Gaussian approximation in the PDA method degrades, when the modulation order is increased. More specifically, as analyzed in Section 4.3 and shown in Fig. 4.5 as well as Fig. 4.6, the interference-plus-noise term \mathbf{v}_i obeys a multimodal Gaussian distribution associated with M^{N_t-1} Gaussian component-distributions. When M is large, there exist many interfering Gaussian component-distributions, where the effect of each might be trivial, but their accumulated effect may render the estimated $P(s_i = a_m|\mathbf{y})$ inaccurate, and hence inaccurate bit-based extrinsic LLRs might be calculated using (4.36).

5) Impact of the number of transmit antennas

The impact of the number of transmit antennas N_t on the achievable performance of the AB-Log-PDA based IDD scheme is shown in Fig. 4.16. On the one hand, upon increasing N_t (and N_r), an increased diversity gain is obtained, and a more accurate Gaussian approximation is achieved according to the central limit theorem. Hence we observe a significant performance improvement, when moving from a (2×2) -element to a (4×4) -element MIMO system. On the other hand, however, it is observed that when N_t (and N_r) is increased, the performance gap between the AB-Log-PDA and the Exact-Log-MAP based IDD receivers is also increased. This is because the achievable diversity gain of the Exact-Log-MAP de-

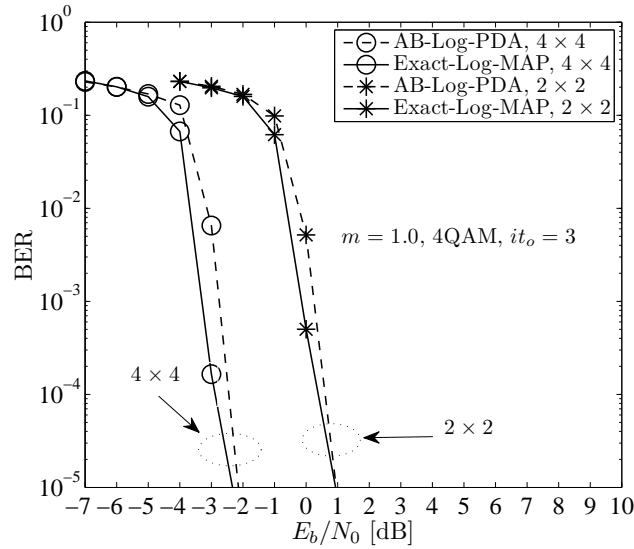


FIGURE 4.16: Impact of the number of transmit antennas on the achievable BER of the AB-Log-PDA ($it_i = 0$) based IDD scheme of Fig. 4.7 and the Exact-Log-MAP based IDD scheme of [75]. The scenario-dependent simulation parameters used for obtaining these results are shown in the figure, while other simulation parameters are given in Table 4.2. we observe a significant performance improvement, when moving from a (2×2) -element to a (4×4) -element MIMO system. Additionally, when N_t (and N_r) is increased, the performance gap between the AB-Log-PDA and the Exact-Log-MAP based IDD receivers is also increased.

tector is higher than that of the AB-Log-PDA detector, although a higher N_t results in an improved Gaussian approximation quality.

6) Impact of channel-estimation error

Finally, the impact of the channel-estimation errors on the achievable BER performance of both the AB-Log-PDA and the Exact-Log-MAP based IDD schemes is investigated in Fig. 4.17. The estimated channel matrix is given by $\hat{\mathbf{H}} = \rho\mathbf{H} + \sqrt{(1.0 - \rho^2)}\Delta\mathbf{H}$, where $0 \leq \rho \leq 1$ indicates the accuracy of channel-estimation. For example, $\rho = 1.0$ represents perfect channel-estimation and each entry of $\Delta\mathbf{H}$ obeys a zero-mean, unit-variance complex Gaussian distribution. It can be observed from Fig. 4.17 that the achievable BER performance of both IDD schemes is moderately degraded upon increasing the value of ρ and that the AB-Log-PDA based IDD still achieves a performance similar to that of its Exact-Log-MAP based IDD counterpart, even when the channel-estimation accuracy is as low as $\rho = 0.97$.

4.6.2 Computational Complexity Analysis

Because the turbo codec module is common to both IDD schemes, and since we have shown that both the AB-Log-PDA and the Exact-Log-MAP based IDD schemes converge after

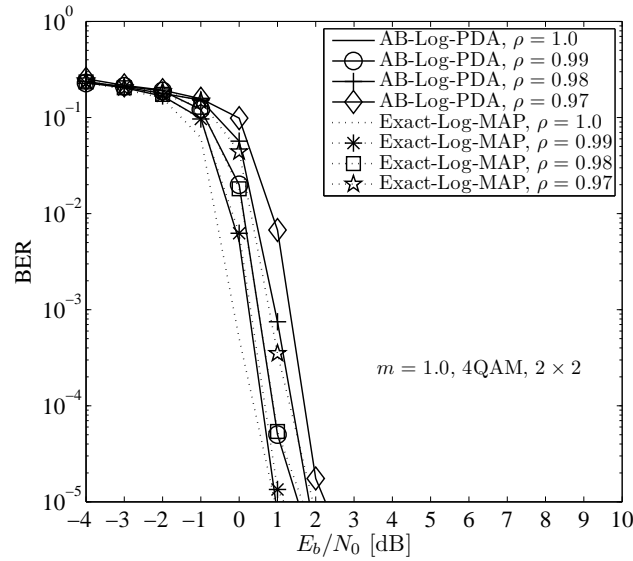


FIGURE 4.17: Impact of channel-estimation error on the achievable BER of the AB-Log-PDA ($it_i = 0$) based IDD scheme of Fig. 4.7 and the Exact-Log-MAP based IDD scheme of [75]. The scenario-dependent simulation parameters used for obtaining these results are shown in the figure, while other simulation parameters are given in Table 4.2. We see that the achievable BER performance of both IDD schemes is moderately degraded upon increasing the value of the channel-estimation accuracy indicator ρ and that the AB-Log-PDA based IDD still achieves a performance similar to that of its Exact-Log-MAP based IDD counterpart, even when the channel-estimation accuracy is as low as $\rho = 0.97$.

three iterations in the scenarios considered, the computational complexity of the proposed AB-Log-PDA based IDD scheme can be evaluated by simply comparing its complexity to that of the Exact-Log-MAP in a single iteration. As shown in Table 4.1, the major computational cost of the AB-Log-PDA per transmit symbol is the calculation of $\mathbf{\Lambda}_i^{-1}$ and the matrix multiplication of (4.19). Direct calculation of $\mathbf{\Lambda}_i^{-1}$ imposes a computational cost of $\mathcal{O}(8N_r^3)$ real-valued operations (additions/multiplications), which is still relatively expensive. Fortunately, by using the Sherman-Morrison-Woodbury formula based “speed-up” techniques of [219], the computational cost of calculating $\mathbf{\Lambda}_i^{-1}$ can be reduced to $\mathcal{O}(4N_r^2)$ real operations per transmit symbol, or $\mathcal{O}(4N_t N_r^2)$ real-valued operations per iteration. Additionally, the calculation of (4.19) requires $\mathcal{O}(4MN_r^2 + 2MN_r)$ real operations per transmit symbol, or $\mathcal{O}(4MN_t N_r^2 + 2MN_t N_r)$ real-valued operations per iteration. In summary, the computational complexity of the AB-Log-PDA method is $\mathcal{O}(4MN_t N_r^2 + 2MN_t N_r) + \mathcal{O}(4N_t N_r^2)$ per iteration.

By comparison, the Exact-Log-MAP algorithm has to calculate the Euclidean distance $\|\mathbf{y} - \mathbf{H}\mathbf{s}\|^2$ for M^{N_t} times, hence its complexity order is $\mathcal{O}(M^{N_t})$. More specifically, $\|\mathbf{y} - \mathbf{H}\mathbf{s}\|^2$ requires $\mathcal{O}(4N_r N_t + 6N_r)$ real-valued operations. Therefore, the Exact-Log-MAP algorithm has a computational complexity of $\mathcal{O}[M^{N_t}(4N_r N_t + 6N_r)]$ real-valued operations per iteration, which is significantly higher than that of the AB-Log-PDA, especially when N_t , N_r and M have large values. This observation is further confirmed by the results of Fig.

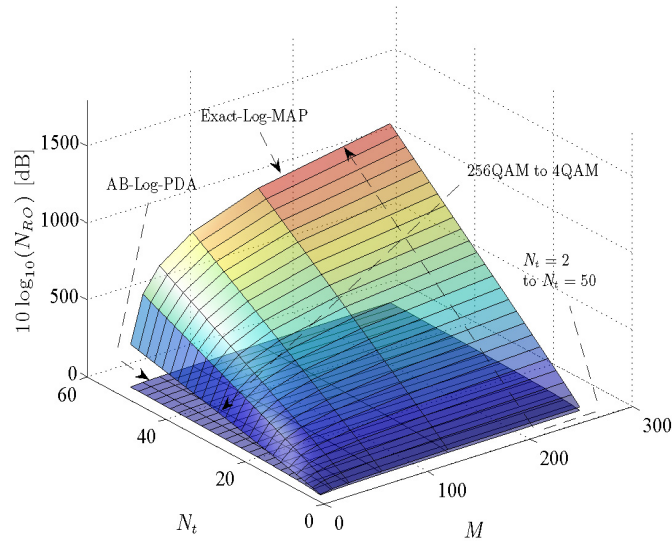


FIGURE 4.18: Computational complexity comparison of the AB-Log-PDA ($it_i = 0$) algorithm of Table 4.1 and the Exact-Log-MAP algorithms of [75] in terms of the number of real-valued operations N_{RO} . The upper surface and the lower surface represent the computational complexity of the Exact-Log-MAP algorithm and of the proposed AB-Log-PDA algorithm, respectively. Since we assume $N_r = N_t$, the computational complexity of both algorithms becomes a function of the number of transmit antennas N_t and of the modulation order M . We observe that upon increasing N_t and/or M , the computational complexity of the Exact-Log-MAP algorithm increases substantially faster than that of the AB-Log-PDA algorithm. Additionally, compared to M , N_t plays a more significant role in determining the computational complexity of the two algorithms.

4.18, where the computational complexity of the two algorithms is compared in terms of the number of real-valued operations N_{RO} , while considering the scenario of $N_r = N_t$ as an example. To elaborate a little further, the upper surface and the lower surface represent the computational complexity of the Exact-Log-MAP algorithm and of the proposed AB-Log-PDA algorithm, respectively. Since we assume $N_r = N_t$, the computational complexity of both algorithms becomes a function of the number of transmit antennas N_t and of the modulation order M . We can observe from Fig. 4.18 that upon increasing N_t and/or M , the computational complexity of the Exact-Log-MAP algorithm increases substantially faster than that of the AB-Log-PDA algorithm. Additionally, compared to M , N_t plays a more significant role in determining the computational complexity of the two algorithms.

Finally, compared to the popular list sphere decoding (LSD) algorithm [75], which has an exponential complexity lower bound, especially for low SNR values [61], the proposed AB-Log-PDA has the distinct advantage of a polynomial-time complexity (roughly a *cubic* function of N_t , as shown above) for all SNR values. Although there exist other reduced-complexity variants of LSD, such as the list fixed-complexity sphere-decoder (LFSD) [82] and the soft K -best sphere-decoder using an improved “look-ahead path metric” [74], in general they still have a higher complexity than the AB-Log-PDA algorithm if the SNR

value is low and/or the problem size (i.e. N_t and M) is large. This is because finding the closest point in lattices is an NP-hard problem [55]. To be more specific, the computational complexity of the K -best SD of [74] is indeed reduced, but it remains of similar order to that of the LFSD, which is on the order of $\mathcal{O}(M^{\sqrt{N_t}})$ [83].

4.7 Chapter Summary and Conclusions

We demonstrate that the classic candidate-search based method of calculating bit-based extrinsic LLRs is not applicable to the family of PDA-based detectors. Additionally, in stark contrast to the existing literature, we demonstrate that the output symbol probabilities of the existing PDAs are not the true APPs, they are rather constituted by the normalized symbol likelihoods. Hence, surprisingly, the classic relationship, where the extrinsic LLRs are given by subtracting the *a priori* LLRs from the *a posteriori* LLRs does not hold for the existing PDA-based detectors, when the output probabilities of the existing PDAs are interpreted as APPs to generate *a posteriori* LLRs. Based on these insights, we conceive the AB-Log-PDA method and identify the technique of calculating the bit-based extrinsic LLRs for the AB-Log-PDA, which results in a simplified IDD receiver structure. Additionally, we demonstrate that we may completely dispense with any inner iterations within the AB-Log-PDA in the context of IDD receivers. Our complexity analysis and numerical results recorded for transmission over Nakagami- m fading MIMO channels demonstrate that the proposed AB-Log-PDA based IDD scheme is capable of achieving a comparable performance to that of the optimal MAP detector based IDD receiver, while imposing a significantly lower computational complexity in the scenarios considered.

Exact Bayes' Theorem Based PDA for Iterative MIMO Detection and Channel Decoding

5.1 Introduction

IT was conventionally regarded that the approximate Bayes' theorem based PDA algorithms output the estimated symbol-wise APPs as soft information [193, 219, 226, 227, 242]. However, in Chapter 4, we demonstrated that these probabilities are *not* actually the true APPs in the rigorous mathematical sense, but a type of nominal APPs that are unsuitable for the *classic IDD architecture* shown in Fig. 4.4. Naturally, in order to design PDA-based IDD receivers, there are two possible strategies to choose from. One of them is to adapt the IDD receiver architecture so that the conventional approximate Bayes' theorem based PDA algorithms can be applied in the modified IDD architecture. This strategy has been studied in Chapter 4, where an AB-Log-PDA based IDD receiver relying on a simplified IDD architecture of Fig. 4.7 was investigated. The other strategy is to remain the classic IDD architecture of Fig. 4.4, but appropriately adapt the conventional PDA algorithm so that it becomes applicable to the classic architecture of IDD receiver seen in Fig. 4.4. In this chapter, we will investigate the second strategy and elucidate the relationship between the two strategies.

Since we have revealed in Chapter 4 that the symbol-wise probabilities output by the family of approximate Bayes' theorem based PDAs are not the true APPs, the classic relationship that the extrinsic LLRs may be generated by the subtraction of the *a priori* LLRs from the *a posteriori* LLRs no longer holds for the approximate Bayes' theorem based PDAs, including the AB-Log-PDA proposed in Chapter 4.

The potential reasons as to why the output symbol probabilities of the conventional PDA detectors/equalizers have been widely misinterpreted as true APPs without causing any notable problems [193, 219, 226, 227, 242] are as follows:

1. They qualify as some form of *a posteriori* estimates based on the *a priori* known received signal and the channel matrix, and hence were roughly treated as the true APPs;
2. They are eminently applicable to numerous applications, including the MUD of uncoded CDMA systems [219], the multi-stream symbol detection of uncoded MIMO systems [41, 226], the soft decision equalization of frequency-selective MIMO channels [193, 227, 242], as well as the distributed soft reception in base station cooperation [43];
3. Additionally, the equivalent bit-wise LLRs generated from these probabilities are also applicable to FEC-coded MIMO systems employing the traditional *open loop* receiver architecture, in which the PDA detector is not required to generate bit-wise *extrinsic* LLRs [230].

Although the AB-Log-PDA based IDD scheme of Fig. 4.7 has been proposed in Chapter 4 upon identifying the above-mentioned misconception, this IDD scheme relies on an irregular IDD architecture that might be inconvenient in practice. Therefore, it is beneficial to perform an in-depth investigation of other alternative PDA designs that are applicable in the classic IDD architecture of Fig. 4.4. Note that the iterative receiver proposed in [233] was essentially an MAP detection aided IDD scheme, employing the hard-output PDA detector for generating the candidate-search list. Since the PDA used in [233] was unable to generate the true APPs for FEC decoding, it did not solve the problem of interest to us.

Against this background, the main contributions of this chapter are summarized as follows.

1. We propose an exact Bayes' theorem based logarithmic domain PDA (EB-Log-PDA) approach for the IDD scheme of FEC-coded MIMO systems using arbitrary M -ary modulation for transmission over fading MIMO channels. As opposed to that of the existing PDAs based on an approximate version of the Bayes' theorem [193, 219, 226, 227, 242], the estimated symbol-wise output probabilities of the EB-Log-PDA exhibit similar characteristics to the true APPs. Hence the bit-wise extrinsic LLRs \mathbf{L}_E delivered by the proposed EB-Log-PDA to the outer FEC decoder may be calculated simply by subtracting the bit-wise *a priori* LLRs \mathbf{L}_A from the bit-wise *a posteriori* LLRs \mathbf{L}_D , which are generated from the symbol-wise output APPs of the EB-Log-PDA. Furthermore, in contrast to the existing probabilistic-domain PDAs [193, 219, 226, 227, 242], the proposed EB-Log-PDA based detector operates in the logarithmic domain, which results in a better numerical stability and a higher numerical accuracy in the context of IDD receivers.
2. We investigate the relationship between the EB-Log-PDA based IDD scheme and the AB-Log-PDA aided IDD scheme proposed in Chapter 4. We demonstrate that the two schemes achieve a similar performance when dispensing with inner iterations within the PDAs. However, this does not mean that the extrinsic LLRs output by the two PDAs

are identical. Actually, the EB-Log-PDA may be viewed as a scheme using the same *a priori* information twice in different processing blocks, whereas the AB-Log-PDA utilizes the corresponding *a priori* information once. Our analysis of the cumulative distribution functions (CDFs) and the probability density functions (PDFs) concerning the *differences* between the two types of extrinsic LLRs reveal that these two types of extrinsic LLRs are different, even though they might be similar in certain scenarios.

3. We provide a comparative study of the impact of the inner iterations within both the AB-Log-PDA and the EB-Log-PDA on the achievable performance of the corresponding IDD schemes. We will demonstrate that, similar to the case of AB-Log-PDA based IDD as discussed in Chapter 4, the performance of the EB-Log-PDA based IDD scheme is also degraded when inner iterations of the EB-Log-PDA are invoked. More specifically, the performance of the EB-Log-PDA based IDD scheme is consistently degraded as the number of inner iterations within the EB-Log-PDA is increased. By contrast, the performance degradation profile of the AB-Log-PDA based IDD scheme exhibits fluctuations upon increasing the number of inner iterations within the AB-Log-PDA. The reasons accounting for these phenomena are discussed as well.
4. When dispensing with inner iterations within both the EB-Log-PDA and the AB-Log-PDA in the context of their respective IDD architecture, the resultant IDD receiver exhibits a performance close to that of the optimal MAP-based IDD scheme, while imposing a significantly lower computational complexity in the scenarios considered.

The remainder of the chapter is organized as follows. In Section 5.2, the FEC-coded MIMO system model relying on the classic IDD architecture is detailed. In Section 5.3, the proposed EB-Log-PDA relying on an external source of *a priori* soft information is presented. Then, in Section 5.4, the method of calculating the extrinsic LLRs for the EB-Log-PDA is derived, and the relationship between the extrinsic LLRs of the EB-Log-PDA and that of the AB-Log-PDA is elucidated as well. Our simulation results and discussions are provided in Section 5.5, while our conclusions are offered in Section 5.6.

5.2 System Model

The AB-Log-PDA based IDD scheme proposed in Chapter 4 has a non-standard architecture of Fig. 4.7. In this chapter we consider the FEC-coded SDM-MIMO system that relies exactly on the classic IDD architecture of Fig. 4.4. To elaborate a little further, the IDD scheme conceived in this chapter has an architecture of Fig. 5.1, in which the EB-Log-PDA detector will be detailed in Section 5.3. Since the description of the FEC-coded SDM-MIMO system considered has been given in Section 4.2, it is omitted here.

the term $s_i \mathbf{e}_i$, which implies that \mathbf{u}_i does not impose interference on s_i . However, it is the interference-plus-noise term \mathbf{v}_i that contaminates the detection of the symbol s_i .

For uncoded MIMO systems, where no outer source of *a priori* soft information about the transmitted symbols is available, the existing PDA methods typically use the received signal \mathbf{y} and the channel matrix \mathbf{H} as input quantities, and then generate the estimated symbol-wise nominal APPs of the transmitted symbols $\{s_i\}_{i=1, \dots, N_t}$ as its output. By contrast, for FEC-coded MIMO systems, we have an extra input quantity, which is the soft information feedback gleaned from the outer FEC decoder. In this scenario, because the reliability of the FEC decoder's output is typically higher than that of the soft MIMO detector at the previous stage, some of the key operations of the proposed EB-Log-PDA are implemented in the logarithmic domain in order to improve the achievable numerical stability and accuracy.

Although the interference-plus-noise term \mathbf{v}_i obeys a multimodal Gaussian mixture distribution [44, 230], initially it is plausible to obtain a coarse estimate of s_i by assuming that \mathbf{v}_i obeys a single N_t -variate Gaussian distribution. It is worth noting that in the circumstances considered each element of \mathbf{v}_i is the sum of only two scalar random variables for any $N_t \geq 2$, hence, according to the central limit theorem, the Gaussian approximation of \mathbf{v}_i does *not* become more accurate when N_t is increased.¹ This trend is different from that of the non-decoupled signal model based PDA [44]. In order to fully characterize the complex random vector \mathbf{v}_i which is not necessarily *proper* [363, 398, 399], we specify the mean of

$$\boldsymbol{\mu}_i \triangleq \mathcal{E}(\mathbf{v}_i) = \sum_{k \neq i} \mathcal{E}(s_k) \mathbf{e}_k, \quad (5.2)$$

the covariance of

$$\boldsymbol{\Upsilon}_i \triangleq \mathcal{C}(\mathbf{v}_i) = \sum_{k \neq i} \mathcal{C}(s_k) \mathbf{e}_k \mathbf{e}_k^T + 2\sigma^2 (\mathbf{H}^H \mathbf{H})^{-1}, \quad (5.3)$$

and the pseudo-covariance of

$$\boldsymbol{\Omega}_i \triangleq \mathcal{C}_p(\mathbf{v}_i) = \sum_{k \neq i} \mathcal{C}_p(s_k) \mathbf{e}_k \mathbf{e}_k^T. \quad (5.4)$$

Note that (5.4) holds, because $\tilde{\mathbf{n}}$ is a circularly symmetric complex-valued Gaussian noise vector and hence it is proper [363, 398, 399].

Considering the IDD architecture of Fig. 4.4, we define an $(N_t \times M)$ -element probability matrix $\mathbf{P}^{(z, z')}$, whose element $P_{n, m}^{(z, z')}$ represents the estimate of the APP that we have $s_n = a_m$ at the z -th/ z' -th outer/inner iteration of the EB-Log-PDA approach. More precisely,

¹From another point of view, for a given data symbol s_k , the corresponding element of \mathbf{v}_i has a Gaussian PDF centered around s_k . However, s_k itself is a non-Gaussian random variable, which leads to a random displacement of the Gaussian PDF. As such, the accuracy of the Gaussian assumption for \mathbf{v}_i does not improve, when N_t or N_r is increased.

we have

$$P_{n,m}^{(z,z')} = P_m^{(z,z')}(s_n|\tilde{\mathbf{y}}) \triangleq P^{(z,z')}(s_n = a_m|\tilde{\mathbf{y}}), \quad (5.5)$$

where z and z' are nonnegative integers, $n = 1, \dots, N_t$ and $m = 1, \dots, M$. Then we have

$$\mathcal{E}(s_k) = \sum_{m=1}^M a_m P_m^{(z,z')}(s_k|\tilde{\mathbf{y}}), \quad (5.6)$$

$$\mathcal{C}(s_k) = \sum_{m=1}^M [a_m - \mathcal{E}(s_k)][a_m - \mathcal{E}(s_k)]^* P_m^{(z,z')}(s_k|\tilde{\mathbf{y}}), \quad (5.7)$$

and

$$\mathcal{C}_p(s_k) = \sum_{m=1}^M [a_m - \mathcal{E}(s_k)]^2 P_m^{(z,z')}(s_k|\tilde{\mathbf{y}}), \quad (5.8)$$

for (5.2), (5.3) and (5.4), respectively, where the pseudo-covariance of a complex random vector \mathbf{x} is defined as [363, 398, 399]

$$\mathcal{C}_p(\mathbf{x}) \triangleq \mathcal{E} \left[(\mathbf{x} - \mathcal{E}(\mathbf{x})) (\mathbf{x} - \mathcal{E}(\mathbf{x}))^T \right]. \quad (5.9)$$

Note that from Eq. (5.2) to Eq. (5.8) we effectively use $(N_t - 1)$ probability vectors of $\{\mathbf{P}^{(z,z')}(k, :)\}_{k \neq i}$ associated with the interference signal $\{s_k\}_{k \neq i}$ to model \mathbf{v}_i , where $\mathbf{P}^{(z,z')}(k, :)$ represents the k th row of the matrix $\mathbf{P}^{(z,z')}$. Since we do not have any *a priori* knowledge about the distribution of $s_n|\tilde{\mathbf{y}}$ at the beginning, $P_m^{(z,z')}(s_n|\tilde{\mathbf{y}})$ is initialized using the uniform distribution of

$$P_m^{(0,0)}(s_n|\tilde{\mathbf{y}}) = \frac{1}{M}, \quad (5.10)$$

for $\forall n = 1, \dots, N_t$ and $\forall m = 1, \dots, M$.

Based on the assumption that \mathbf{v}_i obeys the Gaussian distribution, $\tilde{\mathbf{y}}|s_i$ is also Gaussian distributed. We define

$$\mathbf{w} \triangleq \tilde{\mathbf{y}} - s_i \mathbf{e}_i - \sum_{k \neq i} \mathcal{E}(s_k) \mathbf{e}_k \quad (5.11)$$

and

$$\alpha_{i,m}^{(z,z'+1)} \triangleq - \begin{bmatrix} \Re(\mathbf{w}) \\ \Im(\mathbf{w}) \end{bmatrix}^T \mathbf{\Lambda}_i^{-1} \begin{bmatrix} \Re(\mathbf{w}) \\ \Im(\mathbf{w}) \end{bmatrix}, \quad (5.12)$$

where the *composite* covariance matrix $\mathbf{\Lambda}_i$ is defined as

$$\mathbf{\Lambda}_i \triangleq \begin{bmatrix} \Re(\mathbf{\Upsilon}_i + \mathbf{\Omega}_i) & -\Im(\mathbf{\Upsilon}_i - \mathbf{\Omega}_i) \\ \Im(\mathbf{\Upsilon}_i + \mathbf{\Omega}_i) & \Re(\mathbf{\Upsilon}_i - \mathbf{\Omega}_i) \end{bmatrix}, \quad (5.13)$$

where $\Re(\cdot)$ and $\Im(\cdot)$ represent the real and imaginary part of a complex variable, respectively.

Then the likelihood function of $\tilde{\mathbf{y}}|s_i = a_m$ at the $(z, z' + 1)$ th iteration satisfies

$$p_m^{(z, z'+1)}(\tilde{\mathbf{y}}|s_i) \propto \exp\left(\alpha_{i,m}^{(z, z'+1)}\right). \quad (5.14)$$

In the next step, the existing PDA methods employed in uncoded MIMO systems typically invoked an approximate form of the Bayes' theorem to estimate the symbol-wise APPs [41, 43, 193, 219, 226], which is

$$\mathcal{P}_m^{(z, z'+1)}(s_i|\tilde{\mathbf{y}}) \approx \frac{p_m^{(z, z'+1)}(\tilde{\mathbf{y}}|s_i)}{\sum_{m=1}^M p_m^{(z, z'+1)}(\tilde{\mathbf{y}}|s_i)}. \quad (5.15)$$

However, we argue that (5.15) does not conform to the formal mathematical definition of the APP in Bayesian statistics,² which is [400]

$$P(\theta|X) \propto P(\theta)P(X|\theta), \quad (5.16)$$

where the probability $P(\theta)$ is an *a priori* belief of the random variable θ , and $P(X|\theta)$ is the likelihood of the observation X . Therefore, $\mathcal{P}_m^{(z, z'+1)}(s_i|\tilde{\mathbf{y}})$ calculated with the aid of (5.15) does not represent the true APPs, but instead the normalized likelihoods, which may be regarded as a type of nominal APPs.³

To obtain the true APP of symbol s_i at the $(z, z' + 1)$ th iteration of the PDA-aided IDD receiver, we advocate to use the *exact* form of the Bayes' theorem. Hence the true APP estimated at the output of the PDA method is given as

$$\begin{aligned} & P_m^{(z, z'+1)}(s_i|\tilde{\mathbf{y}}) \\ &= \frac{p_m^{(z, z'+1)}(\tilde{\mathbf{y}}|s_i)P_m^{(z, z')}(s_i)}{\sum_{m=1}^M p_m^{(z, z'+1)}(\tilde{\mathbf{y}}|s_i)P_m^{(z, z')}(s_i)} \\ &= \frac{\exp\left(\beta_{i,m}^{(z, z'+1)} - \gamma\right)}{\sum_{m=1}^M \exp\left(\beta_{i,m}^{(z, z'+1)} - \gamma\right)}, \end{aligned} \quad (5.17)$$

where $P_m^{(z, z')}(s_i)$ is the *a priori* probability generated from the extrinsic LLRs fed back by the soft FEC decoder, and $\beta_{i,m}^{(z, z'+1)} \triangleq \alpha_{i,m}^{(z, z'+1)} + \ln\left(P_m^{(z, z')}(s_i)\right)$. Note that $\gamma \triangleq \max_{m=1, \dots, M} \beta_{i,m}^{(z, z'+1)}$ is introduced for further improving the numerical stability and accuracy. For the same

²For the sake of clarity, here we use $\mathcal{P}()$ to denote the symbol-wise probabilities estimated using the approximate Bayes' formula given by (5.15), while using $P()$ to represent ordinary probabilities otherwise.

³Note that these nominal APPs were invoked in the uncoded systems of [193, 219, 226, 227, 242] and in the coded system of [230] without imposing any notable problems. This is because the calculation of extrinsic LLRs was not required in those contexts.

reason, (5.17) is reformulated in the logarithmic domain as

$$\begin{aligned} & \psi_{i,m}^{(z,z'+1)} \\ \triangleq & \ln \left(P_m^{(z,z'+1)}(s_i|\tilde{\mathbf{y}}) \right) \\ = & \tilde{\beta}_{i,m}^{(z,z'+1)} - \ln \left(\sum_{m=1}^M \exp \left(\tilde{\beta}_{i,m}^{(z,z'+1)} \right) \right), \end{aligned} \quad (5.18)$$

where we have $\tilde{\beta}_{i,m}^{(z,z'+1)} \triangleq \beta_{i,m}^{(z,z'+1)} - \gamma$, and the second term of the right-hand-side expression may be computed by invoking the ‘‘Jacobian logarithm’’ of [75]. When invoking the Max-log approximation, (5.18) may be further simplified as

$$\psi_{i,m}^{(z,z'+1)} \approx \tilde{\beta}_{i,m}^{(z,z'+1)} - \max_{m=1,\dots,M} \tilde{\beta}_{i,m}^{(z,z'+1)} = \tilde{\beta}_{i,m}^{(z,z'+1)}. \quad (5.19)$$

As a result, the estimated symbol-wise APP of s_i is given by

$$P_m^{(z,z'+1)}(s_i|\tilde{\mathbf{y}}) \approx e^{\psi_{i,m}^{(z,z'+1)}}, \quad (5.20)$$

which will be used for replacing the corresponding element $P_m^{(z,z')}(s_i|\tilde{\mathbf{y}})$ in the probability matrix $\mathbf{P}^{(z,z')}$. Based on these updated symbol-wise APPs, the procedure presented above may be repeated either in the next inner iteration within the PDA or in the next outer iteration exchanging extrinsic information between the FEC-decoder and the MIMO detector to obtain new estimates of the symbol-wise APPs. For the sake of clarity, the EB-Log-PDA algorithm relying on the *a priori* soft information feedback gleaned from the outer FEC decoder is summarized in Table 5.1.

5.4 Extrinsic LLR Calculation For EB-Log-PDA

5.4.1 Method of Calculating the Extrinsic LLRs for EB-Log-PDA

For ease of exposition, in the following we will denote the left-hand-side term of (5.15) and (5.17) as $\mathcal{P}(s_i = a_m|\mathbf{y})$ and $P(s_i = a_m|\mathbf{y})$, respectively. As a beneficial result of replacing (5.15) by (5.17), the extrinsic LLRs may be calculated according to the classic relationship by subtracting the *a priori* LLRs from the *a posteriori* LLRs that are generated from the

TABLE 5.1: Summary of the EB-Log-PDA algorithm

Given the received signal \mathbf{y} , the channel matrix \mathbf{H} and the modulation constellation \mathbb{A} , make preprocessing on the received signal \mathbf{y} to obtain $\tilde{\mathbf{y}} = (\mathbf{H}^H \mathbf{H})^{-1} \mathbf{H}^H \mathbf{y}$.

Step 1. Set the initial value of the inner iteration index to $z' = 0$. If the outer iteration index $z = 0$, initialize the values of the symbol-wise APPs as $P_m^{(z, z')}(s_n | \tilde{\mathbf{y}}) = 1/M$, for $\forall n = 1, 2, \dots, N_t$ and $\forall m = 1, 2, \dots, M$. Otherwise, initialize the values of $P_m^{(z, z')}(s_n | \tilde{\mathbf{y}})$ using the *a priori* probabilities generated from the feedback extrinsic LLRs of the soft FEC decoder.

Step 2. Based on the values of $\left\{ \mathbf{P}^{(z, z')}(k, :) \right\}_{k \neq i}$, calculate $P_m^{(z, z'+1)}(s_i | \tilde{\mathbf{y}})$:

for $i = 1 : N_t$

calculate the statistics of the interference-plus-noise term \mathbf{v}_i using (5.2) - (5.8), as well as the inverse of $\mathbf{\Lambda}_i$ in (5.13),

for $m = 1 : M$

calculate $P_m^{(z, z'+1)}(s_i | \tilde{\mathbf{y}})$ using (5.11), (5.12), (5.18) and (5.20).

end

end

Step 3. If $|P_m^{(z, z'+1)}(s_i | \tilde{\mathbf{y}}) - P_m^{(z, z')}(s_i | \tilde{\mathbf{y}})| < \varepsilon$, $\forall i$ and $\forall m$, i.e. the probability-matrix $\mathbf{P}^{(z, z'+1)}$ has converged, where ε is a given small positive real number, or the index z' has reached a given number of iterations, terminate the iteration and output $\mathbf{P}^{(z, z'+1)}$. Otherwise, let $z' = z' + 1$ and return to Step 2.

estimated symbol-wise APPs of the EB-Log-PDA detector, hence we have

$$\begin{aligned}
L_E^{EB}(b_{il} | \mathbf{y}) &= L_D(b_{il} | \mathbf{y}) - L_A(b_{il}) \\
&= \ln \frac{P(b_{il} = +1 | \mathbf{y})}{P(b_{il} = -1 | \mathbf{y})} - L_A(b_{il}) \\
&\quad \sum_{\forall a_m \in \mathbb{A}_l^+} P(s_i = a_m | \mathbf{y}) \\
&= \ln \frac{\sum_{\forall a_m \in \mathbb{A}_l^+} P(s_i = a_m | \mathbf{y})}{\sum_{\forall a_m \in \mathbb{A}_l^-} P(s_i = a_m | \mathbf{y})} \\
&\quad - \underbrace{\ln \frac{P(b_{il} = +1)}{P(b_{il} = -1)}}_{L_A(b_{il})}, \tag{5.21}
\end{aligned}$$

where \mathbb{A}_l^\pm denotes the set of $M/2$ constellation points whose l th bit is $+1$ or -1 , respectively. It is noteworthy that (5.21) represents a simpler technique of generating the bit-wise extrinsic LLRs $L_E^{EB}(b_{il} | \mathbf{y})$, as long as the *true* symbol-wise APPs of $P(s_i = a_m | \mathbf{y})$ may be obtained.

By contrast, this approach is not applicable to the conventional *approximate* Bayes' theorem based PDA methods [41, 43, 193, 219, 226, 227, 242]. Our study reveals that the estimated symbol-wise nominal APPs obtained from (5.15) are *unsuitable* for generating the correct extrinsic bit-wise LLRs upon invoking the classic formula (5.21). This *hidden fact* is corroborated by the simulation results of Fig. 5.2. In the scenarios where the number of outer iterations it_o was set to be higher than zero, it was observed in Fig. 5.2 that the BER results of the IDD scheme using the AB-Log-PDA and (5.21) became abnormally poor, when

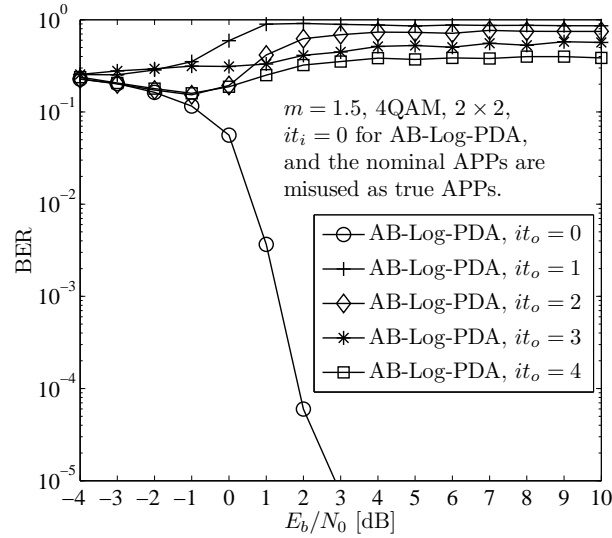


FIGURE 5.2: BER of the AB-Log-PDA based IDD scheme, where the nominal symbol-wise APPs were misinterpreted as the true symbol-wise APPs.

the nominal symbol-wise APPs produced by (5.15) were *misinterpreted* as true symbol-wise APPs. More specifically, we can observe from Fig. 5.2 that except for $it_o = 0$, the BER of the AB-Log-PDA based IDD scheme unexpectedly degrades upon increasing E_b/N_0 , and it also deteriorates when it_o increases from 1 to 4. The BER curve of the $it_o = 0$ scenario characterized in Fig. 5.2 exhibits a trend in line with our expectations, because in this case no soft information is fed back from the FEC decoder and hence the term $P_m^{(z, z')}(s_i)$ in (5.17) can be eliminated. In other words, (5.15) becomes equivalent to (5.17) in this scenario. These results further demonstrate that (5.15) should be regarded as a sort of symbol-wise nominal APP, rather than the symbol-wise true APP, as calculated in (5.17). As a result, we argue that in order to generate the correct symbol-wise APPs, which are readily applicable to (5.21), the calculation of $P_m^{(z, z'+1)}(s_i|\tilde{\mathbf{y}})$ has to rely on (5.17) instead of (5.15) that is used by the conventional PDA based MIMO detector.

Slightly differently from the above-mentioned M -ary modulation scenarios, there exist two alternative methods of generating the extrinsic bit-wise LLRs for BPSK modulation aided MIMO systems. On the one hand, the extrinsic LLR of b_{il} , simplified as b_i , may be formulated as

$$\begin{aligned} L_E^{EB}(b_i|\mathbf{y}) &= L_D(b_i|\mathbf{y}) - L_A(b_i) \\ &= \ln \frac{P(b_i = +1|\mathbf{y})}{P(b_i = -1|\mathbf{y})} - \ln \frac{P(b_i = +1)}{P(b_i = -1)}, \end{aligned} \quad (5.22)$$

where $P(b_i = \pm 1|\mathbf{y})$ is the final output of the EB-Log-PDA algorithm for BPSK modulation.

Alternatively, we have

$$L_D(b_i|\mathbf{y}) = \ln \frac{p(\mathbf{y}|b_i = +1)}{p(\mathbf{y}|b_i = -1)} + \ln \frac{P(b_i = +1)}{P(b_i = -1)}. \quad (5.23)$$

Since $p(\mathbf{y}|b_i = \pm 1)$ constitutes the intermediate output of the EB-Log-PDA algorithm for BPSK modulation, we can directly obtain

$$L_E^{EB}(b_i|\mathbf{y}) = \ln \frac{p(\mathbf{y}|b_i = +1)}{p(\mathbf{y}|b_i = -1)}. \quad (5.24)$$

5.4.2 On the Relationship Between the Extrinsic LLRs of the EB-Log-PDA and AB-Log-PDA

According to Conjecture 1 of [44], the bit-wise extrinsic LLRs of the AB-Log-PDA algorithm relying on (5.15) may be approximated by

$$L_E^{AB}(b_{il}|\mathbf{y}) \approx \ln \frac{\sum_{\forall a_m \in \mathbb{A}_l^+} \mathcal{P}(s_i = a_m|\mathbf{y})}{\sum_{\forall a_m \in \mathbb{A}_l^-} \mathcal{P}(s_i = a_m|\mathbf{y})}, \quad (5.25)$$

where $\mathcal{P}(s_i = a_m|\mathbf{y})$ is calculated by invoking (5.15). The resultant $L_E^{AB}(b_{il}|\mathbf{y})$ in (5.25) was shown to work well in the AB-Log-PDA aided IDD scheme of [44], although the right-hand-side expression of (5.25) appears to be in the form of $L_D^{AB}(b_{il}|\mathbf{y})$ compared with (5.21). Therefore, it is important to investigate the relationship between the extrinsic LLRs of the EB-Log-PDA formulated in (5.21) and that of the AB-Log-PDA calculated by (5.25).

Theorem 5.1. *For a specific bit b_{il} , the extrinsic LLR of the EB-Log-PDA algorithm is typically different from that of the AB-Log-PDA algorithm.*

Proof. Based on $b_{il} = +1$ or -1 , the symbols set \mathbb{A} may be divided into the pair of subsets \mathbb{A}_l^+ and \mathbb{A}_l^- , each hosting half of the constellation symbols. Without loss of generality, we assume that $\mathbb{A}_l^+ = \{a_1, a_2, \dots, a_{M/2}\}$, and $\mathbb{A}_l^- = \{a_{M/2+1}, a_{M/2+2}, \dots, a_M\}$. By substituting (5.15)

into (5.25), we arrive at

$$\begin{aligned}
& L_E^{AB}(b_{il}|\mathbf{y}) \\
&= \ln \frac{\left(\sum_{\forall a_m \in \mathbb{A}_l^+} p(\mathbf{y}|s_i = a_m) \right) / \left(\sum_{m=1}^M p(\mathbf{y}|s_i = a_m) \right)}{\left(\sum_{\forall a_m \in \mathbb{A}_l^-} p(\mathbf{y}|s_i = a_m) \right) / \left(\sum_{m=1}^M p(\mathbf{y}|s_i = a_m) \right)} \\
&= \ln \frac{\sum_{\forall a_m \in \mathbb{A}_l^+} p(\mathbf{y}|s_i = a_m)}{\sum_{\forall a_m \in \mathbb{A}_l^-} p(\mathbf{y}|s_i = a_m)}. \tag{5.26}
\end{aligned}$$

On the other hand, by substituting (5.17) into (5.21), we have

$$\begin{aligned}
L_E^{EB}(b_{il}|\mathbf{y}) &= \ln \frac{\sum_{\forall a_m \in \mathbb{A}_l^+} p(\mathbf{y}|s_i = a_m)P(s_i = a_m)}{\sum_{\forall a_m \in \mathbb{A}_l^-} p(\mathbf{y}|s_i = a_m)P(s_i = a_m)} \\
&\quad - \ln \frac{P(b_{il} = +1)}{P(b_{il} = -1)} \\
&= \ln \frac{\sum_{\forall a_m \in \mathbb{A}_l^+} p(\mathbf{y}|s_i = a_m)P(s_i = a_m)}{\sum_{\forall a_m \in \mathbb{A}_l^-} p(\mathbf{y}|s_i = a_m)P(s_i = a_m)} \\
&\quad - \ln \frac{\sum_{\forall a_m \in \mathbb{A}_l^+} P(s_i = a_m)}{\sum_{\forall a_m \in \mathbb{A}_l^-} P(s_i = a_m)}. \tag{5.27}
\end{aligned}$$

Note that (5.26) and (5.27) are typically not equal to each other, because i) the term $p(\mathbf{y}|s_i = a_m)$ in (5.26) and in (5.27) might be different if the number of inner iterations within the PDAs is higher than zero⁴; ii) even if the term $p(\mathbf{y}|s_i = a_m)$ in (5.26) and in (5.27) would be equal to each other at the same iteration index (z, z') , typically (5.26) and (5.27) would still be different from each other, except in some specific circumstances, for example, when $P(s_i = a_m)$ in (5.27) has the same value for the different constellation symbols a_m . \square

Apart from the nature of difference between the two types of extrinsic LLRs encapsulated in Theorem 5.1, the following proposition further characterizes the degree of difference between the two types of extrinsic LLRs.

Proposition 5.2. *Let us consider the difference $\Delta L_{il} = L_E^{EB}(i, l) - L_E^{AB}(i, l)$ between the*

⁴The estimated symbol-wise probabilities which are used for calculating the statistics of the interference-plus-noise term \mathbf{v}_i via (5.2) - (5.8) might be different for the AB-Log-PDA and EB-Log-PDA algorithms, even if the iteration index (z, z') with $z' > 0$ is the same for them.

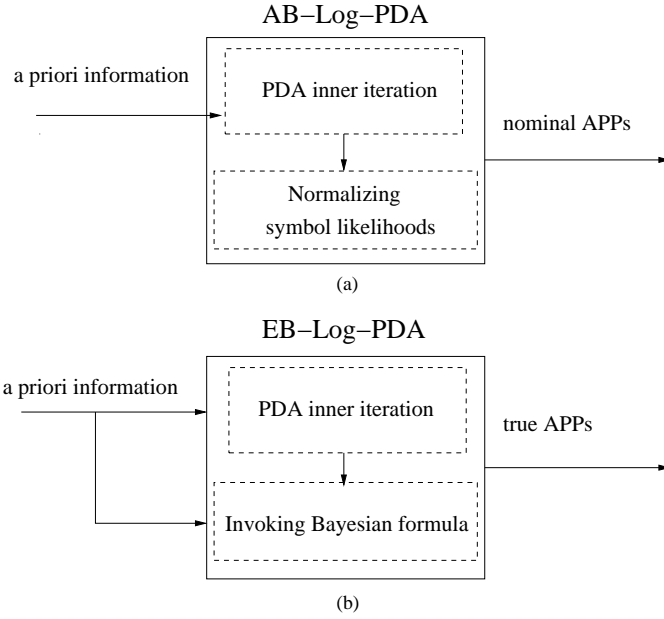


FIGURE 5.3: The role of the *a priori* information in the AB-Log-PDA and the EB-Log-PDA algorithms. These two blocks distinguish Fig. 4.7 and Fig. 5.1.

two types of extrinsic LLRs for each specific bit b_{il} , and also the difference between the hard-decision results $\text{sgn}[L_E^{EB}(i,l)]$ and $\text{sgn}[L_E^{AB}(i,l)]$ based on the two types of extrinsic LLRs for each specific bit b_{il} . Then, the bit-wise extrinsic LLRs $L_E^{EB}(i,l)$ of the EB-Log-PDA and $L_E^{AB}(i,l)$ of the AB-Log-PDA are found to be statistically closest to each other, when the mutual information (MI) between the bit-sequence output by the interleaver and the corresponding *a priori* LLRs fed back by the outer FEC decoder, namely $I_A(\mathbf{d}_2, \mathbf{L}_{A_2})$, approaches either its minimum value of 0.0 or its maximum value of 1.0.

Remarks:

1. This proposition is inferred from the statistical results shown in Table 5.2, Fig. 5.9 and Fig. 5.10. It can also be verified by comparing (5.26) and (5.27). More specifically, in the first case, if we have no *a priori* information about the bit-sequence output by the interleaver, then $I_A(\mathbf{d}_2, \mathbf{L}_{A_2})$ has a minimum value of 0.0, and $P(s_i = a_m)$ in (5.27) becomes a constant for all a_m . Hence (5.27) may be simplified to the form of (5.26). Similarly, in the second case, when the reliability of the *a priori* LLRs fed back by the outer FEC decoder becomes sufficiently high, namely $I_A(\mathbf{d}_2, \mathbf{L}_{A_2})$ approaches its maximum value of 1.0, then there exists a single dominant probability which approaches 1.0 among the *a priori* symbol-wise probabilities $P(s_i = a_m)$ for all a_m . In this case, (5.27) can also be approximated by the form of (5.26), albeit due to the associated approximation, the number of identical pairs of the two types of extrinsic LLRs becomes lower than that in the first case, as shown in the second column of Table 5.2.
2. As shown in Fig. 5.3 and (5.15), the AB-Log-PDA has already invoked the *a priori* information as the input of the PDA's inner iteration for generating the symbol-wise

nominal APPs. By comparison, the EB-Log-PDA invokes the same *a priori* information twice: one for the PDA's inner iteration (similar to the case of AB-Log-PDA), and the other for invoking the Bayes' formula. In other words, the same *a priori* information is invoked twice for providing different functions in two different processing blocks. This feature is also distinct from the case of the MAP-based MIMO detection, where the *a priori* information is used once and it is uncorrelated with the function of generating the *symbol-vector likelihoods* $p(\mathbf{y}|\mathbf{s})$. ■

5.5 Simulation Results and Discussions

In this section, we characterize both the convergence behavior and the achievable performance of the proposed EB-Log-PDA based IDD scheme with the aid of both the semi-analytical extrinsic information transfer (EXIT) charts [402] and Monte-Carlo simulations. Furthermore, we investigate the impact of inner PDA iterations on the attainable performance of both the EB-Log-PDA and the AB-Log-PDA based IDD schemes, as well as the relationship between the extrinsic LLRs of the EB-Log-PDA and the AB-Log-PDA. Additionally, the complexity of the proposed EB-Log-PDA based IDD scheme is compared both to that of the AB-Log-PDA and to that of the optimal MAP based IDD schemes, which demonstrates the attractive performance versus complexity tradeoff achieved by the proposed EB-Log-PDA based IDD scheme. The turbo code employed uses two constituent recursive systematic convolutional (RSC) codes concatenated in parallel [365]. The RSC codes have a constraint length of $L = 3$ and generator polynomials of (7, 5) expressed in octal form, where half of the parity bits generated by each of the two RSC codes are punctured, so that the turbo code employed has a coding rate of $R = \frac{k}{n} = 1/2$. The turbo code is decoded by the Approximate-Log-MAP algorithm using $it_{tc} = 4$ inner iterations. The interleaver employed is a 2400-bit random sequence interleaver. The remaining scenario-dependent simulation parameters are shown in the respective figures, where the MIMO arrangement is represented in the form of $(N_t \times N_r)$.

5.5.1 Convergence and Performance of the EB-Log-PDA based IDD

Fig. 5.4 compares the convergence behavior of both the proposed EB-Log-PDA based IDD, as well as of the AB-Log-PDA based IDD and of the optimal Exact-Log-MAP based IDD schemes using EXIT chart [402] analysis. It is observed that the EXIT curve of the EB-Log-PDA is close to that of the Exact-Log-MAP, and almost overlaps with that of the AB-Log-PDA. More particularly, when the *a priori* MI is $I_{A,inner} = 0$, the Exact-Log-MAP has the highest extrinsic MI of $I_{E,outer} = 0.5596$, while the EB-Log-PDA has a higher extrinsic MI than the the AB-Log-PDA, which is $I_{E,outer} = 0.5334$ versus $I_{E,outer} = 0.5332$. This indicates that the achievable performances of the EB-Log-PDA and of the AB-Log-PDA are

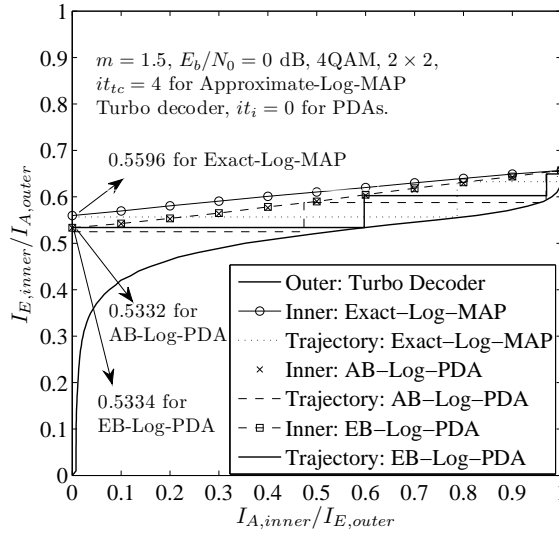


FIGURE 5.4: EXIT chart analysis of the EB-Log-PDA, AB-Log-PDA and Exact-Log-MAP based IDD schemes.

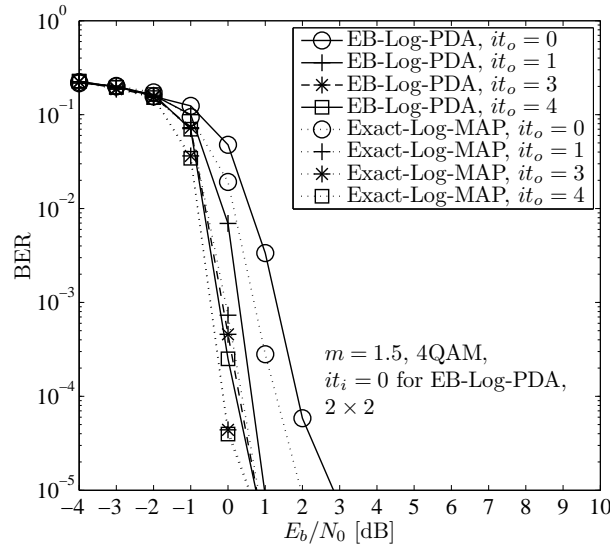


FIGURE 5.5: Impact of the number of outer iterations on BER of the EB-Log-PDA based IDD scheme.

similar to each other, and both of them are close to that of the optimal Exact-Log-MAP in the scenario considered. Additionally, the Monte-Carlo simulation based detection/decoding trajectories indicate that the EB-Log-PDA, the AB-Log-PDA and the Exact-Log-MAP based IDD schemes converge after three iterations. Furthermore, the performance improvements achieved at each iteration by the EB-Log-PDA are more significant than those of the AB-Log-PDA, but less significant than those of the Exact-Log-MAP.

The above EXIT chart based performance predictions and the convergence behavior of the IDD schemes considered are also characterized in terms of the BER performance results of

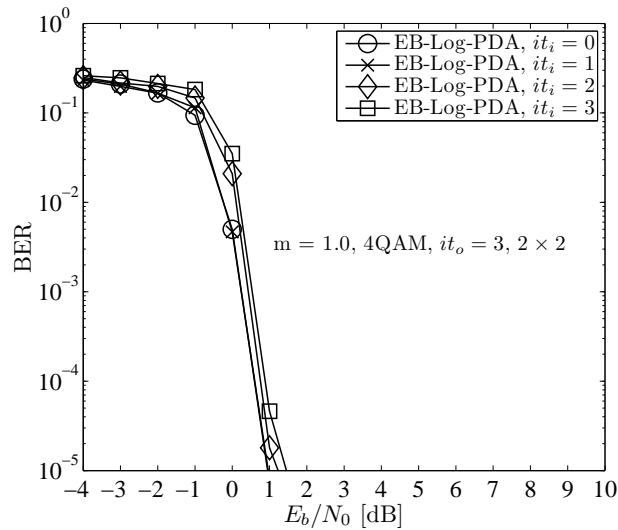


FIGURE 5.6: Impact of the number of inner iterations within the EB-Log-PDA on BER of the EB-Log-PDA based IDD scheme.

Fig. 5.5, where the Nakagami- m fading parameter is set to $m = 1.5$. Observe from Fig. 5.5 that the performance of the EB-Log-PDA based IDD scheme is improved upon increasing the number of outer iterations it_o , where $it_o = 0$ represents the conventional receiver structure in which the MIMO detector and the FEC decoder are serially concatenated, but operate without exchanging soft information. However, the attainable improvements become gradually smaller and the performance achieved after three outer iterations in Fig. 5.5 becomes similar to that of four outer iterations. This implies that the EB-Log-PDA based IDD scheme essentially converges after three outer iterations. A similar convergence profile is also observed in Fig. 5.5 for the optimal Exact-Log-MAP based IDD, although its performance is always marginally better than that of the corresponding EB-Log-PDA based IDD.

5.5.2 Impact of Inner PDA Iterations on the EB-Log-PDA Based IDD

In Fig. 5.6, we investigate the impact of the number of inner iterations of the EB-Log-PDA on the achievable performance of the IDD scheme. We observe that the performance of the IDD scheme is degraded as the number of its inner iterations increases, despite its increased computational complexity.⁵ This implies that the optimal number of inner iterations of the EB-Log-PDA conceived for the IDD receiver is $it_i = z' = 0$. This is because the inner PDA iterations typically fail to assist the repeated Gaussian approximation process in finding the global optimum [41]. Hence, when the reliability of the soft information fed back from the FEC decoder is beyond the reliability limit that the inner iteration aided PDA can achieve,

⁵This observation was found to be also valid for other system configurations, for example, for $N_t = N_r = 4$ and $it_o = 2$. However, due to page limitations, these numerical results are not provided here.

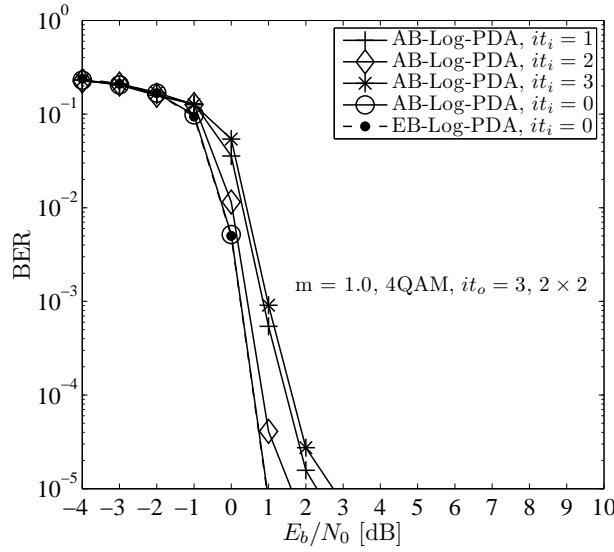


FIGURE 5.7: Impact of the number of inner PDA iterations on BER of the AB-Log-PDA based IDD scheme, as well as the BER comparison between the EB-Log-PDA and AB-Log-PDA based IDD schemes with $it_o = 3$.

the better-quality feedback of the FEC decoder tends to be degraded towards this limit.

In Fig. 5.7 the impact of the number of inner AB-Log-PDA iterations on the achievable performance of the IDD scheme is investigated. More specifically, it is observed from Fig. 5.7 that the optimal number of inner PDA iterations of the AB-Log-PDA based IDD is also $it_i = 0$, but the specific performance degradation experienced upon increasing the number of inner AB-Log-PDA iterations is slightly different from that of the EB-Log-PDA based IDD, as shown in Fig. 5.6. This indicates that the numerical stability of the AB-Log-PDA based IDD scheme incorporating inner PDA iterations is not as good as that of its counterpart using the EB-Log-PDA. Additionally, it is shown in Fig. 5.7 that the best achievable performance of the AB-Log-PDA based IDD scheme using $it_i = 0$ is almost identical to that of the EB-Log-PDA based IDD scheme.

Additionally, in Fig. 5.8 we investigate the intermediate BER evaluated at the output of the soft MIMO detectors, namely the BER recorded upon applying hard-decision to \mathbf{L}_{D_2} for recovering the bits in \mathbf{d}_2 as shown in Fig. 5.1, when the soft MIMO detector employed is the EB-Log-PDA and AB-Log-PDA, respectively⁶. It is observed that the EB-Log-PDA has a better intermediate BER performance than the AB-Log-PDA. This is because \mathbf{L}_{D_2} represents the true *a posteriori* LLR for the EB-Log-PDA, whereas \mathbf{L}_{D_2} is actually its extrinsic LLR generated in (5.25) for the AB-Log-PDA, where the nominal symbol-wise APPs are used.

By jointly considering the results of Fig. 5.6 - Fig. 5.8, we conclude that it is not rec-

⁶Note that this intermediate BER is different from the BER in uncoded systems, because the outer iterations also contribute to the output of the soft MIMO detectors.

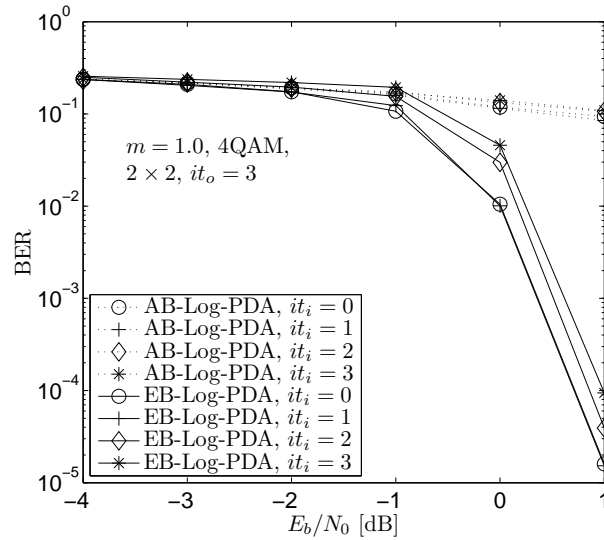


FIGURE 5.8: Impact of the number of inner iterations on BER of the AB-Log-PDA and EB-Log-PDA MIMO detectors, evaluated using \mathbf{L}_{D_2} at the output of the MIMO detectors for FEC-coded bits \mathbf{d}_2 in Fig. 5.1, $it_o = 3$.

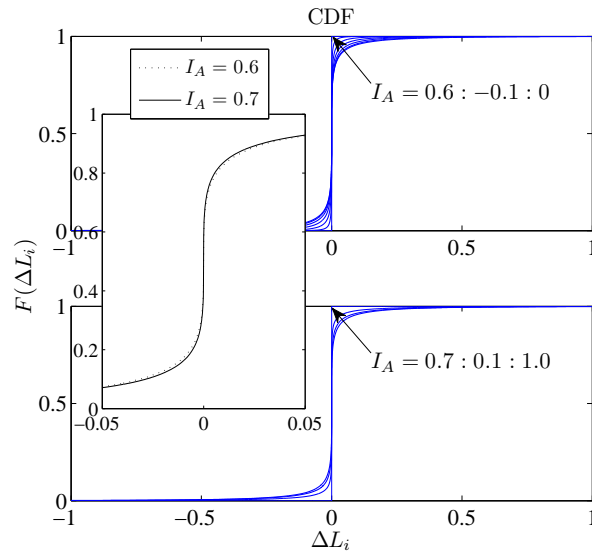


FIGURE 5.9: The cumulative distribution functions of $\Delta L_i = L_E^{EB}(i) - L_E^{AB}(i)$, for samples of 240,000 bits, $it_i = 0$ inner PDA iteration, and $m = 1.0$.

ommended to incorporate inner iterations into the PDA algorithms, when designing the PDA-based IDD schemes.

5.5.3 Relationship between Extrinsic LLRs of EB-Log-PDA and AB-Log-PDA

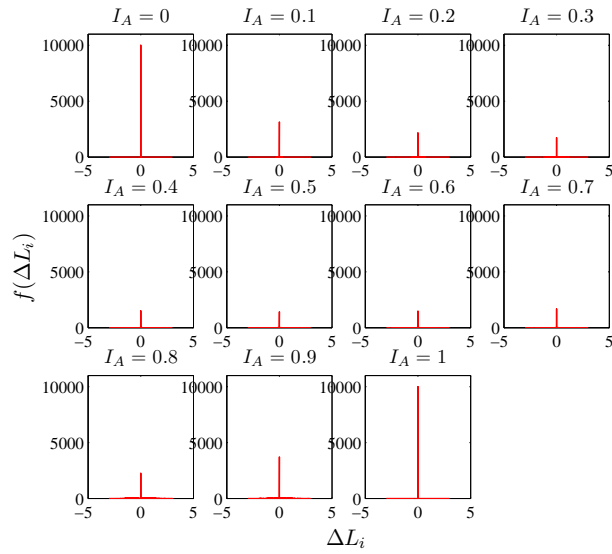
In Fig. 5.9, the CDFs of the difference between the two types of extrinsic LLRs, defined as $\Delta L_{il} = L_E^{EB}(i, l) - L_E^{AB}(i, l)$, is presented for scenarios associated with different values

TABLE 5.2: Statistical comparison of \mathbf{L}_E^{EB} and \mathbf{L}_E^{AB} for samples of 240,000 bits, $it_i = 0$ inner PDA iteration, and $m = 1.0$.

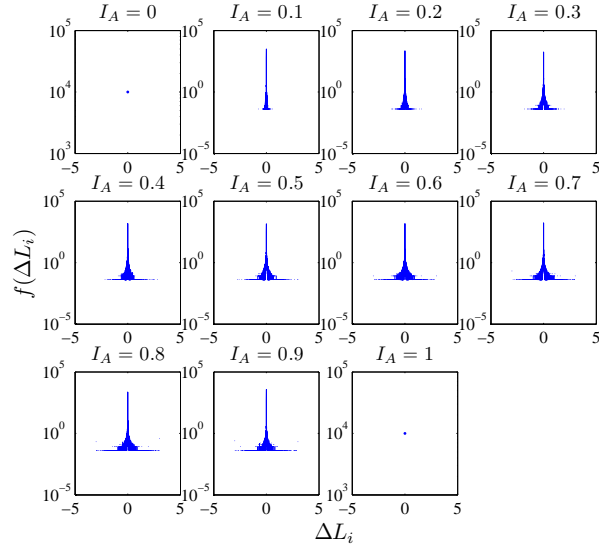
I_A	# of $\Delta L_i = 0$	min ΔL_i	max ΔL_i	min $ \Delta L_i $	max $ \Delta L_i $	mean($ \Delta L_i $)	mean(ΔL_i)	var($ \Delta L_i $)	var(ΔL_i)	# of $\text{sgn}(L_E^{EB}(i)) \neq \text{sgn}(L_E^{AB}(i))$
0	132564	-5.3291e-15	7.1054e-15	0	7.1054e-15	2.1777e-16	1.2659e-18	1.0895e-31	1.5637e-31	0
0.1	0	-0.7602	0.5945	1.7764e-15	0.7602	0.0029	-1.0932e-05	1.0259e-04	1.1092e-04	93
0.2	1	-1.2742	1.5731	0	1.5731	0.0087	1.1815e-04	8.2980e-04	9.0512e-04	236
0.3	0	-1.8188	1.9493	1.5099e-14	1.9493	0.0159	5.9897e-05	0.0025	0.0027	453
0.4	0	-2.1574	2.8015	2.6645e-15	2.8015	0.0231	3.7206e-05	0.0049	0.0055	575
0.5	1	-2.7502	3.7835	0	3.7835	0.0296	-6.2531e-05	0.0080	0.0089	738
0.6	0	-3.8543	3.6252	3.5527e-15	3.8543	0.0339	-2.1830e-05	0.0113	0.0124	859
0.7	0	-3.4085	3.1513	5.3291e-15	3.4085	0.0344	-3.9238e-05	0.0132	0.0144	794
0.8	0	-3.4185	5.2725	3.5527e-15	5.2725	0.0300	-8.3517e-05	0.0131	0.0140	685
0.9	3	-4.6007	3.1890	0	4.6007	0.0190	8.8096e-06	0.0088	0.0091	369
1.0	6334	-3.3751e-14	3.0198e-14	0	3.3751e-14	9.3921e-15	-2.6836e-17	4.4944e-29	1.3315e-28	0

of $I_A(\mathbf{d}_2, \mathbf{L}_{A_2})$, which represents the MI between the bit-sequence output by the interleaver and the corresponding *a priori* LLRs fed back by the outer FEC decoder. For convenience, $I_A(\mathbf{d}_2, \mathbf{L}_{A_2})$ is simply denoted as I_A in Fig. 5.9 and Table 5.2. Observed in Fig. 5.9 that the CDFs may be divided into two groups of functions exhibiting rotational symmetry with respect to the point of (0, 0.5). The first group represents the CDFs associated with the I_A value spanning from 0 to 0.6, while the other group hosts the CDFs associated with the I_A value ranging from 0.7 to 1.0. Interestingly, the two groups of CDFs exhibit opposite trends, when increasing the value of I_A . More specifically, upon considering the CDF curves falling within the right half-plane, we notice that when I_A increases from 0 to 0.6 with a step size of 0.1, the CDF curves of the first group move along from the point (0, 1) to its right-downwards direction. By contrast, when I_A increases from 0.7 to 1.0 with the step size of 0.1, the CDF curves of the second group move along in the opposite direction compared to the first group. Additionally, by zooming in for observing the curve of $I_A = 0.6$ and $I_A = 0.7$, we note that the two curves almost overlap with each other and hence they serve as the boundary between the two groups. In line with Proposition 5.2, the above observations clearly show that the bit-wise extrinsic LLRs of the EB-Log-PDA and of the AB-Log-PDA are statistically closest to each other, when I_A approaches either its minimum value of 0.0 or its maximum value of 1.0, and the difference between the two types of extrinsic LLRs becomes most significant, when the value of I_A is in the middle region, say, between 0.4 to 0.7. These conclusions are also confirmed by the corresponding PDFs shown in Fig. 5.10, where both the “linear scale” and the “semilogy⁷ scale” are used for facilitating accurate observations. Finally, in Table 5.2, the detailed statistical metrics of $\Delta L_{il} = L_E^{EB}(i, l) - L_E^{AB}(i, l)$ are provided, which also support our conclusions.

⁷This means only the y-axis is in logarithmic scale.



(a) linear scale



(b) "semilogy" scale

FIGURE 5.10: The probability density functions of $\Delta L_i = L_E^{EB}(i) - L_E^{AB}(i)$, for samples of 240,000 bits, $it_i = 0$ inner PDA iteration, and $m = 1.0$.

5.5.4 Computational Complexity Comparison

The computational complexity of the proposed EB-Log-PDA based IDD scheme may be evaluated by simply comparing its complexity to those of the AB-Log-PDA and the Exact-Log-MAP based IDD schemes in a single (outer) iteration. This is because i) the turbo codec module is common to all the IDD schemes considered; 2) we have shown that the EB-Log-PDA, as well as the AB-Log-PDA and the Exact-Log-MAP based IDD schemes all converge after three outer iterations in the scenarios considered; 3) the PDAs' inner iterations should not be invoked when designing IDD schemes. As shown in Table 5.1, the major computational

cost of the EB-Log-PDA per transmit symbol is the calculation of $\mathbf{\Lambda}_i^{-1}$ and the matrix multiplication of (5.12). Direct calculation of $\mathbf{\Lambda}_i^{-1}$ imposes a computational cost of $\mathcal{O}(8N_t^3)$ real-valued operations (additions/multiplications), which is still relatively expensive. Fortunately, by using the Sherman-Morrison-Woodbury formula based complexity-reduction techniques of [219], the computational cost of calculating $\mathbf{\Lambda}_i^{-1}$ can be reduced to $\mathcal{O}(4N_t^3)$ real operations per iteration. Additionally, the calculation of (5.12) requires $\mathcal{O}(4MN_t^3 + 2MN_t^2)$ real operations per iteration. In summary, in terms of real operations, the computational complexity of the decoupled signal model based EB-Log-PDA method is $\mathcal{O}(4MN_t^3 + 2MN_t^2) + \mathcal{O}(4N_t^3)$ per outer iteration, which is not related to the number of receive antennas N_r , as opposed to the IDD scheme using the non-decoupled signal model based AB-Log-PDA, which has a computational complexity of $\mathcal{O}(4MN_tN_r^2 + 2MN_tN_r) + \mathcal{O}(4N_tN_r^2)$ per outer iteration [44, 45]. This implies that the decoupled model based EB-Log-PDA has a lower computational complexity than the non-decoupled model based AB-Log-PDA in the scenario of $N_r > N_t$, which is particularly important, because $N_r > N_t$ is a typical configuration for spatial multiplexing based MIMO systems.

By comparison, the Exact-Log-MAP algorithm has to calculate the Euclidean distance of $\|\mathbf{y} - \mathbf{H}\mathbf{s}\|^2$ M^{N_t} times per bit per outer iteration [75], hence its complexity order is $\mathcal{O}(M^{N_t}N_t \log_2 M)$ per outer iteration. More specifically, the evaluation of $\|\mathbf{y} - \mathbf{H}\mathbf{s}\|^2$ requires $\mathcal{O}(4N_rN_t + 6N_r)$ real operations. Therefore, the Exact-Log-MAP algorithm has a computational complexity of $\mathcal{O}[M^{N_t}N_t \log_2 M(4N_rN_t + 6N_r)]$ real operations per outer iteration. There exist other types of reduced-complexity MAP algorithms, such as the look-up-table based Approximate-Log-MAP algorithm and the Max-Log-MAP algorithm [75]. Unfortunately, although they exhibit some advantages in terms of their DSP implementation, in essence both of them are still based on the exhaustive search, hence the computational complexity of calculating the extrinsic LLR for each bit increases exponentially with both the number of transmit antennas N_t and the constellation size M , because $M^{N_t} = 2^{M_b N_t}$ hypotheses have to be evaluated for each bit [75]. Therefore, all the three representative Log-MAP algorithms have a complexity that is significantly higher than that of the EB-Log-PDA, especially when N_t , N_r and M have large values.

5.6 Chapter Summary and Conclusions

We have demonstrated that the estimated symbol-wise probabilities output by the existing approximate Bayes' theorem based PDA algorithms are not the true APPs, they rather constitute nominal APPs, which are unsuitable for the classic IDD architecture of MIMO systems using general M -ary modulations. By contrast, the estimated symbol-wise probabilities at the output of the proposed EB-Log-PDA exhibit similar characteristics to the true APPs, hence they are readily applicable to the classic IDD architecture of M -ary

modulation aided MIMO systems. Furthermore, we demonstrated that introducing inner iterations within both the EB-Log-PDA and the AB-Log-PDA, actually degrades the IDD receiver's performance despite significantly increasing the overall computational complexity of the IDD receiver, which implies that the optimal number of inner iterations of both the EB-Log-PDA and the AB-Log-PDA is zero when they are invoked in IDD receivers. Additionally, the relationship between the EB-Log-PDA and the AB-Log-PDA was investigated, and it was revealed that the bit-wise extrinsic LLRs of the EB-Log-PDA and of the AB-Log-PDA are statistically closest to each other, when the MI between the bit-sequence output by the interleaver and the corresponding *a priori* LLRs fed back by the outer FEC decoder approaches its minimum value of 0.0 and maximum value of 1.0. The difference between the two types of extrinsic LLRs becomes most significant, when the value of the MI is in the middle region of the interval $[0, 1.0]$. Finally, the IDD scheme based on the proposed EB-Log-PDA using no inner PDA iterations is shown to achieve a comparable performance to that of the optimal MAP detector based IDD receiver, while imposing a significantly lower computational complexity in the scenarios considered.

Distributed PDA Based Soft Reception for Base Station Cooperation in Multiuser Multicell MIMO Systems

6.1 Introduction

FROM Chapter 2 to Chapter 5, we have investigated the PDA and the SDPR based MIMO detectors invoked for both the point-to-point MIMO system depicted in Fig. 1.5 and the single-cell multiple-access MIMO system shown in Fig. 1.6. To elaborate a little further, Chapters 2 and 3 focused on uncoded systems, while Chapters 4 and 5 considered FEC-coded systems. However, in order to satisfy the growing demand for high-rate mobile multimedia services, high-spectral-efficiency techniques such as MIMO and near-unity frequency reuse (FR) are expected to be employed in the next-generation cellular networks in a more efficient manner. Although the achievable performance gain of MIMOs is significant in point-to-point links and single-cell multiuser systems [184], it is predominantly limited by the effect of inter-cell CCI in multiuser multicell MIMO systems [32–35]. Conventional interference management primarily relies on the radio resource allocation techniques [404, 405], such as the careful design of FR pattern, accurate power control and judicious spreading code assignment in order to mitigate the inter-cell CCI. However, these conventional techniques may reduce the achievable spectral efficiency and/or lead to inadequate suppression of the inter-cell CCI [36].

Recently, motivated by the information-theoretic capacity analysis of cellular networks [27–31], advanced receiver techniques using base station (BS) cooperation for exploiting

the potential capacity of cellular systems were advocated [129, 133, 135]. The simplest conceptual approach to BS cooperation is to assume that there is a controller, or central signal processing unit (CSPU), which coordinates the operation of all BSs [133]. More specifically, a turbo detection based BS cooperation aided inter-cell interference cancellation scheme was proposed in [133]. This scheme considered a simple model comprising a BS controller (BSC), two BSs and two MSs, where each BS and MS has a single antenna as well as a single interferer. During each iteration of this scheme, the conventional single-user detection (SUD) was used initially and the soft-bits output by the Max-Log-MAP decoder were then calculated and exchanged at the BSC to further perform interference cancellation for each BS. Similarly, the MMSE-SIC based iterative MUD was employed in the CSPU of the distributed antenna system (DAS) [406]. where a single CSPU controls several access points (APs) receiving the signals of user equipments (UEs). For this approach, the performance of different bits-to-symbol mappings was investigated and the set partitioning (SP) scheme was shown to perform best. However, the CSPU constitutes a single point of potential failure, thus the entire network is vulnerable. Additionally, since the complexity of MUD is dominated by the number of users, having a CSPU imposes a potentially excessive computational burden and huge backhaul traffic, thus may become less attractive.

By contrast, distributed processing across a network of interacting BSs was shown to strike an attractive compromise [129, 134, 135]. A distributed iterative detection (DID) scheme was proposed for single-antenna aided multiuser systems in [134]. This approach is a decentralized implementation of the iterative interference cancellation framework used in [133, 406]. Each BS initially performs either SUD or single-antenna interference cancellation (SAIC) [407–411] implemented as joint maximum likelihood detection (JMLD) for the strongest MSs. Then the LLRs generated by the FEC decoder are exchanged between neighboring BSs, followed by a repeated application of SUD at each iteration in order to reconstruct and subtract the interference imposed by the neighboring BSs. Although this scheme was shown to strike an attractive compromise, it has an exponentially increased computational complexity imposed by the computation of the soft information using the Max-Log-MAP algorithm. Furthermore, the multiple rounds of iterative message exchange operations between the cooperative BSs may still impose a potentially excessive backhaul traffic. Additionally, in [134] the DID scheme was shown to be sensitive to the quantization errors of the exchanged LLRs. On the other hand, the belief propagation (BP) algorithm was applied to the problem of distributed detection in the single-antenna aided one-dimensional Wyner model [129], which was thereafter extended to a two-dimensional rectangular grid based Wyner cellular model in [135]. The distributed BP algorithm performs a chain-like message passing between all the BSs and provides a globally near-optimum solution, where none of the received signals is deemed to be interference, instead it is exploited to increase the achievable diversity gain in the single-antenna aided Gaussian multiple access channel. However, the BP algorithm relies on network-wide optimum information exchange, which

unfortunately results in a potentially excessive backhaul traffic and latency, especially for a star-like architecture routinely used for interconnecting the BSs [134].

As regards to the single-antenna aided multiuser system considered in [133,135], the impairments imposed by the interference on the attainable detection performance of the individual MSs are limited to those of the co-channel MSs roaming in the interfering cells. Nevertheless, for multi-antenna aided multiple access systems, where each interfering sub-channel is *not a scalar- but a matrix-channel*, the *inter-antenna interference* should also be considered by each MS, in addition to the inter-cell CCI.

As pointed out in Section 1.8.5 and seen in Chapters 2, 4 and 5, the PDA based MIMO detector represents a low-complexity SISO detection approach that has a self-iterative structure. Taking into account this attractive property, in this chapter we propose an effective low-complexity soft combining (SC) technique aided distributed PDA soft-reception scheme designed for the uplink of multiuser multicell MIMO systems. The proposed scheme is capable of mitigating the prohibitive computational complexity and the huge amount of backhaul traffic faced by multicell processing that relies on BS cooperation. More specifically, a realistic 19-cell hexagonal cellular MIMO-aided network model relying on either perfect or imperfect channel estimation is considered. In this model, the entire channel consists of multiple matrix sub-channels, rather than of scalar/vector sub-channels considered in [129, 133–135, 406]. SC is used at each BS to generate the final soft-decision information, which indicates that the fundamental philosophy of the proposed method is not that of “interference cancellation” but “knowledge sharing and data fusion”. Additionally, we investigate the impact of quantization on both the backhaul traffic and the BER performance of the proposed scheme. Since in practice only the index of the possible discrete value of the converged soft information has to be exchanged for SC operation, the proposed scheme is relatively robust to quantization errors of the soft information exchanged, which dramatically reduces the backhaul traffic at a negligible performance degradation. We also considered the challenging rank-deficient scenario, where the number of transmitters is higher than that of the receivers. Despite its significant performance gain over the conventional non-cooperative MUD schemes, the proposed distributed PDA aided SC (DPDA-SC) approach imposes a modest complexity that increases cubically as a function of the number of concurrent streams processed, while maintaining a low backhaul traffic. Low complexity is achieved as a benefit of the PDA algorithm’s rapid convergence, as well as of the fact that only the converged soft-information is exchanged amongst the BSs of the specific cooperative BS-cluster, requiring a single action.

The rest of this chapter is organized as follows. Section 6.2 presents the topology of the MIMO-aided multiuser multicell network considered. In Section 6.3.1 the uplink received signal model is detailed for both perfect and imperfect channel state information (CSI) scenarios. Subsequently, the proposed DPDA-SC scheme for both full-rank and rank-deficient

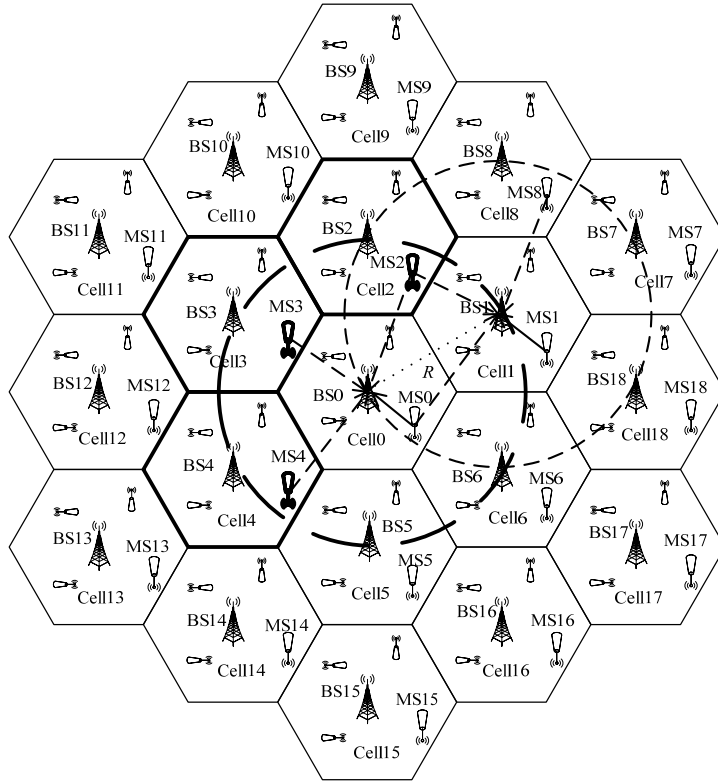


FIGURE 6.1: An example setup showing a 19-cell hexagonal cellular model with inter-cell CCI and unity FR. In this model, the number of *effective* interferers with respect to each user may be different. For instance, when the signal of MS0 is expected to be detected by its home BS, namely by BS0, only MS2, MS3 and MS4, which are emphasized as bold, are the effective interferers. By contrast, for MS7, MS10 and MS11, the number of interferers is two, one and zero, respectively, as shown in Fig. 6.2.

scenarios is discussed in Section 6.3.2-6.3.4, which is followed by the complexity analysis in Section 6.3.5. In Section 6.4 a comprehensive set of numerical results are presented for characterizing the performance of the proposed DPDA-SC scheme in both perfect and imperfect CSI scenarios, as well as in both the full-rank and rank-deficient scenarios. Furthermore, the computational complexity, the convergence properties, as well as the impact of the quantization errors on the achievable performance and the backhaul traffic of the proposed DPDA-SC scheme are numerically investigated. Finally, our conclusions are offered in Section 6.5.

6.2 Hexagonal Cellular Network Model

Consider a hexagonal cellular network model, where both the BSs and MSs are equipped with multiple antennas. Therefore, instead of having a conventional point-to-point channel impulse response (CIR) between each BS and MS [134, 135], we have a CIR matrix, where

the interference imposed on each MS stems not only from other MSs, but also from their own multiple antennas. Channel quality information (CQI) based frequency allocation may be applied for the MSs' uplink transmissions, in order to allow for optimum opportunistic resource scheduling. A unity FR is employed for all the cells and an orthogonal multiple access technique such as for example TDMA [99], orthogonal frequency-division multiple-access (OFDMA) [412], or single-carrier frequency-division multiple-access (SC-FDMA) [413] suggested for the LTE uplink may be applied, in order to create orthogonal signatures for all the different MSs roaming in the same cell. Therefore, the intra-cell interference is assumed to be negligible, while the inter-cell CCI imposed by MSs of the interfering cells is dominant.

Let us consider the topology shown in Fig. 6.1 as an example, which constitutes a *snapshot* of the dynamic network at a specific scheduling interval. Assume that there are N_b BSs and N_u MSs in this network (for the sake of comparability with classic cellular networks, N_b is set to 19 in Fig. 6.1), and K_i MSs in each cell, $i = 1, 2, \dots, N_b$. Although in practice each BS and MS may have a different number of activated antennas at different traffic loads, for simplicity of analysis we assume that each of them is equipped with M_b and M_u activated antennas, respectively. The position of each network entity is represented by its *dynamically updated polar coordinates* with respect to the specific *servicing* BS. This dynamic coordinate system naturally lends itself to distributed processing. For example, if the central cell (Cell0) of Fig. 6.1 is considered, the point at BS0 may be defined as the origin and the BS in the upper-right adjacent cell of Cell0 may be described as BS1= $(R, \pi/6)$, where R is the distance between two immediate neighbor BSs.

Let us assume that the available frequency band is dynamically allocated to the MSs according to their uplink CQI evaluated by each BS, where the CQI metric may be the SNR of each link. For simplicity of graphical illustration, the same frequency slot is tentatively assigned to the MSs situated at the same relative position in their corresponding home cell, as shown in Fig. 6.1¹. For example, MS0, MS1, MS2, \dots , MS18 in the lower-right corner of each cell are all the co-channel users. When invoking dynamic frequency allocation, *not all* the co-channel users but only those located within the *detectable range (DR)* of a specific BS are considered to be interfering with the desired user. Hence the number of *effective* interferers with respect to each user may be different. For instance, when the signal of MS0 is expected to be detected by its home BS, namely by BS0, only MS2, MS3 and MS4, which are emphasized as bold, are the effective interferers. By contrast, the other co-channel users, such as MS1, MS5 and MS6 are not deemed to be effective interferers, since they are outside the disk that is centered at BS0 and has a radius of R . More explicitly, they are outside the DR of BS0. Similarly, for MS1 there are also three effective interferers shown as MS8, MS2, MS0, whereas for MS7, MS10 and MS11, the number of interferers is two, one and zero, respectively, although they are all at the boundary of the network. For the sake of

¹Note that this does not mean the dynamical nature of the network and the adaptive frequency allocation scheme are ignored.

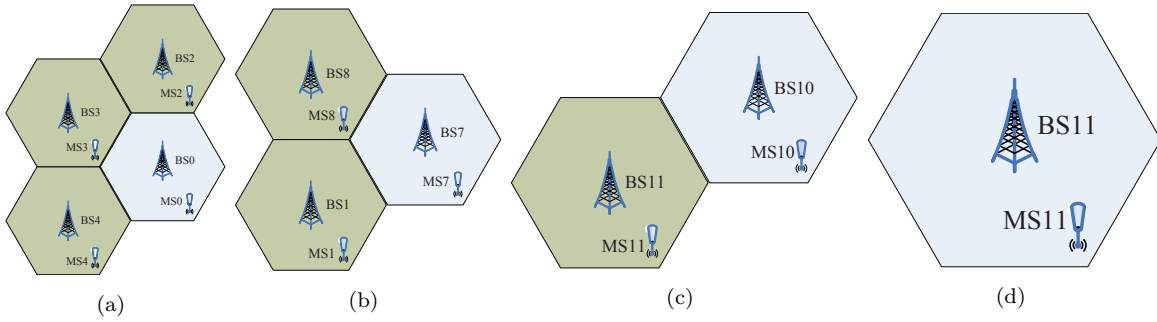


FIGURE 6.2: Various types of location-dependent interferer distributions for a specific MS roaming in the cellular network of Fig. 6.1.

explicit clarity, these various location-dependent interferer distributions corresponding to a specific MS are illustrated in Fig. 6.2. We emphasize that the interfering MSs contaminating the reception of each MS may be different in the next scheduling interval owing to the dynamic nature of the network, since MSs may move to other positions at a certain speed, leading to time-variant traffic density in different areas of the network. On the other hand, the signal of MS0 may also be adequately received at BS1, BS5 and BS6, which therefore have the potential to act as the serving BSs of MS0. Similarly, the number of adjacent BSs supporting each MS may be different as well. We assume in general that for each served MS there are C_u such effective co-channel MSs and C_b adjacent serving BSs, respectively. Then the four-tuple (M_b, M_u, C_b, C_u) may be used to represent the cooperating BS-cluster, which is dynamically changing for the different served MSs.

Remark: The strong interference that is decodable is explicitly considered in this model, while the weak interference is treated implicitly as noise. This strategy is supported by the recent results of information theory on the properties of the interference channel. From the perspective of information theory, the fundamental underlying principle of distributed decoding and MUD is that the interference is sufficiently strong for it to become decodable. This also explains, why the classic Wyner model only considers the immediate neighboring cells and why the strongest layer is cancelled first in the SIC technique. The related capacity results on the “very strong interference” scenario [120] and on the “strong interference” [121, 122] scenario theoretically validate our decoding/detection strategy. On the other hand, if the interference is weak, then the interfering signal should be treated as noise and hence employing single-user decoding would suffice. Treating the weak interference as noise is natural in practice. Very recently, this arrangement was shown to be the *optimal* scheme in the weak interference regime, and it was also found that introducing structure into the weak interfering signals is *not* beneficial [128, 414–416].

6.3 Cooperative Distributed Soft Reception

6.3.1 Signal Model

Based on the hexagonal topology of Fig. 6.1, we consider an idealized synchronous uplink where the signal received at BS k is modeled as

$$\mathbf{y}^k = \mathbf{H}_k^k \mathbf{x}^k + \sum_{\alpha_i \neq k} \mathbf{H}_{\alpha_i}^k \mathbf{x}^{\alpha_i} + \mathbf{n}^k = \mathbf{H}_k^k \mathbf{x}^k + \mathbf{N}^k + \mathbf{n}^k, \quad (6.1)$$

where \mathbf{x}^{α_i} is the length- M_u vector of symbols transmitted from MS α_i in Cell α_i , and each symbol is from the modulation constellation $\mathcal{A} = \{a_1, a_2, \dots, a_M\}$ with cardinality M . Still referring to Eq. (6.1), $\mathbf{H}_{\alpha_i}^k$ is the $(M_b \times M_u)$ -element channel matrix between MS α_i and BS k , $i = 1, 2, \dots, C_u$, $k = 1, 2, \dots, N_b$, while \mathbf{n}^k is the length- M_b complex-valued circular symmetric Gaussian noise vector² with zero mean and covariance matrix $N_0 \mathbf{I}_{M_b}$ at BS k , where \mathbf{I}_{M_b} is an $(M_b \times M_b)$ -element identity matrix.

Let us now define the interference intensity as the channel gain ratio of the interfering users over that of the local desired user, namely as

$$\rho_{\alpha_i}^k = \frac{\|\mathbf{H}_{\alpha_i}^k\|_F}{\|\mathbf{H}_k^k\|_F}, 0 \leq \rho_{\alpha_i}^k \leq 1, \quad (6.2)$$

where $\|\cdot\|_F$ represents the Frobenius norm of a matrix.

As opposed to conventional non-cooperative detection, the distributed detection of \mathbf{x}^k carried out with the aid of BS cooperation detects the desired user's signal not only in the local cell, but rather jointly detects all the co-channel users' signals over-heard from the neighboring cells. More explicitly, the co-channel users' signals are no longer considered as detrimental interference, we rather consider these co-channel users' soft decision information as useful source of further information to be exploited by cooperative processing via message passing amongst the BSs. To this end, the received signal model of Eq. (6.1) may be reformulated as a **virtual** or **distributed MIMO** model, where the cooperating BSs may be viewed as MIMO elements, yielding

$$\mathbf{y}^k = \mathbf{G}^k \mathbf{s}^k + \mathbf{n}^k, \quad (6.3)$$

where we have $\mathbf{G}^k = [\mathbf{H}_k^k, \mathbf{H}_{\alpha_1}^k, \dots, \mathbf{H}_{\alpha_{C_u}}^k]$, $\mathbf{s}^k = [(\mathbf{x}^k)^T, (\mathbf{x}^{\alpha_1})^T, \dots, (\mathbf{x}^{\alpha_{C_u}})^T]^T$ and the elements of \mathbf{s}^k are denoted as s_t^k , $t = 1, 2, \dots, M_u(C_u + 1)$. For the sake of generality, the constraint of $M_u(C_u + 1) \leq M_b$ is not assumed here.

In the case of *imperfect* channel knowledge, the estimated channel matrix $\hat{\mathbf{H}}_k^k$ and $\hat{\mathbf{H}}_{\alpha_i}^k$ associated with the channel-estimation error matrices \mathbf{E}_k and \mathbf{E}_{α_i} may be deemed to obey

²Note that the noise considered here consists of both the ordinary channel noise and weak interference that is not decodable. Treating the weak interference as noise has been recently proved optimal in the weak interference regime [416].

the standard Gaussian distribution of $\mathcal{CN}(0, 1)$. They can be written as

$$\hat{\mathbf{H}}_k^k = \beta_k \mathbf{H}_k^k + \sqrt{1 - \beta_k^2} \mathbf{E}_k \quad (6.4)$$

and

$$\hat{\mathbf{H}}_{\alpha_i}^k = \beta_{\alpha_i} \mathbf{H}_{\alpha_i}^k + \sqrt{1 - \beta_{\alpha_i}^2} \mathbf{E}_{\alpha_i}, \quad (6.5)$$

respectively [417], where β_k and β_{α_i} indicate the channel estimation quality and may be assumed to be close to 1, but not higher than 1. Thus the received signal models of Eq. (6.1) and Eq. (6.3) may be rewritten as

$$\mathbf{y}^k = \hat{\mathbf{H}}_k^k \mathbf{x}^k + \sum_{\alpha_i \neq k} \hat{\mathbf{H}}_{\alpha_i}^k \mathbf{x}^{\alpha_i} + \mathbf{n}^k \quad (6.6)$$

and

$$\mathbf{y}^k = \hat{\mathbf{G}}^k \mathbf{s}^k + \mathbf{n}^k, \quad (6.7)$$

respectively, where we have $\hat{\mathbf{G}}^k = [\hat{\mathbf{H}}_k^k, \hat{\mathbf{H}}_{\alpha_1}^k, \dots, \hat{\mathbf{H}}_{\alpha_{C_u}}^k]$, or

$$\hat{\mathbf{G}}_k = \bar{\beta}_k \mathbf{G} + \sqrt{1 - \bar{\beta}_k^2} \bar{\mathbf{E}}_k \quad (6.8)$$

with $\bar{\beta}_k$ and $\bar{\mathbf{E}}_k$ being the composite-channel estimation error indicators. Note that when we have $\beta_k = \beta_{\alpha_i} = 1$, the signal model under imperfect CSI transforms into that of perfect CSI.

Without loss of generality, below we will continue by considering perfect channel estimation while presenting the proposed DPDA-SC scheme. The case of imperfect channel knowledge may be readily considered by the substitution of the corresponding perfect channels with the estimated channels.

6.3.2 Parallel Detection Using the PDA Algorithm

The first action of the DPDA-SC scheme is that the BSs perform parallel detection employing the PDA algorithm as a low complexity solution, in order to estimate the decision probability of each transmitted symbol without carrying out an exhaustive search in the space of all possible symbol combinations. Each BS jointly detects the signals of multiple users, including both the local user and other cells' users roaming close to this BS, which would be termed as interfering users in conventional non-cooperative systems. For example, BS0 jointly detects MS0, MS2, MS3 and MS4; BS1 jointly detects MS1, MS8, MS2, MS0; similarly, all the other BSs carry out an analogous task. For ease of exposition, we consider detection at BS k as an example and omit the BS index k in our forthcoming exposition.

i) When we have $M_u (C_u + 1) \leq M_b$, for the sake of computational efficiency the decorrelated

signal model of [234] is adopted, and hence Eq. (6.3) may be further formulated as

$$\tilde{\mathbf{y}} = \mathbf{s} + \tilde{\mathbf{n}} = s_t \mathbf{e}_t + \sum_{l \neq t} s_l \mathbf{e}_l + \tilde{\mathbf{n}} \triangleq s_t \mathbf{e}_t + \mathbf{v}_t, \quad (6.9)$$

where $\tilde{\mathbf{y}} = (\mathbf{G}^H \mathbf{G})^{-1} \mathbf{G}^H \mathbf{y}$, $\tilde{\mathbf{n}}$ is a colored Gaussian noise with a zero mean and covariance of $N_0 (\mathbf{G}^H \mathbf{G})^{-1}$, \mathbf{e}_l is a column vector with 1 in the l th position and 0 elsewhere, and \mathbf{v}_t denotes the interference plus noise term for symbol s_t , for $t, l = 1, 2, \dots, M_u (C_u + 1)$.

For the symbol vector \mathbf{s} , we define an $M_u(C_u + 1) \times M$ probability matrix $\mathbf{P}^{(z)}$ whose (t, m) th element $P^{(z)}(s_t = a_m | \mathbf{y})$ is the estimate of the APP that $s_t = a_m$ at the z th iteration, where $m = 1, 2, \dots, M$, with a_m being the m th element of the modulation constellation \mathbb{A} . The key philosophy of the PDA algorithm is to approximate \mathbf{v}_t obeying the multimodal Gaussian mixture distribution as a single multivariate colored Gaussian distributed random vector [219] with an updated mean of

$$\boldsymbol{\mu}_t \triangleq \mathcal{E}(\mathbf{v}_t) = \sum_{l \neq t} \mathcal{E}(s_l) \mathbf{e}_l, \quad (6.10)$$

covariance of

$$\boldsymbol{\Upsilon}_t \triangleq \mathcal{C}(\mathbf{v}_t) = \sum_{l \neq t} \mathcal{C}\{s_l\} \mathbf{e}_l \mathbf{e}_l^T + N_0 (\mathbf{G}^H \mathbf{G})^{-1}, \quad (6.11)$$

and pseudo-covariance [363] of

$$\boldsymbol{\Omega}_t \triangleq \mathcal{C}_p(\mathbf{v}_t) = \sum_{l \neq t} \mathcal{C}_p\{s_l\} \mathbf{e}_l \mathbf{e}_l^T, \quad (6.12)$$

where

$$\mathcal{E}(s_l) = \sum_{m=1}^M a_m P^{(z)}(s_l = a_m | \mathbf{y}), \quad (6.13)$$

$$\mathcal{C}(s_l) = \sum_{m=1}^M [a_m - \mathcal{E}(s_l)][a_m - \mathcal{E}(s_l)]^* P^{(z)}(s_l = a_m | \mathbf{y}), \quad (6.14)$$

$$\mathcal{C}_p(s_l) = \sum_{m=1}^M [a_m - \mathcal{E}(s_l)][a_m - \mathcal{E}(s_l)]^T P^z(s_l = a_m | \mathbf{y}). \quad (6.15)$$

Here $P^{(z)}(s_l = a_m | \mathbf{y})$ is initialized as a uniform distribution and will be replaced with an updated probability at $(z + 1)$ th iteration of the PDA algorithm.

Let

$$\mathbf{w}_m^{(t)} = \tilde{\mathbf{y}} - a_m^{(t)} \mathbf{e}_t - \boldsymbol{\mu}_t, \quad (6.16)$$

and

$$p^{(z+1)}(\mathbf{y}|s_t = a_m) \propto \varphi_m^{(z+1)}(s_t) \triangleq \exp \left(- \left(\begin{array}{c} \Re(\mathbf{w}_m^{(t)}) \\ \Im(\mathbf{w}_m^{(t)}) \end{array} \right)^T \boldsymbol{\Lambda}_t^{-1} \left(\begin{array}{c} \Re(\mathbf{w}_m^{(t)}) \\ \Im(\mathbf{w}_m^{(t)}) \end{array} \right) \right), \quad (6.17)$$

where we have

$$\boldsymbol{\Lambda}_t \triangleq \left(\begin{array}{cc} \Re(\boldsymbol{\Upsilon}_t + \boldsymbol{\Omega}_t) & -\Im(\boldsymbol{\Upsilon}_t - \boldsymbol{\Omega}_t) \\ \Im(\boldsymbol{\Upsilon}_t + \boldsymbol{\Omega}_t) & \Re(\boldsymbol{\Upsilon}_t - \boldsymbol{\Omega}_t) \end{array} \right), \quad (6.18)$$

while $a_m^{(t)}$ indicates that a_m is assigned to s_t , and $\Re(\cdot)$ as well as $\Im(\cdot)$ represent the real and imaginary part of a complex variable, respectively.

Then, the APP that we have $s_t = a_m$ is estimated as

$$P^{(z+1)}(s_t = a_m|\mathbf{y}) \approx \frac{p^{(z+1)}(\mathbf{y}|s_t = a_m)}{\sum_{m=1}^M p^{(z+1)}(\mathbf{y}|s_t = a_m)} = \frac{\varphi_m(s_t)}{\sum_{m=1}^M \varphi_m(s_t)}. \quad (6.19)$$

In summary, the symbol-based PDA algorithm considered proceeds as follows.

1) Initialization: set the initial values of the symbol probabilities $P(s_t = a_m|\mathbf{y})$ using a uniform distribution for $\forall t = 1, 2, \dots, M_u(C_u + 1)$, $\forall m = 1, 2, \dots, M$, i.e. $P(s_t = a_m|\mathbf{y}) = 1/M$; set the iteration counter to $z = 0$.

2) Set the symbol index to $t = 1$.

3) Based on the current values of $\{\mathbf{P}^{(z)}(l, :)\}_{l \neq t}$, compute $P^{(z+1)}(s_t = a_m|\mathbf{y})$ via Eq. (6.13) \sim Eq. (6.19), which will replace the (t, m) th element of $\mathbf{P}^{(z)}$.

4) If $t < M_u(C_u + 1)$, let $t = t + 1$ and go to step 3). Otherwise, go to step 5).

5) If \mathbf{P} has converged, or the iteration index z has reached its maximum, terminate the iteration. Otherwise, let $z = z + 1$ and return to step 2).

ii) When we have $M_u(C_u + 1) > M_b$, the appropriately modified version of the PDA method [220] may be applied to the current problem. Alternatively, the non-decorrelated signal model of [230] may be applied, which yields an equivalent performance to that of the decorrelated signal model based PDA [235] when $M_u(C_u + 1) \leq M_b$. In the case of the non-decorrelated model, Eq. (6.3) may be expanded as

$$\mathbf{y} = \mathbf{g}_t s_t + \sum_{l \neq t} \mathbf{g}_l s_l + \mathbf{n} \triangleq \mathbf{g}_t s_t + \mathbf{u}_t, \quad (6.20)$$

where \mathbf{g}_l is the l th column of \mathbf{G}^k . Then the PDA algorithm is obtained using a similar derivation to that of its counterpart in case (i), as outlined throughout Eq. (6.13) \sim Eq. (6.19).

6.3.3 Parallel Message Exchange via Unified-Client-Server Mode

The effective neighboring BSs incorporated in the same cooperative BS-cluster will then exchange their soft decision information produced by the PDA algorithm in parallel, assuming the presence of an idealized optical fibre backbone. The impairments of a realistic optical fibre were quantified in [418]. It is emphasized that each BS plays the role of both client and server. In other words, each BS operates in a unified-client-server (UCS) mode. As a server, it helps detect the signals of all co-channel users at all the cooperating cells, and then the soft decision information is sent to each user's home BS. This message passing action substantially benefits the signal detection process in neighboring cells. As a client, each BS receives multiple copies of soft decision information for its own desired user's signal. The exchange of soft information is carried out with the aid of BS cooperation. For example, BS0 estimates the APP of its own user MS0, and additionally forwards the APPs of MS2, MS3 and MS4 to the corresponding sites of BS2, BS3 and BS4, respectively. On the other hand, in order to aid the detection of MS0, the surrounding BS0, BS1, BS5 and BS6 output $P(s_t^0 = a_m | \mathbf{y}^0)$, $P(s_t^0 = a_m | \mathbf{y}^1)$, $P(s_t^0 = a_m | \mathbf{y}^5)$, $P(s_t^0 = a_m | \mathbf{y}^6)$, respectively, and all these probabilities will be forwarded to BS0, namely to the home BS of MS0. Therefore, BS0, BS1, BS5 and BS6 assist in the detection of MS0.

6.3.4 Soft Combining (SC) and Final Decision

Based on the aggregated soft decision information, each BS individually performs SC of all the copies of its own desired user's soft information according to

$$P(s_t = a_m | \mathbf{y}_{coop}) = P(s_t = a_m | \mathbf{y}^k) \prod_{j=1}^{C_b} P(s_t = a_m | \mathbf{y}^{\beta_j}), \quad (6.21)$$

where \mathbf{y}_{coop} stands for the received signal used for BS cooperation, i.e. \mathbf{y}^k and \mathbf{y}^{β_j} , $j = 1, \dots, C_b$. $P(s_t = a_m | \mathbf{y}_{coop})$ represents the composite soft decision information³. Again, let us consider the detection of MS0's signal as an example, where the composite soft decision information is $P(s_t^0 = a_m | \mathbf{y}_{coop}) = P(s_t^0 = a_m | \mathbf{y}^0) P(s_t^0 = a_m | \mathbf{y}^1) P(s_t^0 = a_m | \mathbf{y}^5) P(s_t^0 = a_m | \mathbf{y}^6)$. Note that for the sake of numerical stability, the soft information should be further normalized as

$$P(s_t = a_m | \mathbf{y}_{coop})_{norm} = \frac{P(s_t = a_m | \mathbf{y}_{coop})}{\sum_m P(s_t = a_m | \mathbf{y}_{coop})}. \quad (6.22)$$

Finally, make a decision for each transmitted symbol s_t , yielding $\hat{s}_t = a_{m'}$ at each corre-

³Equation (6.21) may also be interpreted as the sum of bit LLRs, where "multiplication" is converted to "addition" in the logarithmic domain.

sponding BS, where

$$m' = \arg \max_{d=1,2,\dots,M} \{P(s_t = a_d | \mathbf{y}_{coop})_{norm}\}. \quad (6.23)$$

6.3.5 Complexity Analysis

The proposed DPDA-SC scheme has a worst-case complexity at each BS per iteration, which is on the order of $O\left[(M_u(C_u + 1))^3\right]$, provided that the Sherman-Morrison-Woodbury formula is applied for the computation of $\mathbf{\Lambda}_t^{-1}$ [219]. No exhaustive network-wide information exchange is applied, since this would impose an excessive complexity. As a reduced-complexity alternative, the converged APPs are exchanged among the adjacent BSs in the cooperative BS-cluster only once, namely after the PDA detection was completed at each of the participating BSs. Furthermore, SC requires only a few simple arithmetic operations, as seen in Eq. (6.21). Hence both the complexity and the backhaul traffic imposed by the associated message exchange and SC remain modest, as will be demonstrated by the numerical complexity comparison results of Fig. 6.8 in Section 6.4. With respect to the backhaul traffic, in the entire reception process of a symbol vector, only $C_u M$ messages are passed from each cooperating BS to the others, and it can be further reduced by transferring the index of the quantized soft information instead of the soft information itself. As will be seen in Fig. 6.5 of Section 6.4, the uniform quantization using even just a single bit imposes only a negligible performance loss.

6.4 Simulation Results and Discussions

In this section, we characterize the achievable performance of the proposed DPDA-SC approach using Monte Carlo simulations in the hexagonal cellular network of Fig. 6.1 consisting of 19 cells. As mentioned before, since the decorrelated model based PDA and the non-decorrelated model based PDA exhibit an equivalent performance, but the former imposes a lower computational complexity when $M_u(C_u + 1) \leq M_b$, we use the decorrelated model based DPDA-SC for the scenario of $M_u(C_u + 1) \leq M_b$. Additionally, the non-decorrelated model aided DPDA-SC is used for the scenario of $M_u(C_u + 1) > M_b$ where the decorrelated PDA model is no longer applicable. QPSK modulation is used and the knowledge of the average equivalent SNR per receive antenna formulated as $\text{SNR} \triangleq 10 \log_{10} \left(\mathcal{E} \left\{ \|\mathbf{G}\mathbf{s}\|^2 \right\} / \mathcal{E} \left\{ \|\mathbf{n}\|^2 \right\} \right) = 10 \log_{10} [M_u(C_u + 1)/N_0]$ is exploited at each BS. Flat Rayleigh fading channels are considered, i.e. the entries of each sub-channel matrix between an MS and a BS are chosen as independent and identically distributed (i.i.d.), zero mean, unit-variance complex-valued Gaussian random variables. A new realization of each channel matrix is drawn for each data burst consisting of 1000 transmitted symbol vectors, and each element of the noise vector \mathbf{n}^k is i.i.d. $\mathcal{CN}(0, N_0)$. We set $(M_u = 2, M_b = 8)$ and

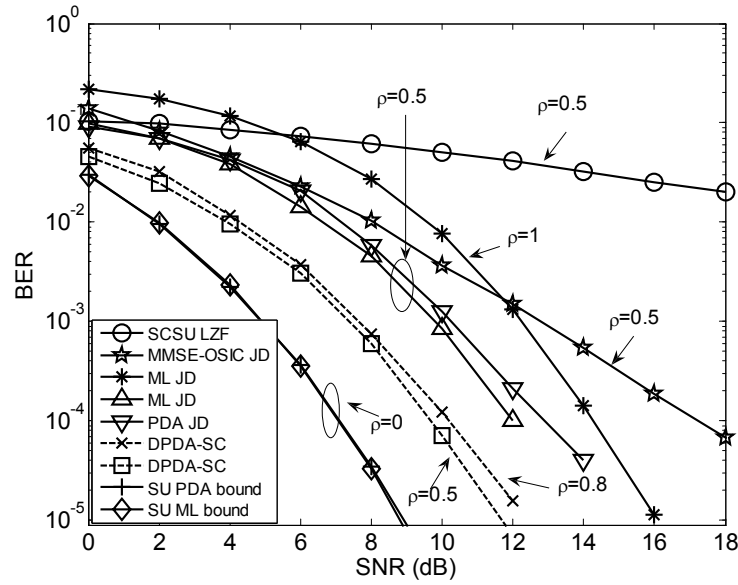


FIGURE 6.3: BER performance comparison of DPDA-SC, ML JD, SCSU LZF, SU ML bound and SU PDA bound under perfect CSI and different interference intensity ρ , which is defined in (6.2). Each individual BS may have a BER record for its own MS, and without loss of generality, the BER shown here is recorded at BS0 for MS0. QPSK modulation is used at each MS.

($M_u = 4, M_b = 8$) for the scenarios of $M_u(C_u + 1) \leq M_b$ and $M_u(C_u + 1) > M_b$, respectively. For simplicity, we consider MS0 in the following investigation where $C_u = 3$, without loss of generality. Since the PDA algorithm typically converges within $3 \sim 5$ iterations [219], we set the maximum number of iterations to $I = 5$.

6.4.1 Perfect CSI

In the case of *perfect CSI*, Fig. 6.3 compares the BER performance of 9 different setups, including the PDA and the ML single-user bounds recorded at BS0 for MS0, where ρ represents the interference intensity $\rho_{\alpha_i}^k$ defined in (6.2). To be specific, each $\rho_{\alpha_i}^k$ value may be different, but for simplicity, an identical interference intensity was assumed for the interfering MSs. This is justified because all the MSs imposing interference on each of the desired MSs are situated in the neighboring cells and have similar distances from the desired MS's home BS.

The “SCSU LZF” scheme refers to the linear zero-forcing (LZF) based single-cell SUD invoked at each BS, where the co-channel users' signals arriving from the other cells are simply treated as background noise. Naturally, this low-complexity SUD leads to a poor performance. The “MMSE-OSIC JD”, the “PDA JD” and the “ML JD” refer to the joint detection (JD) of multiple co-channel MSs at each BS using the MMSE-OSIC, the PDA and the ML approaches, respectively, where again, no SC is invoked. The ML detector

is implemented with the aid of a reduced-complexity sphere decoder [54], where the sphere radius is adaptively adjusted according to the prevalent SNR-level, in order to avoid a search failure. All the JD setups require knowledge of all the channel matrices between the co-channel users and the local BS for mitigating the CCI, but they do not share soft decision information with other cells, since no message exchange and no SC is used. Nonetheless, a substantial BER improvement is shown in comparison to the SCSU LZF, especially when ρ is small.

The dashed curves represent the proposed DPDA-SC scheme operating under $\rho = 0.5$ and $\rho = 0.8$. Observe in Fig. 6.3 that a significant further BER improvement is achieved, which is attributed to the spatial diversity gain provided by joint cooperative BS processing. The PDA and the ML single-user bounds, namely the ‘‘SU PDA bound’’ and ‘‘SU ML bound’’, are obtained by setting $\rho = 0$, which implies that the CCI vanishes. This scenario is equivalent to a single-user (2×8)-element spatial multiplexing MIMO system. It is observed in Fig. 6.3 that the PDA bound is extremely close to the ML bound. The results recorded in Fig. 6.3 for different ρ values characterize the impact of ρ on the attainable reception performance. It may be concluded from Fig. 6.3 that the interference intensity ρ is the key factor limiting the achievable performance of cellular MIMO networks.

Observe furthermore in Fig. 6.3 that the cooperative DPDA-SC reception scheme exploiting the knowledge of the *matrix sub-channels* substantially improves the BER performance, but still fails to approach the single-user bound in the presence of strong interference, which is a direct consequence of the inter-layer interference of the matrix sub-channel⁴. More explicitly, let us consider the equivalent post-channel signal power at BS0:

$$\begin{aligned} \mathcal{E} \left\{ \|\mathbf{G}\mathbf{s}\|^2 \right\} &= \mathcal{E} \left\{ \left\| \sum_{t=1}^{M_u(C_u+1)} \mathbf{g}_t s_t \right\|^2 \right\} \\ &= \sum_{t=1}^{M_u} \mathcal{E} \left\{ \|\mathbf{g}_t\|^2 \right\} + \sum_{t=M_u+1}^{M_u(C_u+1)} \mathcal{E} \left\{ \|\mathbf{g}_t\|^2 \right\}, \end{aligned} \quad (6.24)$$

where \mathbf{g}_t , the t th column of \mathbf{G} , $t = 1, \dots, M_u$, corresponds to the specific sub-channel of the desired user, and \mathbf{g}_t , $t = M_u + 1, \dots, M_u(C_u + 1)$, corresponds to that of the co-channel users. We may randomly select one element $g_{t,i}$, $i = 1, \dots, M_b$, from each \mathbf{g}_t , $t = 1, \dots, M_u(C_u + 1)$ to form a sample channel gain vector. When ρ is increased for example from 0.5 to 0.8, the power vector corresponding to the sample channel gain vector varies from $[1, 1, 0.25, 0.25, 0.25, 0.25, 0.25, 0.25]$ to $[1, 1, 0.64, 0.64, 0.64, 0.64, 0.64, 0.64]$ for MS0, when we have $M_u = 2$ and $M_b = 8$. Hence, although the increased interference power may benefit the reception quality of the distant MSs roaming in the cooperative cells, it still degrades the reception performance of MS0.

⁴For spatial multiplexing aided MIMO systems interference exists among all the layers at the transmitter side, which is also known as multiple-stream interference (MSI).

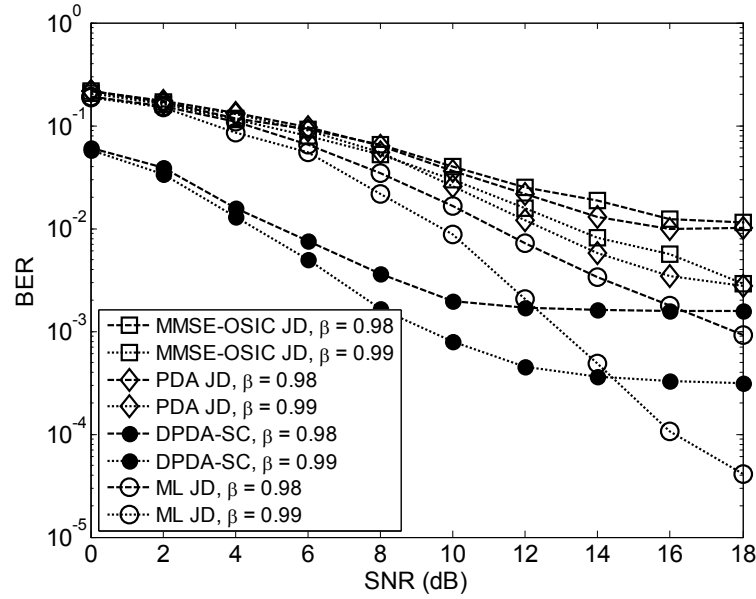


FIGURE 6.4: Performance comparison of different reception schemes under different levels of channel estimation quality $\beta = 0.98$ and $\beta = 0.99$, and a given interference intensity $\rho = 0.8$, using QPSK modulation.

6.4.2 Imperfect CSI

When considering the more practical *imperfect CSI* scenario, Fig. 6.4 compares the performance of the proposed DPDA-SC scheme to the MMSE-OSIC JD, the ML JD and the PDA JD schemes at different levels of channel estimation quality of $\beta = 0.98$ and $\beta = 0.99$, and a given interference intensity of $\rho = 0.8$. It is observed in Fig. 6.4 that the achievable performance of all the schemes considered is dramatically degraded by the channel estimation error. Basically, different error floors are observed for these schemes, because the fixed level of relatively strong interference plays a dominant role, when the SNR is high. More specifically, in the imperfect CSI scenario of Fig. 6.4 the PDA JD scheme only marginally outperforms the MMSE-OSIC JD scheme, although it enjoys a notable advantage in the perfect CSI scenario. In other words, the PDA JD scheme is more sensitive to the channel estimation error than the MMSE-OSIC JD scheme. This is because the MMSE-OSIC JD is a hard-decision method, while the PDA JD vitally relies on an iterative soft information update process. In general, the accuracy of the soft information is a key factor in determining the success of soft information based algorithms. Therefore, we can further observe in Fig. 6.4 that the DPDA-SC scheme has a substantial performance advantage over that of the PDA JD, because the spatial diversity originating from BS cooperation using SC considerably improves the accuracy of the soft information. Compared to the ML JD, the DPDA-SC is remarkably superior in the moderate-SNR region of practical interest, although its advantage erodes in the high-SNR region of Fig. 6.4. This phenomenon is a consequence of the different sensitivity of soft information based and hard information

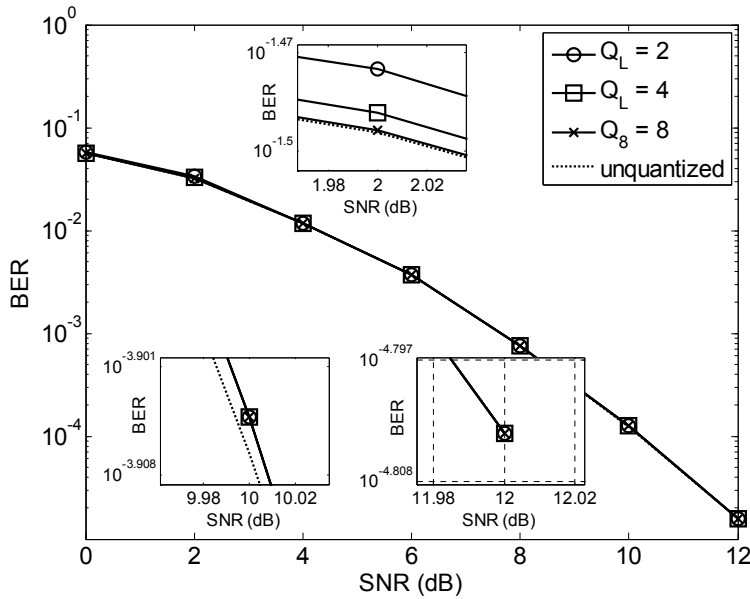


FIGURE 6.5: Uniform quantization impact on the performance of DPDA-SC under perfect CSI and a given interference intensity $\rho = 0.8$, using QPSK modulation.

based methods. Therefore, we conclude that the BS cooperation aided DPDA-SC scheme is capable of mitigating the effects of the error floor imposed by imperfect CSI by exploiting that the strong interference becomes a useful source of increased signal energy as a benefit of the more sophisticated distributed processing. Note that although the error floor is not very obvious for the ML JD in the SNR range considered in Fig. 6.4, it is expected to become more evident at higher SNRs.

6.4.3 Impact of Quantization on the Backhaul Traffic and Performance

The backhaul traffic is a significant challenge that has to be addressed before the BS cooperation aided distributed processing can be implemented in the practical applications. Therefore, it is of practical interest to investigate the cost of backhaul traffic in the parallel message exchange stage using the UCS mode in the proposed DPDA-SC scheme. Instead of transferring the quantized probability value itself, the index of each probability value is transferred between the cooperative BSs, where a quantized probability lookup table is pre-stored. When considering the perfect CSI scenario, where the interference intensity is $\rho = 0.8$, Fig. 6.5 illustrates the performance of the DPDA-SC employing uniform quantization, which is performed on the converged probabilities before they are transferred to the cooperative BSs. It is shown that the performance loss due to the different quantization levels in uniform quantization is marginal in the proposed DPDA-SC scheme. This performance loss diminishes as the SNR increases, and completely vanishes at high SNRs. This is because the converged soft information has been obtained individually using the PDA algorithm at each BS before the parallel message exchange stage, and the SC aided final decision

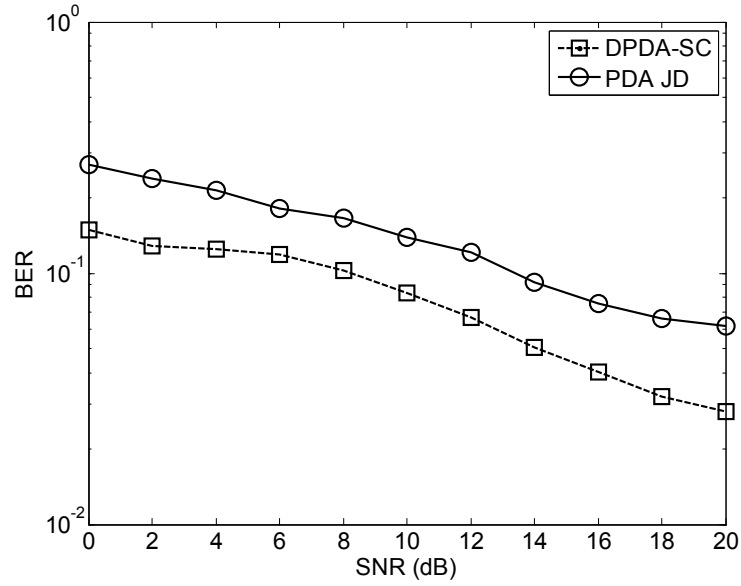


FIGURE 6.6: Performance of DPDA-SC in rank-deficient scenario, $M_b = 8$, $M_u = 4$, $C_u = 3$, $C_b = 3$, with perfect CSI and a given interference intensity $\rho = 0.8$, using QPSK modulation.

relies on which probability is the highest, rather than on the exact values of the probabilities themselves. By comparison, the soft information is obtained via multiple iterations between BSs in [134], where the performance is more sensitive to the quantization loss. Based on our results, if the $Q_L = 2$ uniform quantization scheme is used, only $M \log_2 Q_L = 4$ bits will be transferred from each BS to one of the cooperating BSs, when QPSK is used.

6.4.4 Rank-Deficient Scenario

Fig. 6.6 presents the performance of the proposed DPDA-SC scheme in the scenario of $M_u(C_u + 1) > M_b$, where $M_u = 4$, $M_b = 8$, $C_u = 3$. The non-decorrelated signal model is applied in both the PDA JD and the DPDA-SC schemes. We observed in Fig. 6.6 that the DPDA-SC is still superior to the PDA-JD, although both of them suffered a significant performance loss due to the much stronger inter-layer interference compared to the scenario of $M_u(C_u + 1) > M_b$.

6.4.5 Convergence Property

In Fig. 6.7 we characterize the convergence performance of the proposed DPDA-SC scheme under both perfect and imperfect CSI conditions. It may be observed in Fig. 6.7 that the DPDA-SC converges within a few iterations, which is a contributing factor of the low complexity of the DPDA-SC, as shown in Fig. 6.8.

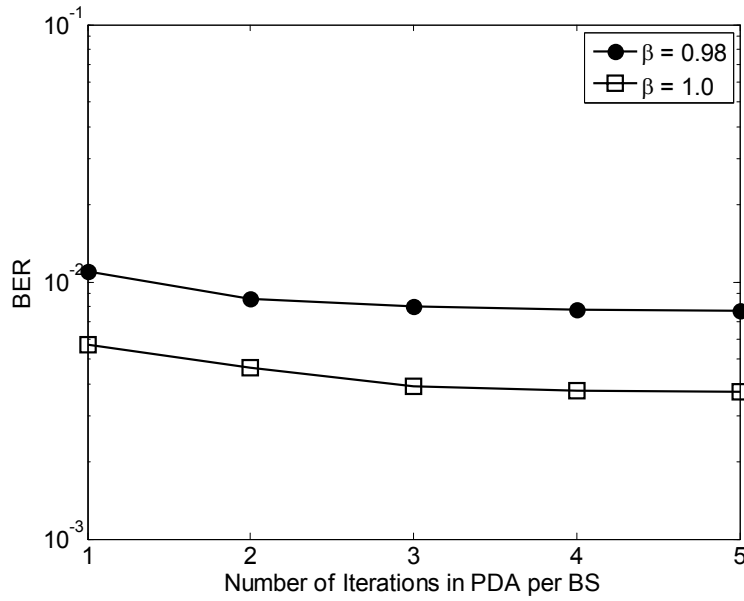


FIGURE 6.7: Convergence property of DPDA-SC, SNR = 6dB, QPSK, $\rho = 0.8$.

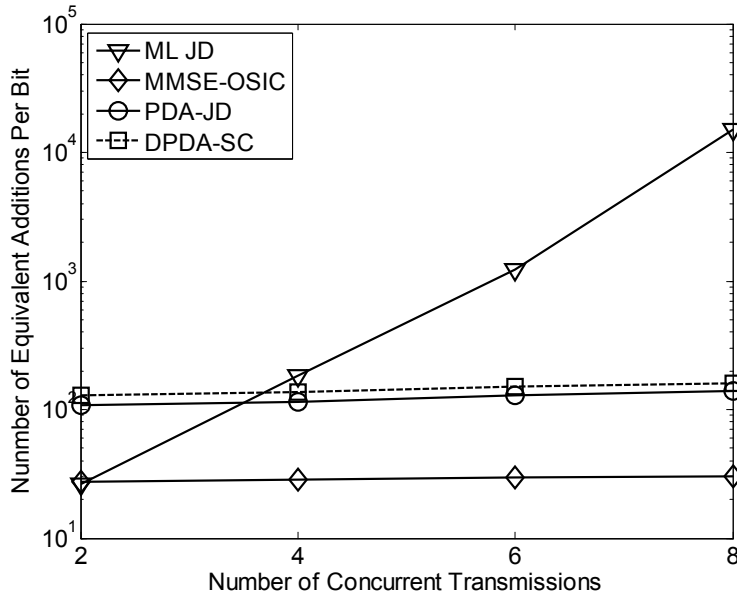


FIGURE 6.8: Complexity comparison of different reception schemes, measured in terms of the number of equivalent additions per bit, SNR = 6dB, QPSK, $\beta = 0.98$, $\rho = 0.8$.

6.4.6 Complexity Comparison

Finally, the complexity comparison between the DPDA-SC, the PDA JD, the MMSE-OSIC JD and the ML JD is provided in Fig. 6.8. The complexity is quantified in terms of the number of equivalent additions required for decoding a single bit. We may observe that as the number of concurrent transmissions increases, the complexity of ML JD increases rapidly, while the other three maintain a near-constant normalized complexity. Furthermore, the

complexity of the proposed DPDA-SC is marginally higher (contributed by SC) than that of the conventional PDA JD, but significantly lower than that of ML JD (about 1% when the number of concurrent transmissions is 8). Although the relatively coarse complexity analysis using $O(\cdot)$ function shows that the DPDA-SC approach enjoys the same $O(L^3)$ order of complexity as the SIC based algorithm, the numerical results show that the DPDA-SC is about five times more complex than the MMSE-OSIC JD scheme.

6.5 Chapter Summary and Conclusions

We proposed a DPDA-SC scheme for BS cooperation in the uplink of multiuser multicell MIMO systems. The realistic hexagonal cellular model relying on unity frequency reuse was considered. The DPDA-SC scheme was shown to converge in few iterations, hence it constitutes a low-complexity solution for jointly estimating the initial soft decision information at each BS. Each BS shares the MSs' soft information with the aid of their message exchange and generates the final soft decision information with the aid of SC. The simulation results as well as our complexity analysis demonstrate that the proposed scheme significantly outperforms the conventional non-cooperative schemes, while imposing a modest additional complexity and backhaul traffic. We also investigated the performance of the proposed DPDA-SC scheme in the more practical imperfect CSI scenario and demonstrated that the DPDA-SC scheme succeeds in mitigating the system's error floor. The impact of quantization on both the backhaul traffic and the achievable performance was also investigated, and it was shown that even when using single-bit uniform quantization the performance loss is trivial, while leading to a low backhaul traffic.

Conclusions and Future Research

THIS thesis has studied the challenging MIMO detection problem, which is of central importance for both wireless and wireline communication systems aiming for striking an attractive compromise between the achievable spectrum-efficiency and energy-efficiency. For example, a new type of digital subscriber line (DSL) technology (gigabit DSL) [419] has been proposed based on the binder MIMO channels of [420]. Although the MIMO detection problem has been studied since the late 1960s [146], the interests in this challenging fundamental problem revive again and again during the evolution of telecommunications. As a retrospective of this thesis, its inherent logical structure depicted in Fig. 1.14 may be interpreted from the following two perspectives.

- Firstly, in terms of the *fundamental detection algorithm improvement*, both the PDA and the SDPR based MIMO detectors highlighted in Fig. 1.11 were improved by using a virtually antipodal (VA) model transformation technique, which was conceived for MIMO systems employing the family of rectangular M -ary QAM constellations. As a rigorous mathematical approach of describing the bit vector to symbol vector mapping process that takes place at the transmitter of MIMO systems, the VA technique is capable of explicitly transforming the symbol-based MIMO system model into a BPSK-like model, and hence providing an increased flexibility in terms of designing MIMO detection algorithms. For a given MIMO system, the VA transformation matrix is determined by three factors, which are the number of transmit antennas, the size of the rectangular QAM constellations and the bit-to-symbol mapping rule. Hence, the VA techniques advocated are applicable to all symbol-based MIMO detection algorithms in principle. As application examples, we considered the PDA and the SDPR detectors employing our VA techniques, and demonstrated that either their achievable performance is improved or their computational complexity is reduced, as compared to their symbol-based counterparts. The evidence of these statements was presented in Chapters 2 and 3.
- Secondly, in terms of the *evolution of the application context of MIMO detection*, on the

one hand, both the uncoded and FEC-coded MIMO systems were considered; on the other hand, the point-to-point MIMO systems, the uplink of single-cell multiuser MIMO systems and the multicell multiuser MIMO systems were all investigated. More specifically, the VA-aided detection of high-order rectangular QAM in uncoded MIMO systems was conceived in Chapters 2 and 3, and then the PDA-based IDD design of an FEC-coded MIMO system was detailed in Chapters 4 and 5. The system models considered throughout Chapters 2 to 5 implicitly include both point-to-point MIMO systems and the uplink of single-cell multiuser MIMO systems, while the system model considered in Chapter 6 is the multicell multiuser MIMO system that relies on both distributed transmitters and distributed receivers. Therefore, the representative MIMO system models depicted in Fig. 1.5, Fig. 1.6, and Fig. 1.8 have been studied. Note that since MIMO detection is rarely used in the downlink of MIMO systems, the MIMO broadcast channel shown in Fig. 1.7 is not considered in this thesis.

The remainder of this concluding chapter is organized as follows. First, the summary and major conclusions of this thesis are presented in Section 7.1. Second, several key challenges and open problems concerning MIMO detection are identified for future research in Section 7.2.

7.1 Summary and Conclusions

The summary and major conclusions of this thesis are as follows.

- **Chapter 1:**

In Chapter 1, we provided a comprehensive overview of the generic MIMO detection problem and discussed a variety of representative MIMO detectors. More specifically, in Section 1.1 we elucidated the nature and essence of CCI from both theoretic and engineering practice perspectives. In Section 1.2, we clarified the concept and generality of MIMO detection techniques from the perspective of physical-layer CCI management. Then, a more rigorous formal definition of the MIMO detection problem was given in Section 1.3. Additionally, from Section 1.4 to Section 1.6, several frequently used MIMO system models were described, including that of the linear memoryless channels, as well as of the dispersive channels exhibiting memory. The relationship between the complex-valued and the real-valued MIMO system models was also detailed. Furthermore, the historical development and the state-of-the-art of the representative MIMO detectors, as shown in Fig. 1.10 and Fig. 1.11, were reviewed in Section 1.8, including the optimal ML/MAP based detector, the family of linear detectors, the family of interference cancellation based detectors, the tree-search based detectors, the PDA based detectors and the SDPR based detectors. The milestones in the development of these MIMO detectors

were summarized from Table 1.1 to Table 1.8, respectively. Finally, the organization and novel contributions of this thesis were briefly presented in Section 1.9.

- **Chapter 2:** [40, 41]

In Chapter 2, a unified B-PDA detection approach was investigated in uncoded MIMO systems employing high-order rectangular QAM. The proposed novel approach transforms the symbol detection process of QAM to a bit-based process by introducing a unified matrix representation (UMR) of QAM. With the aid of simulation results given in Fig. 2.9 to Fig. 2.12, we demonstrated that the linear natural mapping based B-PDA approach typically attained an improved detection performance (measured in terms of both BER and SER) in comparison to the conventional symbol-based PDA aided MIMO detector, despite its dramatically reduced computational complexity as shown in Section 2.5.4 and Fig. 2.6. The only exception is that at low SNRs, the linear natural mapping based B-PDA is slightly inferior in terms of its BER to the conventional symbol-based PDA using binary reflected Gray mapping. Furthermore, the simulation results of Fig. 2.9 to Fig. 2.12 showed that the linear natural mapping based B-PDA MIMO detector may approach the best-case performance provided by the nonlinear binary reflected Gray mapping based B-PDA MIMO detector under ideal conditions. Additionally, as shown in Section 2.3 and Section 2.4, the implementation of the B-PDA MIMO detector is shown to be much simpler in the case of the linear natural mapping. Based on these two points, we conclude that in the context of the uncoded B-PDA MIMO detector it is preferable to use the linear natural bit-to-symbol mapping, rather than the nonlinear Gray mapping.

More specifically, the UMR of the linear natural mapping based scenario was derived in Section 2.3, where the ($N_t = 2$)-aided SDM-MIMO systems employing BPSK, 4-QAM, 8-QAM, 16-QAM, 32-QAM and 64-QAM were first considered as examples, followed by the generic UMR formulae derived for rectangular M -QAM in Section 2.3.3. Note that the linear natural mapping is defined as a mapping that satisfies (2.3) with a single unique solution. Therefore, for linear natural mapping aided MIMO systems, the relationship between the transmitted bit vector \mathbf{b} and the symbol vector \mathbf{s} can be characterized by $\mathbf{s} = \mathbf{W}\mathbf{b}$, where \mathbf{W} is the transformation matrix. Additionally, the UMR of the nonlinear binary reflected Gray mapping based scenario was derived in Section 2.4, where both 16-QAM and 64-QAM were first considered as examples, and then the generic method of obtaining the UMR for rectangular M -QAM was outlined in Section 2.4.3. It was shown, for example in Table 2.4, that the UMR of Gray mapping depends on the pattern of the transmitted bits, and hence the relationship between the transmitted bit vector and symbol vector is characterized by $\mathbf{s} = \mathbf{W}(\mathbf{b})\mathbf{b}$ in the Gray mapping scenario, rather than $\mathbf{s} = \mathbf{W}\mathbf{b}$. However, since the linear natural mapping and the Gray mapping are identical for 4-QAM, the transformation matrices of 4-QAM under both mappings are the same, which is an exception compared to other higher-order rectangular QAM constellations.

After obtaining the UMR for both linear natural mapping and nonlinear Gray mapping scenarios, a novel B-PDA detector was derived in Section 2.5, followed by an example of the proposed B-PDA in Section 2.5.2. Then, both the positive and negative impacts of the UMR based operation were discussed in Section 2.5.3.1, where the iterative Gaussian approximation processes of both the conventional symbol-based PDA and the proposed B-PDA were visualized in Fig. 2.4 and Fig. 2.5 respectively for intuitively illuminating why the proposed B-PDA detector may achieve a better performance than the conventional symbol-based PDA detector. Additionally, the impact of constellations labelling on the BER and/or SER performance of both symbol-based detectors and bit-based detectors were elucidated in Section 2.5.3.2 for uncoded systems, and the insights obtained here were beneficial for interpreting the simulation results of Section 2.6. Furthermore, the practical feasibility of the proposed UMR for Gray mapping was discussed in Section 2.5.3.3, which answers the question as to why the B-PDA detector becomes impractical when it is based on the UMR derived in Section 2.4 for the Gray mapping scenario. However, in order to provide a benchmark, in the simulations of Section 2.6 we assumed that the transformation matrix $\mathbf{W}(\mathbf{b})$ of the Gray mapping scenario is perfectly known to the receiver. As a result, in Fig. 2.9 to Fig. 2.12, the simulation results associated with the B-PDA of Gray mapping scenario serves only as a theoretical performance benchmark for the linear natural mapping based B-PDA.

In Section 2.5.4, the complexity of the proposed B-PDA was analyzed. It was shown that the complexity of B-PDA is significantly lower than that of the conventional symbol-based PDA detector when the constellation size M is far greater than 4. This conclusion is supported by the FLOP-based complexity results of Fig. 2.6. Additionally, Fig. 2.7 evaluates the complexity of the proposed B-PDA detector for different SNR values. It can be seen from Fig. 2.7 that the B-PDA has a near-constant complexity for different SNR values. This near-constant complexity may be regarded as another merit of the B-PDA detector, especially in the context of circuit-based implementation. By comparison, some other reduced-complexity MIMO detectors, for example the tree-search based methods, typically have a complexity that is quite sensitive to the SNR values encountered.

Finally, in Section 2.6, a range of simulation results were provided for evaluating the performance of the proposed B-PDA detector against other representative MIMO detectors. To elaborate a little further, Fig. 2.8 compared the impact of the number of iterations on the achievable performance of both the B-PDA and the conventional symbol-based PDA. It was shown that both of them exhibit quite a good convergence, since they typically converge within 3 to 5 iterations. Furthermore, from Fig. 2.9 to Fig. 2.12, the BER and SER performances of the proposed B-PDA are compared with that of the conventional symbol-based PDA, the MMSE-OSIC and the ML detectors, while using both the linear natural mapping and nonlinear Gray mapping in the context of rectangular 16-QAM and 64-QAM. Apart from the aforementioned major conclusions regarding the performance

of the B-PDA and the conventional symbol-based PDA, we observed that the achievable performance of the proposed B-PDA is better than of the MMSE-OSIC detector, but inferior to that of the ML detector in the context considered.

- **Chapter 3:** [48, 49]

In Chapter 3, an efficient generalized SDPR based VA detection approach was proposed for Gray-coded high-order rectangular QAM signalling over MIMO channels. As shown in Chapter 2, albeit the decomposition of symbol-based detection to a bit-based one is desirable owing to its reduced complexity and increased flexibility, Gray-mapping is non-linear, and hence the direct bit-based detection of MIMO systems employing Gray-coded rectangular QAM constitutes a challenging problem. In Section 3.4, we further conceived a way of exploiting the structural regularity of Gray-coded high-order rectangular QAM, and transforms the classic symbol-based MIMO detection model to a low-complexity bit-based detection model. As an appealing benefit, the conventional three-step “signal-to-symbols-to-bits” decision process can be substituted by a simpler “signal-to-bits” decision process for the classic Gray-mapping aided high-order rectangular QAM in practice, and hence any bit-based detection method becomes potentially applicable. As an application example, in Section 3.5 we proposed a direct-bit-based VA-SDPR (DVA-SDPR) MIMO detector, which is capable of directly making binary decisions concerning the individual information bits of the ubiquitous Gray-mapping aided high-order rectangular QAM, while dispensing with symbol-based detection. Furthermore, the proposed model transformation method facilitates the exploitation of the UEP property of high-order QAM with the aid of the low-complexity bit-flipping based “hill climbing” method, as seen in Section 3.5.3 and Fig. 3.7. As a result, the proposed DVA-SDPR detector achieves the best BER performance among the known SDPR-based MIMO detectors in the context considered, while still maintaining the lowest-possible worst-case complexity order of $O[(N_t \log_2 M + 1)^{3.5}]$.

In order to make the thesis more self-contained, the essential mathematical foundation of the SDPR based detectors was briefly introduced in Section 3.2. More specifically, in Section 3.2.1 the basic concepts of convex sets, convex functions and convex optimization models were first introduced, and then several frequently used techniques for identifying convex functions were presented. Additionally, the basic framework of solving mathematical optimization problems using convex optimization was illustrated in Fig. 3.3. Furthermore, in Section 3.2.2, we presented three widely used forms of the SDP model and clarified the relationship between them. The three forms are the inequality form, the LMI standard form (with equality constraints) and the standard form. It is possible to convert from one form to another, although the conversion might not be straightforward. Additionally, an example of the SDP problem was provided, and the Lagrangian dual problem of the standard-form SDP was formulated as well.

Subsequently, in Section 3.3, the basic concept of the existing IVA-SDPR detector, which is used as a benchmark of the proposed DVA-SDPR detector, was highlighted. Then, in Section 3.4 the structure of the Gray mapping based rectangular QAM constellations was revisited, and a novel XOR-operation based transformation approach was conceived for explicitly characterizing the relationship between the Gray-coded symbol and the corresponding information bits. To elaborate another step further, the Gray-coded rectangular 16-QAM and 64-QAM were considered as examples, and the generic transformation formulae were obtained for even higher-order Gray-coded rectangular QAM constellations, as summarized in Table 3.1. In contrast to the transformation approach proposed in Section 2.4, that conceived in Section 3.4 is readily applicable in nonlinear Gray mapping scenario in practice, because the latter approach does not rely on a transformation matrix that is dependent on the transmitted bit vector. Based on the transformation approach of Section 3.4, the DVA-SDPR detector is capable of directly making decisions on the information bits of a Gray-coded symbol vector, as formulated in Section 3.5.1. A modified version of the efficient primal-dual interior-point algorithm was presented in Section 3.5.2. Since the transformation approach proposed in Table 3.1 of Section 3.4 facilitates the exploitation of the UEP property of QAM bits, a bit-flipping technique was conceived in Section 3.5.3 for improving the performance of the DVA-SDPR detector. Furthermore, the complexity of the proposed DVA-SDPR detector was analyzed in Section 3.5.4, where it was shown that the worst-case complexity of recovering the original information bit vector by using the DVA-SDPR detector is on the order of $O[(N_t \log_2 M + 1)^{3.5}]$.

Finally, our simulation results and discussions were offered in Section 3.6 for characterizing the proposed DVA-SDPR detector's achievable performance and its computational complexity. To elaborate a little further, Fig. 3.5 quantified the impact of the convergence tolerance of $\epsilon = 10^{-k}$ on the performance of the DVA-SDPR detector. It was shown that the DVA-SDPR detector converges for $k = 8$ or 9 . We observed from Fig. 3.6 that the complexity of the DVA-SDPR detector increased almost linearly upon increasing the value of k . Fig. 3.7 showed the UEP characteristics of the proposed DVA-SDPR detector. It was observed that the first and the third bits (resp. the second and the fourth bits) of a single 16-QAM symbol exhibit an identical BER performance, which is better (resp. worse) than the overall average BER performance. Fig. 3.8 showed that the DVA-SDPR detector has a performance better than the MMSE-OSIC, but worse than the SD relying on an adaptive sphere radius. Additionally, it was shown in Fig. 3.8 that bit-flipping is capable of improving the performance of the DVA-SDPR detector. However, when bit-flipping is not invoked, the DVA-SDPR has a similar performance to the IVA-SDPR. We observed from Fig. 3.9 that as usual, the SD imposed a significantly higher complexity in the low-SNR region than in the high-SNR region. By comparison, the complexities of the DVA-SDPR and of the IVA-SDPR are almost identical and near-constant, and they are considerably lower than that of the SD across the entire SNR region considered.

Nonetheless, observe in Fig. 3.9 that the complexity of all the SDPR based detectors is still higher than that of the MMSE-OSIC detector. Furthermore, Fig. 3.10 compared the complexity of the DVA-SDPR, of the classic SD as well as of the FCSD detectors in the context of “massive MIMO” systems [25, 384], where the number of transmit antennas N_t can be extremely high. The results of Fig. 3.10 imply that although the SD based detectors are competitive in the relatively low-throughput MIMO systems associated with moderate values of N_t , it might be difficult to use them in the massive MIMO systems, where the DVA-SDPR detector might be more promising.

- **Chapter 4:** [44, 45]

Having considered the MIMO detection problem in uncoded MIMO systems in Chapters 2 and 3, in Chapter 4, the issue of designing an IDD aided receiver relying on the low-complexity PDA method is addressed for turbo-coded MIMO systems using general M -ary modulations. We demonstrated in Section 4.5.1 that the classic candidate-search aided bit-based extrinsic LLR calculation method is not applicable to the family of PDA-based detectors. Additionally, in Section 4.5.2 we revealed that in contrast to the interpretation in the existing literature, the output symbol probabilities of existing PDA algorithms are not the true APPs, but rather the normalized symbol likelihoods. Therefore, the classic relationship, where the extrinsic LLRs are given by subtracting the *a priori* LLRs from the *a posteriori* LLRs does not hold for the existing PDA-based detectors. Motivated by these revelations, we proposed a new AB-Log-PDA method in Section 4.4 and unveiled the technique of calculating bit-based extrinsic LLRs for the AB-Log-PDA in Section 4.5.2, which facilitates the employment of the AB-Log-PDA in a simplified IDD receiver structure, as shown in Fig. 4.7. Additionally, in Section 4.6.1 numerous numerical results were provided to evaluate the performance of the AB-Log-PDA based IDD. In particular, it was demonstrated that we may dispense with inner iterations within the AB-Log-PDA in the context of IDD receivers. Furthermore, the complexity of the AB-Log-PDA based IDD was analyzed and compared with other benchmark IDDs in Section 4.6.2, which, together with the numerical results recorded in Section 4.6.1, demonstrated that the proposed AB-Log-PDA based IDD scheme is capable of achieving a comparable performance to that of the optimal MAP detector based IDD receiver, while imposing a significantly lower computational complexity in the scenarios considered.

More specifically, in order to provide more insights into the fundamental principle underlying the PDA based methods, an interference-plus-noise distribution analysis was provided in Section 4.3. It was shown that the interference-plus-noise term typically obeys a multimodal Gaussian mixture distribution, whose parameters are updated by the PDA iterations. This process was visualized in Fig. 4.5 and 4.6 by considering two examples that correspond to the effects both before and after using the PDA iterations, respectively.

Subsequently, in Section 4.4, the AB-Log-PDA detector was derived and the algorithm

was summarized in Table 4.1, while in Section 4.5, the challenges of calculating extrinsic LLRs from the output of the family of PDA based methods were analyzed. It was demonstrated in Proposition 4.1 of Section 4.5.2 that for all PDA algorithms which output the probabilities $P(s_i|\mathbf{y})$, or the likelihood functions $p(\mathbf{y}|s_i)$, the bit-based extrinsic LLR $L_E(b_k|\mathbf{y})$ cannot be calculated using the candidate-search method that relies on $p(\mathbf{y}|\mathbf{b})$ or $p(\mathbf{y}|\mathbf{s})$. Additionally, it was pointed out in Section 4.5.2 that the conventional interpretation of the nature of the estimated symbol probabilities output by the approximate Bayes' theorem based PDA methods is incorrect. In fact, they are not the true APPs, but rather the normalized symbol likelihoods. Based on this insight, a simple approach of calculating the extrinsic LLRs from the output symbol probabilities of AB-Log-PDA was given in Conjecture 1 of Section 4.5.2.

Finally, in Section 4.6.1 a range of simulation results were provided for evaluating the impact of various design parameters on the achievable performance of the AB-Log-PDA based IDD. These results include the impact of inner PDA iterations (Fig. 4.8 to 4.11), the impact of outer iterations (Fig. 4.12 and 4.13), the impact of the Nakagami- m fading parameter m (Fig. 4.14), the influence of the modulation order (Fig. 4.15), the impact of the number of transmit antennas (Fig. 4.16) and the effect of channel-estimation errors (Fig. 4.17). In particular, it was shown in Fig. 4.8 that the performance of the AB-Log-PDA based IDD is degraded upon increasing the number of inner iterations of the AB-Log-PDA, despite the fact that the computational complexity increases dramatically. Therefore, the AB-Log-PDA based IDD should not invoke any inner PDA iteration. The reasons as to why the inner PDA iterations fail to provide BER improvements were investigated from three different perspectives, as shown in Fig. 4.9 to 4.11. Additionally, the complexity analysis of Section 4.6.2 showed that the computational complexity of the proposed AB-Log-PDA based IDD is significantly lower than that of the Exact-Log-MAP based IDD, of the fixed-complexity list SD based IDD, and of the soft K -best SD using an improved "look-ahead path metric". This conclusion was also confirmed by the numerical result of Fig. 4.18.

- **Chapter 5:** [46, 47]

As a further extension of Chapter 4, in Chapter 5 we provided another design alternative for the PDA-based IDD receiver of MIMO systems. Since the AB-Log-PDA based IDD proposed in Chapter 4 is still based on the approximate Bayes' theorem, the symbol probabilities estimated by the AB-Log-PDA are not the true APPs in the rigorous mathematical sense, but a type of nominal APPs, which are unsuitable for the *classic* architecture of IDD aided receivers. To circumvent this predicament, in Chapter 5.3 we proposed a novel EB-Log-PDA method, whose output has similar characteristics to the true APPs, and hence it is readily applicable to the classic IDD architecture of MIMO systems using arbitrary M -ary memoryless modulation. Additionally, in Section 5.4, the method of calculating the extrinsic LLRs for the EB-Log-PDA was derived, and the re-

relationship between the extrinsic LLRs of the EB-Log-PDA and the AB-Log-PDA was analyzed. Furthermore, in Section 5.5 a range of simulation results and their interpretations were provided for evaluating the EB-Log-PDA based IDD receiver's convergence property, its achievable performance and its computational complexity, and for illuminating the relationship between the EB-Log-PDA based IDD and other benchmark IDD schemes.

More specifically, the EB-Log-PDA algorithm derived in Section 5.3 was summarized in Table 5.1. The methods of calculating the extrinsic LLRs for the proposed EB-Log-PDA in the context of both high-order M -ary modulation as well as BPSK modulation was detailed in Section 5.4.1. Additionally, the relationship between the extrinsic LLRs of the EB-Log-PDA and of the AB-Log-PDA was analyzed in Section 5.4.2, where Theorem 5.1 demonstrated that for a specific bit b_{il} , the extrinsic LLR of the EB-Log-PDA algorithm is typically different from that of the AB-Log-PDA algorithm. As a further result, Proposition 5.2 characterized the degree of difference between the two types of extrinsic LLRs. In order to provide more insights on the relationship between the AB-Log-PDA and the EB-Log-PDA, Fig. 5.2 showed the BER of the AB-Log-PDA based IDD scheme for the scenario where the nominal symbol APPs were deliberately misinterpreted as the true symbol APPs. More explicitly, Fig. 5.3 illuminated the role of the *a priori* information in the AB-Log-PDA and the EB-Log-PDA algorithms, which indicated the essential difference between the two PDA algorithms.

In Fig. 5.4 of Section 5.5.1, the convergence behavior of the EB-Log-PDA, the AB-Log-PDA and the Exact-Log-MAP based IDD schemes were compared with the aid of the EXIT chart analysis. Explicitly, it was shown in Fig. 5.4 that all of them converge after three outer iterations. This conclusion was also supported by the numerical results of Fig. 5.5, which characterized the impact of the number of outer iterations on the BER performance of the EB-Log-PDA. Additionally, in Section 5.5.2 the impact of the EB-Log-PDA algorithm's inner iteration on the design of EB-Log-PDA aided IDD receiver was also investigated, as shown in Fig. 5.6 and Fig. 5.7. We demonstrated that introducing inner iterations into the EB-Log-PDA scheme, which is common practice in conventional-PDA aided uncoded MIMO systems, would actually degrade the IDD receiver's performance, despite significantly increasing the overall computational complexity of the IDD receiver. This observation may be deemed to be somewhat similar to the scenario of the AB-Log-PDA based IDD, as shown in Fig. 4.8. In order to show the difference between the AB-Log-PDA and the EB-Log-PDA more explicitly, Fig. 5.8 depicted the intermediate BER evaluated at the output of the two PDA detectors in the context of FEC-coded MIMO systems. It may be observed that the EB-Log-PDA has a better intermediate BER performance than the AB-Log-PDA. Furthermore, in Section 5.5.3 we investigated the relationship between the extrinsic LLRs of the proposed EB-Log-PDA and of the AB-Log-PDA by examining the CDFs and PDFs of the difference between the two types

of extrinsic LLRs. The CDF and PDF results were provided in Fig. 5.9 and Fig. 5.10, respectively, while a variety of statistical data concerning the difference between the two types of extrinsic LLRs were provided in Table 5.2. These numerical results coincide with the analytical results of Proposition 5.2, which points out the condition when the bit-wise extrinsic LLRs of the EB-Log-PDA and of the AB-Log-PDA are statistically closest to each other, and the condition when the difference between the two types of extrinsic LLRs becomes most significant. Finally, in Section 5.5.4 the complexity of the EB-Log-PDA based IDD was analytically compared to that of the AB-Log-PDA and to that of the family of Log-MAP based IDD schemes. It was shown that the decoupled model based EB-Log-PDA has a lower complexity than the non-decoupled model based AB-Log-PDA when the number of receive antennas is higher than that of transmit antennas. By comparing the results of Fig. 5.5, Fig. 5.7 and Fig. 4.18, we showed that although the IDD schemes employing the EB-Log-PDA and the AB-Log-PDA without incorporating any inner PDA iterations have a similar achievable performance close to that of the optimal MAP detector based IDD receiver, the PDA-based IDD schemes impose a significantly lower computational complexity in the scenarios considered.

- **Chapter 6:** [42, 43]

The MIMO detectors studied in Chapter 2 to Chapter 5 are equally applicable both to single-user MIMO systems and to the uplink of multiuser MIMO systems. By contrast, in Chapter 6, we considered the MIMO detection problem in the uplink of a multicell multiuser MIMO system, where a DPDA-SC scheme was proposed for the sake of exploiting the CCI. A realistic 19-cell hexagonal cellular model relying on unity frequency reuse was considered, as seen in Fig. 6.1 of Section 6.2, where both the BSs and the MSs are equipped with multiple antennas. Therefore, the performance of the system is limited by the CCI, including not only the traditional inter-cell and/or intra-cell interference, but also the inter-antenna interference. As seen in Section 6.3, cooperative joint processing of the uplink signals received from multiple co-channel MSs roaming within both the serving cell and the interfering cells is performed by introducing a so-called unified-client-server mode at the BSs. Local cooperation based message passing was used instead of a global message passing chain for the sake of reducing the backhaul traffic. The classic symbol-based PDA algorithm that had been used as a benchmark in Chapter 2 was employed as a low complexity solution for producing soft information, which facilitates the employment of SC at the individual BSs in order to generate the final soft decision metric. The simulations and discussions provided in Section 6.4 demonstrated that despite its low additional complexity and modest backhaul traffic, the proposed DPDA-SC reception scheme significantly outperforms the conventional non-cooperative benchmarks. Furthermore, since only the index of the possible discrete value of the quantized converged soft information has to be exchanged for SC in practice, the proposed DPDA-SC scheme is relatively robust to the quantization errors of the soft information exchanged. As a beneficial re-

sult, the backhaul traffic is dramatically reduced at a negligible performance degradation.

More specifically, in Section 6.2, the realistic 19-cell hexagonal cellular network model relying on the unity frequency reuse principle was described in detail, where both the BSs and MSs are equipped with multiple antennas. A snapshot of the dynamic network topology considered was depicted in Fig. 6.1, where each individual BS may serve multiple co-channel MSs located in different neighboring cells, and may also be assisted by another set of neighboring cells. For each BS, the two sets of neighboring cells, namely the sets of neighboring cells assisting or to be assisted by this particular BS, may have different set-size and different entries owing to the geographical distribution of co-channel MSs, which is a realistic situation rarely considered by existing literature [24]. Based on the topology of Fig. 6.1, the corresponding virtual MIMO uplink signal model was presented in Section 6.3.1, where both the perfect and imperfect CSI scenarios were considered. In Section 6.3.2, we described the first action of the DPDA-SC scheme, namely performing parallel detection using the classic symbol-based PDA algorithm discussed in Chapter 2 at each BS. Both the non-overloaded and overloaded scenarios were characterized. Then, the parallel message passing and sharing process, which is the second action of the DPDA-SC scheme, was described in Section 6.3.3. In Section 6.3.4, the SC and our final decision technique, namely the third action of the DPDA-SC scheme, was detailed. Having described the procedures of the DPDA-SC scheme, the complexity analysis of the DPDA-SC scheme was provided in Section 6.3.5, which demonstrated that at each BS the DPDA-SC has a low complexity increasing cubically with the number of simultaneously transmitted data streams in the uplink.

In Section 6.4, a comprehensive set of simulation results were provided for evaluating both the performance and the complexity of the proposed DPDA-SC scheme. To elaborate a little further, in the case of perfect CSI, the BER performance of the DPDA-SC and of several non-cooperative single-cell MUD schemes was compared in Fig. 6.3. It was observed that the BS cooperation aided DPDA-SC scheme of Section 6.3 substantially outperforms other benchmark receivers, including the optimal single-cell ML based MUD. Additionally, Fig. 6.4 compared the performance of the proposed DPDA-SC to that of several representative benchmark receivers in a realistic imperfect CSI scenario. It was observed in Fig. 6.4 that in the low-SNR region the DPDA-SC performs better than all the benchmark schemes considered, while in the high-SNR region, where the CCI plays a dominant role, all schemes considered suffer from different degrees of error floor due to the impact of channel estimation error. However, in Fig. 6.4 the DPDA-SC scheme was still seen to perform better than most of the benchmark schemes, except for the ML based MUD. Since the backhaul traffic constitutes a significant challenge faced by BS cooperation aided distributed processing, Fig. 6.5 investigated the impact of uniform quantization on the backhaul traffic and on the overall performance of the proposed DPDA-SC scheme, where uniform quantization of the converged probabilities

was performed and only the index of each probability value was transferred between the cooperative BSs. As a beneficial result, the backhaul traffic of the DPDA-SC scheme was significantly reduced. Additionally, it was shown in Fig. 6.5 that the performance loss due to the different number of quantization levels used for uniform quantization is marginal in the proposed DPDA-SC scheme. Furthermore, Fig. 6.6 characterized the performance of the DPDA-SC scheme in an overloaded rank-deficient scenario. It was observed in Fig. 6.6 that the DPDA-SC scheme's performance is still superior to that of the PDA based single-cell MUD, but both of them suffer from a significant performance loss due to the much stronger multi-stream interference. Fig. 6.7 characterized the convergence behavior of the proposed DPDA-SC scheme under both perfect and imperfect CSI conditions. It was observed in Fig. 6.7 that the DPDA-SC converges within a few iterations, which is another factor contributing to the low complexity of the DPDA-SC. Finally, in Fig. 6.8 the complexity of the DPDA-SC was numerically compared to that of three single-cell MUD schemes. It was shown in Fig. 6.8 that the complexity of the DPDA-SC is significantly lower than that of the ML based single-cell MUD, but marginally higher than that of the PDA and MMSE-OSIC based single-cell MUDs.

7.2 Future Work

In this section, a number of future research ideas concerning MIMO detection are discussed.

- **Performance Analysis of PDA-Based MIMO Detectors**

The family of PDA-based detectors, such as those studied in Chapters 2, 4, 5 and 6, have an iterative structure and the accuracy of the Gaussian approximation invoked in each iteration depends on the specific system parameters, including the number of transmit antennas, the size of modulation constellations and the operating SNR etc. Therefore, most of the existing contributions on PDA-based MIMO detectors rely on Monte Carlo simulations, rather than on rigorous mathematical analysis. However, in order to deepen our understanding of the PDA-based MIMO detectors, the rigorous analysis of their exact BER performance, diversity of order, convergence behavior and optimality condition should be the subject of future research, although these problems are particularly challenging. Furthermore, since the Gaussian approximation invoked in the PDA-based detectors becomes more accurate in large-scale systems [232, 421], it would be interesting to investigate the performance of the family of PDA-based detectors in “massive MIMO” systems [25], where the interference imposed on each user or each antenna tends to be Gaussian distributed. In this context, using large-system analysis techniques such as random matrix theory might be essential.

- **Performance Analysis of SDPR-Based MIMO Detectors in High-Order M -ary Modulation**

Most of the existing studies concerning the SDPR-based MIMO detectors, including our contributions in Chapter 3, are based on simulations and numerical results. Some analytical results on SDPR detectors are available in the limited context of BPSK/QPSK modulation [248, 249]. For example, in [248] the first analytical study of the SDPR detector was provided for BPSK-aided MIMO systems. It was shown that the SDPR detector is capable of achieving the same BER performance as that of the ML detector in high-SNR scenarios, while at the low-SNR region, the SDPR detector serves as a constant-factor approximation of the ML detector in large systems. Additionally, it was analytically demonstrated in [249] that the SDPR based detector is capable of achieving the full receive diversity order in BPSK-aided real-valued MIMO channels. However, the diversity order and performance bound of the SDPR detector in high-order M -ary modulation scenarios are unknown. Therefore, it would be valuable to provide the theoretical analysis of the SDPR detector in the context of high-order M -ary modulation scenarios.

- **Design of Near-Optimal SDPR-Based MIMO Detectors for High-Order M -ary Modulation**

The family of SDPR-based MIMO detection methods investigated in Chapter 3 have an attractive “polynomial-time” worst-case computational complexity. Both simulation and analytical results have shown that the SDPR-based MIMO detector may achieve a near-optimal performance in BPSK/QPSK scenario [248, 249]. However, as shown in [250–256] and in Chapter 3, the existing SDPR detectors suffer from a significant performance loss in high-order M -ary modulation scenarios. Therefore, two important questions have to be answered. Firstly, is it possible to design SDPR-based MIMO detectors capable of achieving near-optimal performance in the high-order M -ary modulation scenario, while still maintaining a low computational complexity? Secondly, if the answer to the first question is yes, then how can we design the near-optimal SDPR-based MIMO detectors for high-order M -ary modulation?

- **Design of SDPR-Based Soft Multi-Symbol Differential Detector**

Most of the SDPR-based MIMO detectors proposed in the existing literature [245–247, 250–256, 373] and in Chapter 3 are coherent detectors, which rely on the knowledge of the CSI of the MIMO channel considered. It is known that [422–426] the sphere decoder can be used for both coherent MIMO detection and non-coherent multi-symbol differential detection (MSDD). Similar to the case of a sphere decoder, the MSDD can also be implemented with the SDPR technique. For example, in [427] a SDPR-based MSDD scheme was proposed for a single-antenna aided system that uses differential QPSK (DQPSK) modulation. However, the scheme proposed in [427] is a hard-decision based scheme. Hence, it is beneficial to investigate how to design a soft-decision based SDPR-MSDD scheme. Additionally, the scheme proposed in [427] is only applicable to a single-antenna aided system. Therefore, it is promising to investigate how to design both the hard-decision and soft-decision based SDPR-MSDD schemes for MIMO systems.

- **Transceiver Design for “massive MIMO” systems**

In the emerging “massive MIMO” system [25], the BS might be equipped with numerous antennas to serve dozens of users. In the uplink of this system, the number of transmit antennas might be significantly lower than that of the receive antennas. Therefore, a potentially enormous receive diversity gain becomes available at the receiver, and the performance gap between the various detectors of the traditional small-scale MIMO systems might be compensated by the receive diversity gain. In other words, if a detector has a worse performance and a lower complexity than another in traditional small-scale MIMO systems, it is possible that the former becomes more attractive in the uplink of massive MIMO systems. This is because in this context both detectors may achieve a similar performance, but the former will have a significantly lower computational complexity. Therefore, it is necessary to examine the specific behavior of an entire suite of MIMO detectors in large-scale MIMO systems.

On the other hand, in the downlink of massive MIMO systems, it is expected that sophisticated precoding and beamforming techniques will be employed, and it is possible that some of the transmit antennas might not be activated if sophisticated antenna selection is used. Then the joint optimization of the transmitter and the receiver for massive MIMO systems constitutes an interesting and important problem. Additionally, if no precoding is used in the downlink, the downlink receiver faces a severely overloaded rank-deficient MIMO detection problem, which is very challenging. This is because the number of transmit antennas is significantly higher than that of the receive antennas, and hence the channel’s covariance matrix becomes rank-deficient.

Glossary

3GPP	Third Generation Partnership Project.
A-CPDA	approximate complex-valued probabilistic data association.
AB-Log-PDA	approximate Bayes' theorem based logarithmic-domain probabilistic data association.
AME	asymptotic-multiuser-efficiency.
AP	access point.
APP	<i>a posteriori</i> probability.
ASIC	application-specific integrated circuit.
AWGN	additive white Gaussian noise.
B-PDA	bit-based probabilistic data association.
BALM	block alternating likelihood maximization.
BC-SDPR	bound-constrained semidefinite programming relaxation.
BER	bit error rate.
BICM	bit-interleaved coded modulation.
BP	belief propagation.
BPSK	binary phase-shift keying.
BQP	Boolean quadratic programming.
BS	base station.
BSC	base station controller.
CAGR	compound annual growth rate.
CCI	co-channel interference.
CDF	cumulative density function.
CDM	code-division multiplexing.
CDMA	code-division multiple-access.
CIR	channel impulse response.
CLPS	closest lattice-point search.

CPDA	complex-valued probabilistic data association.
CQI	channel quality information.
CSI	channel state information.
CSPU	central signal processing unit.
DAS	distributed antenna system.
DFD	decision-feedback detector.
DID	distributed iterative detection.
DPDA	distributed probabilistic data association.
DQPSK	differential quadrature phase-shift keying.
DR	detectable range.
DS-CDMA	direct-sequence code-division multiple-access.
DSL	digital subscriber line.
DSNR	decreasing signal-to-noise ratio.
DVA-SDPR	direct-bit-based virtually antipodal semidefinite programming relaxation.
EB	exabytes.
EB-Log-PDA	exact Bayes' theorem based logarithmic-domain probabilistic data association.
EXIT	extrinsic information transfer.
FCSD	fixed-complexity sphere decoding/decoder.
FDM	frequency-division multiplexing.
FDMA	frequency-division multiple-access.
FEC	forward-error-correction.
FH-CDMA	frequency-hopped code-division multiple-access.
FIR	finite impulse response.
FLOP	floating point operation.
FR	frequency reuse.
GSNR	greatest signal-to-noise ratio.
HSPA	high speed packet access.
IAI	interantenna interference.
IC	interference cancellation.
ICI	interchannel interference.
IDD	iterative detection and decoding.
IEEE	Institute of Electrical and Electronics Engineers.
IMSE	increasing mean-square error.
IPA	interior point algorithm.
ISI	intersymbol interference.

IVA-SDPR	index-bit-based virtually antipodal semidefinite programming relaxation.
JD	joint detection.
JMLD	joint maximum likelihood detection.
JPDA	joint probabilistic data association.
LDPC	low-density parity-check.
LLR	logarithmic likelihood ratio.
LMI	linear matrix inequality.
LMR	linear matrix representation.
LMSE	least mean-square error.
LS	least-squares.
LSD	list sphere decoding.
LTE	Long Term Evolution.
LZF	linear zero-forcing.
M2M	machine-to-machine.
MAI	multiple-access interference.
MAME	maximum asymptotic-multiuser-efficiency.
MAP	maximum <i>a posteriori</i> .
MBER	minimum bit error rate.
MC-CDMA	multicarrier code-division multiple-access.
MF	matched filter.
MFSK	multiple frequency-shift keying.
MIC	multistage interference cancellation.
MIMO	multiple-input multiple-output.
ML	maximum likelihood.
MLSE	maximum likelihood sequence estimator/estimation.
MMSE	minimum mean-square error.
MS	mobile station.
MSDD	multi-symbol differential detection/detector.
MSI	multiple-stream interference.
MUD	multiuser detection/detector.
MUI	multiuser interference.
NP-complete	nondeterministic polynomial-time complete.
NP-hard	nondeterministic polynomial-time hard.
OFDMA	orthogonal frequency-division multiple-access.
OSIC	ordered successive interference cancellation.

PAM	pulse-amplitude modulation.
PD-IPA	primal-dual interior-point algorithm.
PDA	probabilistic data association.
PDF	probability density function.
PE	partial equalisation.
PI-SDPR	polynomial-inspired semidefinite programming relaxation.
PIC	parallel interference cancellation.
PSD	positive semidefinite.
PSK	phase-shift keying.
QAM	quadrature amplitude modulation.
QPSK	quadrature phase-shift keying.
RPDA	real-valued probabilistic data association.
SAIC	single-antenna interference cancellation.
SC	soft combining.
SC-FDMA	single-carrier frequency-division multiple-access.
SD	sphere decoding/decoder.
SDM	space-division multiplexing.
SDMA	space-division multiple-access.
SDP	semidefinite programming.
SDPR	semidefinite programming relaxation.
SE	Schnorr-Euchner.
SER	symbol error rate.
SIC	successive interference cancellation.
SISO	soft-input soft-output.
SNR	signal-to-noise ratio.
SP	set partitioning.
STBC	spacetime block code.
SUD	single-user detection.
SUMF	single-user matched filter.
TDM	time-division multiplexing.
TDMA	time-division multiple-access.
UCS	unified-client-server.
UE	user equipment.
UEP	unequal error protection.
UMR	unified matrix representation.

VA	virtually antipodal.
VA-SDPR	virtually antipodal semidefinite programming relaxation.
VB	Viterbo-Boutros.
VBLAST	vertical Bell Laboratories layered space-time.
VLSI	very-large-scale integration.
VNI	visual network index.
WiMAX	Worldwide Interoperability for Microwave Access.
WLS	weighted least-squares.
XOR	exclusive or.
ZF	zero-forcing.

List of Figures

1.1	Cisco VNI: global mobile data traffic forecast, 2012-2017.	2
1.2	Cisco VNI: share of different devices in the global mobile traffic forecast, 2012-2017.	2
1.3	Three fundamental domains of characterizing signals.	4
1.4	Limited duration-time vs infinite bandwidth: the reason why every active radio transmitter has an impact on every operating radio receiver.	4
1.5	Schematic of the point-to-point MIMO channel.	6
1.6	Schematic of the MIMO multiple-access channel.	7
1.7	Schematic of the MIMO broadcast channel.	7
1.8	Schematic of the MIMO broadcast channel.	8
1.9	Schematic of VBLAST-style SDM-MIMO systems.	10
1.10	The three historical periods in the development of MIMO detection.	14
1.11	Overview of representative MIMO detectors considered in this thesis.	15
1.12	Example of the optimal ML based MIMO detector in the context of $N_I = 2$ and BPSK modulation.	18
1.13	Euler digram for P, NP, NP-complete, NP-hard set of problems under both $P \neq NP$ and $P = NP$ assumptions.	19
1.14	Organization of the thesis.	34
1.15	The framework of novel contributions of the thesis.	38
2.1	Signal space diagram for 16-QAM under Gray mapping.	51
2.2	Signal space diagram for 64-QAM under Gray mapping.	53
2.3	Flow chart of the B-PDA algorithm.	59
2.4	The process of approximating a single-variate four-modal Gaussian mixture distribution by a single Gaussian distribution.	65
2.5	The process of approximating a single-variate bimodal Gaussian mixture distribution by a single Gaussian distribution.	66
2.6	Computational complexity comparison in terms of FLOPs per iteration and per symbol vector for B-PDA with natural bit mapping and CPDA with Gray bit mapping. BPSK ($M_c = 1$), 4-QAM ($M_c = 2$), 16-QAM ($M_c = 4$), and 64-QAM ($M_c = 6$) are considered, SNR = 20dB, and $N_t = N_r = 2$	69
2.7	Computational complexity of B-PDA under different SNR values for 16-QAM and 64-QAM, $N_t = N_r = 2$	69
2.8	Impact of the number of iterations on the achievable performance of CPDA and B-PDA in VBLAST using 16-QAM, $N_t = N_r = 2$	71
2.9	BER comparison of B-PDA and CPDA, MMSE-OSIC, ML in VBLAST with 16-QAM, $I_{max}=5$, $N_t = N_r = 2$	71
2.10	BER comparison of B-PDA and CPDA, MMSE-OSIC, ML in VBLAST with 64-QAM, $I_{max}=5$, $N_t = N_r = 2$	72
2.11	SER comparison of B-PDA and CPDA, MMSE-OSIC, ML in VBLAST with 16-QAM, $I_{max}=5$, $N_t = N_r = 2$	72
2.12	SER comparison of B-PDA and CPDA, MMSE-OSIC, ML in VBLAST with 64-QAM, $I_{max}=5$, $N_t = N_r = 2$	73
3.1	Convex set versus nonconvex set.	79

3.2	Example of a convex function.	80
3.3	Framework of solving problems using convex optimization.	82
3.4	Constellation decomposition of the Gray-mapping aided 16-QAM.	88
3.5	Impact of the convergence tolerance $\epsilon = 10^{-k}$ on the performance of the DVA-SDPR for 16-QAM aided (8×8) -element MIMO over uncorrelated flat Rayleigh fading channels.	97
3.6	Impact of the convergence tolerance $\epsilon = 10^{-k}$ on the complexity of the DVA-SDPR for 16-QAM aided (8×8) -element MIMO over uncorrelated flat Rayleigh fading channels.	97
3.7	UEP effect of the DVA-SDPR for Gray-coded 16-QAM aided (8×8) -element MIMO over uncorrelated flat Rayleigh fading channels, with the convergence tolerance $\epsilon = 10^{-9}$	98
3.8	Performance comparison of the DVA-SDPR, IVA-SDPR, SD and MMSE-OSIC detectors for 16-QAM aided (8×8) -element MIMO over uncorrelated flat Rayleigh fading channels.	99
3.9	Complexity comparison of the DVA-SDPR, IVA-SDPR, SD and MMSE-OSIC detectors for 16-QAM aided (8×8) -element MIMO.	100
3.10	Complexity comparison of the DVA-SDPR and the SD based detectors for 16-QAM aided massive MIMOs where the value of N_t can be very high.	101
4.1	The optimal vector-by-vector based detection strategy for uncoded MIMO systems.	106
4.2	The optimal MLSE based joint detection-and-decoding strategy conceived for FEC-coded MIMO systems.	106
4.3	The near-optimal MAP based iterative detection and decoding strategy designed for FEC-coded MIMO systems.	107
4.4	The FEC-coded MIMO system relying on the classic IDD receiver architecture, where we have both $\mathbf{L}_{E_1} = \mathbf{L}_{D_1} - \mathbf{L}_{A_1}$ and $\mathbf{L}_{E_2} = \mathbf{L}_{D_2} - \mathbf{L}_{A_2}$	110
4.5	The initial multimodal Gaussian mixture PDF of the interference-plus-noise term, when we have no <i>a priori</i> knowledge about the interference symbols before performing symbol detection.	113
4.6	The multimodal Gaussian mixture PDF of the interference-plus-noise term after performing the PDA-based detection, when we have a relatively strong belief about the correct value of the desired symbol.	114
4.7	Schematic of the FEC-coded MIMO system relying on a simplified structure for the AB-Log-PDA based IDD receiver, where we have $\mathbf{L}_{E_2} = \mathbf{L}_{D_2}$ rather than the classical $\mathbf{L}_{E_2} = \mathbf{L}_{D_2} - \mathbf{L}_{A_2}$	122
4.8	Impact of the number of inner iterations on the achievable BER of the AB-Log-PDA based IDD scheme.	124
4.9	The fine details of the impact of inner PDA iterations on the achievable performance of the symbol-based PDA detector in an uncoded MIMO system, where we have $N_t = N_r = 2$, and 4QAM is used.	125
4.10	The fine details of the convergence profile of a single symbol's probability $P(s_i = a_m \mathbf{y})$ in an uncoded MIMO system, where we have $N_t = N_r = 2$, and 4QAM is used.	126
4.11	The impact of inner PDA iterations on the consistency of LLRs output by the AB-Log-PDA detector.	127
4.12	EXIT chart analysis of the AB-Log-PDA (dispensing with its inner iterations) and the Exact-Log-MAP based IDD schemes.	128
4.13	Impact of the number of outer iterations on the achievable BER of the AB-Log-PDA (dispensing with its inner iterations) and the Exact-Log-MAP based IDD schemes.	128
4.14	Impact of Nakagami- m fading parameter m on the achievable BER of the AB-Log-PDA (dispensing with its inner iterations) and the Exact-Log-MAP based IDD schemes.	129
4.15	Impact of the modulation order on the achievable BER of the AB-Log-PDA (dispensing with its inner iterations) and the Exact-Log-MAP based IDD schemes.	130
4.16	Impact of the number of transmit antennas on the achievable BER of the AB-Log-PDA (dispensing with its inner iterations) and the Exact-Log-MAP based IDD schemes.	131
4.17	Impact of channel-estimation error on the achievable BER of the AB-Log-PDA (dispensing with its inner iterations) and the Exact-Log-MAP based IDD schemes.	132

4.18	Computational complexity comparison of the AB-Log-PDA (dispensing with its inner iterations) and the Exact-Log-MAP algorithms in terms of the number of real-valued operations N_{RO} .	133
5.1	The FEC-coded MIMO system relying on the EB-Log-PDA method based IDD receiver.	138
5.2	BER of the AB-Log-PDA based IDD scheme, where the nominal symbol-wise APPs were misinterpreted as the true symbol-wise APPs.	144
5.3	The role of the <i>a priori</i> information in the AB-Log-PDA and the EB-Log-PDA algorithms. These two blocks distinguish Fig. 4.7 and Fig. 5.1.	147
5.4	EXIT chart analysis of the EB-Log-PDA, AB-Log-PDA and Exact-Log-MAP based IDD schemes.	149
5.5	Impact of the number of outer iterations on BER of the EB-Log-PDA based IDD scheme.	149
5.6	Impact of the number of inner iterations within the EB-Log-PDA on BER of the EB-Log-PDA based IDD scheme.	150
5.7	Impact of the number of inner PDA iterations on BER of the AB-Log-PDA based IDD scheme, as well as the BER comparison between the EB-Log-PDA and AB-Log-PDA based IDD schemes with $it_o = 3$.	151
5.8	Impact of the number of inner iterations on BER of the AB-Log-PDA and EB-Log-PDA MIMO detectors, evaluated using \mathbf{L}_{D_2} at the output of the MIMO detectors for FEC-coded bits \mathbf{d}_2 in Fig. 5.1, $it_o = 3$.	152
5.9	The cumulative distribution functions of $\Delta L_i = L_E^{EB}(i) - L_E^{AB}(i)$, for samples of 240,000 bits, $it_i = 0$ inner PDA iteration, and $m = 1.0$.	152
5.10	The probability density functions of $\Delta L_i = L_E^{EB}(i) - L_E^{AB}(i)$, for samples of 240,000 bits, $it_i = 0$ inner PDA iteration, and $m = 1.0$.	154
6.1	An example setup showing a 19-cell hexagonal cellular model with inter-cell CCI and unity FR.	160
6.2	Various types of location-dependent interferer distributions for a specific MS roaming in the cellular network of Fig. 6.1.	162
6.3	BER performance comparison of DPDA-SC, ML JD, SCSU LZF, SU ML bound and SU PDA bound under perfect CSI and different interference intensity ρ , which is defined in (6.2). Each individual BS may have a BER record for its own MS, and without loss of generality, the BER shown here is recorded at BS0 for MS0. QPSK modulation is used at each MS.	169
6.4	Performance comparison of different reception schemes under different levels of channel estimation quality $\beta = 0.98$ and $\beta = 0.99$, and a given interference intensity $\rho = 0.8$, using QPSK modulation.	171
6.5	Uniform quantization impact on the performance of DPDA-SC under perfect CSI and a given interference intensity $\rho = 0.8$, using QPSK modulation.	172
6.6	Performance of DPDA-SC in rank-deficient scenario, $M_b = 8, M_u = 4, C_u = 3, C_b = 3$, with perfect CSI and a given interference intensity $\rho = 0.8$, using QPSK modulation.	173
6.7	Convergence property of DPDA-SC, SNR = 6dB, QPSK, $\rho = 0.8$.	174
6.8	Complexity comparison of different reception schemes, measured in terms of the number of equivalent additions per bit, SNR = 6dB. QPSK, $\beta = 0.98, \rho = 0.8$.	174

List of Tables

1.1	Milestones in the development of the optimal MIMO detector	20
1.2	Milestones in the development of linear MIMO detectors	23
1.3	Milestones in the development of interference cancellation MIMO detectors	27
1.4	Milestones in the development of the tree-search MIMO detectors: Depth-first type	29
1.5	Milestones in the development of the tree-search MIMO detectors: Breadth-first type	30
1.6	Milestones in the development of the tree-search MIMO detectors: best-first type	30
1.7	Milestones in the development of the PDA-based MIMO detectors	32
1.8	Milestones in the development of the SDPR-based MIMO detectors	35
2.1	Look-up table for Gray constellation mapping of 4-QAM	45
2.2	Generating units of 16-QAM using Gray mapping	52
2.3	Generating units of 64-QAM using Gray mapping	55
2.4	UMR rule of Gray mapping	56
2.5	An example of updating probability table for B-PDA.	63
2.6	Probabilities computed in one iteration of conventional symbol-based CPDA	68
2.7	Probabilities computed in one iteration for B-PDA	68
3.1	Gray-mapping based QAM transformation	90
4.1	Summary of the AB-Log-PDA based IDD algorithm	118
4.2	Global simulation parameters	123
5.1	Summary of the EB-Log-PDA algorithm	143
5.2	Statistical comparison of \mathbf{L}_E^{EB} and \mathbf{L}_E^{AB} for samples of 240,000 bits, $it_i = 0$ inner PDA iteration, and $m = 1.0$	153

Bibliography

- [1] D. Mcqueen, “The momentum behind LTE adoption,” *IEEE Communications Magazine*, vol. 47, no. 2, pp. 44–45, Feb. 2009.
- [2] K. Lee, J. Lee, Y. Yi, I. Rhee, and S. Chong, “Mobile data offloading: how much can WiFi deliver?” in *Proc. ACM 6th International Conference on emerging Networking EXperiments and Technologies (CoNEXT’10)*, Philadelphia, Pennsylvania, USA, Dec. 2010, pp. 26:1–26:12. [Online]. Available: <http://doi.acm.org/10.1145/1921168.1921203>
- [3] M. El-Sayed, A. Mukhopadhyay, C. Urrutia-Valdés, and Z. J. Zhao, “Mobile data explosion: monetizing the opportunity through dynamic policies and QoS pipes,” *Bell Labs Technical Journal*, vol. 16, no. 2, pp. 79–99, Sep. 2011. [Online]. Available: <http://dx.doi.org/10.1002/bltj.20504>
- [4] P. Ranganathan, “From microprocessors to nanostores: rethinking data-centric systems,” *IEEE Computer Magazine*, vol. 44, no. 1, pp. 39–48, Jan. 2011.
- [5] B. Han, P. Hui, V. S. A. Kumar, M. V. Marathe, J. Shao, and A. Srinivasan, “Mobile data offloading through opportunistic communications and social participation,” *IEEE Transactions on Mobile Computing*, vol. 11, no. 5, pp. 821–834, May 2012.
- [6] “Cisco Visual Networking Index: Global Mobile Data Traffic Forecast Update, 2012-2017,” White Paper, Cisco, Feb. 2013. [Online]. Available: http://www.cisco.com/en/US/solutions/collateral/ns341/ns525/ns537/ns705/ns827/white_paper_c11-520862.pdf
- [7] Cisco Visual Networking Index (VNI). Cisco. [Online]. Available: http://www.cisco.com/en/US/netsol/ns827/networking_solutions_sub_solution.html
- [8] G. Lawton, “Machine-to-machine technology gears up for growth,” *IEEE Computer Magazine*, vol. 37, no. 9, pp. 12–15, Sep. 2004.
- [9] I. Cha, Y. Shah, A. U. Schmidt, A. Leicher, and M. V. Meyerstein, “Trust in M2M communication,” *IEEE Vehicular Technology Magazine*, vol. 4, no. 3, pp. 69–75, Sep. 2009.
- [10] B. Emmerson, “M2M: the internet of 50 billion devices,” *Huawei WinWin Magazine*, no. 4, pp. 19–22, Jan. 2010. [Online]. Available: <http://www-cnc.huawei.com/de/static/HW-072296.pdf>

- [11] M. Starsinic, "System architecture challenges in the home M2M network," in *Proc. IEEE 6th Annual Conference on Long Island Systems Applications and Technology (LISAT'10)*, Farmingdale, NY, USA, May 2010, pp. 1–7.
- [12] Y. Chen and W. Wang, "Machine-to-machine communication in LTE-A," in *Proc. IEEE 72nd Vehicular Technology Conference (VTC'10-Fall)*, Ottawa, ON, Canada, Sep. 2010, pp. 1–4.
- [13] Z. M. Fadlullah, M. M. Fouda, N. Kato, A. Takeuchi, N. Iwasaki, and Y. Nozaki, "Toward intelligent machine-to-machine communications in smart grid," *IEEE Communications Magazine*, vol. 49, no. 4, pp. 60–65, Apr. 2011.
- [14] D. Niyato, L. Xiao, and P. Wang, "Machine-to-machine communications for home energy management system in smart grid," *IEEE Communications Magazine*, vol. 49, no. 4, pp. 53–59, Apr. 2011.
- [15] S.-Y. Lien, K.-C. Chen, and Y. Lin, "Toward ubiquitous massive accesses in 3GPP machine-to-machine communications," *IEEE Communications Magazine*, vol. 49, no. 4, pp. 66–74, Apr. 2011.
- [16] R. Lu, X. Li, X. Liang, X. Shen, and X. Lin, "GRS: the green, reliability, and security of emerging machine to machine communications," *IEEE Communications Magazine*, vol. 49, no. 4, pp. 28–35, Apr. 2011.
- [17] G. Wu, S. Talwar, K. Johansson, N. Himayat, and K. D. Johnson, "M2M: from mobile to embedded internet," *IEEE Communications Magazine*, vol. 49, no. 4, pp. 36–43, Apr. 2011.
- [18] Y. Zhang, R. Yu, S. Xie, W. Yao, Y. Xiao, and M. Guizani, "Home M2M networks: architectures, standards, and QoS improvement," *IEEE Communications Magazine*, vol. 49, no. 4, pp. 44–52, Apr. 2011.
- [19] S.-Y. Lien and K.-C. Chen, "Massive access management for QoS guarantees in 3GPP machine-to-machine communications," *IEEE Communications Letters*, vol. 15, no. 3, pp. 311–313, Mar. 2011.
- [20] United States Frequency Allocation Chart: August 2011 Edition. National Telecommunications and Information Administration, United States Department of Commerce. [Online]. Available: http://www.ntia.doc.gov/files/ntia/publications/spectrum_wall_chart_aug2011.pdf
- [21] A. Paulraj, R. Nabar, and D. Gore, *Introduction to Space-Time Wireless Communications*. Cambridge University Press, 2003.
- [22] D. Gesbert, M. Kountouris, R. W. Heath, C.-B. Chae, and T. Salzer, "Shifting the MIMO paradigm: from single-user to multiuser communications," *IEEE Signal Processing Magazine*, vol. 24, no. 5, pp. 36–46, Oct. 2007.
- [23] J. Mietzner, R. Schober, L. Lampe, W. H. Gerstacker, and P. A. Hoeher, "Multiple-antenna techniques for wireless communications – a comprehensive literature survey," *IEEE Communications Surveys & Tutorials*, vol. 11, no. 2, pp. 87–105, Second Quarter 2009.
- [24] D. Gesbert, S. V. Hanly, H. Huang, S. Shamai (Shitz), O. Simeone, and W. Yu, "Multi-cell MIMO cooperative networks: a new look at interference," *IEEE Journal on Selected Areas in Communications*, vol. 28, no. 9, pp. 1380–1408, Dec. 2010.

- [25] F. Rusek, D. Persson, B. K. Lau, E. G. Larsson, T. L. Marzetta, O. Edfors, and F. Tufvesson, "Scaling up MIMO: opportunities and challenges with very large arrays," *IEEE Signal Processing Magazine*, vol. 30, no. 1, pp. 40–60, Jan. 2013.
- [26] C. Han, T. Harrold, S. Armour, I. Krikidis, S. Videv, P. M. Grant, H. Haas, J. S. Thompson, I. Ku, C.-X. Wang, T. A. Le, M. R. Nakhai, J. Zhang, and L. Hanzo, "Green radio: radio techniques to enable energy-efficient wireless networks," *IEEE Communications Magazine*, vol. 49, no. 6, pp. 46–54, Jun. 2011.
- [27] S. V. Hanly and P. Whiting, "Information-theoretic capacity of multi-receiver networks," *Telecommunication Systems*, vol. 1, no. 1, pp. 1–42, 1993.
- [28] A. D. Wyner, "Shannon-theoretic approach to a Gaussian cellular multiple-access channel," *IEEE Transactions on Information Theory*, vol. 40, no. 6, pp. 1713–1727, Nov. 1994.
- [29] S. Shamai (Shitz) and A. D. Wyner, "Information-theoretic considerations for symmetric, cellular, multiple-access fading channels – Part I," *IEEE Transactions on Information Theory*, vol. 43, no. 6, pp. 1877–1894, Nov. 1997.
- [30] —, "Information-theoretic considerations for symmetric, cellular, multiple-access fading channels – Part II," *IEEE Transactions on Information Theory*, vol. 43, no. 6, pp. 1895–1911, Nov. 1997.
- [31] O. Somekh and S. Shamai (Shitz), "Shannon-theoretic approach to a Gaussian cellular multiple-access channel with fading," *IEEE Transactions on Information Theory*, vol. 46, no. 4, pp. 1401–1425, Jul. 2000.
- [32] S. Catreux, P. F. Driessen, and L. J. Greenstein, "Simulation results for an interference-limited multiple-input multipleoutput cellular system," *IEEE Communications Letters*, vol. 4, no. 11, pp. 334–336, Nov. 2000.
- [33] —, "Attainable throughput of an interference-limited multiple-input multiple-output (MIMO) cellular system," *IEEE Transactions on Communications*, vol. 49, no. 8, pp. 1307–1311, Aug. 2001.
- [34] R. S. Blum, J. H. Winters, and N. R. Sollenberger, "On the capacity of cellular systems with MIMO," *IEEE Communications Letters*, vol. 6, no. 6, pp. 242–244, Jun. 2002.
- [35] H. Dai, A. F. Molisch, and H. V. Poor, "Downlink capacity of interference-limited MIMO system with joint detection," *IEEE Transactions on Wireless Communications*, vol. 3, no. 2, pp. 442–453, Mar. 2004.
- [36] D. N. C. Tse and P. Viswanath, *Fundamentals of Wireless Communication*. Cambridge, UK: Cambridge University Press, 2005.
- [37] P. van Emde Boas, "Another NP-complete partition problem and the complexity of computing short vectors in a lattice," Department of Mathematics, University of Amsterdam, The Netherlands, Tech. Rep. 81-04, Apr. 1981.
- [38] S. Verdú, "Computational complexity of optimum multiuser detection," *Algorithmica*, vol. 4, no. 1-4, pp. 303–312, Jun. 1989. [Online]. Available: <http://dx.doi.org/10.1007/BF01553893>
- [39] D. Micciancio, "The hardness of the closest vector problem with preprocessing," *IEEE Transactions on Information Theory*, vol. 47, no. 3, pp. 1212–1215, Mar. 2001.

- [40] S. Yang, T. Lv, and L. Hanzo, "Unified bit-based probabilistic data association aided MIMO detection for high-order QAM," in *Proc. IEEE Wireless Communications and Networking Conference (WCNC'11)*, Cancun, Mexico, Mar. 2011, pp. 1629–1634.
- [41] S. Yang, T. Lv, R. G. Maunder, and L. Hanzo, "Unified bit-based probabilistic data association aided MIMO detection for high-order QAM constellations," *IEEE Transactions on Vehicular Technology*, vol. 60, no. 3, pp. 981–991, Mar. 2011.
- [42] S. Yang, T. Lv, and L. Hanzo, "Base station cooperation in MIMO-aided multi-user multi-cell systems employing distributed probabilistic data association based soft reception," in *Proc. IEEE International Conference on Communications (ICC'11)*, Kyoto, Japan, Jun. 2011, pp. 1–5.
- [43] S. Yang, T. Lv, R. G. Maunder, and L. Hanzo, "Distributed probabilistic-data-association-based soft reception employing base station cooperation in MIMO-aided multiuser multicell systems," *IEEE Transactions on Vehicular Technology*, vol. 60, no. 7, pp. 3532–3538, Sep. 2011.
- [44] S. Yang and L. Hanzo, "Iterative detection and decoding using approximate Bayesian theorem based PDA method over MIMO Nakagami- m fading channels," in *Proc. IEEE Global Communications Conference (GLOBECOM'12)*, Anaheim, CA, USA, Dec. 2012, pp. 3588–3593.
- [45] S. Yang, L. Wang, T. Lv, and L. Hanzo, "Approximate Bayesian probabilistic-data-association-aided iterative detection for MIMO systems using arbitrary M -ary modulation," *IEEE Transactions on Vehicular Technology*, vol. 62, no. 3, pp. 1228–1240, Mar. 2013.
- [46] S. Yang and L. Hanzo, "Exact Bayes' theorem based probabilistic data association for iterative MIMO detection and decoding," in *Proc. IEEE Global Communications Conference (GLOBECOM'13)*, Atlanta, GA, USA, Dec. 2013.
- [47] S. Yang, T. Lv, R. G. Maunder, and L. Hanzo, "From nominal to true *a posteriori* probabilities: an exact Bayesian theorem based probabilistic data association approach for iterative MIMO detection and decoding," *IEEE Transactions on Communications*, vol. 61, no. 7, pp. 2782–2793, Jul. 2013.
- [48] S. Yang and L. Hanzo, "Semidefinite programming relaxation based virtually antipodal detection for Gray coded 16-QAM MIMO signalling," in *Proc. IEEE Global Telecommunications Conference (GLOBECOM'11)*, Houston, TX, USA, Dec. 2011, pp. 1–5.
- [49] S. Yang, T. Lv, and L. Hanzo, "Semidefinite programming relaxation based virtually antipodal detection for MIMO systems using gray-coded high-order QAM," *IEEE Transactions on Vehicular Technology*, vol. 62, no. 4, pp. 1667–1677, 2013.
- [50] A. Duel-Hallen, J. M. Holtzman, and Z. Zvonar, "Multiuser detection for CDMA systems," *IEEE Personal Communications Magazine*, vol. 2, no. 2, pp. 46–58, Apr. 1995.
- [51] S. Moshavi, "Multi-user detection for DS-CDMA communications," *IEEE Communications Magazine*, vol. 34, no. 10, pp. 124–136, Oct. 1996.
- [52] S. Verdú, *Multiuser Detection*. Cambridge, UK: Cambridge University Press, 1998.
- [53] M. L. Honig, Ed., *Advances in Multiuser Detection*. John Wiley & Sons, Inc., 2009.

- [54] E. Viterbo and J. Boutros, "A universal lattice code decoder for fading channels," *IEEE Transactions on Information Theory*, vol. 45, no. 7, pp. 1639–1642, Jul. 1999.
- [55] E. Agrell, T. Eriksson, A. Vardy, and K. Zeger, "Closest point search in lattices," *IEEE Transactions on Information Theory*, vol. 48, no. 8, pp. 2201–2214, Aug. 2002.
- [56] M. O. Damen, A. Chkeif, and J.-C. Belfiore, "Lattice code decoder for space-time codes," *IEEE Communications Letters*, vol. 4, no. 5, pp. 161–163, May 2000.
- [57] M. O. Damen, K. Abed-Meraim, and J.-C. Belfiore, "Generalised sphere decoder for asymmetrical space-time communication architecture," *Electronics Letters*, vol. 36, no. 2, pp. 166–167, Jan. 2000.
- [58] M. O. Damen, H. El Gamal, and G. Caire, "On maximum-likelihood detection and the search for the closest lattice point," *IEEE Transactions on Information Theory*, vol. 49, no. 10, pp. 2389–2402, Oct. 2003.
- [59] B. Hassibi and H. Vikalo, "On the sphere-decoding algorithm I. expected complexity," *IEEE Transactions on Signal Processing*, vol. 53, no. 8, pp. 2806–2818, Aug. 2005.
- [60] H. Vikalo and B. Hassibi, "On the sphere-decoding algorithm II. generalizations, second-order statistics, and applications to communications," *IEEE Transactions on Signal Processing*, vol. 53, no. 8, pp. 2819–2834, Aug. 2005.
- [61] J. Jaldén and B. Ottersten, "On the complexity of sphere decoding in digital communications," *IEEE Transactions on Signal Processing*, vol. 53, no. 4, pp. 1474–1484, Apr. 2005.
- [62] A. Burg, M. Borgmann, M. Wenk, M. Zellweger, W. Fichtner, and H. Bolcskei, "VLSI implementation of MIMO detection using the sphere decoding algorithm," *IEEE Journal of Solid-State Circuits*, vol. 40, no. 7, pp. 1566–1577, Jul. 2005.
- [63] K.-W. Wong, C.-Y. Tsui, R. S. Cheng, and W.-H. Mow, "A VLSI architecture of a K-best lattice decoding algorithm for MIMO channels," in *Proc. IEEE International Symposium on Circuits and Systems (ISCAS'02)*, Scottsdale, AZ, USA, May 2002, pp. III-273–III-276.
- [64] Z. Guo and P. Nilsson, "Algorithm and implementation of the K-best sphere decoding for MIMO detection," *IEEE Journal on Selected Areas in Communications*, vol. 24, no. 3, pp. 491–503, Mar. 2006.
- [65] S. Chen, T. Zhang, and Y. Xin, "Relaxed K-best MIMO signal detector design and VLSI implementation," *IEEE Transactions on Very Large Scale Integration (VLSI) Systems*, vol. 15, no. 3, pp. 328–337, 2007.
- [66] C. Studer, A. Burg, and H. Bolcskei, "Soft-output sphere decoding: algorithms and VLSI implementation," *IEEE Journal on Selected Areas in Communications*, vol. 26, no. 2, pp. 290–300, Feb. 2008.
- [67] A. R. Murugan, H. El Gamal, M. O. Damen, and G. Caire, "A unified framework for tree search decoding: rediscovering the sequential decoder," *IEEE Transactions on Information Theory*, vol. 52, no. 3, pp. 933–953, Mar. 2006.
- [68] R. Gowaikar and B. Hassibi, "Statistical pruning for near-maximum likelihood decoding," *IEEE Transactions on Signal Processing*, vol. 55, no. 6, pp. 2661–2675, Jun. 2007.

- [69] K. Lee and J. Chun, "ML symbol detection based on the shortest path algorithm for MIMO systems," *IEEE Transactions on Signal Processing*, vol. 55, no. 11, pp. 5477–5484, Nov. 2007.
- [70] M. Stojnic, H. Vikalo, and B. Hassibi, "Speeding up the sphere decoder with H^∞ and SDP inspired lower bounds," *IEEE Transactions on Signal Processing*, vol. 56, no. 2, pp. 712–726, Feb. 2008.
- [71] T.-H. Kim and I.-C. Park, "High-throughput and area-efficient MIMO symbol detection based on modified Dijkstra's search," *IEEE Transactions on Circuits and Systems I: Regular Papers*, vol. 57, no. 7, pp. 1756–1766, Jul. 2010.
- [72] R. Y. Chang, W.-H. Chung, and S.-J. Lin, "A* algorithm inspired memory-efficient detection for MIMO systems," *IEEE Wireless Communications Letters*, vol. 1, no. 5, pp. 508–511, Oct. 2012.
- [73] R. Y. Chang and W.-H. Chung, "Best-first tree search with probabilistic node ordering for MIMO detection: generalization and performance-complexity tradeoff," *IEEE Transactions on Wireless Communications*, vol. 11, no. 2, pp. 780–789, Feb. 2012.
- [74] J. W. Choi, B. Shim, and A. C. Singer, "Efficient soft-input soft-output tree detection via an improved path metric," *IEEE Transactions on Information Theory*, vol. 58, no. 3, pp. 1518–1533, Mar. 2012.
- [75] B. M. Hochwald and S. ten Brink, "Achieving near-capacity on a multiple-antenna channel," *IEEE Transactions on Communications*, vol. 51, no. 3, pp. 389–399, Mar. 2003.
- [76] J. Boutros, N. Gresset, L. Brunel, and M. Fossorier, "Soft-input soft-output lattice sphere decoder for linear channels," in *Proc. IEEE Global Telecommunications Conference (GLOBECOM'03)*, San Francisco, USA, Dec. 2003, pp. 1583–1587.
- [77] H. Vikalo, B. Hassibi, and T. Kailath, "Iterative decoding for MIMO channels via modified sphere decoding," *IEEE Transactions on Wireless Communications*, vol. 3, no. 6, pp. 2299–2311, Nov. 2004.
- [78] R. Wang and G. B. Giannakis, "Approaching MIMO channel capacity with soft detection based on hard sphere decoding," *IEEE Transactions on Communications*, vol. 54, no. 4, pp. 587–590, Apr. 2006.
- [79] C. Studer and H. Bolcskei, "Soft-input soft-output single tree-search sphere decoding," *IEEE Transactions on Information Theory*, vol. 56, no. 10, pp. 4827–4842, Oct. 2010.
- [80] M. Rachid and B. Daneshrad, "Iterative MIMO sphere decoding throughput guarantees under realistic channel conditions," *IEEE Communications Letters*, vol. 14, no. 4, pp. 342–344, Apr. 2010.
- [81] L. G. Barbero and J. S. Thompson, "Fixing the complexity of the sphere decoder for mimo detection," *IEEE Transactions on Wireless Communications*, vol. 7, no. 6, pp. 2131–2142, Jun. 2008.
- [82] —, "Extending a fixed-complexity sphere decoder to obtain likelihood information for turbo-mimo systems," *IEEE Transactions on Vehicular Technology*, vol. 57, no. 5, pp. 2804–2814, Sep. 2008.

-
- [83] J. Jaldén, L. G. Barbero, B. Ottersten, and J. S. Thompson, “The error probability of the fixed-complexity sphere decoder,” *IEEE Transactions on Signal Processing*, vol. 57, no. 7, pp. 2711–2720, Jul. 2009.
- [84] W. C. Y. Lee, “Overview of cellular CDMA,” *IEEE Transactions on Vehicular Technology*, vol. 40, no. 2, pp. 291–302, May 1991.
- [85] P. Jung, P. W. Baier, and A. Steil, “Advantages of CDMA and spread spectrum techniques over FDMA and TDMA in cellular mobile radio applications,” *IEEE Transactions on Vehicular Technology*, vol. 42, no. 3, pp. 357–364, Aug. 1993.
- [86] A. J. Viterbi, *CDMA: Principles of Spread Spectrum Communication*, 1st ed. Addison-Wesley, 1995.
- [87] R. H. Roy and B. Ottersten, “Spatial division multiple access wireless communication systems,” U.S. Patent 5 515 378, May 7, 1996.
- [88] D. Gerlach, “Adaptive transmitting antenna arrays at the base station in mobile radio networks,” Ph.D. dissertation, Department of Electrical Engineering, Stanford University, California, USA, 1995.
- [89] B. Ottersten, “Array processing for wireless communications,” in *Proc. 8th IEEE Signal Processing Workshop on Statistical Signal and Array Processing*, Corfu, Greece, Jun. 1996, pp. 466–473.
- [90] R. H. Roy, “Spatial division multiple access technology and its application to wireless communication systems,” in *Proc. IEEE 47th Vehicular Technology Conference (VTC’97)*, Phoenix, AZ, USA, May 1997, pp. 730–734.
- [91] M. P. Lotter and P. van Rooyen, “Space division multiple access for cellular CDMA,” in *Proc. IEEE 5th International Symposium on Spread Spectrum Techniques and Applications (ISSSTA ’98)*, Sun City, South Africa, Sep. 1998, pp. 959–964.
- [92] P. Vandenameele, L. Van der Perre, and M. Engels, *Space Division Multiple Access for Wireless Local Area Networks*. Norwell, MA, USA: Kluwer, 2001.
- [93] A. Goldsmith, *Wireless Communications*, 1st ed. Cambridge University Press, 2005.
- [94] A. V. Oppenheim, A. S. Willsky, and S. H. Nawab, *Signals and Systems*, 2nd ed. Upper Saddle River, NJ, USA: Prentice-Hall, 1996.
- [95] B. Sklar, *Digital Communications: Fundamentals and Applications*, 2nd ed. Upper Saddle River, NJ, USA: Prentice-Hall, 2001.
- [96] T. S. Rappaport, *Wireless Communications: Principles and Practice*, 2nd ed. Upper Saddle River, NJ: Prentice Hall, 2002.
- [97] J. G. Proakis, *Digital Signal Processing: Principles, Algorithms and Applications*, 4th ed. Pearson Education, 2007.
- [98] S. Haykin, *Adaptive Filter Theory*, 4th ed. Upper Saddle River, NJ: Prentice Hall, 2002.
- [99] A. Jamalipour, T. Wada, and T. Yamazato, “A tutorial on multiple access technologies for beyond 3G mobile networks,” *IEEE Communications Magazine*, vol. 43, no. 2, pp. 110–117, Feb. 2005.

- [100] S. Kandukuri and S. Boyd, "Optimal power control in interference-limited fading wireless channels with outage-probability specifications," *IEEE Transactions on Wireless Communications*, vol. 1, no. 1, pp. 46–55, Jan. 2002.
- [101] G. J. Foschini, "Layered space-time architecture for wireless communication in a fading environment when using multi-element antennas," *Bell Labs Technical Journal*, vol. 1, no. 2, pp. 41–59, 1996.
- [102] P. W. Wolniansky, G. J. Foschini, G. D. Golden, and R. A. Valenzuela, "V-BLAST: an architecture for realizing very high data rates over the rich-scattering wireless channel," in *Proc. URSI International Symposium on Signals, Systems, and Electronics (ISSSE'98)*, Pisa, Italy, Sep. 1998, pp. 295–300.
- [103] G. D. Golden, G. J. Foschini, R. A. Valenzuela, and P. W. Wolniansky, "Detection algorithm and initial laboratory results using V-BLAST space-time communication architecture," *Electronics Letters*, vol. 35, no. 1, pp. 14–16, Jan. 1999.
- [104] E. G. Larsson, "MIMO detection methods: how they work," *IEEE Signal Processing Magazine*, vol. 26, no. 3, pp. 91–95, May 2009.
- [105] S. Sfar, R. D. Murch, and K. B. Letaief, "Layered space-time multiuser detection over wireless uplink systems," *IEEE Transactions on Wireless Communications*, vol. 2, no. 4, pp. 653–668, Jul. 2003.
- [106] S. Serbetli and A. Yener, "Transceiver optimization for multiuser MIMO systems," *IEEE Transactions on Signal Processing*, vol. 52, no. 1, pp. 214–226, Jan. 2004.
- [107] F. Zhao, J. Liu, J. Liu, L. Guibas, and J. Reich, "Collaborative signal and information processing: an information-directed approach," *Proceedings of the IEEE*, vol. 91, no. 8, pp. 1199–1209, Aug. 2003.
- [108] T. E. Hunter and A. Nosratinia, "Cooperation diversity through coding," in *Proc. IEEE International Symposium on Information Theory (ISIT'02)*, Lausanne, Switzerland, Jul. 2002, p. 220.
- [109] J. N. Laneman and G. W. Wornell, "Distributed space-time-coded protocols for exploiting cooperative diversity in wireless networks," *IEEE Transactions on Information Theory*, vol. 49, no. 10, pp. 2415–2425, Oct. 2003.
- [110] J. N. Laneman, D. N. C. Tse, and G. W. Wornell, "Cooperative diversity in wireless networks: efficient protocols and outage behavior," *IEEE Transactions on Information Theory*, vol. 50, no. 12, pp. 3062–3080, Dec. 2004.
- [111] A. Nosratinia, T. E. Hunter, and A. Hedayat, "Cooperative communication in wireless networks," *IEEE Communications Magazine*, vol. 42, no. 10, pp. 74–80, Oct. 2004.
- [112] M. Janani, A. Hedayat, T. E. Hunter, and A. Nosratinia, "Coded cooperation in wireless communications: space-time transmission and iterative decoding," *IEEE Transactions on Signal Processing*, vol. 52, no. 2, pp. 362–371, Feb. 2004.
- [113] T. E. Hunter and A. Nosratinia, "Diversity through coded cooperation," *IEEE Transactions on Wireless Communications*, vol. 5, no. 2, pp. 283–289, Feb. 2006.

- [114] Q. H. Spencer, A. L. Swindlehurst, and M. Haardt, "Zero-forcing methods for downlink spatial multiplexing in multiuser MIMO channels," *IEEE Transactions on Signal Processing*, vol. 52, no. 2, pp. 461–471, Feb. 2004.
- [115] Q. H. Spencer, C. B. Peel, A. L. Swindlehurst, and M. Haardt, "An introduction to the multiuser MIMO downlink," *IEEE Communications Magazine*, vol. 42, no. 10, pp. 60–67, Oct. 2004.
- [116] L.-U. Choi and R. D. Murch, "A transmit preprocessing technique for multiuser MIMO systems using a decomposition approach," *IEEE Transactions on Wireless Communications*, vol. 3, no. 1, pp. 20–24, Jan. 2004.
- [117] H. Zhang and H. Dai, "Cochannel interference mitigation and cooperative processing in downlink multicell multiuser MIMO networks," *EURASIP J. Wireless Commun. Netw.*, vol. 2004, no. 2, pp. 222–235, doi:10.1155/S1687147204406148, 2004. [Online]. Available: <http://downloads.hindawi.com/journals/wcn/2004/202654.pdf>
- [118] G. Caire, S. A. Ramprasad, H. C. Papadopoulos, C. Pepin, and C.-E. W. Sundberg, "Multiuser MIMO downlink with limited inter-cell cooperation: approximate interference alignment in time, frequency and space," in *Proc. 46th Annual Allerton Conference on Communication, Control, and Computing (Allerton'08)*, Urbana-Champaign, IL, USA, Sep. 2008, pp. 730–737.
- [119] G. Caire, N. Jindal, M. Kobayashi, and N. Ravindran, "Multiuser MIMO achievable rates with downlink training and channel state feedback," *IEEE Transactions on Information Theory*, vol. 56, no. 6, pp. 2845–2866, Jun. 2010.
- [120] A. Carleial, "A case where interference does not reduce capacity," *IEEE Transactions on Information Theory*, vol. 21, no. 5, pp. 569–570, Sep. 1975.
- [121] T. Han and K. Kobayashi, "A new achievable rate region for the interference channel," *IEEE Transactions on Information Theory*, vol. 27, no. 1, pp. 49–60, Jan. 1981.
- [122] H. Sato, "The capacity of the gaussian interference channel under strong interference," *IEEE Transactions on Information Theory*, vol. 27, no. 6, pp. 786–788, Nov. 1981.
- [123] M. H. M. Costa, "On the gaussian interference channel," *IEEE Transactions on Information Theory*, vol. 31, no. 5, pp. 607–615, Sep. 1985.
- [124] M. H. M. Costa and A. El Gamal, "The capacity region of the discrete memoryless interference channel with strong interference," *IEEE Transactions on Information Theory*, vol. 33, no. 5, pp. 710–711, Sep. 1987.
- [125] I. Sason, "On achievable rate regions for the gaussian interference channel," *IEEE Transactions on Information Theory*, vol. 50, no. 6, pp. 1345–1356, Jun. 2004.
- [126] G. Kramer, "Review of rate regions for interference channels," in *Proc. International Zurich Seminar on Communications*, Zurich, Switzerland, Feb. 2006, pp. 162–165.
- [127] S. A. Jafar and M. J. Fakhreddin, "Degrees of freedom for the MIMO interference channel," *IEEE Transactions on Information Theory*, vol. 53, no. 7, pp. 2637–2642, Jul. 2007.
- [128] R. H. Etkin, D. N. C. Tse, and H. Wang, "Gaussian interference channel capacity to within one bit," *IEEE Transactions on Information Theory*, vol. 54, no. 12, pp. 5534–5562, Dec. 2008.

- [129] A. Grant, S. V. Hanly, J. S. Evans, and R. Muller, "Distributed decoding for Wyner cellular systems," in *Proc. 5th Australian Communications Theory Workshop (AusCTW'04)*, Newcastle, Australia, Feb. 2004, pp. 77–81.
- [130] H. Zhang, H. Dai, and Q. Zhou, "Base station cooperation for multiuser MIMO: joint transmission and BS selection," in *Proc. 38th Annual Conference on information sciences and systems (CISS'04)*, Princeton, NJ, USA, Mar. 2004, pp. 17–19.
- [131] H. Zhang, N. B. Mehta, A. F. Molisch, J. Zhang, and H. Dai, "Asynchronous interference mitigation in cooperative base station systems," *IEEE Transactions on Wireless Communications*, vol. 7, no. 1, pp. 155–165, Jan. 2008.
- [132] Y. Hadisusanto, L. Thiele, and V. Jungnickel, "Distributed base station cooperation via block-diagonalization and dual-decomposition," in *Proc. IEEE Global Telecommunications Conference (GLOBECOM'08)*, New Orleans, LO, Nov. 2008, pp. 1–5.
- [133] T. Mayer, H. Jenkac, and J. Hagenauer, "Turbo base-station cooperation for intercell interference cancellation," in *Proc. IEEE International Conference on Communications (ICC'06)*, Istanbul, Turkey, Jun. 2006, pp. 4977–4982.
- [134] S. Khattak, W. Rave, and G. Fettweis, "Distributed iterative multiuser detection through base station cooperation," *EURASIP J. Wireless Commun. Netw.*, vol. 2008, Article ID 390489, 15 pages, doi:10.1155/2008/390489, 2008. [Online]. Available: <http://downloads.hindawi.com/journals/wcn/2008/390489.pdf>
- [135] E. Aktas, J. S. Evans, and S. V. Hanly, "Distributed decoding in a cellular multiple-access channel," *IEEE Transactions on Wireless Communications*, vol. 7, no. 1, pp. 241–250, Jan. 2008.
- [136] B. L. Ng, J. S. Evans, S. V. Hanly, and D. Aktas, "Distributed downlink beamforming with cooperative base stations," *IEEE Transactions on Information Theory*, vol. 54, no. 12, pp. 5491–5499, Dec. 2008.
- [137] R. Zakhour and S. V. Hanly, "Base station cooperation on the downlink: large system analysis," *IEEE Transactions on Information Theory*, vol. 58, no. 4, pp. 2079–2106, Apr. 2012.
- [138] M. A. Maddah-Ali, A. S. Motahari, and A. K. Khandani, "Signaling over MIMO multi-base systems: combination of multi-access and broadcast schemes," in *Proc. IEEE International Symposium on Information Theory (ISIT'06)*, Seattle, WA, Jul. 2006, pp. 2104–2108.
- [139] —, "Communication over X channel: signalling and multiplexing gain," Department of Electrical and Computer Engineering, University of Waterloo, Waterloo, ON, Canada, Tech. Rep. UW-ECE-2006-12, Jul. 2006.
- [140] —, "Communication over MIMO X channel: signalling and performance analysis," Department of Electrical and Computer Engineering, University of Waterloo, Waterloo, ON, Canada, Tech. Rep. UW-ECE-2006-27, Dec. 2006.
- [141] —, "Communication over MIMO X channels: interference alignment, decomposition, and performance analysis," *IEEE Transactions on Information Theory*, vol. 54, no. 8, pp. 3457–3470, Aug. 2008.

- [142] S. A. Jafar and S. Shamai (Shitz), “Degrees of freedom of the MIMO X channel,” in *Proc. IEEE Global Telecommunications Conference (GLOBECOM’07)*, Washington, DC, USA, Nov. 2007, pp. 1632–1636.
- [143] —, “Degrees of freedom region of the MIMO X channel,” *IEEE Transactions on Information Theory*, vol. 54, no. 1, pp. 151–170, Jan. 2008.
- [144] V. R. Cadambe and S. A. Jafar, “Interference alignment and degrees of freedom of the K -user interference channel,” *IEEE Transactions on Information Theory*, vol. 54, no. 8, pp. 3425–3441, Aug. 2008.
- [145] S. A. Jafar, “Interference alignment – a new look at signal dimensions in a communication network,” *Foundations and Trends in Communications and Information Theory*, vol. 7, no. 1, 2010.
- [146] D. A. Shnidman, “A generalized Nyquist criterion and an optimum linear receiver for a pulse modulation system,” *The Bell System Technical Journal*, vol. 46, no. 9, pp. 2163–2177, Nov. 1967.
- [147] A. Kaye and D. George, “Transmission of multiplexed PAM signals over multiple channel and diversity systems,” *IEEE Transactions on Communication Technology*, vol. COM-18, no. 5, pp. 520–526, Oct. 1970.
- [148] W. van Etten, “An optimum linear receiver for multiple channel digital transmission systems,” *IEEE Transactions on Communications*, vol. 23, no. 8, pp. 828–834, Aug. 1975.
- [149] —, “Maximum likelihood receiver for multiple channel transmission systems,” *IEEE Transactions on Communications*, vol. 24, no. 2, pp. 276–283, Feb. 1976.
- [150] D. Horwood and R. Gagliardi, “Signal design for digital multiple access communications,” *IEEE Transactions on Communications*, vol. 23, no. 3, pp. 378–383, Mar. 1975.
- [151] K. S. Schneider, “Optimum detection of code division multiplexed signals,” *IEEE Transactions on Aerospace and Electronic Systems*, vol. AES-15, no. 1, pp. 181–185, Jan. 1979.
- [152] —, “Crosstalk resistant receiver for M -ary multiplexed communications,” *IEEE Transactions on Aerospace and Electronic Systems*, vol. AES-16, no. 4, pp. 426–433, Jul. 1980.
- [153] U. Timor, “Improved decoding scheme for frequency-hopped multilevel FSK system,” *The Bell System Technical Journal*, vol. 59, no. 10, pp. 1839–1855, Dec. 1980.
- [154] —, “Multistage decoding of frequency-hopped FSK system,” *The Bell System Technical Journal*, vol. 60, no. 4, pp. 471–483, Apr. 1981.
- [155] S. Verdú, “Optimum sequence detection of asynchronous multiple-access communications,” in *Abstr. IEEE International Symposium on Information Theory (ISIT’83)*, St. Jovite, Canada, Sep. 1983, p. 80.
- [156] —, “Minimum probability of error for asynchronous multiple access communication systems,” in *Proc. IEEE Military Communications Conference (MILCOM’83)*, Washington, DC, Nov. 1983, pp. 213–219.
- [157] —, “Minimum probability of error for asynchronous Gaussian multiple-access channels,” *IEEE Transactions on Information Theory*, vol. IT-32, no. 1, pp. 85–96, Jan. 1986.

- [158] —, “Optimum multiuser asymptotic efficiency,” *IEEE Transactions on Communications*, vol. 34, no. 9, pp. 890–897, Sep. 1986.
- [159] R. Lupas and S. Verdú, “Linear multiuser detectors for synchronous code-division multiple-access channels,” *IEEE Transactions on Information Theory*, vol. 35, no. 1, pp. 123–136, Jan. 1989.
- [160] —, “Near-far resistance of multiuser detectors in asynchronous channels,” *IEEE Transactions on Communications*, vol. 38, no. 4, pp. 496–508, Apr. 1990.
- [161] R. Kohno and M. Hatori, “Cancellation techniques of co-channel interference in asynchronous spread spectrum multiple access systems,” *Electronics and Communications in Japan (Part I: Communications)*, vol. 66, no. 5, pp. 20–29, May 1983. [Online]. Available: <http://dx.doi.org/10.1002/ecja.4400660504>
- [162] R. Kohno, H. Imai, M. Hatori, and S. Pasupathy, “Combinations of an adaptive array antenna and a canceller of interference for direct-sequence spread-spectrum multiple-access system,” *IEEE Journal on Selected Areas in Communications*, vol. 8, no. 4, pp. 675–682, May 1990.
- [163] —, “An adaptive canceller of cochannel interference for spread-spectrum multiple-access communication networks in a power line,” *IEEE Journal on Selected Areas in Communications*, vol. 8, no. 4, pp. 691–699, May 1990.
- [164] M. K. Varanasi and B. Aazhang, “Multistage detection in asynchronous code-division multiple-access communications,” *IEEE Transactions on Communications*, vol. 38, no. 4, pp. 509–519, Apr. 1990.
- [165] —, “Near-optimum detection in synchronous code-division multiple-access systems,” *IEEE Transactions on Communications*, vol. 39, no. 5, pp. 725–736, May 1991.
- [166] —, “Optimally near-far resistant multiuser detection in differentially coherent synchronous channels,” *IEEE Transactions on Information Theory*, vol. 37, no. 4, pp. 1006–1018, Jul. 1991.
- [167] Y. C. Yoon, R. Kohno, and H. Imai, “A spread-spectrum multiaccess system with cochannel interference cancellation for multipath fading channels,” *IEEE Journal on Selected Areas in Communications*, vol. 11, no. 7, pp. 1067–1075, Sep. 1993.
- [168] D. Divsalar, M. K. Simon, and D. Raphaeli, “Improved parallel interference cancellation for CDMA,” *IEEE Transactions on Communications*, vol. 46, no. 2, pp. 258–268, Feb. 1998.
- [169] R. M. Buehrer and B. D. Woerner, “Analysis of adaptive multistage interference cancellation for CDMA using an improved gaussian approximation,” *IEEE Transactions on Communications*, vol. 44, no. 10, pp. 1308–1321, Oct. 1996.
- [170] T. Masamura, “Spread spectrum multiple access system with intrasystem interference cancellation,” *IEICE Transactions*, vol. E71, no. 3, pp. 224–231, Mar. 1988.
- [171] A. J. Viterbi, “Very low rate convolution codes for maximum theoretical performance of spread-spectrum multiple-access channels,” *IEEE Journal on Selected Areas in Communications*, vol. 8, no. 4, pp. 641–649, May 1990.
- [172] Z. Xie, C. K. Rushforth, and R. T. Short, “Multiuser signal detection using sequential decoding,” *IEEE Transactions on Communications*, vol. 38, no. 5, pp. 578–583, May 1990.

- [173] Z. Xie, R. T. Short, and C. K. Rushforth, "A family of suboptimum detectors for coherent multiuser communications," *IEEE Journal on Selected Areas in Communications*, vol. 8, no. 4, pp. 683–690, May 1990.
- [174] Z. Xie, C. K. Rushforth, R. T. Short, and T. K. Moon, "Joint signal detection and parameter estimation in multiuser communications," *IEEE Transactions on Communications*, vol. 41, no. 8, pp. 1208–1216, Aug. 1993.
- [175] A. Duel-Hallen, "Decorrelating decision-feedback multiuser detector for synchronous code-division multiple-access channel," *IEEE Transactions on Communications*, vol. 41, no. 2, pp. 285–290, Feb. 1993.
- [176] —, "A family of multiuser decision-feedback detectors for asynchronous code-division multiple-access channels," *IEEE Transactions on Communications*, vol. 43, no. 2/3/4, pp. 421–434, Feb./Mar./Apr. 1995.
- [177] P. R. Patel and J. M. Holtzman, "Analysis of a simple successive interference cancellation scheme in a DS/CDMA system," *IEEE Journal on Selected Areas in Communications*, vol. 12, no. 5, pp. 796–807, Jun. 1994.
- [178] M. K. Varanasi, "Decision feedback multiuser detection: a systematic approach," *IEEE Transactions on Information Theory*, vol. 45, no. 1, pp. 219–240, Jan. 1999.
- [179] A. L. C. Hui and K. B. Letaief, "Successive interference cancellation for multiuser asynchronous DS/CDMA detectors in multipath fading links," *IEEE Transactions on Communications*, vol. 46, no. 3, pp. 384–391, Mar. 1998.
- [180] S. Verdú and S. Shamai (Shitz), "Spectral efficiency of CDMA with random spreading," *IEEE Transactions on Information Theory*, vol. 45, no. 2, pp. 622–640, Mar. 1999.
- [181] X. Wang and H. V. Poor, *Wireless Communication Systems: Advanced Techniques for Signal Reception*, 1st ed. Upper Saddle River, NJ, USA: Prentice Hall, 2009.
- [182] A. Paulraj and T. Kailath, "Increasing capacity in wireless broadcast systems using distributed transmission/directional reception," U.S. Patent 5 345 599, Sep. 6, 1994.
- [183] E. Telatar, "Capacity of multi-antenna gaussian channels," Technical Report #BL0112170-950615-07TM, AT & T Bell Laboratories, 1995.
- [184] G. J. Foschini and M. J. Gans, "On limits of wireless communications in a fading environment when using multiple antennas," *Wireless Personal Communications*, vol. 6, no. 3, pp. 311–335, Mar. 1998.
- [185] E. Telatar, "Capacity of multi-antenna gaussian channels," *European Transactions on Telecommunications*, vol. 10, no. 6, pp. 585–595, November-December 1999. [Online]. Available: <http://dx.doi.org/10.1002/ett.4460100604>
- [186] V. Tarokh, N. Seshadri, and A. R. Calderbank, "Space-time codes for high data rate wireless communication: performance criterion and code construction," *IEEE Transactions on Information Theory*, vol. 44, no. 2, pp. 744–765, Mar. 1998.
- [187] A. F. Naguib, V. Tarokh, N. Seshadri, and A. R. Calderbank, "A space-time coding modem for high-data-rate wireless communications," *IEEE Journal on Selected Areas in Communications*, vol. 16, no. 8, pp. 1459–1478, Oct. 1998.

- [188] S. Alamouti, "A simple transmit diversity technique for wireless communications," *IEEE Journal on Selected Areas in Communications*, vol. 16, no. 8, pp. 1451–1458, Oct. 1998.
- [189] V. Tarokh, A. F. Naguib, N. Seshadri, and A. R. Calderbank, "Space-time codes for high data rate wireless communication: performance criteria in the presence of channel estimation errors, mobility, and multiple paths," *IEEE Transactions on Communications*, vol. 47, no. 2, pp. 199–207, Feb. 1999.
- [190] H. El Gamal, A. R. Hammons, Y. Liu, M. P. Fitz, and O. Y. Takeshita, "On the design of space-time and space-frequency codes for MIMO frequency-selective fading channels," *IEEE Transactions on Information Theory*, vol. 49, no. 9, pp. 2277–2292, Sep. 2003.
- [191] T. Abe and T. Matsumoto, "Space-time turbo equalization in frequency-selective MIMO channels," *IEEE Transactions on Vehicular Technology*, vol. 52, no. 3, pp. 469–475, May 2003.
- [192] X. Zhu and R. D. Murch, "Layered space-frequency equalization in a single-carrier MIMO system for frequency-selective channels," *IEEE Transactions on Wireless Communications*, vol. 3, no. 3, pp. 701–708, May 2004.
- [193] S. Liu and Z. Tian, "Near-optimum soft decision equalization for frequency selective MIMO channels," *IEEE Transactions on Signal Processing*, vol. 52, no. 3, pp. 721–733, Mar. 2004.
- [194] X. Ma, L. Yang, and G. B. Giannakis, "Optimal training for MIMO frequency-selective fading channels," *IEEE Transactions on Wireless Communications*, vol. 4, no. 2, pp. 453–466, Mar. 2005.
- [195] Z. Wang and G. B. Giannakis, "Wireless multicarrier communications—Where Fourier meets Shannon," *IEEE Signal Processing Magazine*, vol. 17, no. 3, pp. 29–48, May 2000.
- [196] R. F. H. Fischer and C. Windpassinger, "Real versus complex-valued equalisation in V-BLAST systems," *Electronics Letters*, vol. 39, no. 5, pp. 470–471, Mar. 2003.
- [197] M. Siti and M. P. Fitz, "A novel soft-output layered orthogonal lattice detector for multiple antenna communications," in *Proc. IEEE International Conference on Communications (ICC'06)*, vol. 4, Istanbul, Turkey, Jun. 2006, pp. 1686–1691.
- [198] L. Azzam and E. Ayanoglu, "Reduced complexity sphere decoding via a reordered lattice representation," *IEEE Transactions on Communications*, vol. 57, no. 9, pp. 2564–2569, Sep. 2009.
- [199] T.-H. Liu and C.-N. Chiu, "On fast preprocessing schemes for the real-valued spatially multiplexed MIMO detectors," *International Journal of Communication Systems*, 2012. [Online]. Available: <http://dx.doi.org/10.1002/dac.2365>
- [200] D. W. Tufts, "Nyquist's problem – the joint optimization of transmitter and receiver in pulse amplitude modulation," *Proceedings of the IEEE*, vol. 53, no. 3, pp. 248–259, Mar. 1965.
- [201] Y. G. Li, J. H. Winters, and N. R. Sollenberger, "MIMO-OFDM for wireless communications: signal detection with enhanced channel estimation," *IEEE Transactions on Communications*, vol. 50, no. 9, pp. 1471–1477, Sep. 2002.
- [202] B. Lu, G. Yue, and X. Wang, "Performance analysis and design optimization of LDPC-coded MIMO OFDM systems," *IEEE Transactions on Signal Processing*, vol. 52, no. 2, pp. 348–361, Feb. 2004.

- [203] A. Zanella, M. Chiani, and M. Z. Win, "MMSE reception and successive interference cancellation for MIMO systems with high spectral efficiency," *IEEE Transactions on Wireless Communications*, vol. 4, no. 3, pp. 1244–1253, May 2005.
- [204] S. Chen, A. Livingstone, and L. Hanzo, "Minimum bit-error rate design for space-time equalization-based multiuser detection," *IEEE Transactions on Communications*, vol. 54, no. 5, pp. 824–832, May 2006.
- [205] D. P. Palomar, M. Bengtsson, and B. Ottersten, "Minimum BER linear transceivers for MIMO channels via primal decomposition," *IEEE Transactions on Signal Processing*, vol. 53, no. 8, pp. 2866–2882, Aug. 2005.
- [206] D. Wübben, R. Böhnke, V. Kühn, and K.-D. Kammeyer, "MMSE extension of V-BLAST based on sorted QR decomposition," in *Proc. IEEE 58th Vehicular Technology Conference (VTC'03-Fall)*, Orlando, USA, Oct. 2003, pp. 508–512.
- [207] K.-W. Wong, C.-Y. Tsui, and R. S. Cheng, "A low complexity architecture of the V-BLAST system," in *Proc. IEEE Wireless Communications and Networking Conference (WCNC'00)*, Chicago, IL, USA, Sep. 2000, pp. 310–314.
- [208] R. Böhnke, D. Wübben, V. Kühn, and K.-D. Kammeyer, "Reduced complexity MMSE detection for BLAST architectures," in *Proc. IEEE Global Telecommunications Conference (GLOBECOM'03)*, San Francisco, USA, Dec. 2003, pp. 2258–2262.
- [209] B. Hassibi, "An efficient square-root algorithm for BLAST," in *Proc. IEEE International Conference on Acoustics, Speech, and Signal Processing (ICASSP'00)*, Istanbul, Turkey, Jun. 2000, pp. 737–740.
- [210] J. Benesty, Y. Huang, and J. Chen, "A fast recursive algorithm for optimum sequential signal detection in a BLAST system," *IEEE Transactions on Signal Processing*, vol. 51, no. 7, pp. 1722–1730, Jul. 2003.
- [211] T.-H. Liu, "Some results for the fast MMSE-SIC detection in spatially multiplexed MIMO systems," *IEEE Transactions on Wireless Communications*, vol. 8, no. 11, pp. 5443–5448, Nov. 2009.
- [212] W. H. Chin, A. G. Constantinides, and D. B. Ward, "Parallel multistage detection for multiple antenna wireless systems," *Electronics Letters*, vol. 38, no. 12, pp. 597–599, 2002.
- [213] Z. Luo, M. Zhao, S. Liu, and Y. Liu, "Generalized parallel interference cancellation with near-optimal detection performance," *IEEE Transactions on Signal Processing*, vol. 56, no. 1, pp. 304–312, Jan. 2008.
- [214] C. Studer, S. Fateh, and D. Seethaler, "ASIC implementation of soft-input soft-output MIMO detection using MMSE parallel interference cancellation," *IEEE Journal of Solid-State Circuits*, vol. 46, no. 7, pp. 1754–1765, Jul. 2011.
- [215] E. Viterbo and E. Biglieri, "A universal decoding algorithm for lattice codes," in *Proc. GRETSI 14-ème Colloque*, Juan-les-Pins, France, Sep. 1993.
- [216] Y. H. Wu, Y. T. Liu, H.-C. Chang, Y.-C. Liao, and H.-C. Chang, "Early-pruned K-best sphere decoding algorithm based on radius constraints," in *Proc. IEEE International Conference on Communications (ICC'08)*, Beijing, China, May 2008, pp. 4496–4500.

- [217] T. Fukatani, R. Matsumoto, and T. Uyematsu, "Two methods for decreasing the computational complexity of the MIMO ML decoder," *IEICE Transactions on Fundamentals of Electronics, Communications and Computer Sciences*, vol. E87-A, no. 10, pp. 2571–2576, Oct. 2004.
- [218] A. Okawado, R. Matsumoto, and T. Uyematsu, "Near ML detection using Dijkstra's algorithm with bounded list size over MIMO channels," in *Proc. IEEE International Symposium on Information Theory (ISIT'2008)*, Toronto, ON, Jul. 2008, pp. 2022–2025.
- [219] J. Luo, K. R. Pattipati, P. K. Willett, and F. Hasegawa, "Near optimal multiuser detection in synchronous CDMA using probabilistic data association," *IEEE Communications Letters*, vol. 5, no. 9, pp. 361–363, Sep. 2001.
- [220] J. Luo, "Improved multiuser detection in code-division multiple access systems," Ph.D. dissertation, Univ. of Connecticut, Storrs, May 2002. [Online]. Available: <http://istec.colostate.edu/~rockey/Papers/PhDThesis.pdf>
- [221] D. Pham, J. Luo, K. R. Pattipati, and P. K. Willett, "A PDA-Kalman approach to multiuser detection in asynchronous CDMA," *IEEE Communications Letters*, vol. 6, no. 11, pp. 475–477, Nov. 2002.
- [222] J. Luo, K. R. Pattipati, and P. K. Willett, "A sliding window PDA for asynchronous CDMA, and a proposal for deliberate asynchronicity," *IEEE Transactions on Communications*, vol. 51, no. 12, pp. 1970–1974, 2003.
- [223] P. H. Tan, L. K. Rasmussen, and J. Luo, "Iterative multiuser decoding based on probabilistic data association," in *Proc. IEEE International Symposium on Information Theory (ISIT'03)*, Yokohama, Japan, Jun. 2003, pp. 301–301.
- [224] Y. Yin, Y. Huang, and J. Zhang, "Turbo equalization using probabilistic data association," in *Proc. IEEE Global Telecommunications Conference (GLOBECOM'04)*, Dallas, TX, USA, Dec. 2004, pp. 2535–2539.
- [225] Y. Huang and J. Zhang, "A generalized probabilistic data association multiuser detector," in *Proc. IEEE International Symposium on Information Theory (ISIT'04)*, Chicago, IL, USA, Jun. 2004, p. 529.
- [226] D. Pham, K. R. Pattipati, P. K. Willett, and J. Luo, "A generalized probabilistic data association detector for multiple antenna systems," *IEEE Communications Letters*, vol. 8, no. 4, pp. 205–207, Apr. 2004.
- [227] S. Liu and Z. Tian, "A Kalman-PDA approach to soft-decision equalization for frequency-selective MIMO channels," *IEEE Transactions on Signal Processing*, vol. 53, no. 10, pp. 3819–3830, Oct. 2005.
- [228] G. Latsoudas and N. D. Sidiropoulos, "A hybrid probabilistic data association-sphere decoding detector for multiple-input-multiple-output systems," *IEEE Signal Processing Letters*, vol. 12, no. 4, pp. 309–312, Apr. 2005.
- [229] Y. Jia, C. Andrieu, R. J. Piechocki, and M. Sandell, "Gaussian approximation based mixture reduction for near optimum detection in MIMO systems," *IEEE Communications Letters*, vol. 9, no. 11, pp. 997–999, Nov. 2005.

- [230] J. Fricke, M. Sandell, J. Mietzner, and P. A. Hoeher, "Impact of the Gaussian approximation on the performance of the probabilistic data association MIMO decoder," *EURASIP Journal on Wireless Communications and Networking*, vol. 2005, no. 5, pp. 796–800, 2005.
- [231] J. Wang and S. Li, "MIMO turbo receiver with new probability data association soft interference cancellation," in *Proc. International Conference on Communications, Circuits and Systems (ICCCAS'05)*, Hong Kong, China, May 2005, pp. 232–236.
- [232] P. H. Tan and L. K. Rasmussen, "Asymptotically optimal nonlinear MMSE multiuser detection based on multivariate gaussian approximation," *IEEE Transactions on Communications*, vol. 54, no. 8, pp. 1427–1428, Aug. 2006.
- [233] Y. Cai, X. Xu, Y. Cheng, Y. Xu, and Z. Li, "A SISO iterative probabilistic data association detector for MIMO systems," in *Proc. 10th International Conference on Communication Technology (ICCT'06)*, Guilin, China, Nov. 2006, pp. 1–4.
- [234] Y. Jia, C. M. Vithanage, C. Andrieu, and R. J. Piechocki, "Probabilistic data association for symbol detection in MIMO systems," *Electronics Letters*, vol. 42, no. 1, pp. 38–40, Jan. 2006.
- [235] F. Cao, J. Li, and J. Yang, "On the relation between PDA and MMSE-ISDIC," *IEEE Signal Processing Letters*, vol. 14, no. 9, pp. 597–600, Sep. 2007.
- [236] S. Bavarian and J. K. Cavers, "Reduced complexity distributed base station processing in the uplink of cellular networks," in *Proc. IEEE Global Telecommunications Conference (GLOBECOM'07)*, Washington, DC, USA, Nov. 2007, pp. 4500–4504.
- [237] —, "Reduced-complexity belief propagation for system-wide MUD in the uplink of cellular networks," *IEEE Journal on Selected Areas in Communications*, vol. 26, no. 3, pp. 541–549, Apr. 2008.
- [238] Y. Jia, C. Andrieu, R. J. Piechocki, and M. Sandell, "Depth-first and breadth-first search based multilevel sga algorithms for near optimal symbol detection in mimo systems," *IEEE Transactions on Wireless Communications*, vol. 7, no. 3, pp. 1052–1061, Mar. 2008.
- [239] M. Grossmann and T. Matsumoto, "Nonlinear frequency domain MMSE turbo equalization using probabilistic data association," *IEEE Communications Letters*, vol. 12, no. 4, pp. 295–297, Apr. 2008.
- [240] Y. J. D. Kim and J. Bajcsy, "An iterative receiver for non-coherent MIMO systems with differential encoding," in *Proc. 5th IEEE Consumer Communications and Networking Conference (CCNC'08)*, Las Vegas, NV, Jan. 2008, pp. 46–47.
- [241] S. K. Mohammed, A. Chockalingam, and B. S. Rajan, "Low-complexity near-MAP decoding of large non-orthogonal STBCs using PDA," in *IEEE International Symposium on Information Theory (ISIT'09)*, Seoul, Korea, Jul. 2009, pp. 1998–2002.
- [242] S. Bavarian and J. K. Cavers, "A new framework for soft decision equalization in frequency selective MIMO channels," *IEEE Transactions on Communications*, vol. 57, no. 2, pp. 415–422, Feb. 2009.
- [243] Z.-Q. Luo, W.-K. Ma, A. M.-C. So, Y. Ye, and S. Zhang, "Semidefinite relaxation of quadratic optimization problems," *IEEE Signal Processing Magazine*, vol. 27, no. 3, pp. 20–34, May 2010.

- [244] Z.-Q. Luo and W. Yu, "An introduction to convex optimization for communications and signal processing," *IEEE Journal on Selected Areas in Communications*, vol. 24, no. 8, pp. 1426–1438, Aug. 2006.
- [245] P. H. Tan and L. K. Rasmussen, "The application of semidefinite programming for detection in CDMA," *IEEE Journal on Selected Areas in Communications*, vol. 19, no. 8, pp. 1442–1449, Aug. 2001.
- [246] W.-K. Ma, T. N. Davidson, K. M. Wong, Z.-Q. Luo, and P.-C. Ching, "Quasi-maximum-likelihood multiuser detection using semi-definite relaxation with application to synchronous CDMA," *IEEE Transactions on Signal Processing*, vol. 50, no. 4, pp. 912–922, Apr. 2002.
- [247] W.-K. Ma, T. N. Davidson, K. M. Wong, and P.-C. Ching, "A block alternating likelihood maximization approach to multiuser detection," *IEEE Transactions on Signal Processing*, vol. 52, no. 9, pp. 2600–2611, Sep. 2004.
- [248] M. Kisiailiou and Z.-Q. Luo, "Performance analysis of quasi-maximum-likelihood detector based on semi-definite programming," in *Proc. IEEE International Conference on Acoustics, Speech, and Signal Processing (ICASSP'05)*, vol. 3, Philadelphia, PA, Mar. 2005, pp. III/433–III/436.
- [249] J. Jaldén and B. Ottersten, "The diversity order of the semidefinite relaxation detector," *IEEE Transactions on Information Theory*, vol. 54, no. 4, pp. 1406–1422, Apr. 2008.
- [250] Z.-Q. Luo, X. Luo, and M. Kisiailiou, "An efficient quasi-maximum likelihood decoder for PSK signals," in *Proc. IEEE International Conference on Acoustics, Speech, and Signal Processing (ICASSP'03)*, vol. 6, Hong Kong, China, Apr. 2003, pp. VI/561–VI/564.
- [251] W.-K. Ma, P.-C. Ching, and Z. Ding, "Semidefinite relaxation based multiuser detection for M-ary PSK multiuser systems," *IEEE Transactions on Signal Processing*, vol. 52, no. 10, pp. 2862–2872, Oct. 2004.
- [252] A. Wiesel, Y. C. Eldar, and S. Shamai (Shitz), "Semidefinite relaxation for detection of 16-QAM signaling in MIMO channels," *IEEE Signal Processing Letters*, vol. 12, no. 9, pp. 653–656, Sep. 2005.
- [253] Y. Yang, C. Zhao, P. Zhou, and W. Xu, "MIMO detection of 16-QAM signaling based on semidefinite relaxation," *IEEE Signal Processing Letters*, vol. 14, no. 11, pp. 797–800, Nov. 2007.
- [254] N. D. Sidiropoulos and Z.-Q. Luo, "A semidefinite relaxation approach to MIMO detection for high-order QAM constellations," *IEEE Signal Processing Letters*, vol. 13, no. 9, pp. 525–528, Sep. 2006.
- [255] A. Mobasher, M. Taherzadeh, R. Sotirov, and A. K. Khandani, "A near-maximum-likelihood decoding algorithm for MIMO systems based on semi-definite programming," *IEEE Transactions on Information Theory*, vol. 53, no. 11, pp. 3869–3886, Nov. 2007.
- [256] Z. Mao, X. Wang, and X. Wang, "Semidefinite programming relaxation approach for multiuser detection of QAM signals," *IEEE Transactions on Wireless Communications*, vol. 6, no. 12, pp. 4275–4279, Dec. 2007.
- [257] W.-K. Ma, C.-C. Su, J. Jaldén, T.-H. Chang, and C.-Y. Chi, "The equivalence of semidefinite relaxation MIMO detectors for higher-order QAM," *IEEE Journal of Selected Topics in Signal Processing*, vol. 3, no. 6, pp. 1038–1052, Dec. 2009.

- [258] J. G. Andrews, “Interference cancellation for cellular systems: a contemporary overview,” *IEEE Wireless Communications Magazine*, vol. 12, no. 2, p. 2005, Apr. 19-29.
- [259] A. J. Viterbi, “Error bounds for convolutional codes and an asymptotically optimum decoding algorithm,” *IEEE Transactions on Information Theory*, vol. 13, no. 2, pp. 260–269, Apr. 1967.
- [260] J. Omura, “On the Viterbi decoding algorithm,” *IEEE Transactions on Information Theory*, vol. 15, no. 1, pp. 177–179, Jan. 1969.
- [261] G. D. Forney, “Maximum-likelihood sequence estimation of digital sequences in the presence of intersymbol interference,” *IEEE Transactions on Information Theory*, vol. 18, no. 3, pp. 363–378, May 1972.
- [262] —, “The Viterbi algorithm,” *Proceedings of the IEEE*, vol. 61, no. 3, pp. 268–278, Mar. 1973.
- [263] A. J. Viterbi, “A personal history of the Viterbi algorithm,” *IEEE Signal Processing Magazine*, vol. 23, no. 4, pp. 120–142, Jul. 2006.
- [264] S. U. H. Qureshi, “Adaptive equalization,” *Proceedings of the IEEE*, vol. 73, no. 9, pp. 1349–1387, Sep. 1985.
- [265] M. Honig, U. Madhow, and S. Verdú, “Blind adaptive multiuser detection,” *IEEE Transactions on Information Theory*, vol. 41, no. 4, pp. 944–960, Jul. 1995.
- [266] L. Tong, G. Xu, and T. Kailath, “Blind identification and equalization based on second-order statistics: a time domain approach,” *IEEE Transactions on Information Theory*, vol. 40, no. 2, pp. 340–349, Mar. 1994.
- [267] X. Wang and H. V. Poor, “Blind equalization and multiuser detection in dispersive cdma channels,” *IEEE Transactions on Communications*, vol. 46, no. 1, pp. 91–103, Jan. 1998.
- [268] S. Verdú, “Optimum multi-user signal detection,” Ph.D. dissertation, Department of Electrical and Computer Engineering, University of Illinois at Urbana-Champaign, Urbana, IL, Aug. 1984.
- [269] H. V. Poor and S. Verdú, “Single-user detectors for multiuser channels,” *IEEE Transactions on Communications*, vol. 36, no. 1, pp. 50–60, Jan. 1988.
- [270] S. Verdú, “Demodulation in the presence of multiuser interference: progress and misconceptions,” in *Intelligent Methods in Signal Processing and Communications*, D. Docampo, A. R. Figueiras-Vidal, and F. Pérez-González, Eds. Boston: Birkhäuser, 1997, pp. 15–45. [Online]. Available: http://dx.doi.org/10.1007/978-1-4612-2018-3_2
- [271] K. Abend, T. J. Harley, B. D. Fritchman, and C. Gumacos, “On optimum receivers for channels having memory,” *IEEE Transactions on Information Theory*, vol. 14, no. 6, pp. 819–820, Nov. 1968.
- [272] K. Abend and B. D. Fritchman, “Statistical detection for communication channels with inter-symbol interference,” *Proceedings of the IEEE*, vol. 58, no. 5, pp. 779–785, May 1970.
- [273] L. Bahl, J. Cocke, F. Jelinek, and J. Raviv, “Optimal decoding of linear codes for minimizing symbol error rate,” *IEEE Transactions on Information Theory*, vol. 20, no. 2, pp. 284–287, Mar. 1974.

- [274] S. Verdú and H. V. Poor, “Backward, forward and backward-forward dynamic programming models under commutativity conditions,” in *Proc. the 23rd IEEE Conference on Decision and Control (CDC’84)*, Las Vegas, NV, Dec. 1984, pp. 1081–1086.
- [275] —, “Abstract dynamic programming models under commutativity conditions,” *SIAM Journal on Control and Optimization*, vol. 25, no. 4, pp. 990–1006, Jul. 1987. [Online]. Available: <http://epubs.siam.org/doi/abs/10.1137/0325054>
- [276] M. R. Garey and D. S. Johnson, *Computers and Intractability: A Guide to the Theory of NP-Completeness*. San Francisco, USA: W. H. Freeman and Co., 1979.
- [277] T. H. Cormen, C. E. Leiserson, R. L. Rivest, and C. Stein, *Introduction to Algorithms*, 3rd ed. Cambridge, Massachusetts: MIT Press, 2009.
- [278] R. Lupas and S. Verdú, “Asymptotic efficiency of linear multiuser detectors,” in *Proc. the 25th IEEE Conference on Decision and Control (CDC’86)*, Dec. 1986, pp. 2094–2100.
- [279] —, “Optimum near-far resistance of linear detectors for code-division multiple-access channels,” in *Abstr. IEEE International Symposium on Information Theory (ISIT’88)*, Jun. 1988, p. 14. [Online]. Available: <http://www.princeton.edu/~verdu/reprints/OptimumNear-FarResistanceOfLinearDetectors.pdf>
- [280] S. M. Kay, *Fundamentals of Statistical Signal Processing, Volume I: Estimation Theory*. Prentice Hall, 1993.
- [281] Z. Xie, R. T. Short, and C. K. Rushforth, “Suboptimum coherent detection of direct-sequence multiple-access signals,” in *Proc. IEEE Military Communications Conference (MILCOM’89)*, Boston, MA, Oct. 1989, pp. 128–133.
- [282] H. V. Poor and S. Verdú, “Probability of error in MMSE multiuser detection,” *IEEE Transactions on Information Theory*, vol. 43, no. 3, pp. 858–871, May 1997.
- [283] N. B. Mandayam and B. Aazhang, “Generalized sensitivity analysis of optical code division multiple access systems,” in *Proc. 27th Annual Conference on Information Sciences and Systems (CISS’93)*, Baltimore, MD, Mar. 1993, pp. 302–307.
- [284] —, “Gradient estimation for stochastic optimization of optical code-division multiple-access systems: Part I – generalized sensitivity analysis,” *IEEE Journal on Selected Areas in Communications*, vol. 15, no. 4, pp. 731–741, May 1997.
- [285] —, “Gradient estimation for stochastic optimization of optical code-division multiple-access systems: Part II – adaptive detection,” *IEEE Journal on Selected Areas in Communications*, vol. 15, no. 4, pp. 742–750, May 1997.
- [286] —, “Gradient estimation for sensitivity analysis and adaptive multiuser interference rejection in code-division multiple-access systems,” *IEEE Transactions on Communications*, vol. 45, no. 7, pp. 848–858, Jul. 1997.
- [287] I. N. Psaromiligkos, S. N. Batalama, and D. A. Pados, “On adaptive minimum probability of error linear filter receivers for DS-CDMA channels,” *IEEE Transactions on Communications*, vol. 47, no. 7, pp. 1092–1102, Jul. 1999.
- [288] X. Wang, W.-S. Lu, and A. Antoniou, “Constrained minimum-BER multiuser detection,” in *Proc. IEEE International Conference on Acoustics, Speech, and Signal Processing (ICASSP’99)*, Phoenix, AZ, USA, Mar. 1999, pp. 2603–2606.

- [289] —, “Constrained minimum-BER multiuser detection,” *IEEE Transactions on Signal Processing*, vol. 48, no. 10, pp. 2903–2909, Oct. 2000.
- [290] C.-C. Yeh, R. R. Lopes, and J. R. Barry, “Approximate minimum bit-error rate multiuser detection,” in *Proc. IEEE Global Telecommunications Conference (GLOBECOM’98)*, Sydney, NSW, Australia, Nov. 1998, pp. 3590–3595.
- [291] C.-C. Yeh and J. R. Barry, “Adaptive minimum bit-error rate equalization for binary signaling,” *IEEE Transactions on Communications*, vol. 48, no. 7, pp. 1226–1235, Jul. 2000.
- [292] S. Chen, A. K. Samingan, B. Mulgrew, and L. Hanzo, “Adaptive minimum-BER linear multiuser detection for DS-CDMA signals in multipath channels,” *IEEE Transactions on Signal Processing*, vol. 49, no. 6, pp. 1240–1247, Jun. 2001.
- [293] P. Bergmans and T. M. Cover, “Cooperative broadcasting,” *IEEE Transactions on Information Theory*, vol. 20, no. 3, pp. 317–324, May 1974.
- [294] T. M. Cover, “Some advances in broadcast channels,” in *Advances in Communication Systems*, A. J. Viterbi, Ed. New York: Academic Press, Inc., 1975, vol. 4, pp. 229–260. [Online]. Available: <http://www-isl.stanford.edu/~cover/papers/paper34.pdf>
- [295] P. Dent, B. Gudmundson, and M. Ewerbring, “CDMA-IC: a novel code division multiple access scheme based on interference cancellation,” in *Proc. 3rd IEEE International Symposium on Personal, Indoor and Mobile Radio Communications (PIMRC’92)*, Boston, MA, Oct. 1992, pp. 98–102.
- [296] S. Moshavi, E. G. Kanterakis, and D. L. Schilling, “Multistage linear receivers for DS-CDMA systems,” *International Journal of Wireless Information Networks*, vol. 3, no. 1, pp. 1–17, Jan. 1996. [Online]. Available: <http://dx.doi.org/10.1007/BF02106658>
- [297] S. Kubota, S. Kato, and K. Feher, “Inter-channel interference cancellation technique for CDMA mobile/personal communication systems,” in *Proc. 3rd IEEE International Symposium on Personal, Indoor and Mobile Radio Communications (PIMRC’92)*, Boston, MA, Oct. 1992, pp. 112–117.
- [298] —, “Inter-channel interference cancellation technique for CDMA mobile/personal communication base stations,” in *Proc. 2nd IEEE International Symposium on Spread Spectrum Techniques and Applications (ISSSTA ’92)*, Yokohama, Japan, Nov. 1992, pp. 91–94.
- [299] P. R. Patel and J. M. Holtzman, “Analysis of a DS/CDMA successive interference cancellation scheme using correlations,” in *Proc. IEEE Global Telecommunications Conference (GLOBECOM’93)*, Houston, TX, USA, Dec. 1993, pp. 76–80.
- [300] J. M. Holtzman, “DS/CDMA successive interference cancellation,” in *Proc. IEEE 3rd International Symposium on Spread Spectrum Techniques and Applications (ISSSTA’94)*, Oulu, Finland, Jul. 1994, pp. 69–78.
- [301] —, “Successive interference cancellation for direct sequence code division multiple access,” in *Proc. IEEE Military Communications Conference (MILCOM’94)*, Fort Monmouth, NJ, Oct. 1994, pp. 997–1001.
- [302] A. S. Gupta and A. C. Singer, “Successive interference cancellation using constellation structure,” *IEEE Transactions on Signal Processing*, vol. 55, no. 12, pp. 5716–5730, Dec. 2007.

- [303] J. G. Andrews and T. H. Meng, "Optimum power control for successive interference cancellation with imperfect channel estimation," *IEEE Transactions on Wireless Communications*, vol. 2, no. 2, pp. 375–383, Mar. 2003.
- [304] Y. C. Yoon, R. Kohno, and H. Imai, "A spread-spectrum multi-access system with a cascade of co-channel interference cancelers for multipath fading channels," in *Proc. 2nd IEEE International Symposium on Spread Spectrum Techniques and Applications (ISSTA '92)*, Yokohama, Japan, Nov. 1992, pp. 87–90.
- [305] R. M. Buehrer, S. P. Nicoloso, and S. Gollamudi, "Linear versus nonlinear interference cancellation," *Journal of Communication and Networks*, vol. 1, no. 2, pp. 118–133, Jun. 1999.
- [306] D. Guo, L. K. Rasmussen, S. Sun, and T. J. Lim, "A matrix-algebraic approach to linear parallel interference cancellation in CDMA," *IEEE Transactions on Communications*, vol. 48, no. 1, pp. 152–161, Jan. 2000.
- [307] M. K. Varanasi and B. Aazhang, "An iterative detector for asynchronous spread-spectrum multiple-access systems," in *Proc. IEEE Global Telecommunications Conference (GLOBECOM'88)*, Nov. 1988, pp. 556–560.
- [308] —, "Probability of error comparison of linear and iterative multiuser detectors," in *Proc. International Conference on Advances in Communications and Control Systems*, Baton Rouge, LA, Oct. 1988, pp. 54–65.
- [309] A. Duel-Hallen, "Linear and decision-feedback multiuser detectors," in *Proc. IEEE International Symposium on Information Theory (ISIT'91)*, Budapest, Hungary, Jun. 1991, pp. 24–28.
- [310] —, "Performance of multiuser zero-forcing and MMSE decision-feedback detectors for CDMA channels," in *Proc. IEEE Global Telecommunications Conference (GLOBECOM'93)*, Houston, TX, USA, Nov. 1993, pp. 82–86.
- [311] A. Duel-Hallen and C. Heegard, "Delayed decision-feedback sequence estimation," *IEEE Transactions on Communications*, vol. 37, no. 5, pp. 428–436, May 1989.
- [312] A. Duel-Hallen, "Equalizers for multiple input/multiple output channels and PAM systems with cyclostationary input sequences," *IEEE Journal on Selected Areas in Communications*, vol. 10, no. 3, pp. 630–639, Apr. 1992.
- [313] S. Verdú, "Recent progress in multiuser detection," in *Advances in Communications and Signal Processing*, ser. Lecture Notes in Control and Information Sciences, W. A. Porter and S. C. Kak, Eds. Heidelberg: Springer-Verlag, 1989, vol. 129, pp. 27–38. [Online]. Available: <http://dx.doi.org/10.1007/BFb0042716>
- [314] Z. Xie and C. K. Rushforth, "Multi-user signal detection using sequential decoding," in *Proc. IEEE Military Communications Conference (MILCOM'88)*, San Diego, CA, USA, Oct. 1988, pp. 983–988.
- [315] Z. Xie, C. K. Rushforth, R. T. Short, and T. K. Moon, "A tree-search algorithm for signal detection and parameter estimation in multi-user communications," in *Proc. IEEE Military Communications Conference (MILCOM'90)*, Monterey, CA, USA, Oct. 1990, pp. 796–800.
- [316] L. Wei, L. K. Rasmussen, and R. Wyrwas, "Near optimum tree-search detection schemes for bit-synchronous multiuser CDMA systems over gaussian and two-path rayleigh-fading channels," *IEEE Transactions on Communications*, vol. 45, no. 6, pp. 691–700, Jun. 1997.

- [317] F. Jelinek and J. B. Anderson, *Instrumentable tree encoding of information sources*. School of Electrical Engineering, Cornell University, Ithaca, NY, USA, Sep. 1969.
- [318] —, “Instrumentable tree encoding of information sources,” *IEEE Transactions on Information Theory*, vol. 17, no. 1, pp. 118–119, Jan. 1971.
- [319] W. L. Waltmann and R. J. Lambert, “T-algorithm for tridiagonalization,” *Journal of the Society for Industrial and Applied Mathematics*, vol. 13, no. 4, pp. 1069–1078, Dec. 1965. [Online]. Available: <http://www.jstor.org/stable/2946426>
- [320] S. J. Simmons, “A reduced-computation trellis decoder with inherent parallelism,” Ph.D. dissertation, Department of Electrical and Computer Engineering, Queens University, Kingston, Ontario, Canada, Jun. 1986. [Online]. Available: <http://istec.colostate.edu/~rockey/Papers/PhDThesis.pdf>
- [321] S. J. Simmons and P. Senyshyn, “Reduced-search trellis decoding of coded modulations over ISI channels,” in *Proc. IEEE Global Telecommunications Conference (GLOBECOM'90)*, Dec. 1990, pp. 393–396.
- [322] S. J. Simmons, “Breadth-first trellis decoding with adaptive effort,” *IEEE Transactions on Communications*, vol. 38, no. 1, pp. 3–12, Jan. 1990.
- [323] M. V. Eyuboğlu and S. U. Qureshi, “Reduced-state sequence estimation with set partitioning and decision feedback,” *IEEE Transactions on Communications*, vol. 36, no. 1, pp. 13–20, Jan. 1988.
- [324] R. Fano, “A heuristic discussion of probabilistic decoding,” *IEEE Transactions on Information Theory*, vol. 9, no. 2, pp. 64–74, Apr. 1963.
- [325] K. S. Zigangirov, “Some sequential decoding procedures,” *Problemy Peredachi Informatsii*, vol. 2, no. 4, pp. 13–25, Oct. 1966.
- [326] F. Jelinek, “Fast sequential decoding algorithm using a stack,” *IBM Journal of Research and Development*, vol. 13, no. 6, pp. 675–685, Nov. 1969.
- [327] J. L. Massey, “Variable-length codes and the fano metric,” *IEEE Transactions on Information Theory*, vol. 18, no. 1, pp. 196–198, Jan. 1972.
- [328] J. B. Anderson and S. Mohan, “Sequential coding algorithms: a survey and cost analysis,” *IEEE Transactions on Communications*, vol. 32, no. 2, pp. 169–176, Feb. 1984.
- [329] J. B. Anderson, “Limited search trellis decoding of convolutional codes,” *IEEE Transactions on Information Theory*, vol. 35, no. 5, pp. 944–955, Sep. 1989.
- [330] G. J. Pottie and D. P. Taylor, “A comparison of reduced complexity decoding algorithms for trellis codes,” *IEEE Journal on Selected Areas in Communications*, vol. 7, no. 9, pp. 1369–1380, Dec. 1989.
- [331] M. Pohst, “On the computation of lattice vectors of minimal length, successive minima and reduced bases with applications,” *ACM SIGSAM Bulletin*, vol. 15, no. 1, pp. 37–44, Feb. 1981.
- [332] U. Fincke and M. Pohst, “Improved methods for calculating vectors of short length in a lattice, including a complexity analysis,” *Mathematics of Computation*, vol. 44, no. 170, pp. 463–471, Apr. 1985.

- [333] C. P. Schnorr and M. Euchner, “Lattice basis reduction: improved practical algorithms and solving subset sum problems,” *Mathematical Programming*, vol. 66, no. 1-3, pp. 181–199, Aug. 1994.
- [334] B. Hassibi and H. Vikalo, “On the expected complexity of sphere decoding,” in *Proc. 35th Annual Asilomar Conference on Signals, Systems and Computers (Asilomar’01)*, Pacific Grove, CA, USA, Nov. 2001, pp. 1051–1055.
- [335] —, “On the expected complexity of integer least-squares problems,” in *Proc. IEEE International Conference on Acoustics, Speech, and Signal Processing (ICASSP’02)*, vol. 2, Orlando, FL, USA, May 2002, pp. II–1497–II–1500.
- [336] —, “Maximum-likelihood decoding and integer least-squares: The expected complexity,” in *DIMACS Series in Discrete Mathematics and Theoretical Computer Science: Multiantenna channels: capacity, coding and signal processing*, G. J. Foschini and S. Verdú, Eds. New York: American Mathematical Society, 2003, vol. 62, pp. 161–192.
- [337] J. Jaldén and B. Ottersten, “An exponential lower bound on the expected complexity of sphere decoding,” in *Proc. IEEE International Conference on Acoustics, Speech, and Signal Processing (ICASSP’04)*, vol. 4, Montreal, Canada, May 2004, pp. 393–396.
- [338] B. M. Hochwald and S. ten Brink, “Iterative list sphere decoding to attain capacity on a multi-antenna link,” in *Proc. of 39th Annual Allerton Conference On Communication, Control and Computing (Allerton’01)*, Monticello, IL, USA, Oct. 2001, pp. 815–824.
- [339] L. G. Barbero and J. S. Thompson, “A fixed-complexity MIMO detector based on the complex sphere decoder,” in *Proc. IEEE 7th Workshop on Signal Processing Advances in Wireless Communications (SPAWC’06)*, Cannes, France, Jul. 2006, pp. 1–5.
- [340] E. W. Dijkstra, “A note on two problems in connexion with graphs,” *Numerische Mathematik*, vol. 1, no. 1, pp. 269–271, 1959. [Online]. Available: <http://dx.doi.org/10.1007/BF01386390>
- [341] W. Xu, Y. Wang, Z. Zhou, and J. Wang, “A computationally efficient exact ML sphere decoder,” in *Proc. IEEE Global Telecommunications Conference (GLOBECOM’04)*, Dallas, TX, USA, Dec. 2004, pp. 2594–2598.
- [342] Y. Bar-Shalom and E. Tse, “Tracking in a cluttered environment with probabilistic data association,” *Automatica*, vol. 11, no. 5, pp. 451 – 460, 1975. [Online]. Available: <http://www.sciencedirect.com/science/article/pii/0005109875900217>
- [343] T. E. Fortmann, Y. Bar-Shalom, and M. Scheffe, “Multi-target tracking using joint probabilistic data association,” in *19th IEEE Conference on Decision and Control including the Symposium on Adaptive Processes*, Albuquerque, NM, USA, Dec. 1980, pp. 807–812.
- [344] —, “Sonar tracking of multiple targets using joint probabilistic data association,” *IEEE Journal of Oceanic Engineering*, vol. 8, no. 3, pp. 173–184, Jul. 1983.
- [345] Y. Bar-Shalom and X. R. Li, *Estimation and Tracking: Principles, Techniques and Software*. Dedham, MA: Artech House, 1993.
- [346] Y. Bar-Shalom, X. R. Li, and T. Kirubarajan, *Estimation with Applications to Tracking and Navigation: Theory, Algorithms and Software*. John Wiley & Sons, Inc., 2004.

- [347] Y. Bar-Shalom, T. Kirubarajan, and X. Lin, "Probabilistic data association techniques for target tracking with applications to sonar, radar and EO sensors," *IEEE Aerospace and Electronics Systems Magazine*, vol. 20, no. 8, pp. 37–56, 2005.
- [348] Y. Bar-Shalom, F. Daum, and J. Huang, "The probabilistic data association filter," *IEEE Control Systems Magazine*, vol. 29, no. 6, pp. 82–100, Dec. 2009.
- [349] K.-C. Chang and Y. Bar-Shalom, "Joint probabilistic data association for multitarget tracking with possibly unresolved measurements and maneuvers," *IEEE Transactions on Automatic Control*, vol. 29, no. 7, pp. 585–594, Jul. 1984.
- [350] K.-C. Chang, C.-Y. Chong, and Y. Bar-Shalom, "Joint probabilistic data association in distributed sensor networks," *IEEE Transactions on Automatic Control*, vol. 31, no. 10, pp. 889–897, Oct. 1986.
- [351] J. A. Roecker and G. L. Phillis, "Suboptimal joint probabilistic data association," *IEEE Transactions on Aerospace and Electronic Systems*, vol. 29, no. 2, pp. 510–517, Apr. 1993.
- [352] D. Musicki, R. J. Evans, and S. Stankovic, "Integrated probabilistic data association," *IEEE Transactions on Automatic Control*, vol. 39, no. 6, pp. 1237–1241, Jun. 1994.
- [353] D. J. Kershaw and R. J. Evans, "Waveform selective probabilistic data association," *IEEE Transactions on Aerospace and Electronic Systems*, vol. 33, no. 4, pp. 1180–1188, Oct. 1997.
- [354] H. A. P. Blom and E. A. Bloem, "Probabilistic data association avoiding track coalescence," *IEEE Transactions on Automatic Control*, vol. 45, no. 2, pp. 247–259, Feb. 2000.
- [355] T. Kirubarajan and Y. Bar-Shalom, "Probabilistic data association techniques for target tracking in clutter," *Proceedings of the IEEE*, vol. 92, no. 3, pp. 536–557, Mar. 2004.
- [356] D. Musicki and R. J. Evans, "Joint integrated probabilistic data association: JIPDA," *IEEE Transactions on Aerospace and Electronic Systems*, vol. 40, no. 3, pp. 1093–1099, Jul. 2004.
- [357] I. J. Cox, "A review of statistical data association techniques for motion correspondence," *International Journal of Computer Vision*, vol. 10, no. 1, pp. 53–66, Feb. 1993. [Online]. Available: <http://dx.doi.org/10.1007/BF01440847>
- [358] D. Schulz, W. Burgard, D. Fox, and A. B. Cremers, "Tracking multiple moving targets with a mobile robot using particle filters and statistical data association," in *Proc. IEEE International Conference on Robotics and Automation (ICRA'01)*, Seoul, Korea, May 2001, pp. 1665–1670.
- [359] —, "People tracking with mobile robots using sample-based joint probabilistic data association filters," *International Journal of Robotics Research*, vol. 22, no. 2, pp. 99–116, Feb. 2003.
- [360] C. Rasmussen and G. D. Hager, "Probabilistic data association methods for tracking complex visual objects," *IEEE Transactions on Pattern Analysis and Machine Intelligence*, vol. 23, no. 6, pp. 560–576, Jun. 2001.
- [361] Z. J. Wang, Z. Han, and K. J. R. Liu, "Mimo-ofdm channel estimation via probabilistic data association based toas," in *Proc. IEEE Global Telecommunications Conference (GLOBECOM'03)*, San Francisco, CA, USA, Dec. 2003, pp. 626–630.
- [362] —, "A MIMO-OFDM channel estimation approach using time of arrivals," *IEEE Transactions on Wireless Communications*, vol. 4, no. 3, pp. 1207–1213, May 2005.

- [363] F. D. Neeser and J. L. Massey, "Proper complex random processes with applications to information theory," *IEEE Transactions on Information Theory*, vol. 39, no. 4, pp. 1293–1302, Jul. 1993.
- [364] C. Berrou, A. Glavieux, and P. Thitimajshima, "Near Shannon limit error-correcting coding and decoding: Turbo-codes (1)," in *Proc. IEEE International Conference on Communications (ICC'93)*, vol. 2, Geneva, Switzerland, May 1993, pp. 1064–1070.
- [365] C. Berrou and A. Glavieux, "Near optimum error correcting coding and decoding: turbo-codes," *IEEE Transactions on Communications*, vol. 44, no. 10, pp. 1261–1271, Oct. 1996.
- [366] R. Gallager, "Low-density parity-check codes," *IRE Transactions on Information Theory*, vol. 8, no. 1, pp. 21–28, Jan. 1962.
- [367] D. J. C. MacKay and R. M. Neal, "Near Shannon limit performance of low density parity check codes," *Electronics Letters*, vol. 32, no. 18, pp. 1645–1646, 1996.
- [368] L. Vandenberghe and S. Boyd, "Semidefinite programming," *SIAM Review*, vol. 38, no. 1, pp. 49–95, Mar. 1996.
- [369] S. Boyd and L. Vandenberghe, *Convex Optimization*. New York, USA: Cambridge University Press, 2004.
- [370] P. H. Tan, L. K. Rasmussen, and T. M. Aulin, "The application of semidefinite programming for detection in CDMA," in *Proc. IEEE International Symposium on Information Theory (ISIT'01)*, Washington, DC, Jun. 2001, p. 9.
- [371] W.-K. Ma, T. N. Davidson, K. M. Wong, Z.-Q. Luo, and P.-C. Ching, "Efficient quasi-maximum-likelihood multiuser detection by semi-definite relaxation," in *Proc. IEEE International Conference on Communications (ICC'01)*, Helsinki, Finland, Jun. 2001, pp. 6–10.
- [372] X. Wang, W.-S. Lu, and A. Antoniou, "A near-optimal multiuser detector for CDMA channels using semidefinite programming relaxation," in *Proc. IEEE International Symposium on Circuits and Systems (ISCAS'01)*, Sydney, NSW, Australia, May 2001, pp. 298–301.
- [373] —, "A near-optimal multiuser detector for DS-CDMA systems using semidefinite programming relaxation," *IEEE Transactions on Signal Processing*, vol. 51, no. 9, pp. 2446–2450, Sep. 2003.
- [374] B. Steingrimsson, Z.-Q. Luo, and K. M. Wong, "Soft quasi-maximum-likelihood detection for multiple-antenna wireless channels," *IEEE Transactions on Signal Processing*, vol. 51, no. 11, pp. 2710–2719, Nov. 2003.
- [375] H. Holma and A. Toskala, Eds., *LTE Advanced: 3GPP Solution for IMT-Advanced*. John Wiley & Sons, 2012.
- [376] M. Riegel, A. Chindapol, and D. Kroeselberg, *Deploying Mobile WiMAX*. John Wiley & Sons, 2010.
- [377] S. Ahmadi, *Mobile WiMAX: A Systems Approach to Understanding IEEE 802.16m Radio Access Technology*. Elsevier, 2010.
- [378] L. Hanzo, S. X. Ng, T. Keller, and W. Webb, *Quadrature Amplitude Modulation: From Basics to Adaptive Trellis-Coded, Turbo-Equalised and Space-Time Coded OFDM, CDMA and MC-CDMA Systems*, 2nd ed. West Sussex, UK: Wiley-IEEE Press, 2004.

- [379] T. Matsumoto, S. Ibi, S. Sampei, and R. Thomä, “Adaptive transmission with single-carrier multilevel BICM,” *Proceedings of the IEEE*, vol. 95, no. 12, pp. 2354–2367, Dec. 2007.
- [380] E. Agrell, J. Lassing, E. G. Ström, and T. Ottosson, “On the optimality of the binary reflected Gray code,” *IEEE Transactions on Information Theory*, vol. 50, no. 12, pp. 3170–3182, Dec. 2004.
- [381] F. Schreckenbach, N. Gortz, J. Hagenauer, and G. Bauch, “Optimization of symbol mappings for bit-interleaved coded modulation with iterative decoding,” *IEEE Communications Letters*, vol. 7, no. 12, pp. 593–595, Dec. 2003.
- [382] J. Jaldén, L. G. Barbero, B. Ottersten, and J. S. Thompson, “Full diversity detection in MIMO systems with a fixed-complexity sphere decoder,” in *Proc. IEEE International Conference on Acoustics, Speech, and Signal Processing (ICASSP’07)*, vol. 3, Honolulu, HI, Apr. 2007, pp. II–49–III–52.
- [383] J. Maurer, G. Matz, , and D. Seethaler, “On the diversity-complexity tradeoff in MIMO spatial multiplexing systems,” in *Proc. 40th Asilomar Conference on Signals, Systems, and Computers (ACSSC’06)*, Pacific Grove, CA, USA, Oct. 2006, pp. 2077–2081.
- [384] J. Hoydis, S. ten Brink, and M. Debbah, “Massive MIMO: How many antennas do we need?” in *Proc. 2011 49th Annual Allerton Conference on Communication, Control, and Computing (Allerton’11)*, Sep. 2011, pp. 545–550.
- [385] L. Hanzo, H. Haas, S. Imre, D. O’Brien, M. Rupp, and L. Gyongyosi, “Wireless myths, realities, and futures: From 3G/4G to optical and quantum wireless,” *Proceedings of the IEEE*, vol. 100, no. Special Centennial Issue, pp. 1853–1888, May 2012.
- [386] C. Helmberg, F. Rendl, R. J. Vanderbei, and H. Wolkowicz, “An interior-point method for semidefinite programming,” *SIAM Journal on Optimization*, vol. 6, pp. 342–361, 1996.
- [387] M. Nekui, M. Kisialiou, T. Davidson, and Z.-Q. Luo, “Efficient soft-output demodulation of MIMO QPSK via semidefinite relaxation,” *IEEE Journal of Selected Topics in Signal Processing*, vol. 5, no. 8, pp. 1426–1437, Dec. 2011.
- [388] M. Nekui and T. N. Davidson, “A semidefinite relaxation approach to efficient soft demodulation of MIMO 16-QAM,” in *Proc. IEEE International Conference on Communications (ICC’09)*, Dresden, Germany, Jun. 2009, pp. 1–6.
- [389] M. Breiling and L. Hanzo, “The super-trellis structure of turbo codes,” *IEEE Transactions on Information Theory*, vol. 46, no. 6, pp. 2212–2228, Sep. 2000.
- [390] T. Giallorenzi and S. Wilson, “Multiuser ML sequence estimator for convolutionally coded asynchronous DS-CDMA systems,” *IEEE Transactions on Communications*, vol. 44, no. 8, pp. 997–1008, Aug. 1996.
- [391] J. Hagenauer, “The Turbo principle: tutorial introduction and state of the art,” in *Proc. 1st International Symposium on Turbo Codes and Related Topics*, Brest, France, Sep. 1997, pp. 1–11.
- [392] X. Wang and H. V. Poor, “Iterative (turbo) soft interference cancellation and decoding for coded cdma,” *IEEE Transactions on Communications*, vol. 47, no. 7, pp. 1046–1061, Jul. 1999.

- [393] J. Lodge, R. Young, P. A. Hoeher, and J. Hagenauer, "Separable MAP 'filters' for the decoding of product and concatenated codes," in *Proc. IEEE International Conference on Communications (ICC'93)*, vol. 3, Geneva, Switzerland, May 1993, pp. 1740–1745.
- [394] J. Hagenauer, E. Offer, and L. Papke, "Iterative decoding of binary block and convolutional codes," *IEEE Transactions on Information Theory*, vol. 42, no. 2, pp. 429–445, Mar. 1996.
- [395] M. Sellathurai and S. Haykin, "Turbo-BLAST for wireless communications: theory and experiments," *IEEE Transactions on Signal Processing*, vol. 50, no. 10, pp. 2538–2546, Oct. 2002.
- [396] J. Proakis, *Digital Communications*, 4th ed. New York, USA: McGraw-Hill, 2000.
- [397] T. Aulin, "Characteristics of a digital mobile radio channel," *IEEE Transactions on Vehicular Technology*, vol. 30, no. 2, pp. 45–53, May 1981.
- [398] T. Adali, P. Schreier, and L. Scharf, "Complex-valued signal processing: The proper way to deal with impropriety," *IEEE Transactions on Signal Processing*, vol. 59, no. 11, pp. 5101–5125, Nov. 2011.
- [399] D. Mandic and V. Goh, *Complex Valued Nonlinear Adaptive Filters: Noncircularity, Widely Linear and Neural Models*, ser. Adaptive and Learning Systems for Signal Processing, Communications and Control Series. John Wiley & Sons, 2009.
- [400] P. M. Lee, *Bayesian Statistics: An Introduction*, 3rd ed. Chichester, UK: Wiley, 2004.
- [401] J. Pearl, *Probabilistic Reasoning in Intelligent Systems: Networks of Plausible Inference*. San Mateo, California: Morgan Kaufmann Publishers, 1988.
- [402] S. ten Brink, "Convergence behavior of iteratively decoded parallel concatenated codes," *IEEE Transactions on Communications*, vol. 49, no. 10, pp. 1727–1737, Oct. 2001.
- [403] J. Hagenauer, "The EXIT chart—Introduction to extrinsic information transfer in iterative processing," in *Proc. 12th European Signal Processing Conference (EUSIPCO'04)*, Vienna, Austria, Sep. 2004, pp. 1541–1548.
- [404] J. Zander, S.-L. Kim, and M. Almgren, *Radio Resource Management for Wireless Networks*. Norwood, MA, USA: Artech House, Inc., 2001.
- [405] N. D. Tripathi, J. H. Reed, and H. F. Vanlandingham, *Radio Resource Management for Wireless Networks*. Dordrecht, Netherlands: Kluwer Academic Publishers, 2001.
- [406] S. Khattak, W. Rave, and G. Fettweis, "SIC based multi-user turbo detector for non gray mapping in distributed antenna systems," in *Proc. 9th International Symposium on Wireless Personal Multimedia Communications (WPMC'06)*, San Diego, CA, USA, Sep. 2006, pp. 855–859.
- [407] A. Mostafa, R. Kobylinski, I. Kostanic, and M. Austin, "Single antenna interference cancellation (SAIC) for GSM networks," in *Proc. IEEE 58th Vehicular Technology Conference (VTC'03-Fall)*, Orlando, Florida, Oct. 2003, pp. 1089–1093.
- [408] H. Schoeneich and P. A. Hoeher, "Single antenna interference cancellation: iterative semiblind algorithm and performance bound for joint maximum-likelihood interference cancellation," in *Proc. IEEE Global Telecommunications Conference (GLOBECOM'03)*, San Francisco, USA, Dec. 2003, pp. 1716–1720.

- [409] M. Pukkila, G. P. Mattellini, and P. A. Ranta, "Constant modulus single antenna interference cancellation for GSM," in *Proc. IEEE 59th Vehicular Technology Conference (VTC'04-Spring)*, Milan, Italy, May 2004, pp. 584–588.
- [410] R. Meyer, W. H. Gerstacker, R. Schober, and J. B. Huber, "A single antenna interference cancellation algorithm for increased GSM capacity," *IEEE Transactions on Wireless Communications*, vol. 5, no. 7, pp. 1616–1621, Jul. 2006.
- [411] P. A. Hoeher, S. Badri-Hoeher, W. Xu, and C. Krakowski, "Single-antenna co-channel interference cancellation for TDMA cellular radio systems," *IEEE Wireless Communications Magazine*, vol. 12, no. 2, pp. 30–37, Apr. 2005.
- [412] I. Koffman and V. Roman, "Broadband wireless access solutions based on OFDM access in IEEE 802. 16," *IEEE Communications Magazine*, vol. 40, no. 4, pp. 96–103, Apr. 2002.
- [413] N. Benvenuto, R. Dinis, D. Falconer, and S. Tomasin, "Single carrier modulation with nonlinear frequency domain equalization: an idea whose time has come — again," *Proceedings of the IEEE*, vol. 98, no. 1, pp. 69–96, Jan. 2010.
- [414] A. S. Motahari and A. K. Khandani, "Capacity bounds for the gaussian interference channel," *IEEE Transactions on Information Theory*, vol. 55, no. 2, pp. 620–643, Feb. 2009.
- [415] X. Shang, G. Kramer, and B. Chen, "A new outer bound and the noisy-interference sum-rate capacity for gaussian interference channels," *IEEE Transactions on Information Theory*, vol. 55, no. 2, pp. 689–699, Feb. 2009.
- [416] V. S. Annapureddy and V. V. Veeravalli, "Gaussian interference networks: Sum capacity in the low-interference regime and new outer bounds on the capacity region," *IEEE Transactions on Information Theory*, vol. 55, no. 7, pp. 3032–3050, Jul. 2009.
- [417] T. Weber, A. Sklavos, and M. Meurer, "Imperfect channel-state information in MIMO transmission," *IEEE Transactions on Communications*, vol. 54, no. 3, pp. 543–552, Mar. 2006.
- [418] X. Xu, R. Zhang, and L. Hanzo, "Imperfect radio over fibre aided distributed antennas with fractional frequency reuse," in *Proc. IEEE 72nd Vehicular Technology Conference (VTC'10-Fall)*, Ottawa, Canada, Sep. 2010, pp. 1–5.
- [419] B. Lee, J. M. Cioffi, S. Jagannathan, and M. Mohseni, "Gigabit DSL," *IEEE Transactions on Communications*, vol. 55, no. 9, pp. 1689–1692, Sep. 2007.
- [420] B. Lee, J. M. Cioffi, S. Jagannathan, K. Seong, Y. Kim, M. Mohseni, and M. H. Brady, "Binder MIMO channels," *IEEE Transactions on Communications*, vol. 55, no. 8, pp. 1617–1628, Aug. 2007.
- [421] Y.-C. Liang, G. Pan, and Z. D. Bai, "Asymptotic performance of MMSE receivers for large systems using random matrix theory," *IEEE Transactions on Information Theory*, vol. 53, no. 11, pp. 4173–4190, Nov. 2007.
- [422] L. Lampe, R. Schober, V. Pauli, and C. Windpassinger, "Multiple-symbol differential sphere decoding," in *Proc. IEEE International Conference on Communications (ICC'04)*, vol. 2, Paris, France, Jun. 2004, pp. 787–791.
- [423] —, "Multiple-symbol differential sphere decoding," *IEEE Transactions on Communications*, vol. 53, no. 12, pp. 1981–1985, Dec. 2005.

- [424] V. Pauli, L. Lampe, and R. Schober, "Turbo DPSK using soft multiple-symbol differential sphere decoding," *IEEE Transactions on Information Theory*, vol. 52, no. 4, pp. 1385–1398, Apr. 2006.
- [425] V. Pauli and L. Lampe, "Tree-search multiple-symbol differential decoding for unitary space-time modulation," *IEEE Transactions on Communications*, vol. 55, no. 8, pp. 1567–1576, Aug. 2007.
- [426] —, "On the complexity of sphere decoding for differential detection," *IEEE Transactions on Information Theory*, vol. 53, no. 4, pp. 1595–1603, Apr. 2007.
- [427] Z. Ma, P. Fan, E. G. Larsson, and B. Honary, "Quasi-maximum-likelihood multiple-symbol differential detection for time-varying rayleigh fading channel," *Electronics Letters*, vol. 45, no. 22, pp. 1127–1128, Oct. 2009.

Author Index

- Aazhang, B. 8, 14, 23, 24, 26, 27
- Abe, T. 11
- Abed-Meraim, K. 3
- Abend, K. 17
- Agrell, E. 3, 14, 28, 29, 46, 51, 134
- Ahmadi, S. 42
- Aktas, D. 8
- Aktas, E. 8, 158–160
- Alamouti, S. 8
- Anderson, J. B. 27
- Andrews, J. G. 15, 24, 25
- Andrieu, C. 14, 31, 32, 36, 42, 43, 56, 67, 70, 75, 108, 116, 118, 121, 125, 126, 165
- Antoniou, A. 24, 33, 35, 189
- Armour, S. 1
- Aulin, T. M. 33, 35
- Ayanoglu, E. 13
- Azzam, L. 13
- Bahl, L. 17
- Baier, P. W. 3
- Bajcsy, Jan 14, 31, 32
- Bar-Shalom, Y. 31
- Barbero, L. G. 3, 14, 28, 30, 74, 133, 134
- Barry, J. R. 24
- Batalama, S. N. 22, 24
- Bauch, G. 51
- Bavarian, S. 14, 31, 32, 135, 136, 141, 143
- Belfiore, J.-C. 3
- Benesty, J. 14, 25
- Bengtsson, M. 14, 24
- Bergmans, P. 24, 27
- Berrou, C. 32, 105, 106, 148
- Biglieri, E. 14, 27–29
- Bloem, E. A. 31
- Blom, H. A. P. 31
- Blum, R. S. 1, 157
- Böhnke, R. 14, 25, 27
- Bolcskei, H. 3, 14, 28, 29
- Borgmann, M. 3, 14, 28, 29
- Boutros, J. 3, 14, 27–29, 98, 170

- Boyd, S. 5, 33, 76, 77, 83, 84, 92, 93
- Brunel, L. 3
- Buehrer, R. M. 8, 14, 25, 26
- Burg, A. 3, 14, 28, 29
- Burgard, W. 31
- Cadambe, V. R. 8
- Cai, Yueming 14, 31, 136
- Caire, G. 3, 7, 14, 28–30
- Calderbank, A. R. 8, 105
- Cao, Feifei 14, 31, 166
- Carleial, A. 7, 24, 27, 162
- Catreux, S. 1, 157
- Cavers, J. K. 14, 31, 32, 135, 136, 141, 143
- Cha, Inhyok 1
- Chae, Chan-Byoung 1
- Chang, Hsie-Chia 14, 28
- Chang, Hsiu-Chi 14, 28
- Chang, Kuo-Chu 31
- Chang, Ronald Y. 3, 14, 28, 30
- Chang, Tsung-Hui 14, 33, 35
- Chen, Jingdong 14, 25
- Chen, Kwang-Cheng 1
- Chen, Sheng 14, 23, 24
- Chen, Sizhong 3, 14, 28, 30
- Chen, Yu 1
- Cheng, Roger S. 3, 14, 25, 28, 30
- Cheng, Yunpeng 14, 31, 136
- Chi, Chong-Yung 14, 33, 35
- Chiani, M. 14, 25
- Chin, W. H. 14, 26, 27
- Chindapol, A. 42
- Ching, Pak-Chung 14, 33, 35, 189
- Chiu, Chun-Ning 13
- Chkeif, A. 3
- Chockalingam, A. 14, 31, 32
- Choi, Jun Won 3, 133, 134
- Choi, Lai-U 7
- Chong, Chee-Yee 31
- Chong, Song 1
- Chun, Joohwan 3, 14, 28
- Chung, Wei-Ho 3, 14, 28, 30
- Cocke, J. 17
- Constantinides, A. G. 14, 26, 27
- Cormen, T. H. 18, 19
- Costa, M. H. M. 7
- Cover, T. M. 24, 27
- Cox, I. J. 31
- Cremers, A. B. 31
- Dai, Huaiyu 1, 7, 8, 157
- Damen, M. O. 3, 14, 28–30
- Daneshrad, B. 3
- Daum, F. 31
- Davidson, T. N. 14, 33, 35, 189
- Dent, P. 24, 25
- Dijkstra, E. W. 30
- Ding, Zhi 14, 33, 35, 189
- Divsalar, D. 8, 14, 24, 25

- Driessen, P. F. 1, 157
- Duel-Hallen, A. 3, 6, 8, 14, 24, 26, 27
- Edfors, O. 1, 3, 183, 188, 190
- El Gamal, A. 7
- El Gamal, H. 3, 11, 14, 28–30
- El-Sayed, M. 1
- Eldar, Y. C. 14, 33, 35, 76, 95, 96, 189
- Emmerson, B. 1
- Engels, M. 3, 5, 6
- Eriksson, T. 3, 14, 28, 29, 134
- Etkin, R. H. 7, 162
- Euchner, M. 28, 29
- Evans, J. S. 8, 158–160
- Evans, R. J. 31
- Ewerbring, M. 24, 25
- Eyuboglu, M. V. 27
- Fadlullah, Z. M. 1
- Fakhereddin, M. J. 7
- Fano, R. 27
- Fateh, S. 14, 24, 26, 27
- Feher, K. 25
- Fettweis, G. 8, 158–160, 173
- Fichtner, W. 3, 14, 28, 29
- Fincke, U. 28, 29
- Fischer, R. F. H. 13
- Fitz, M. P. 11, 13
- Forney, G. D. 15, 17
- Fortmann, T. E. 31
- Foschini, G. J. 6, 8, 10, 14, 21–25, 27, 70, 105, 157
- Fossorier, M. 3
- Fouda, M. M. 1
- Fox, D. 31
- Fricke, J. 14, 31–33, 42, 43, 57, 63, 64, 75, 136, 139, 141, 166
- Fritchman, B. D. 17
- Fukatani, T. 14, 28, 30
- Gagliardi, R. 8, 14, 23
- Gallager, R. 33, 105
- Gans, M. J. 8, 157
- Garey, M. R. 18, 19
- George, D. 8, 14, 22, 23
- Gerlach, D. 3, 5, 6, 8
- Gerstacker, W. H. 1
- Gesbert, D. 1, 8, 187
- Giannakis, G. B. 3, 11, 12
- Glavieux, A. 32, 105, 106, 148
- Golden, G. D. 6, 8, 10, 14, 21–25, 27, 70
- Goldsmith, A. 3–7, 10
- Gollamudi, S. 25
- Gore, D. 1, 3–7, 10
- Gortz, N. 51
- Gowaikar, R. 3
- Grant, A. 8, 158, 159
- Grant, P. M. 1
- Greenstein, L. J. 1, 157

- Gresset, N. 3
- Grossmann, M. 14, 31
- Gudmundson, B. 24, 25
- Guibas, L. 7
- Guizani, M. 1
- Gumacos, C. 17
- Guo, Dongning 26
- Guo, Zhan 3, 14, 28, 30
- Gupta, A. S. 25
- Haardt, M. 7
- Haas, H. 1
- Hadisusanto, Y. 8
- Hagenauer, J. 8, 51, 158, 159
- Hager, G. D. 31
- Hammons, A. R. 11
- Han, Bo 1
- Han, Congzheng 1
- Han, Te 7, 162
- Han, Zhu 31
- Hanly, S. V. 1, 8, 157–160, 187
- Hanzo, L. 1, 3, 8, 14, 23, 24, 37–40, 42, 45, 108, 118, 121, 136, 139, 141, 143, 145, 150, 155, 179, 181, 183, 184, 186
- Harley, T. J. 17
- Harrold, T. 1
- Hasegawa, F. 14, 31, 32, 42, 43, 57, 68, 108, 116, 118, 121, 132, 135, 136, 141, 143, 155, 165, 168, 169
- Hassibi, B. 3, 14, 25, 28, 29
- Hatori, M. 8, 14, 24, 25, 27
- Haykin, S. 4
- Heath, R. W. 1
- Hedayat, A. 7
- Heegard, C. 26
- Himayat, N. 1
- Hochwald, B. M. 3, 29, 106, 107, 117, 119, 127–133, 142, 155
- Hoeher, P. A. 1, 14, 31–33, 42, 43, 57, 63, 64, 75, 136, 139, 141, 166
- Holtzman, J. M. 3, 6, 8, 14, 25, 26
- Honig, M. 15
- Horwood, D. 8, 14, 23
- Huang, Howard 1, 8, 187
- Huang, Jim 31
- Huang, Yiteng 14, 25
- Huang, Yufei 14, 31
- Hui, A. L. C. 8, 14, 25
- Hui, Pan 1
- Hunter, T. E. 7
- Ibi, S. 43
- Imai, H. 8, 14, 25, 27
- Iwasaki, N. 1
- Jafar, S. A. 7, 8
- Jaldén, J. 3, 14, 28–30, 33, 35, 74, 98, 99, 102, 107, 133, 134, 189
- Jamalipour, A. 5, 161
- Janani, M. 7
- Jelinek, F. 17, 27, 30

- Jenkac, H. 8, 158, 159
- Jia, Yugang. 14, 31
- Jindal, N. 7
- Johnson, D. S. 18, 19
- Johnson, K. D. 1
- Johnsson, K. 1
- Jung, P. 3
- Jungnickel, V. 8
- Kailath, T. 3, 8, 15
- Kammeyer, K.-D. 14, 25, 27
- Kandukuri, S. 5
- Kanterakis, E. G. 24, 26
- Kato, N. 1
- Kato, S. 25
- Kay, Steven M. 21
- Kaye, A. 8, 14, 22, 23
- Keller, T. 42, 45
- Kershaw, D. J. 31
- Khandani, A. K. 8, 14, 33, 35, 72, 76, 189
- Khattak, S. 8, 158–160, 173
- Kim, Tae-Hwan 3, 14, 28
- Kim, Yong Jin Daniel 14, 31, 32
- Kirubarajan, T. 31
- Kisialiou, M. 14, 33, 35, 189
- Kobayashi, K. 7, 162
- Kobayashi, M. 7
- Kohno, R. 8, 14, 24, 25, 27
- Kountouris, M. 1
- Kramer, G. 7
- Krikidis, I. 1
- Kroeselberg, D. 42
- Ku, Ivan 1
- Kubota, S. 25
- Kühn, V. 14, 25, 27
- Kumar, V. S. A. 1
- Lambert, R. J. 27
- Lampe, L. 1
- Laneman, J. N. 7
- Larsson, E. G. 1, 3, 6, 183, 188, 190
- Lassing, J. 46, 51
- Latsoudas, G. 14, 31, 32
- Lau, Buon Kiong 1, 3, 183, 188, 190
- Lawton, G. 1
- Le, Tuan Anh 1
- Lee, Joohyun 1
- Lee, Kyungchun. 3, 14, 28
- Lee, Kyunghan 1
- Lee, William C. Y. 3
- Leicher, A. 1
- Leiserson, C. E. 18, 19
- Letaief, K. B. 6, 8, 14, 25
- Li, Jiandong 14, 31, 166
- Li, Shaoqian 14, 31
- Li, Xiao Rong 31
- Li, Xu 1
- Li, Ye (Geoffrey) 14, 25
- Li, Zi 14, 31, 136

- Liang, Xiaohui 1
- Liao, Yen-Chin 14, 28
- Lien, Shao-Yu 1
- Lim, Teng Joon 26
- Lin, Sian-Jheng 3, 14, 28, 30
- Lin, Xiangdong 31
- Lin, Xiaodong 1
- Lin, Yonghua 1
- Liu, Jie 7
- Liu, Juan 7
- Liu, K. J. Ray 31
- Liu, Shoumin 11, 14, 31, 32, 42, 43, 75, 108, 118, 121, 135, 136, 141, 143
- Liu, Siyang 14, 26
- Liu, Tsung-Hsien 13, 14, 25
- Liu, Youjian 11
- Liu, Yu Ting 14, 28
- Liu, Yuanan 14, 26
- Livingstone, A. 14, 23, 24
- Lopes, R. R. 24
- Lotter, M. P. 3, 5, 6, 8
- Lu, Ben 14, 25
- Lu, Rongxing 1
- Lu, Wu-Sheng 24, 33, 35, 189
- Luo, Jie 14, 31, 32, 42, 43, 57, 68, 72, 75, 108, 116, 118, 121, 132, 135, 136, 141, 143, 155, 165, 166, 168, 169
- Luo, Xiaodong 14, 33, 35, 189
- Luo, Zhendong 14, 26
- Luo, Zhi-Quan 14, 33, 35, 76, 83, 96, 101, 189
- Lupas, R. 8, 14, 21–23
- Lv, Tiejun 3, 8, 37–40, 108, 118, 121, 136, 141, 143, 150, 155, 179, 181, 183, 184, 186
- Ma, Wing-Kin 14, 33, 35, 83, 189
- Ma, Xiaoli 11
- MacKay, D. J. C. 33, 105
- Maddah-Ali, M. A. 8
- Madhow, U. 15
- Mandayam, N. B. 23, 24
- Mao, Zhiwei 14, 33, 35, 43, 72, 76, 77, 87, 96, 98, 189
- Marathe, M. V. 1
- Marzetta, T. L. 1, 3, 183, 188, 190
- Masamura, T. 8, 14
- Massey, J. L. 27, 31, 115, 139, 140, 165
- Matsumoto, R. 14, 28, 30
- Matsumoto, T. 11, 14, 31, 43
- Matz, G. 74
- Maunder, R. G. 3, 8, 37–40, 108, 118, 121, 136, 141, 143, 150, 179, 184, 186
- Maurer, J. 74
- Mayer, T. 8, 158, 159
- Mcqueen, D. 1
- Mehta, N. B. 8
- Meng, Teresa H. 25
- Meyerstein, M. V. 1
- Micciancio, D. 1, 18, 20

- Mietzner, J. 1, 14, 31–33, 42, 43, 57, 63, 64, 75, 136, 139, 141, 166
- Mobasher, A. 14, 33, 35, 72, 76, 189
- Mohammed, S. K. 14, 31, 32
- Mohan, S. 27
- Molisch, A. F. 1, 8, 157
- Moon, T. K. 8, 14, 26, 27, 30
- Moshavi, S. 3, 6, 24, 26
- Motahari, A. S. 8
- Mow, Wai-Ho 3, 14, 28, 30
- Mukhopadhyay, A. 1
- Mulgrew, B. 24
- Muller, R. 8, 158, 159
- Murch, R. D. 6, 7, 11
- Murugan, A. R. 3, 30
- Musicki, D. 31
- Nabar, R. 1, 3–7, 10
- Naguib, A. F. 8
- Nakhai, M. R. 1
- Nawab, S. H. 4
- Neal, R. M. 33, 105
- Neeser, F. D. 31, 115, 139, 140, 165
- Ng, Boon Loong 8
- Ng, Soon Xin 42, 45
- Nicoloso, S. P. 25
- Nilsson, P. 3, 14, 28, 30
- Niyato, D. 1
- Nosratinia, A. 7
- Nozaki, Y. 1
- Okawado, A. 14, 28
- Omura, J. 15, 17
- Oppenheim, A. V. 4
- Ottersten, B. 3, 5, 6, 8, 14, 24, 28–30, 33, 35, 74, 98, 99, 102, 107, 133, 134, 189
- Ottosson, T. 46, 51
- Pados, D. A. 22, 24
- Palomar, D. P. 14, 24
- Papadopoulos, H. C. 7
- Park, In-Cheol 3, 14, 28
- Pasupathy, S. 8, 14, 25, 27
- Patel, P. R. 8, 14, 25
- Pattipati, K. R. 14, 31, 32, 42, 43, 57, 68, 72, 75, 108, 116, 118, 121, 132, 135, 136, 141, 143, 155, 165, 168, 169
- Paulraj, A. 1, 3–8, 10
- Peel, C. B. 7
- Pepin, C. 7
- Persson, D. 1, 3, 183, 188, 190
- Pham, D. 14, 31, 32, 42, 43, 68, 72, 75, 108, 116, 118, 121, 135, 136, 141, 143
- Phillis, G. L. 31
- Piechocki, R. J. 14, 31, 32, 36, 42, 43, 56, 67, 70, 75, 108, 116, 118, 121, 125, 126, 165
- Pohst, M. 28, 29
- Poor, H. V. 1, 8, 10, 14–18, 22, 26, 157
- Pottie, G. J. 27
- Proakis, J. G. 4
- Psaromiligkos, I. N. 22, 24

- Qureshi, S. U. 27
- Qureshi, Shahid U. H. 15
- Rachid, M. 3
- Rajan, B. S. 14, 31, 32
- Ramprashad, S. A. 7
- Ranganathan, P. 1
- Raphaeli, D. 8, 14, 24, 25
- Rappaport, T. S. 4, 15
- Rasmussen, C. 31
- Rasmussen, L. K. 14, 26, 27, 30–33, 35, 93, 188, 189
- Rave, W. 8, 158–160, 173
- Ravindran, N. 7
- Raviv, J. 17
- Reich, J. 7
- Rhee, Injong 1
- Riegel, M. 42
- Rivest, R. L. 18, 19
- Roecker, J. A. 31
- Roy, R. H. 3, 5, 6, 8
- Rusek, F. 1, 3, 183, 188, 190
- Rushforth, C. K. 8, 14, 22–24, 26, 27, 29, 30
- Salzer, T. 1
- Samingan, A. K. 24
- Sampei, S. 43
- Sandell, M. 14, 31–33, 42, 43, 57, 63, 64, 75, 136, 139, 141, 166
- Sason, I. 7
- Sato, H. 7, 162
- Scheffe, M. 31
- Schilling, D. L. 24, 26
- Schmidt, A. U. 1
- Schneider, K. S. 8, 14, 21, 23
- Schnorr, C. P. 28, 29
- Schober, R. 1
- Schreckenbach, F. 51
- Schulz, D. 31
- Seethaler, D. 14, 24, 26, 27
- Senyshyn, P. 27
- Serbetli, S. 6
- Seshadri, N. 8, 105
- Sfar, S. 6
- Shah, Y. 1
- Shamai (Shitz), S. 1, 8, 14, 24, 33, 35, 76, 95, 96, 157, 187, 189
- Shao, Jianhua 1
- Shen, Xuemin 1
- Shim, Byonghyo 3, 133, 134
- Shnidman, D. A. 8, 14, 21–23, 177
- Short, R. T. 8, 14, 22–24, 26, 27, 29, 30
- Sidiropoulos, N. D. 14, 31–33, 35, 76, 96, 189
- Simeone, O. 1, 8, 187
- Simmons, S. J. 27
- Simon, M. K. 8, 14, 24, 25
- Singer, A. C. 3, 25, 133, 134
- Siti, M. 13
- Sklar, B. 4

- So, A. M.-C. 14, 33, 83
- Sollenberger, N. R. 1, 14, 25, 157
- Somekh, O. 1, 157
- Sotirov, R. 14, 33, 35, 72, 76, 189
- Spencer, Q. H. 7
- Srinivasan, A. 1
- Stankovic, S. 31
- Starsinic, M. 1
- Steil, A. 3
- Stein, C. 18, 19
- Steingrimsson, B. 35, 101
- Stojnic, M. 3, 14, 28
- Ström, E. G. 46, 51
- Studer, C. 3, 14, 24, 26, 27
- Su, Chao-Cheng 14, 33, 35
- Sun, Sumei 26
- Sundberg, C.-E. W. 7
- Swindlehurst, A. L. 7
- Taherzadeh, M. 14, 33, 35, 72, 76, 189
- Takeshita, O. Y. 11
- Takeuchi, A. 1
- Talwar, S. 1
- Tan, Peng Hui 14, 31–33, 35, 93, 188, 189
- Tarokh, V. 8, 105
- Taylor, D. P. 27
- Telatar, E. 8, 13
- ten Brink, S. 3, 29, 106, 107, 117, 119, 127–133, 142, 155
- Thiele, L. 8
- Thitimajshima, P. 32, 105, 106
- Thomä, R. 43
- Thompson, J. S. 1, 3, 14, 28, 30, 74, 133, 134
- Tian, Zhi 11, 14, 31, 32, 42, 43, 75, 108, 118, 121, 135, 136, 141, 143
- Timor, U. 8, 14, 24, 26, 27
- Tong, Lang 15
- Tse, D. N. C. 1, 3, 5–7, 10, 157, 162
- Tse, Edison 31
- Tsui, Chi-Ying 3, 14, 25, 28, 30
- Tufts, D. W. 14
- Tufvesson, F. 1, 3, 183, 188, 190
- Urrutia-Valdés, C. 1
- Uyematsu, T. 14, 28, 30
- Valenzuela, R. A. 6, 8, 10, 14, 21–25, 27, 70
- Van der Perre, L. 3, 5, 6
- van Emde Boas, P. 1, 18, 20
- van Etten, W. 8, 14, 15, 20–23
- van Rooyen, P. 3, 5, 6, 8
- Vandenameele, P. 3, 5, 6
- Vandenberghe, L. 33, 76, 77, 83, 84, 92, 93
- Varanasi, M. K. 8, 14, 24, 26, 27
- Vardy, A. 3, 14, 28, 29, 134
- Verdú, S. 1, 3, 6, 8, 10, 12, 14–18, 20–24, 26
- Videv, S. 1
- Vikalo, H. 3, 14, 28, 29
- Viswanath, P. 1, 3, 5–7, 10, 157
- Viterbi, A. J. 3, 5, 8, 14, 15, 17, 24, 25, 27

- Viterbo, E. 3, 14, 27–29, 98, 170
- Vithanage, C. M. 14, 31, 32, 36, 42, 43, 56, 67, 70, 75, 108, 116, 118, 121, 125, 126, 165
- Wada, T. 5, 161
- Waltmann, W. L. 27
- Wang, Cheng-Xiang 1
- Wang, Hua 7, 162
- Wang, Jing 30
- Wang, Jun 14, 31
- Wang, Li 3, 39, 155, 183
- Wang, Ping 1
- Wang, Renqiu 3
- Wang, Wei 1
- Wang, Xianmin 14, 33, 35, 43, 72, 76, 77, 87, 96, 98, 189
- Wang, Xiaodong 8, 10, 14, 15, 25, 26
- Wang, Xiaofeng 14, 24, 33, 35, 43, 72, 76, 77, 87, 96, 98, 189
- Wang, Youzheng 30
- Wang, Z. Jane 31
- Wang, Zhendao 11, 12
- Ward, D. B. 14, 26, 27
- Webb, W. 42, 45
- Wei, Lei 26, 27, 30
- Wenk, M. 3, 14, 28, 29
- Whiting, P. 1, 157
- Wiesel, A. 14, 33, 35, 76, 95, 96, 189
- Willett, P. K. 14, 31, 32, 42, 43, 57, 68, 72, 75, 108, 116, 118, 121, 132, 135, 136, 141, 143, 155, 165, 168, 169
- Willsky, A. S. 4
- Win, M. Z. 14, 25
- Windpassinger, C. 13
- Winters, J. H. 1, 14, 25, 157
- Woerner, B. D. 8, 14, 26
- Wolniansky, P. W. 6, 8, 10, 14, 21–25, 27, 70
- Wong, Kon Max 14, 33, 35, 101, 189
- Wong, Kwan-Wai 3, 14, 25, 28, 30
- Wornell, G. W. 7
- Wu, Geng 1
- Wu, Yi Hsuan 14, 28
- Wübben, D. 14, 25, 27
- Wyner, A. D. 1, 157
- Wyrwas, R. 26, 27, 30
- Xiao, Lu 1
- Xiao, Yang 1
- Xie, Shengli 1
- Xie, Zhenhua 8, 14, 22–24, 26, 27, 29, 30
- Xin, Yan 3, 14, 28, 30
- Xu, Guanghan 15
- Xu, Wei 14, 33, 76, 189
- Xu, Weiyu 30
- Xu, Xin 14, 31, 136
- Xu, Youyun 14, 31, 136
- Yamazato, T. 5, 161
- Yang, Jiawei 14, 31, 166
- Yang, Liuqing 11

- Yang, Shaoshi 3, 8, 37–40, 108, 118, 121, 136, 139, 141, 143, 145, 150, 155, 179, 181, 183, 184, 186
- Yang, Yijin 14, 33, 76, 189
- Yao, Wenqing 1
- Ye, Yinyu 14, 33, 83
- Yeh, Chen-Chu 24
- Yener, A. 6
- Yi, Yung 1
- Yin, Yufang 14, 31
- Yoon, Young C. 8, 14, 25
- Yu, Rong 1
- Yu, Wei 1, 8, 14, 33, 76, 83, 187
- Yue, Guosen 14, 25
- Zakhour, R. 8
- Zanella, A. 14, 25
- Zeger, K. 3, 14, 28, 29, 134
- Zellweger, M. 3, 14, 28, 29
- Zhang, Hongyuan 7, 8
- Zhang, Jianqiu 14, 31
- Zhang, Jiayi 1
- Zhang, Jin 8
- Zhang, Shuzhong 14, 33, 83
- Zhang, Tong 3, 14, 28, 30
- Zhang, Yan 1
- Zhao, Chunming 14, 33, 76, 189
- Zhao, Feng 7
- Zhao, Ming 14, 26
- Zhao, Z. John 1
- Zhou, Peng 14, 33, 76, 189
- Zhou, Quan 8
- Zhou, Zucheng 30
- Zhu, Xu 11
- Zigangirov, K. Sh. 27
- Zvonar, Z. 3, 6, 26

